3

NASA CR 147541

ORSER-SSEL Technical Report 4-76

INTERDISCIPLINARY APPLICATIONS AND INTERPRETATIONS OF EREP DATA WITHIN THE SUSQUEHANNA RIVER BASIN

Final Report: Mar 1 [illegible] – November 30 1975

Skylab EREP Investigation
NASA Contract Number [illegible]

THE PENNSYLVANIA STATE UNIVERSITY

OFFICE FOR REMOTE SENSING OF EARTH RESOURCES
SPACE SCIENCE AND [illegible] APPLICATIONS

219 Electrical Engineering West
The Pennsylvania State University
University Park, Pennsylvania 16802

Principal Investigators:

January 1976

Prepared for NASA
LYNDON B. JOHNSON
Houston, Texas

1. Report No.	2. Government Accession No.	3. Recipient's Catalog No.
ORSER-SSEL TR 2-76		

4. Title and Subtitle	5. Report Date
INTERDISCIPLINARY APPLICATIONS AND INTERPRETATIONS OF EREP DATA WITHIN THE SUSQUEHANNA RIVER BASIN	January 1976
	6. Performing Organization Code

7. Author(s)	8. Performing Organization Report No.
Principal Investigators: G. J. McMurtry and G. W. Petersen	

9. Performing Organization Name and Address	10. Work Unit No.
Office for Remote Sensing of Earth Resources 219 Electrical Engineering West Building University Park, Pa. 16802	
	11. Contract or Grant No. NAS9-13406
	13. Type of Report and Period Covered

12. Sponsoring Agency Name and Address	Final Report 1 May 1973-30 Nov. 1975
NASA/Lyndon B. Johnson Space Center Houston, Texas 77058 Technical Monitor: Martin Miller	14. Sponsoring Agency Code

15. Supplementary Notes	
Original photography may be purchased from: EROS Data Center 10th and Dakota Avenue Sioux Falls, SD 57198	ORIGINAL CONTAINS COLOR ILLUSTRATIONS

16. ABSTRACT This report describes an interdisciplinary effort to analyze Skylab/EREP data for test sites in Pennsylvania. The research findings are presented for two major subject areas: 1) photographic analysis for geomorphic and geologic applications, and 2) evaluation of S192 multispectral scanner digital data. Photography from the S190A and S190B sensors were compared, with the result that the S190B color positive film was selected as the best in overall quality for terrain analysis. S190B photographs were then used for terrain mapping of three test areas selected as being representative of major physiographic regions in Pennsylvania. Skylab photography was superior to both Landsat imagery and high altitude aircraft photography for purposes of accurate location of lineaments. Analysis of Skylab photography has shown that long lineaments originally plotted on Landsat images are actually made up of shorter segments. As a result of a comparison between Skylab and Landsat-1 lineaments, lineament sampling bias on both types of data was shown. Correlation of lineaments with ore deposits was determined following the preparation of a Pennsylvania mineral deposit map. Lineaments were also related to groundwater well yields in the carbonate areas of Pennsylvania. A zone of lineation determined on Skylab photography was used in a study to investigate the origin and extent of a thermal anomaly in central Pennsylvania. Digital wavenumber analysis (spatial filtering) was attempted to determine if it can be used to enhance certain subtle features and, in particular, to locate and verify lineaments. The various spectral bands and channels of the S192 (MSS) digital data were evaluated for their value (information content and redundancy) in the classification and thematic mapping. Following mapping and classification, three methods (correlation, principal components, and canonical analysis) were used to evaluate the spectral channels. The most important channels in defining both total information content and discriminatory variance cover the long visible through short IR wavelengths (0.68-1.75 μ) and the long reflected IR band (2.10-2.35 μ). The band contributing the least information is the thermal IR (10.20-12.50 μ).

17. Key Words (Selected by Author(s))	18. Distribution Statement
Interdisciplinary, geology, photography, digital MSS, channel evaluation, lineaments, minerals, groundwater, principal components, and canonical analysis	

19. Security Classif. (of this report)	20. Security Classif. (of this page)	21. No. of Pages	22. Price*
Unclassified	Unclassified	253	

PREFACE

This report presents a review of the efforts of the Office for Remote Sensing of Earth Resources (ORSER) of the Space Science and Engineering Laboratory (SSEL) at The Pennsylvania State University in analyzing Skylab EREP data over the period 1 May 1973 through 30 November 1975. This has been an interdisciplinary effort involving seven faculty members and several graduate students from five departments in three colleges of the University. The geographical area of interest has been the State of Pennsylvania.

Objectives and Scope

The scope and general objectives of this project, as defined in Contract NAS 9-13406, included the:

1) determination of the content of geological information in S190A and S190B photography, and S192 imagery, and comparison of these to Landsat-1 imagery and high and low altitude aerial photography;

2) processing of S192 digital data and comparison of the classification results with those from Landsat-1 data;

3) evaluation of the use of spacecraft remote sensing data for geologic interpretation and for predicting potentially favorable areas for mineral exploration; and

4) evaluation of the potential extension of analysis techniques developed and used on this project to wide areas of the United States or of the world.

The specific objectives to be met under this contract were to:

1) compile an inventory of known mineral deposits and geological structures in the Susquehanna River Basin;

2) correlate Skylab/EREP data with Landsat data and verify Landsat-identified lineaments in Pennsylvania;

3) correlate lineaments identified on Skylab and Landsat imagery with known mineral deposits;

4) correlate Skylab/EREP data with known geothermal "hot-spots" in central and eastern Pennsylvania;

5) perform analyses on the digital MSS data and select the most useful spectral channels for classification purposes;

6) apply spatial filtering to digital MSS data as a means of enhancing geologic and other features;

7) evaluate and compare the photographic data from the S190A and S190B sensors; and

8) evaluate the effectiveness of terrain mapping from the best of the photographic formats (determined in objective 7).

Conclusions

The significant findings and conclusions based upon the analysis of Skylab data are:

1. The S190B color positive photography was clearly superior, for interpretive purposes, to any of the S190A photography. Within the S190A films, the panchromatic black and white is generally superior to the infrared black and white, although water feature definition and that of water and wind gaps are distinctly clearer on the infrared film. The visible color film of the S190A is superior to the color infrared film.

2. Photoanalysis techniques applied to Skylab S190B photography can yield a regional map of considerable value. Landforms with minimum relief differences of 150-240 m can be mapped relatively consistently, and lesser relief differences can be discerned in some instances, with the assistance of shadows and vegetation differences.

3. Drainage pattern mapping is a major key to successful identification of many features. The consistency with which three operators have identified features in three different geographic areas indicates that generalized regional mapping using S190B photography is feasible for areas for which little or no ground truth is available.

4. Skylab S190B photography was shown to be a very effective form of ground truth data when digitally processing Landsat MSS data. Its quality and resolution are excellent for this purpose. It is useful to a lesser degree as ground truth support for processing Skylab MSS data. Aircraft underflight photography with better resolution is more suitable as ground truth in this latter case.

5. Skylab photography is superior to both Landsat imagery and high altitude (U2 or RB57) aircraft photography for purposes of accurate location of lineaments initially detected on Landsat imagery.

6. A comparison of lineaments plotted on Skylab scenes with those plotted on Landsat images has revealed that the Landsat plots suffer from a significant bias by illumination and scan line directions.

7. Analysis of Skylab photography has shown that lineaments originally plotted on Landsat images are actually made up of several shorter segments. These segments may differ in orientation by several degrees from the mean orientation of the long lineament originally plotted from the Landsat data.

8. Groundwater studies have shown that intersections of lineaments and fracture traces should be used to obtain maximum well yields. The large number and wide distribution of lineaments and fracture traces in all terrains means that almost any community can exploit these features to increase their water supplies, avoiding the need for costly long distance pipe lines and reservoirs. Formations known to be very poor aquifers have been shown to yield large volumes of water from fractured zones.

9. Based upon relations observed between the mineral deposit map prepared for Pennsylvania and structural features identified from Skylab and Landsat scenes, there appears to be an indication that lineaments provide clues to possible controls of metallic mineralization in Pennsylvania. The Tyrone-Mount Union lineament complex and the Perkiomen Creek lineament are the most strongly associated with mineralization in Pennsylvania. Several other unnamed lineaments were geographically associated with 3 - 5 mineral occurrences each.

10. As a result of studying the wavenumber spectrum of the individual Skylab channels, it is concluded that each channel provides unique wavenumber information about a particular scene. The peaks and troughs produced in the wavenumber domain by a scene are shaped differently in different channels, and the separations of the intensities of peaks and troughs vary for different channels. The most detailed wavenumber spectrum is produced by the thermal IR which has greater intensities in the higher wavenumbers than in the other channels. The channels in the IR and near IR show a relatively distinct wavenumber signature for the dominant periodic feature in the scene. The channels in the visible range have a flatter wavenumber response, and the wavenumber signature associated with the dominant feature is not as sharp and as well defined as in the IR channels.

11. Channels which were duplicates in the bandwidth of their spectral response appear to contain approximately duplicate information and discriminatory power as applied to the types of ground targets being classified by ORSER. Therefore, the choice of the best sensor in each band should be determined by other factors, such as cost, design, and reliability.

12. The most important channels in defining both total information content and discriminatory variance cover the long visible through short IR wavelengths (0.68-1.75 μ) and the long reflected IR band from 2.10-2.35 μ; and, finally, the least important band is the thermal IR band (10.20-12.50 μ).

13. The relatively low information content in the thermal IR channels is somewhat surprising, but it is believed that such channels should not be considered useless in land use classification applications. After canonical transformation, three axes in the transformed data were found to be useful for classification. The third of these axes, although it contained the least discriminatory information (smallest variance), was still significant and the thermal IR content in this axis was relatively high. One possible explanation for the overall low rating of the thermal IR channels may be that their discriminatory power is relatively low in the daytime, since the energy measured is both reflected and radiated

(as opposed to night sensing of radiated energy alone). Thermal IR measurements are more sensitive to time of day, atmospheric disturbances, etc., and calibration is very critical.

14. Skylab MSS data have greater resolution than Landsat data and this makes land use mapping somewhat easier in some cases. Simultaneously, however, the system features which result in greater resolution, along with the many spectral channels of Skylab, generate a much greater data volume to be handled and processed. This results in increased costs and time for processing. Overall, the quality of Skylab MSS data is quite good.

15. As a result of the application of principal components and canonical analysis to the MSS data, it was determined that a considerable reduction in data volume can be achieved by use of such transformations followed by feature selection (dimension reduction) based on information content of the transformed axes. The resulting savings in time and cost are substantial. In addition, the transformed data is ideally suited for use with color display devices.

It should be noted that the above results from this study of the S192 digital data are for the general mix of land use patterns existing in the growing season for an area representative of western Pennsylvania. It would be conjectural to extrapolate the results to other substantially different climatic areas, such as semi-arid ones, or to another very different season of the year, such as winter. Although the methodology would be expected to be as satisfactory in channel evaluation under other conditions, the specific results might very well be quite different.

Summary of Recommendations

As a result of the analysis of Skylab data, the following recommendations are submitted:

1. The S190B color positive photography should be used for all terrain analysis studies involving Skylab photography, and studies of this nature should utilize an instrument such as the Bausch and Lomb Zoom 95R stereoscope mounted on an X-Y stage.

2. A "foreign" area - one for which there is little or no ground truth available and one with which the photointerpreter is unfamiliar - should be studied using Skylab S190B photography in an attempt to define the landforms, nature of the bedrock, structural features, nature of the soil cover, and relative depth to the groundwater table. After such a study, the ground truth should be established and the percentage of the area correctly mapped should be determined.

3. Skylab photography, or imagery at that scale and resolution, should be obtained on a seasonal basis and over major geographical areas for continued lineaments work. Repetitive Skylab coverage is lacking for most areas, and some areas are not covered at all. Stereo coverage

4. Investigation should be continued into the effects of operator, scan line, and illumination bias on Skylab and Landsat photography and imagery. Multiple operators should be used to increase the probability of detecting more subtle lineaments.

5. There should be an investigation to determine from ground-based observations the nature of the structural features which underlie lineaments and to determine the nature and tectonic significance of well known major lineaments to establish their relationship to less prominent surrounding lineaments.

6. An accurate lineament map of the Commonwealth of Pennsylvania should be prepared using Skylab-type data and evaluated for its use in groundwater and mineral prospecting, siting of proposed construction, and pollution controls.

7. It is recommended that thermal infrared channels be included on future geological remote sensing missions since the Skylab thermal channel consistently produced a wavenumber spectrum with contributions in all wavenumbers, with a greater intensity in the higher wavenumbers than in the other channels. Since periodic ground features, such as folds and multiple lineaments, are of interest geologically, channels containing a great amount of wavenumber character would be desirable for geological studies.

8. To realize the full potential of wavenumber analysis in remote sensing and geologic applications, computer programs must be developed which are capable of operating on large data blocks representing ground areas of the order of 1 to 4 x 10^4 km^2. Basically, the area considered must be large enough to contain the salient shape characteristics of the feature(s) of interest.

9. Future earth resources missions should use fewer spectral bands (and channels) and provide more areal coverage. Six bands (e.g., 0.5-0.7 μ, 0.7-0.9 μ, 0.9-1.1 μ, 1.1-1.3 μ, 2.10-2.35 μ, and 10.20-12.50 μ) would appear to be adequate.

10. The techniques used for channel evaluation in this investigation (correlation, principal components, and canonical analysis) should be applied to S192 data over other geographical areas and for other types of targets.

11. There is a need for a more extensive investigation of the value of daytime thermal IR data for land use mapping using digital MSS data. Consideration should be given to calibration, types of target, time of day, etc.

12. Canonical analysis should be applied to digital S192 data and the results displayed on color display devices for evaluation by photo-interpreters.

ACKNOWLEDGMENTS

The work reported herein was primarily supported by the National Aeronautics and Space Administration, Goddard Space Flight Center, under Contract NAS 9-13406. In addition to the Skylab data supplied, the aircraft data acquired by NASA personnel were invaluable to the success of our research activities. Special appreciation is expressed to James Lindeman and James Weber of NASA-Houston for coordinating the RB57 and C130 missions, and to Larry Keyser of NASA-Houston for processing the multispectral scanner data. The efforts of Martin Miller and Victor Mazade for providing liaison as Technical Monitors of this project are also appreciated.

Supplementary support was provided by the Space Science and Engineering Laboratory at The Pennsylvania State University. In addition, the contribution of significant amounts of unfunded computer time by the University is gratefully acknowledged.

Five Penn State faculty members conducted and supervised the major research work described in the various sections of this report. These were:

Dr. Shelton S. Alexander, Professor of Geophysics
Dr. F. Yates Borden, Associate Professor of Forestry
Dr. David P. Gold, Professor of Geology
Dr. Richard R. Parizek, Professor of Geology
Dr. Harmer A. Weeden, Professor of Civil Engineering

In addition to faculty personnel, 12 graduate students and one undergraduate were involved in various phases of the investigations. These are listed below, with the degrees on which they were working:

Civil Engineering

S. G. Daelhausen, Ph.D.
G. M. Hesler, B.S.
C. L. Kleeman, M.S.

Electrical Engineering

W. A. Chren, M.S.
E. G. Crenshaw, Ph.D.

Forest Resources

D. M. Barr, M.S.
B. F. Merembeck, Ph.D.

Geophysics

D. R. Baumgardt, Ph.D.
C. W. Nichols, M.S.
B. L. Weinman, M.S.

Geosciences

M. R. Canich, M.S.
R. G. Craig, Ph.D.
W. S. Kowalik, M.S.

The persons involved in the various aspects of the research described herein are identified by name in parentheses after the title of the sections in which their work is described.

In addition to the above persons, a special note of appreciation is given to Ms. Danielle N. Applegate for her services as computer programmer and to Ms. Nanna B. Bolling, as image analyst and for compilation, editing, and production of this report.

CONTENTS

CONTENTS (continued)

CONTENTS (continued)

LIST OF TABLES

LIST OF FIGURES

LIST OF FIGURES (continued)

LIST OF FIGURES (continued)

1.0 INTRODUCTION

The Office for Remote Sensing of Earth Resources (ORSER), operating as a division of the Space Science and Engineering Laboratory at The Pennsylvania State University, is an interdisciplinary group established in 1970 for the purpose of participating in projects involving the use of remotely-sensed data of earth resources. Investigators involved in ORSER research projects have been from the fields of agronomy, civil engineering, computer science, electrical engineering, forestry, geology, geophysics, hydrology, plant pathology, pattern recognition, regional planning, and soils. A problems-oriented, rather than a discipline-oriented approach is taken in the completion of tasks, in order that associates from various disciplines may work together toward a common goal.

ORSER has directed most of its efforts toward processing, analysis, and interpretation of multispectral remotely-sensed data, most of which have been supplied by NASA in both imagery and digital format. Photointerpretation has been a vital part of the overall analytical process, but the emphasis has been on the use of digital computer algorithms for data processing. The end product of most projects is typically a computer map showing various environmental and land use characteristics of data points in the analyzed scenes.

Data processing facilities include unlimited access (via the remote job entry system) to the IBM 370/168 computer, housed and operated by the Penn State Computation Center. The source language is FORTRAN IV. Computation cost efficiency has been emphasized throughout, as ORSER personnel have developed algorithms for pattern recognition, analysis of statistical information, etc. A well-equipped photointerpretation laboratory includes Bausch and Lomb Zoom 70 and 95R stereoscopic systems and a Bausch and Lomb Zoom Transferscope.

Work on NASA Contract NAS 9-13406 has been concerned with Skylab EREP data, both in photographic and digital form, obtained from the Skylab 3 and 4 missions over Pennsylvania. The general and specific objectives of this work are described in the preface to this report, along with the conclusions and summary of recommendations.

2.0 DATA

The Skylab and aircraft data provided by NASA to support this study are described below.

2.1 SKYLAB DATA

2.1.1 Photographic Data (S190A and B)

Two camera systems, the S190A and the S190B, provided the photographic transparencies studied in this investigation. Table 2-1 lists the major characteristics of these two systems. The S190A, a multispectral photographic system, consisted of a bank of camera stations which simultaneously recorded six frames within specified bandwidths of the photographic spectrum. Two infrared black and white, two panchromatic black and white, one infrared color, and one high resolution visible color photograph were simultaneously exposed for each scene. The S190B camera recorded a single visible color or black and white frame for each field of view. A summary of the camera and film package characteristics appears in Table 2-2 and descriptions of the individual films can be found in Table 2-3. Photographic data from the two camera systems were received for all Skylab orbits shown on Figure 2-1. The missions, orbits, and data types collected are summarized below:

Mission	Orbit	Data Collected
SL 3	14	S190A, S190B, S192
	30	S190B
	44	S190A, S190B
	52	S190A, S190B, S192
SL 4	73	S190A, S190B

Table 2-1: Skylab Camera Characteristics

S190A:	Six multispectral cameras F/2.8 lenses with 15.25 cm focal length 163 x 163 km field of view Original film size - 70 x 70 mm, with 6.4 x 6.4 cm format Original scale - 1:3,000,000 Scale of 4X enlargements - 1:690,000
S190B:	Earth terrain camera f/4 lens with 45.7 cm focal length 111 x 111 km field of view Original film size - 12.7 x 12.7 cm, with 11.4 x 11.4 cm format Original scale - 1:920,000 Scale of 2X enlargements - 1:500,000

Table 2-2: Film/Filter Characteristics of Skylab Photographic Data

Sensor	Camera Station	ORIGINAL FILM					DUPLICATING FILM		
		Film Type	Bandwidth with Filter (μ)	Approximate Color Range	Resolution[a] (ℓ/mm)	(meters)	Film Type	Resolution[a] (ℓ/mm)	(meters)
S190A	1	IR Aerographic B&W EK-2424	0.7-0.8	Red to near IR	32-100	388-124	Blue-sensitive Aerial Duplicating EK-2420	80-125	155-99
	2	IR Aerographic B&W EK-2424	0.8-0.9	Near IR	32-100	388-124	Blue-sensitive Aerial Duplicating EK-2420	80-125	155-99
	3	Aerochrome IR Color EK-2443	0.5-0.88	Green to near IR	32-63	388-197	Low contrast color reversal duplicating SO-360	63-125	197-99
	4	Aerial Color SO-356	0.4-0.7	Blue to red	100-200	124-62	Low contrast color reversal duplicating SO-360	63-125	197-99
	5	Pan-X Aerial B&W SO-022	0.6-0.7	Orange to red	80-200	155-62	Blue-sensitive Aerial Duplicating EK-2430	160-320	78-39
	6	Pan-X Aerial B&W SO-022	0.5-0.6	Green	80-200	155-62	Blue-sensitive Aerial Duplicating EK-2430	160-320	78-39
S190B		Aerial Color SO-242	0.4-0.7	Blue to red	100-200	41-20	Low contrast color reversal duplicating SO-360	63-125	133-66
		High Resolution Pan B&W EK-3414	0.5-0.7	Green to red	250-630	33-7	Blue-sensitive Aerial duplicating EK-2430	160-320	26-13

[a]No attempt has been made to compute the ground resolution of the final photographic product, because the influences of the camera lenses and filters, and of the enlarging lens, are unknown.

REPRODUCIBILITY OF THE ORIGINAL PAGE IS POOR

Table 2-3: Skylab Film Characteristics

S190A Films

Kodak Infrared Aerographic Black and White, EK-2424

-Sensitive from ultraviolet to infrared (0.9μ)
-Maximum sensitivity from 0.76 to 0.88μ
-Suited well for haze effects

Kodak Aerochrome Infrared Color, EK-2443

-A "false color" film for infrared discrimination
-False color films differ from conventional films in that three layers are sensitized to green, red, and infrared radiation rather than to blue, green, and red.
-When used with yellow filter, as in the S190A:
Green appears Blue
Red appears Green
IR appears Red

Kodak Aerial Color, SO-356

-A Kodak special order color reversal film
-High resolution
-High contrast
-Good color separation

Kodak Panchromatic-X Aerial Black and White, SO-022

-Panchromatic negative film
-Intermediate speed
-High contrast
-Extended red sensitivity

S190B Film

Kodak Aerial Color, SO-242 (High Definition)

-A daylight balanced color reversal film
-High contrast
-Good color saturation characteristics
-Extremely fine grain
-High resolving power and definition

(continued)

Table 2-3 (continued)

S190B Film (Continued)

Kodak High Definition Aerial Black and White, EK-3414

-Panchromatic negative film
-Slow speed
-Extremely fine grain
-High definition
-Extended red sensitivity

Duplicating Films

Kodak Duplicating Film, EK-2420

-Blue sensitive aerial duplicating film
-Fine grain
-High dimensional stability
-Intended for use both as the intermediate positive and for the final negative

Kodak Duplicating Film, EK-2430

-Blue sensitive, aerial duplicating film
-Extremely fine grain
-Extremely good dimensional stability
-Designed for duplicating high-definition aerial negatives

Kodak Duplicating Film, SO-360

-Low-contrast color reversal duplicating film
-Extremely fine grain
-High resolution
-Dimensionally stable
-Designed for duplicating Kodak Ektachrome and Aerochrome film originals from aerial surveying and reconnaissance photography

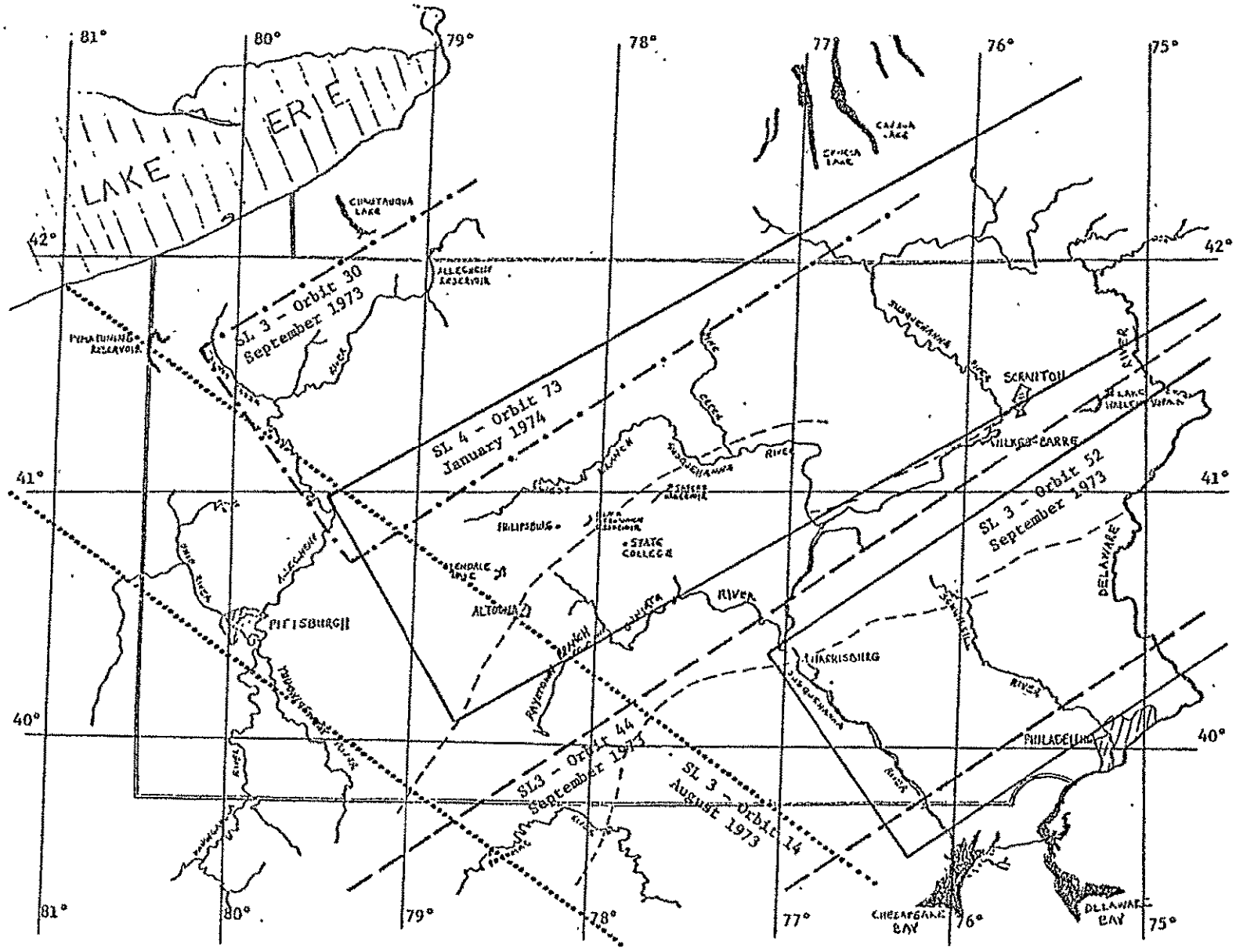

Figure 2-1: Skylab orbits from which ORSER received data from NASA.

2.1.2 Multispectral Scanner Data (S192)

The S192 multispectral scanner (MSS) had a conical scan of 360° of which the forward 110° provided the data, covering 68.5 km on the ground. The 22 channels of data collected covered 13 discrete bands of the electromagnetic spectrum. These data were processed to produce computer compatible tapes in both the original conical-scan form and in line-straightened form. Preview film of three channels of imagery was provided for all the MSS data available over Pennsylvania. This film was used as a basis for ordering data tapes and single-band black and white imagery for selected areas. (A more detailed description of the S192 scanner and data is provided in sections 5.3 and 5.4, in which the channels and data are evaluated.)

S192 data were available over Pennsylvania for SL3 orbits 14 and 52. Evaluating the quality of the data available from the preview film provided, ORSER ordered S192 digital and image data from three areas covered by orbit 14 (see Figure 2-2). These data were received as follows:

Data Form	Scan Type	Channels
Digital Tape	Conical	1-22
Digital Tape	Straight	1-22
Imagery	Conical	1,3,5,7,9,11,13,17-22

2.2 AIRCRAFT UNDERFLIGHT DATA

Two types of aircraft data were flown for ORSER as sources of "ground truth" for this project. The RB57 aircraft flew at an approximate altitude of 18,300 m (60,000 ft), collecting color and black and white photographic data in both the visible and near IR portions of the spectrum. The C130 aircraft flew within an altitude range of 1520 to 4500 m (5000 to 15,000 ft), collecting color and black and white photographic data in both the visible and near IR portions of the spectrum, as well as multispectral scanner (MSS) digital data. Photographs and MSS imagery were supplied to ORSER on 25 cm (9 in.) reels. MSS digital data for selected portions of C130 Missions 238 and 247 were supplied on computer compatible tapes. The aircraft support mission dates and approximate lengths of flight are shown below. The flight lines are shown on Figure 2-3 (RB57) and 2-4 (C130).

Aircraft	Mission	Dates	Approximate Kilometers Flown
RB 57	248	29 Aug 1973	877
C130	238	15 Jun 1973	153
	247	6 Aug 1973	386
	258-A	12 Dec 1973	257
	258-B	12 Feb 1974	829

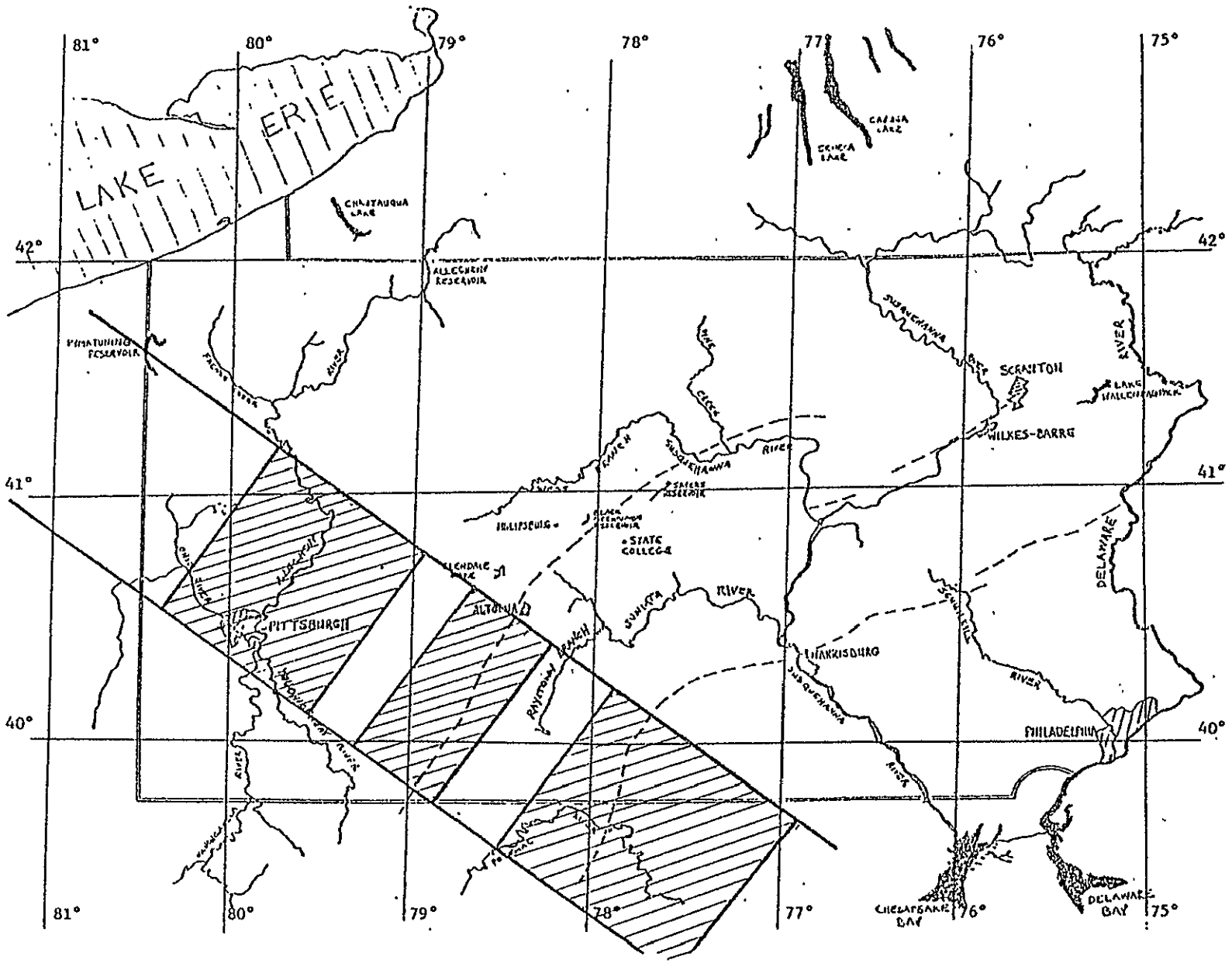

Figure 2-2: Areas (shaded) for which Skylab S192 digital data and imagery were received by ORSER. (SL3, orbit 14, 5 Aug 1973.)

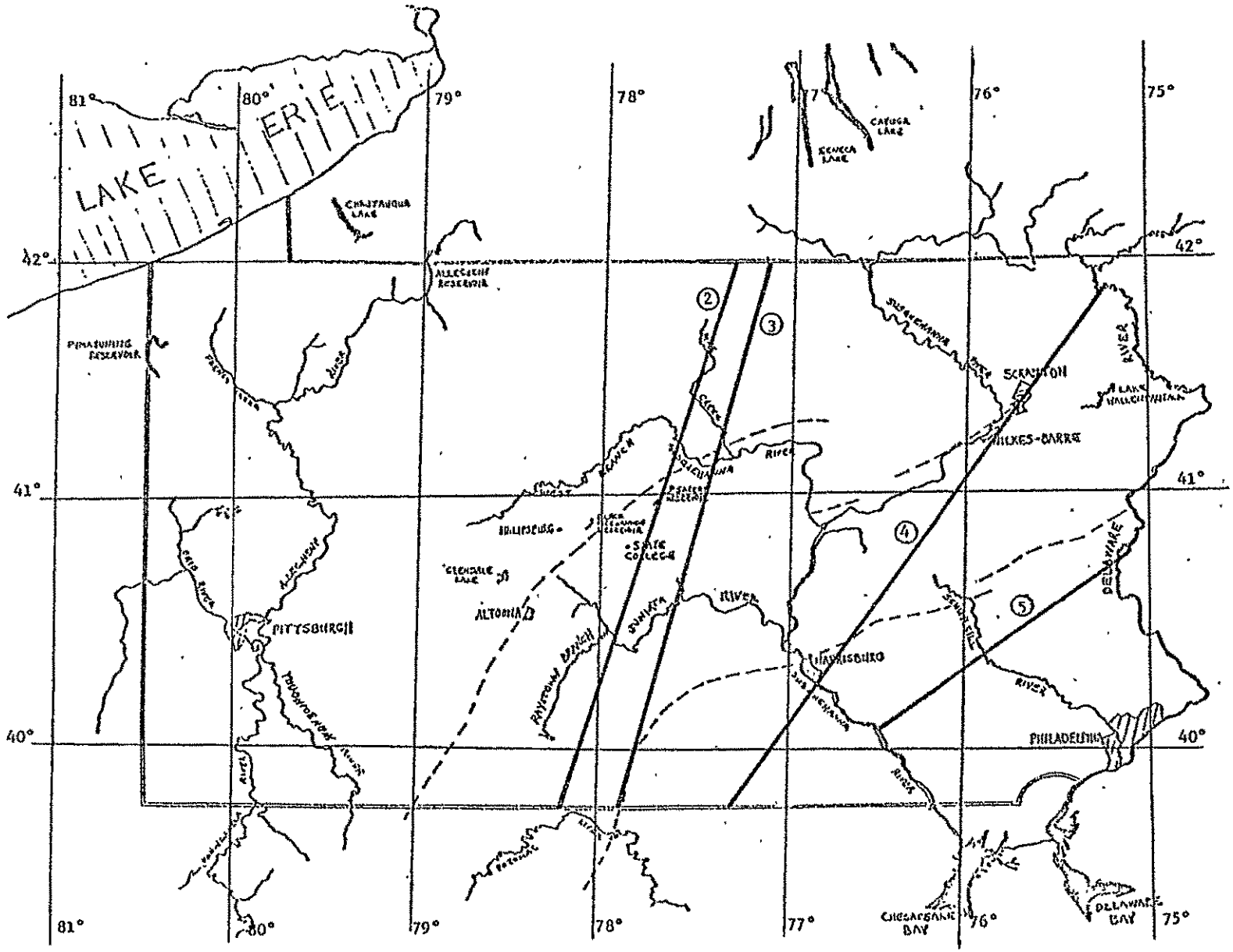

Figure 2-3: The four RB57 flight lines from which ORSER received data. (Mission 248, 29 Aug 1973.)

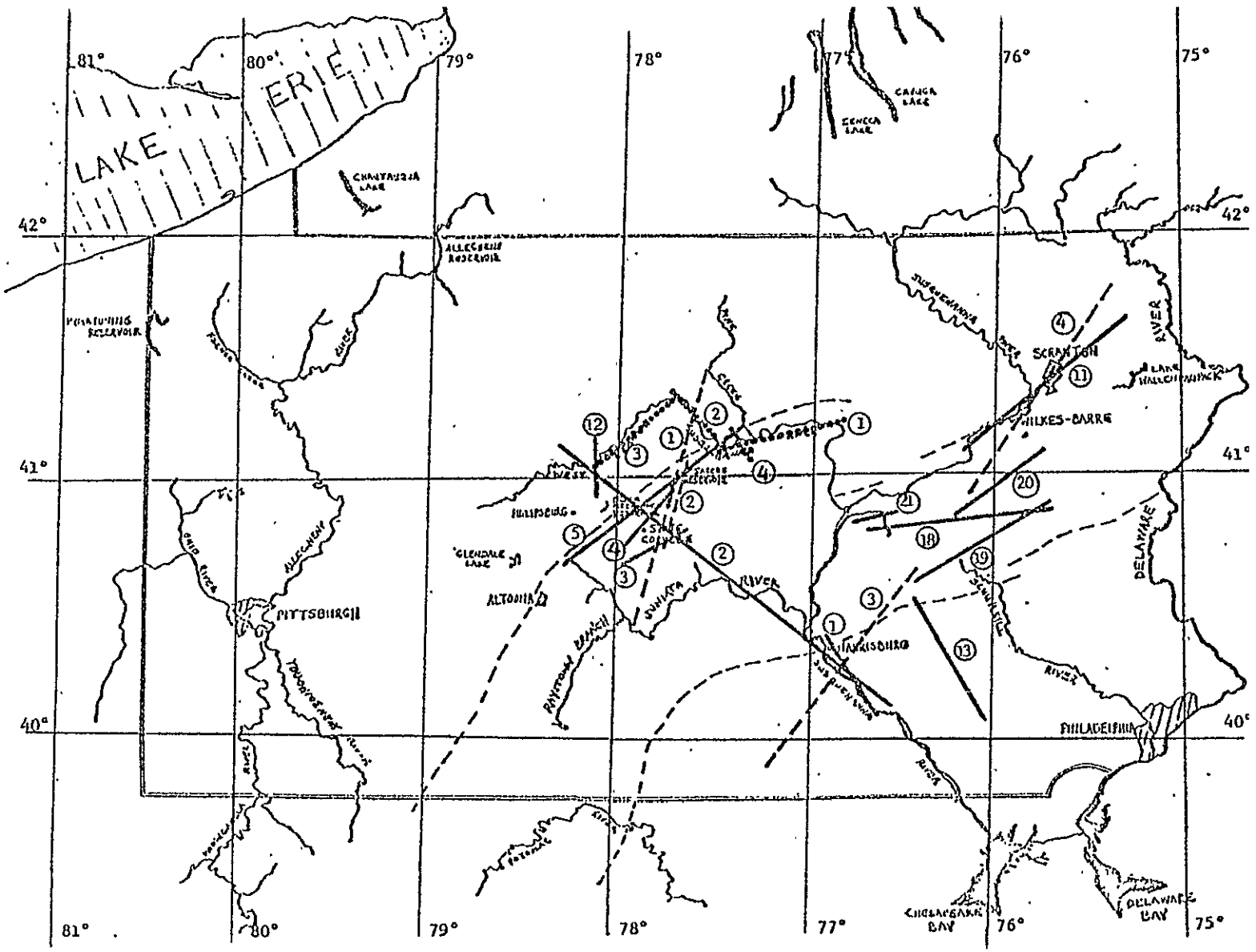

Figure 2-4: C130 flight lines from which ORSER received data.

. . . . Mission 238 - - - - Mission 247 ———— Mission 258

3.0 PHOTOGRAPHIC APPLICATIONS ANALYSIS

Before commencing application of Skylab photography in detailed geologic studies, it was decided that Skylab photography should be evaluated for its general interpretive potential, especially in terrain mapping applications. A comparison should be made for test sites selected as being representative of major physiographic regions in Pennsylvania. Standard techniques used for aerial photointerpretation were to be applied during the evaluation. The basis for the evaluation was to be an analysis and comparison of the various Skylab sensor/film/filter combinations available, utilizing study guides prepared from ground truth information for each test site.

After this analysis and comparison was completed, terrain mapping could be performed using the optimum Skylab sensor/film/filter combinations for each test site. Selected scenes should be analyzed then for the amount of detailed information contained in the Skylab photography. This analysis should be performed both with and without the aid of aircraft underflight photography as ground truth.

Finally, it was felt that Skylab photography could be a useful form of ground truth which would be helpful in digital analysis of Landsat MSS data. A study was conducted to evaluate this potential application of Skylab photography.

3.1 SENSOR AND FILM/FILTER ANALYSIS (Weeden, Kleeman, Daelhausen, Hesler)

The initial study of Skylab data was undertaken to determine the limits of refinement within which landscape units could be identified from Skylab photography. The term "landscape unit" is intended to define a portion of terrain which is separable from adjacent units on the basis of a difference in soil character or underlying bedrock conditions. The term landscape unit is in many ways identical with the term "land form", as defined in texts on geomorphology. Landscape units are recognized on air photos by their unique relief features, related drainage and erosion characteristics, vegetative cover, cultural development, and color or tonal patterns. Historically, civil engineers, landscape architects, and others have defined these units on aerial photographs at scales varying from 1:10,000 to 1:60,000. With the present availability of Skylab photography, it is most important that studies be conducted to assess the ways in which these scenes, covering larger areas per frame, can contribute to terrain analysis.

The area of interest was the Susquehanna River Basin within the State of Pennsylvania, for which ORSER had received various photographic forms of data from the S190A and S190B sensors collected on the third (SL3) and fourth (SL4) missions. The Susquehanna River Basin is located in the central portion of Pennsylvania, bounded approximately by longitude 75° 45'W and 78° 30'W. As seen on Figure 2-1, nearly complete Skylab coverage of this area was available from the combined data sources of SL3 and SL4. Orbit 44 of SL3 and orbit 73 of SL4 provided the best coverage and are the only orbits referred to in the remainder of this section. Unfortunately, seasonal variability of the data sources limited the degree of comparison possible between SL3 and SL4 photography; however, it permitted assessment of seasonal advantages or disadvantages. NASA U2 and C130 seasonal aircraft underflight photography was available for limited regions covered by the Skylab photography.

Within the coverage limits of SL3 and SL4, three specific test sites were selected to evaluate the interpretive potential of the Skylab photography (Figure 3-1). These sites, well documented in the available literature, are representative of several Pennsylvania physiographic regions. They are located in central and south-central Pennsylvania and are identified herein by the local prominent cultural feature of the area. The sites are centered around Sayers Dam in Clinton County; the Harrisburg area in Dauphin, Perry, York, and Cumberland Counties; and the Reading area in Berks County. These study areas satisfied the specific requirements of 1) a variety of landscape units of different magnitude, 2) several types of drainage systems, 3) various soil and bedrock units, 4) a variety of land uses for which ground truth was available, and 5) two seasonal coverages (for one of the areas only).

Study guides, consisting of ground-truth information on each area, were prepared from the literature. The Skylab photography and corresponding aircraft underflight photography were analyzed using techniques for aerial photography interpretation developed for civil engineering purposes. These techniques are described in detail in ORSER-SSEL Technical Report 17-75.

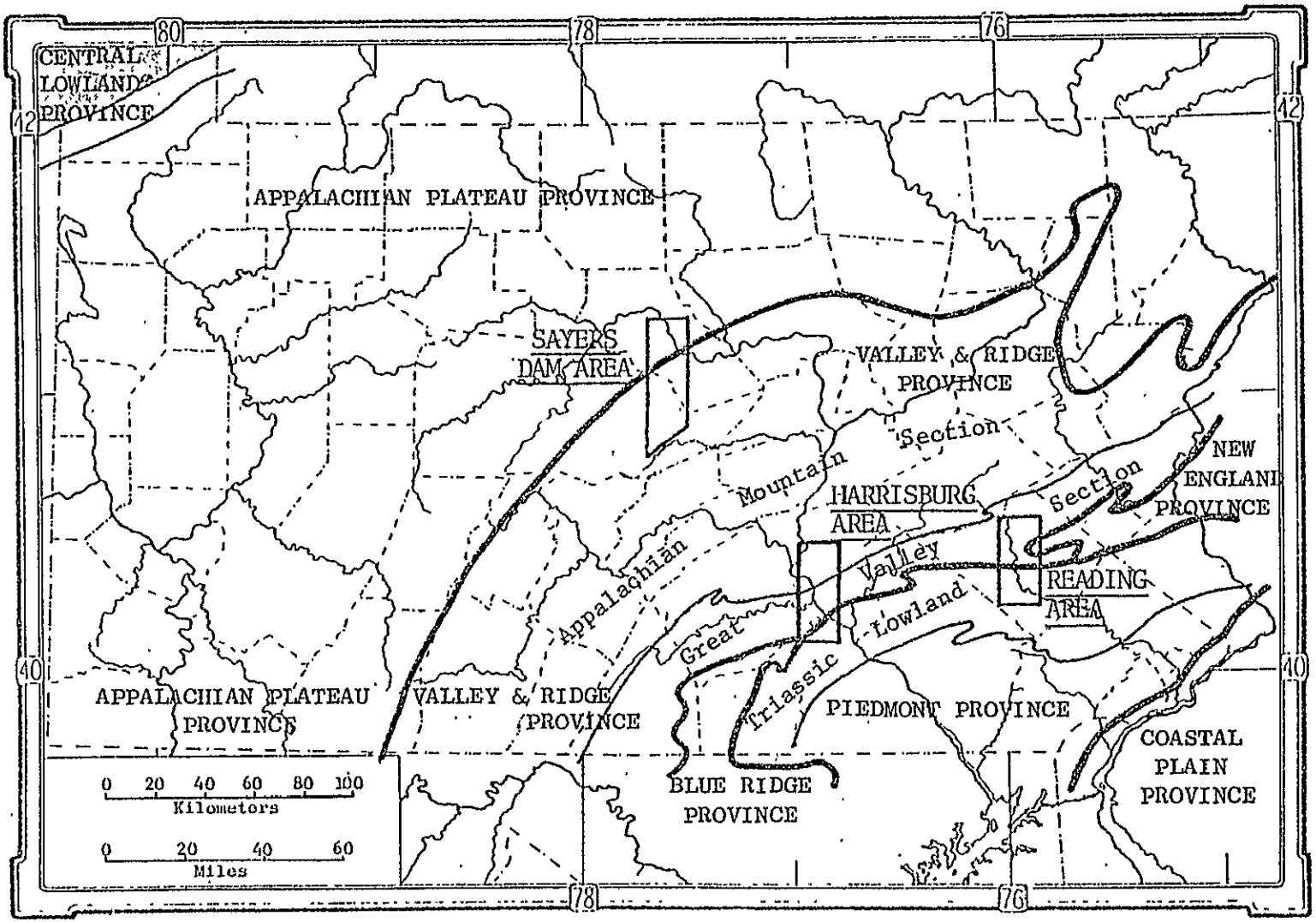

Figure 3-1: Physiographic sketch map of Pennsylvania, showing the three test sites.

Initially, all the photographic forms available in the ORSER laboratories for the study areas were reviewed. Selected scenes from these were then compared, in order to determine in more detail the sensor/filter combination best suited for photointerpretive analysis.

3.1.1 Procedures

The S190A and S190B camera systems provided the photographic transparencies studied in this investigation. The evaluation was performed by two graduate students and one undergraduate senior in Civil Engineering, under the supervision of a professor in that department. The analysts performed their first look using black and white film on a light table with the Old Delft Scanning Stereoscope at magnifications of 1.5 and 4.5X. This was the observing tool to which they could best adapt for obtaining a stereoscopic model.

It became apparent quite early that the interpretation of Skylab photography would be heavily dependent upon detailed drainage delineation. This was attempted using: 1) a high quality overhead projector, 2) a Bausch and Lomb Zoom Transferscope (ZTS), and 3) the Old Delft scanning stereoscope. After some initial trials, the method adopted was a combination of methods 2 and 3; that is, mapping using the ZTS with verification from the stereo model of the Old Delft. Although a Bausch and Lomb Zoom 95 stereoscope with image rotation was available, the students found it difficult to adjust because it was not mounted on an X-Y stage[1].

An effective method of analysis requires that the analyst should map slope breaks as well as drainage. Each interpreter established his own degree of accuracy in mapping these two features. A systematic approach was developed which centered around the use of a data form designed by the group. This form was filled out for each Skylab and aircraft scene studied. A sample of such a form appears as Figure 3-2.

The six S190A photographs and the one S190B photograph (plus adjacent frames for stereo viewing) were studied for each test site. A series of photo-elements was chosen for analysis (e.g., slope breaks, street patterns, railroad rights-of-way, etc.) and it was determined whether each of these was visible on a particular photograph. A data sheet, such as that shown in Figure 3-2, was compiled for each photograph, and the results of these individual photo-studies were later compiled. The area study guides and aircraft photography were used as source material, where necessary, to verify the identity of smaller features.

---

[1] ORSER has since acquired an X-Y mounting for the Zoom 95R, and it is now the preferred instrument for studies of this nature.

Mission	*SL-3*	Sensor:	*S190A*
Roll No.:	*48*	Film Type:	*SO-022 Pan-X B&W*
Frame No.:	*29,30,31*	Bandwidth, μ:	*0.5-0.6*
Orbit No.:	*44*	Filter Type:	*AA*
Location:	*Harrisburg*	Camera Station:	*6*
Date:	*9-16-73*	Transparency Size:	*9 x 9 [23 x 23 cm]*
		Original Size:	*70 mm*

General Quality: *Fair to Good; less contrast and detail than on Roll 47.*

Smallest Identifiable Units: *Highways, bridges, interchanges, islands in Susquehanna River, some individual farm fields.*

ANTICIPATED FEATURES	OBSERVED FEATURES & COMMENTS
1. *Major folding of Appalachian Ridges.*	1. *Sandstone ridges and slope breaks visible. Sandstone-to-shale slope breaks visible from vegetative change. Less contrast between woodlands and lowlands.*
2. *Major Drainage.*	2. *Tonal variations in Susquehanna River present. All other major creeks visible.*
3. *Minor Drainage.*	3. *Dendritic tributaries to Swatara, Paxton, and Conodoguinet Creeks present. All minor drainage less visible than on Roll 47.*
4. *Great Valley rolling hills topography.*	4. *Visible but much less so than Roll 47.*
5. *Mountains of Triassic Lowland.*	5. *Visible from their vegetative cover.*
6. *Great Valley carbonates.*	6. *Visible only from the absence of drainage.*
7. *Little Mountain water gaps.*	7. *Little Mountain water gaps not visible.*

Figure 3-2: Sample Skylab photoanalysis data sheet.

3.1.2 Results

The results of the comparison of the various Skylab film formats from the three test areas were closely similar in spite of the fact that each area was studied by a different interpreter. In Table 3-1, each of the seven sensor/film/filter combinations is related to a series of terrain-related features. In the discussion below, each of the formats is described[1].

S190A, Sta. 1, B&W IR (0.7-0.8μ): This photography appears at first to be of little value in terrain studies, as elements of fine detail, such as cultural and farm features, are not at all visible. On the other hand, this photography is excellent for the location of major streams, rivers, and reservoirs, which are usually difficult to spot amid the abundant vegetative, farm, and cultural features found on other Skylab photography. However, as this film appears to be sensitive to water surfaces, rather than vegetation, it is extremely difficult to locate first or second order drainage, such as small streams, creeks, and gullies, which are usually spotted by their accompanying vegetation. Braiding features in the Susquehanna River are prominent in this photography. Water gaps are visible. Limestone quarries appear as very dark spots and can be confirmed from underflight photography.

S190A, Sta. 2, B&W IR (0.8-0.9μ): This film package differs from that of station 1 only in the filter sensitivity. Its value for analyzing terrain features is basically the same as that described under station 1, although many of the terrain features used for comparison are slightly more visible. Water gaps can be seen most readily in this photography.

S190A, Sta. 3, Color IR (0.5-0.88μ): The largest contrast between wooded and cultivated land can be seen in this photography. Minor drainage (second order) can only be identified from accompanying vegetation. The resolution of this photography is poor, and the film is grainy. The presence of slight color variations and streaking in parts of the Great Valley may indicate carbonate material. Some very distinct variations in the color of the Susquehanna River over most of its length are seen. This was also seen, to a lesser extent, as tonal variations in the black and white photography. The sandstone ridges and Triassic igneous intrusions appear in sharp contrast to the lowlands and valleys, probably due to this film's sensitivity to vegetation. Quarries can be located, particularly after identifying them on underflight photography.

S190A, Sta. 4, Color Pos. (0.4-0.7μ): This photography may be the most useful of the S190A photographic packages. It is a fine grained film which exhibits very good detail. It is sensitive to farming practice and valley features, and highly sensitive to vegetation. This color positive photography is much sharper in detail than the IR color photography, particularly with respect to valley features and farmland detail. Color variations and streaking provide an indication of the

---

[1] These comments were prepared from the Harrisburg area scenes. Results from the other two scenes were closely similar.

Table 3-1: Evaluation of Skylab Sensor Systems

Feature	S190A Sta 1 B&W IR	S190A Sta 2 B&W IR	S190A Sta 3 Color IR	S190A Sta 4 Color Pos	S190A Sta 5 B&W Pan-X	S190A Sta 6 B&W Pan-X	S190B 1 sta Color Pos
Grain Texture	coarse	medium	medium	fine	fine	medium	fine
Drainage:							
2nd order	no	no	yes(nc)[a]	no	yes	no	yes
3rd order & up	yes	yes	yes	yes	yes	yes	yes
Geology:							
Sandstone ridges	yes	yes	yes	yes	yes	yes	yes
Triassic intrusions	no	no	yes	yes	yes	yes(nc)	yes
150-240 m relief	no	no	yes	yes	yes	no	yes
Strike & dip	no	no	yes	yes	yes	no	yes
Water gaps	yes	yes	yes(nc)	yes	no	no	yes
Slope breaks	no	no	no	no	no	no	no
Cultural Features:							
City street patterns	no	no	no	yes	yes	no	yes
Utility right-of-way	yes(nc)	yes(nc)	yes(nc)	yes	yes	yes(nc)	yes
RR right-of-way	no	no	no	yes	no	no	yes
Highways & bridges	no	no	yes(nc)	yes	yes	yes(nc)	yes
Airports	no	no	yes	yes	yes	yes	yes
Agricultural practices	yes(nc)	yes(nc)	yes	yes	yes	yes	yes
Quarrying - SL3	yes	yes	yes(nc)	yes	no	no	yes
SL4	no	no	yes	no	yes	yes	yes
Large industrial bldgs.	no	no	yes(nc)	yes	yes	yes(nc)	yes
Tonal Variations:							
Water turbidity[b]	no	no	yes	yes	yes	yes(nc)	yes
Forest vs. cleared land	no	no	yes	yes	yes	yes	yes
Soils	no	no	no	no	no	no	no

[a] nc = not clear

[b] None in Sayers Dam area

underlying material in the Great Valley as do quarries and drainage patterns, which indicate structural and/or stratigraphic control. Color variations in the Susquehanna River are easily seen. The Appalachian Mountain ridges and the Triassic igneous intrusions stand out sharply. Nothing present in this photography serves to identify distinct soil types or characteristics, although moisture content as a function of proximity to drainage is occasionally indicated.

S190A, Sta. 5, B&W Pan X (0.6-0.7μ): This photography is by far the best black and white coverage of the Skylab package. It is a very fine grained film, providing excellent detail. Both major and minor drainage are distinctly seen, including smaller streams and creeks, although first order drainage cannot be reliably identified. Valley streams and related features stand out well. The photography is sensitive to vegetation, farm, and cultural features. However, water gaps are not visible. The sensitivity of this film to minor drainage patterns lends much to the analysis of the underlying material. Unlike station 1 and station 2 photography, which showed the sandstone ridges of the Appalachian mountains but not the ridges and knobs of the Triassic igneous intrusions, this photography shows both features in fine detail. These features are enhanced both by relief and by forest vegetation. The detail of farm and cultural practices in this photography obscures tonal variations which might provide clues to the underlying soil or rock material.

S190A, Sta. 6, B&W Pan X (0.5-0.6μ): This photography was probably the most dissappointing of all the Skylab photography for the purposes of this study. Nearly every terrain feature compared was either less visible or of poorer quality in the station 6 photography than its counterpart in the station 5 photography. Only the contrast between wooded and cultivated land seemed to be somewhat better. (It is known that there was some degree of camera malfunction at station 6 prior to exposure.)

S190B, Color Pos. (0.5-0.9μ): A few minutes spent in examining Table 3-1 will lead one to the immediate conclusion that the S190B color photography is unquestionably the best of the seven film combinations considered. Its resolution is far better than any of the S190A photographic systems. The detail of valley features is excellent. Major and minor drainage patterns are clearly shown, down to second and sometimes first order drainage. Mountain ridges appear in sharp contrast to lowlands and valleys. There is excellent overall contrast and excellent color separation. Street patterns, buildings, warehouses, factories, and similar structures can be distinguished. A few quarries can be identified without the aid of underflight photography. The color variations in the Susquehanna River are also visible. Determinations of soil types at this scale, however, is still very unlikely.

For the sake of completeness, the high resolution panchromatic black and white EK-3414 photography from the S190B sensor should be mentioned. Although this coverage was not available for the selected study areas, frames 344 and 345 from roll 85 of orbit 30 data, which covered the Finger Lakes region in Heen Park State, were reviewed for

purposes of comparison. This film compares with the S190B color positive photographs in every respect, as viewed under the Old Delft Scanning Stereoscope at 4.5X. Interpretability, however, is not as good because of the lack of color. Judgments related to tracing drainage, identifying the absence of ground cover, and grouping vegetative cover, are less assured. The study of this black and white film positive included the use of the Bausch and Lomb Zoom 95R Stereoscopic viewing system, with the mount permitting "X-Y" scanning. At low magnification (2x), relief features on the order of 300 m were easily observed. At high magnification (10x), relief features on the order of 30 to 60 m were observed. The quality of the image was slightly degraded by graininess at the 10x magnification. However, the trade-off of graininess for better relief definition is considered acceptable.

3.1.3 Summary, Conclusions, and Recommendations

ORSER received S190A and S190B photography from several passes of Skylab-3 and one of Skylab-4. The Skylab-4 scenes were of limited usefulness, being largely snow and cloud covered. Photography in the 230 mm format is clearly superior to the 127 mm or 70 mm formats.

Skylab scenes from three different areas in Pennsylvania were viewed under the Old Delft scanning stereoscope in order to determine their usefulness in terrain analysis. Selected terrain elements seen on photography from the S190A and S190B sensors were systematically studied and the results compared. It was determined that the S190B color positive film was the best in overall quality for terrain analysis.

In terms of film grain texture and object definition of the duplicating film, the S190B color positive photography is distinctly superior to the S190A photography when both are compared in the 230 mm format. It is possible, however, that this is a function of the fact that the original S190B film is 127 mm, whereas the original S190A film is 70 mm. Thus, the S190B film has been magnified to a lesser extent than the S190A to obtain the same size transparency.

Within the S190A films, the panchromatic black and white is generally superior to the infrared black and white, although water feature definition and that of water gaps are distinctly clearer on the infrared film. The color positive film of the S190A is superior to the color infrared film. This may be a function of the fact that the three wavelengths registered by the emulsion of the color IR film are longer than those of the color positive film. As the photography is enlarged, the distortion brought about by this difference is accentuated. It should be noted that some inconsistency in performance between S190A camera stations 5 and 6 was detected.

The sensor/film/filter analysis revealed that the following features are visible on all of the photography: 1) major drainage, such as rivers and their tributary creeks and 2) the sandstone ridges of the Appalachian Ridge and Valley region.

The following features are visible on all photography with the exception of that from S190A stations 1 and 2 (0.7 to 0.8 and 0.8 to 0.9μ, respectively): 1) differences in vegetation (forest versus agricultural land), 2) color/tone variations in water bodies, 3) most cultural features, such as railroad rights-of-way, large industrial buildings, and roads (some with verification from underflight aircraft photography), and 4) hills formed by the Triassic igneous intrusions. Water bodies are most clearly visible on photography from stations 1 and 2 of the S190A photography, and on the S190B photography. Limestone quarries are visible on all photography but that of stations 5 and 6 (0.6-0.7 and 0.5-0.6μ) from the snow-free passes of Skylab-3. Slope breaks and soil differences are not clearly seen on any of the Pennsylvania scenes. Differences in relief of 150-240 m can be seen on all but stations 1, 2 and 6 photographs, using the Old Delft stereoscope. With the Bausch & Lomb Zoom 95R stereoscope, however, relief differences down to 30 m were seen on a black and white S190B scene from New York State.

It is recommended that: 1) future studies of this nature utilize an instrument such as the Bausch and Lomb Zoom 95R stereoscope mounted on an X-Y stage, and 2) the S190B color positive photography, when available, be used for all terrain analysis studies involving Skylab photography.

3.2 TERRAIN MAPPING FROM S190B PHOTOGRAPHY (Weeden, Kleeman, Daelhausen, Hesler)

After the initial analysis of the films available, each of the three students chose a scene from the S190B sensor, determined during the sensor and film/filter analysis to be the most promising film format, for evaluation of his test area. Standard techniques for aerial photo-interpretation developed for civil engineering purposes, and the Old Delft Scanning Stereoscope, were used to analyze the photographs.

The scenes were initially examined to determine the level of refinement possible for identifying detail without assistance from aircraft photography or other ground truth information. This was accomplished by delineating the details of drainage, slope breaks, vegetation, culture, and soils.

The Skylab S190B photography was then re-evaluated on the basis of details observed on the aircraft underflight photography (see Table 3-2) and from information obtained from the study guides. In this way, the level of maximum refinement possible in the interpretation from Skylab photography was determined.

In the discussion below, the results of the photographic study are summarized for each site, after a brief description of the site obtained from the literature study.

3.2.1 Harrisburg Area (Kleeman)

The Harrisburg study area is located in the south-central portion of Pennsylvania, including portions of Perry, Dauphin, Cumberland, and York Counties. Portions of the Ridge and Valley, the Appalachian Valley, and the Triassic Lowland Sections are represented within the area (see Figure 3-1). Elevations vary from 120 to 400 m. Slopes vary from level to steeply sloping, and the terrain is well drained, with the exception of a few low lying areas and associated streams. The bedrock geology is dominantly sedimentary. In the Ridge and Valley Section, the sandstones, shales, and limestones are folded into a major syncline cut by the Susquehanna River. In the Appalachian Valley (the Great Valley), the rocks are generally flat lying shale, limestone and sandstone. The sedimentary rocks of the Triassic Lowland are also relatively flat-lying, with knobs and ridges consisting of igneous basaltic rock. Trellis drainage dominates in the Ridge and Valley Section, whereas dendritic drainage, at times subsurface, characterizes the Appalachian Valley and the Triassic Lowland Sections. Woodlands dominate the rocky ridges, while farmlands in grazing, grains, or fruits are found in the valleys. Much of this farmland is rapidly being replaced by urban and industrial development surrounding cities such as Harrisburg and York.

Frame 67 from roll 88 of sensor S190B, SL3, orbit 44, was chosen for study of the Harrisburg area. The photography was taken in September, 1973. The results of this study are described below, and a few features seen on the C130 photographs and the Skylab photograph are compared in Table 3-3.

Table 3-2: Aircraft Data Used in Terrain Analysis[a]

Test Sites:	Sayers Dam		Harrisburg		Reading	
Aircraft:	U2	C130	U2	C130	U2	C130
Mission:	74-060A	258B	74-016	271	74-016	271
Flight Line:	--	5B	--	24C	--	22
Roll No:						
Color IR:	17	145	23	30	23	30
Color Pos:	--	144	--	29	--	29
Frame Nos:						
Color IR:	8097-8098	23-25	6052-6057 6090-6093	90-113	5987-5990	176-179
Color Pos:	--	23-25	--	90-113	--	176-179
Date (1974):	Apr 25	Feb 12	Feb 5	Apr 28	Feb 5	Apr 28
Scale:	1:130,000	1:33,000	1:130,000	1:31,200	1:130,000	1:20,760

[a]All frames were in 230 X 230 mm format.

Table 3-3: Comparison of Skylab S190B Photography of the Harrisburg Area with Aircraft Photography of the Same Area

C130 Aircraft Mission 271	Skylab S190B
Paxton Creek visible to Wildwood Lake and through Harrisburg until it joins the Susquehanna River.	Paxton Creek visible only as far as Wildwood Lake -- not at all through the city of Harrisburg.
Minor streams -- Spring Run and Hogestown Run -- visible to the Conodoguinet from the south.	Minor streams -- Spring Run and Hogestown Run -- visible, but due only to vegetation along them.
Well-dissected hills visible rising to 150 m just north of Steelton and just south of Harrisburg terrace.	Hills just north of Steelton are not visible. Only indication is drainage in that area.
Deep-cutting Spring Creek and other short running streams visible disecting the hills above Steelton.	Spring Creek and other parallel streams are visible mainly from vegetation on the stream banks.
A terrace of glacial outwash along the Susquehanna River on which Harrisburg is built is visible.	Harrisburg terrace visible from relief and city street and building patterns.
Elevated hills rising 30 m above stream level between meanders of Conodoguinet Creek indicate shale joint control.	30 m relief not visible between meanders of Conodoguinet Creek.
Hilly terrain typical of Great Valley south of railroad at Rutherford Heights is visible.	Hilly relief south of railroad at Rutherford Heights not visible.
Grid-type pattern of minor (1st and 2nd order) drainage on Spring Creek above I-83 in Harrisburg is visible.	1st order drainage not visible; 2nd order drainage visible where assisted by vegetation.
Grid-type pattern of minor (1st and 2nd order) drainage and topography just south of the Conodoguinet near the Susquehanna River is visible.	1st order drainage not visible; some 2nd order drainage visible; relief not visible.

(continued)

Table 3-3 (continued)

C130 Aircraft Mission 271	Skylab S190B
Bethlehem Steel quarries and slag pits at Steelton on east bank of Susquehanna River visible.	Relief visible in larger quarries. Slag pits visible after locating on C130 photography.
Water filled quarries at I-83 in Harrisburg and NE of Hershey visible.	Both sets of quarries visible with aid of C130 photography.
Nuclear reactor and cooling towers at Three Mile Island power generating facility visible.	Nuclear reactor building and four cooling towers visible.
Farmland and plowed fields in the Great Valley visible.	Individual plowed fields and cultivated fields visible.

Landforms and Geology: The sandstone ridges of the Ridge and Valley Section, and the resistant rocks of the Triassic Lowlands, representing relief differences of 210 - 240 m, are distinct. The rounded hills of the Martinsburg shale cannot be discerned, nor can this shale be differentiated from the limestones of the valleys. Regional strike and dip can be determined in the case of the sandstone ridges.

Drainage and Erosion: A large change in drainage density reflects the underlying bedrock. On the basis of drainage density, an approximate boundary can be drawn separating the Martinsburg shales from the limestones to the south and the sandstone ridges to the north. All first and most second order drainage cannot be discerned; however, all third and higher orders are easily traced. Large scale erosional features, such as water gaps, are easily identified. First order gully erosion is not visible at the small scale of the Skylab photography.

Color-Tone-Texture: Color, tone, and texture patterns at the Skylab scale do not provide clues for differentiating soils or bedrock in the Harrisburg area. The patterns do assist in classifying general vegetation features. The heavily forested regions reflect a much darker tone than the surrounding developed land. A noticeable tonal variation is seen in the Susquehanna River, most likely caused by increased turbidity resulting from the 10.0 cm of rain which fell over a two-day period prior to the Skylab orbit. It is possible, on occasion, to differentiate between concrete and asphalt highways, from the lighter tone reflected by the concrete.

Vegetation: The tonal contrast between major vegetation types was a prime indicator of slope breaks, drainage, and lithologic formations, in that darker tones were reflected from forested regions and lighter tones indicated other land use areas. Second order streams, which could not be seen in themselves, were sometimes traced out by the aid of vegetation along their courses. Forested areas indicated land which was excessively steep and stony, or where the soil was poor. Using such indicators, it is possible to roughly separate topographic features and to map the igneous rock areas in the Triassic Lowland Section. Agricultural field patterns are clearly seen on this September photography, but it is not possible to discriminate between crops because of the low resolution of this small scale photography.

Cultural features: Urban areas and suburban areas were readily distinguished on the basis of street pattern density. Agricultural areas were easily identified by the field patterns. Limestone quarries are identifiable with the assistance of aerial underflight photography; in a few cases, of quarries several hundred meters in length, some relief could be detected.

Soils: Soil associations could only be identified on a regional basis, and no sharp boundary could be drawn separating soil associations. It is believed that the reddish tonal variation observed in the Great Valley area reflects the underlying limestone.

3.2.2 Sayers Dam Area (Daelhausen)

The Sayers Dam study area is located in the center of Pennsylvania and includes portions of Centre and Clinton counties (see Figure 3-1). Portions of the Ridge and Valley and the Allegheny Mountain Sections are represented within the area. Elevations vary from 168 to 672 m. In the three broad valleys traversing this region, the slopes are gentle to moderate, whereas they are moderate to very steep in the mountains. The bedrock, which is entirely sedimentary, varies from nearly horizontal in the Allegheny Mountain Section to tilted and folded in the Ridge and Valley Section. Sandstones form the higher elevations of the mountains, while limestones and dolomites (with some shales) are the dominant feature of the valleys. Sinkholes and limestone quarries are common valley features. In areas of surface drainage, the streams exhibit a trellis pattern. Locally, the groundwater table is seasonably high; evidence of this is seen as a mottled soil pattern on aerial photographs. Trees, originally covering the area, are now limited to steep and stony mountain slopes and valley regions of soil too poor for cultivation or urban development.

Frame 324 from roll 91 of sensor S190B, SL4 orbit 73, was chosen for study of the Sayers Dam area. There is a light snow cover on this January scene. The results of this study are described below.

Landforms and Geology: The landforms are detectable on a regional basis only. They can be related to the underlying geology, but no sharp boundary line can be drawn separating them. In the stereoscopic model of the area, the resistant sandstone formations of the Ridge and Valley Section (where greater than approximately 240 m in relief) stand out. However, no detectable slope break can be observed between the ridges and the valleys. Relief features of a lesser order of magnitude than the sandstone ridges can be observed in the dissected shale hills of the Allegheny Front. Effective shadows, produced by the combination of the low sun angle and topographic relief, assisted in differentiating the shale hills. Separation of individual members within the shale formation was not possible. A detectable break in terrain is seen separating the Catskill formation from the Chemung-Portage shale formations and Pocono sandstone.

Drainage and Erosion: Although relief features separating the Pocono from the Pottsville sandstone formations of the Allegheny Mountain Section cannot be seen, as the slope differences are not readable at the Skylab scale, the separation of lithologies, from the Pocono and Pottsville sandstones through the Catskill formation and to the shales, is made possible by the noticeable change of the surface drainage patterns, reflecting the change in the underlying bedrock. The Juniata formation, separating the Tuscarora and Oswego formations, is identifiable; however, no sharp erosional boundary is discernible. Large-scale erosion features, such as water gaps, are easily seen. First order drainage gullies cannot be seen at this scale. One minor erosional feature was observed. The Catskill formation is believed to be exposed along the slopes north of the West Branch of the Susquehanna River. The south-facing slopes permit early snow melt, exposing the Catskill formation underlying the Pocono and Pottsville sandstones. An example of this may be seen in the vicinity of North Bend and Renovo.

Color-Tone-Texture: Color, tonal, and textural patterns, which provide valuable assistance in detecting and identifying geological features on aircraft photography, are almost completely obscured on winter Skylab photography of the Sayers Dam area due to the 7 to 10 cm of snow on the ground. Only the Catskill formation, described above, is revealed by a reddish color on the photograph.

Vegetation: In January the vegetation is dormant; however, a sharp tonal contrast between forested and other land use categories was provided by the light snow cover in this scene. Forested regions (darker in tone) indicate areas of poor soils or steep terrain, and thus are a clue to the underlying geology. The Gatesburg formation, defining an area of scrub oak known as "the Barrens," is easily identified as a forested area within Nittany Valley. The snow cover prevented significant identification of agricultural vegetation.

Cultural features: Urban areas are easily separated from surrounding land uses. The street patterns in the medium-sized towns of State College, Bellefonte, and Lock Haven are identifiable. Snow cover prevented identification of agricultural field patterns. Major highways can be seen when not obscured by snow. Railroad rights-of-way, large industrial buildings, and limestone quarries can be identified with the aid of aircraft underflight photography.

Soils: The snow cover at this time of year prevents identification of soil associations.

3.2.3 Reading Area (Hesler)

The Reading area is located in the southwestern portion of Berks County. It includes parts of the Appalachian Valley and the Traissic Lowland Sections (see Figure 3-1). Elevations vary from 43 to 324 m. Slopes range from level to very steep. A considerable variety of bedrock types is found in the area. The Appalachian Valley Section (the Great Valley) consists of gently dipping limestones and shales, with the highlands of Reading (the Reading Prong) composed of granitic and gneissic rocks. In the Triassic Lowlands to the south, several high ridges of diabase rock are surrounded by limestones, shales, and conglomerates. In the Reading highlands, drainage is structurally controlled by a complex fault system, whereas in the remainder of the Appalachian Valley Section and in the Triassic Lowlands Section the drainage has a trellis pattern on folded shale. Just northwest of the Highlands area, drainage in a limestone valley is subsurface to the Schuylkill River. Forest lands are largely confined to slopes too steep for agricultural use, with the exception of a few cultivated lots of conifers found on moderate slopes. The large areal extent of deep, productive soils has led to the development of a large variety of agricultural activities. Chief among these is dairy farming, grains, truck crops, and orchards. Growth of the suburban areas around the city of Reading is encroaching on the agricultural land to some extent. A few limestone quarries are found in the area.

From the comparisons described earlier, it was determined that the S190B color positive film was the most promising for analysis. Accordingly, frame 69 from roll 88 of sensor S190B, SL3 orbit 44, was chosen for study of the Reading area. The photography was taken in September. The results of this study are described below.

Landforms and Geology: Separation of the varied lithologies within this area can only be done on a regional scale. The igneous formations of the Reading Prong are roughly delineated from the surrounding lowlands (representing a relief of approximately 225 m). The dissected shale hills cannot be seen, nor can the limestones be separated from the shale formations.

Drainage and Erosion: Changes in drainage density can be effectively used as indicators of changes in bedrock lithology. For example, a change in drainage density indicates the approximate boundary between the Martinsburg shales and the bordering limestones in the area. First order drainage cannot be seen. Some second order drainage is discernible; however, aircraft underflight photography was not available to verify the mapping of these. All drainage of higher order than second was easily traced. First order gully erosion cannot be detected.

Color-Tone-Texture: In this area, darker tones generally indicate limestones and lighter tones indicate underlying shales. In some instances, a mottling effect appears to be observable, further substantiating the presence of limestone. Drainage features show up as a dark color tone, and a reservoir just northwest of Reading shows a tonal variation similar to that seen in the Susquehanna River in the Harrisburg area. The lighter water tones occur only at the inlet to the reservoir and, as in the Susquehanna River, these are probably an indication of turbidity resulting from the 9.65 cm of rain which fell in the Reading area two days prior to the Skylab pass. Tonal variations are not detectable in the smaller streams of the area. Forest vegetation can be separated from other land uses on the basis of tone.

Vegetation: Vegetation, in the form of tonal contrasts, is a prime indicator of differences in lithology. Forested areas, dark in tone, form a rough boundary separating igneous intrusions from the surrounding sedimentary formations, as the forests are largely confined to stony and steep slopes. This characteristic, in turn, leads to the determination of an approximate boundary between slope breaks. Agricultural field patterns are clearly visible, but discrimination between crop types is not possible at the scale of the Skylab photography. Vegetation is occasionally of aid in tracing second order drainage.

Cultural features: Differentiation between urban, suburban, and agricultural areas is comparable to that found in the Harrisburg area, and considerably better than that found in the January, snow-covered, scene of the Sayers Dam area.

Soils: It is possible to roughly identify regional soil associations. The variety of soils series present and the small scale of the photography prevented more detailed discrimination.

3.2.4 Summary of Results

Landforms and Geology: Minimum relief differences on the order of 150 to 240 m could be detected by stereoscopic study; however, it is recognized that vegetation and cultural practices assist in such delineations. The line of separation between highs and lows could not be consistently mapped. Secondary clues, such as shadows on winter photographs, led to an interpretation of relief in some instances. Gentle rolling relief related to limestone, dolomite, and shale in the valleys could not be detected. The igneous rock highs of the Reading Prong in the Great Valley were easily seen, in part due to vegetation and in part as a function of relief. Regional geologic features could be delineated, using topography, drainage patterns, vegetation, and cultural patterns. However, specific lithologic members of a formation could not be differentiated. Strike and dip could be determined on a regional basis, but verification from ground truth was needed.

Drainage and Erosion: Water and wind gaps through major ridges were easily seen. Streams of third order and larger were clearly visible and easy to trace. Second order streams could sometimes be identified and traced, but not with consistency. First order streams and gullies, on which much erosion analysis depends, could not be detected. Changes in drainage density frequently could be used as an indicator of differences in lithology. Shadows, especially on the winter scene, and vegetation were of assistance in tracing drainage.

Color-Tone-Texture: Differences in color, tone, and textural patterns rarely supplied clues for differentiating soils or bedrock. In some instances, darker tones indicated underlying limestones and lighter tones indicated shales. Rarely, mottling substantiated the presence of limestone. In one instance, it was thought that a reddish tone indicated the presence of the Catskill formation; in another, that it indicated limestone in the Great Valley. Tonal variations were detected in the Susquehanna River and in one reservoir. It is suspected that this was a function of suspended silt from a heavy rain. Forest vegetation was easily separated from other land uses on the basis of tone, and developed land was separated from agricultural land on the basis of the textural pattern of streets.

Vegetation: The separation of naturally forested areas from areas of cultivation and pasture was effective and a valuable clue to the underlying geology. It was possible to separate large plantings of conifers from deciduous trees, especially on winter scenes. Field patterns were not seen on the snow covered winter scenes, but were readily seen on the September scenes, although crops could not be identified. Vegetation was frequently a valuable clue in tracing second order drainage.

Cultural features: Suburban and industrial developments were clearly differentiated from urban areas and surrounding agricultural fields. Street patterns, field patterns, reservoirs, highways, and large bridges were identifiable. Utility and railroad rights-of-way, quarries, and large industrial buildings could occasionally be identified of themselves, but most often had to be verified from underflight photography and/or ground truth.

Soils: Soil associations could be identified on a regional basis, but no sharp boundary could be drawn separating soil associations. Occasional tonal variations seemed to indicate the presence of particular soils, but again no sharp boundary could be drawn. No soils information was obtained from the January snow-covered scene.

3.2.5 Conclusions and Recommendations

S190B photographs from three areas in Pennsylvania were studied using standard aerial photointerpretation techniques and the Old Delft Scanning Stereoscope. Initially, the photos were analyzed without the assistance of ground truth information; later, a study guide for each area (prepared in advance) was used for re-evaluation of the scenes, in order to determine the maximum level of refinement possible.

It is clear that drainage pattern mapping is a key to identification of many features. Drainage to the level of third order streams (source streams are first order) can be consistently mapped, and second order streams are frequently discernible with the aid of vegetation and shadows. Vegetation at the level of forests versus agricultural land can be consistently mapped, and in some cases larger areas of conifers can be differentiated from deciduous trees, especially on color winter scenes. Regional geological features can be delineated from topography, and from patterns of drainage, vegetation, and cultural features. Regional strike and dip may be indicated, but should be verified by ground truth. Water and wind gaps, and drainage larger than second order are clearly visible. Changes in drainage density are an important indicator of lithologic types.

Color and tonal changes give inconclusive evidence of soil and underlying bedrock. Tonal differences clearly differentiated forest vegetation from cultivated fields. Tonal differences in water bodies may indicate the presence of silt. Textural differences were used to identify urban, suburban and industrial, and agricultural land uses. The presence of utility and railroad rights-of-way, quarries, and large industrial buildings require aircraft underflight photography for verification. Field patterns can easily be seen, although crops cannot be identified. The level of generalization at which soils can be mapped compares well with the soil association maps prepared by the Soil Conservation Service.

Photoanalysis techniques applied to Skylab S190B photography can yield a regional map of considerable value. Landforms with minimum relief differences of 150 to 240 m can be mapped relatively consistently, using the Old Delft Stereoscope, and lesser relief differences can be discerned in some instances, with the assistance of shadows and vegetation differences. Clues such as topography, drainage pattern differences, vegetation, and cultural patterns reveal the regional geology on the formation level, and regional structural orientation can often be determined.

A brief study of the S190B black and white photography available only for an area outside of the study areas chosen here, indicated that the quality of this form of data is equal to that of the S190B color photography except for the loss of definition resulting from the lack of

color. Use of the Bausch and Lomb Zoom 95R stereoscopic system mounted on the X-Y scanning stage with this photography indicated that relief features down to 30 m could be discerned. It is clear that such a viewing system should be used in all future studies of photography of this nature.

Extensive ground truth, underflight photography, and information from the literature were used to verify the identification of features seen on the Skylab photography in the study areas. However, the consistency with which three operators identified features in the three different geographic areas seems to indicate that regional mapping on the level herein described, using S190B photography, is feasible for areas for which little or no ground truth is available.

The successful experience in mapping at small scale on a regional basis is significant to persons conducting reconnaissance studies. This would hold true for civil engineers involved in route location, pedologists mapping soil associations, forest resource evaluators, land use mappers, and others. Moreover, the quality of a detailed analysis of soils or bedrock characteristics is heavily dependent on proper regional relationships. That is to say, studies should always proceed from the general to the particular in order to appreciate the interrelationships of the several map units which evolve.

Skylab photography would have enhanced the reconnaissance studies for the Interstate System of Highways, for instance. When conducting analyses pertinent to such regions as the Adirondock Park area, Skylab data provides an excellent overview of regional geology, drainage systems, land use, and interrelationships with adjacent areas pertinent to land use restrictions. From our limited experience, it can be predicted with reasonable assurance that it is possible to construct regional terrain classification maps for military and civilian applications from Skylab S190B photography.

It is suggested that the next step should be a detailed study of Skylab S190B photography of a "foreign" area in an attempt to define the landforms, nature of the bedrock, structural features, nature of the soil cover, and relative depth to the groundwater table. This study should be done with a viewing system such as the Zoom 95R mounted on an X-Y stage, and without the aid of prior knowledge of the area. After such a study, the ground truth should be established and the percentage of the area correctly mapped should be determined.

It is recommended further that an attempt be made to develop spectral signatures for bare soil areas, and an effort made to relate these areas to lithology. This calls for the development of improved spectral analysis for small ground areal units.

3.3 USE OF SKYLAB PHOTOGRAPHY AS GROUND TRUTH FOR LANDSAT DIGITAL DATA (McMurtry and Chren)

Skylab S190B photography was used as a form of ground truth data in a land use mapping project. Digital MSS data from Landsat-1 was processed using various classifiers in the ORSER System (see section 5.1).

An area along the Allegheny River, just west of Oil City, Pennsylvania, was chosen as the test area, because large, visually uniform areas were present and because unbanded and cloud-free Landsat data for the scene were available. Skylab photographs, the only photographic source available, were used as ground truth. It was later decided that lower altitude (more detailed) photos would not be necessary, since a relatively non-detailed classification map was sought. Topographic maps were also used.

The Skylab data was S190B photography taken on September 10, 1973, on orbit 30 of SL3. The film format was 127 mm black and white. Frame 342 of roll 85 was used. The Landsat digital data were from scene 1028-15295, collected on 20 August 1972. All four Landsat MSS channels were used in the classification.

A five-class land use analysis was made of the area using the Landsat digital data. The five classes were: water, city (urban and suburban), agricultural land (of all types), forest (all kinds), and abused land (strip mines, etc.). Each of the classes had to be made broad enough to include all of the various subclasses which conceivably could be formed in other analyses with these data. Hence, large values of critical distances were used in the classification algorithms, and classes with several different training areas for each class were defined. Some classes had to be broken down into two or three subclasses. For example, it was found in the analysis that there were three types of forest (deciduous, coniferous, and shaded trees). Shaded trees are those located in valleys (where there is a different intensity of ambient light). The three types of forest present in the scene each had its own training area, but in the resultant map these were given the same "forest" mapping symbol. Only one water class (for the Allegheny River) was needed Two classes for abused land and city were needed.

The various classes were sufficiently large that NMAP (an intensity map similar to a grey-scale map), in conjunction with the Skylab pictures, was sufficient to indicate training areas of adequate purity. UMAP is normally used after NMAP in the ORSER sequence of programs in order to identify homogeneous training areas. However, in this case, UMAP was not used since it was thought that the visual ground truth in the form of Skylab S190B photography provided assurance of training area homogeneity.

In order to determine classifier accuracy, an attempt was made to use the Bausch and Lomb zoom transfer scope (ZTS) to compare the computer-produced map output with the Skylab photo, but it was found that the difference in scale between the 127 mm photograph and the computer-produced map necessitated reducing the map to such a scale as to make

individual mapping symbols indistinguishable. Enlarging the Skylab photo an equal amount made class boundaries much less distinct. Thus, the zoom transfer scope was not used. Instead, a very detailed and slow process of "eyeball" point-by-point comparison of Skylab ground truth and the classification map was used to determine classifier accuracy. After this investigation was concluded, ORSER received a 230 mm Skylab photograph of the same area. Had this been available, the ZTS could probably have been used very effectively.

In addition to the Skylab photos, topographic maps were used to great advantage in classifying this scene. During analysis of the data, it was realized that because of the similarity between abused land and some urban areas, such as roads, railroad tracks and large oil bins, a large number of the city signatures were being misclassified as abused land. Upon reference to the topographic maps, which detail such information, it was found that much of the area originally classified as abused land actually was urban. The presence and locations of the various categories were verified, using the ZTS, by superimposing the topographical map onto the computer map.

The classification results on the Oil City scene indicate the difficulty encountered when trying to map such diverse categories as agricultural land, disturbed land, and city. The classification percentage for these categories was relatively poor (78%, 70%, and 77%, respectively), and better results would only have been achieved at a great expenditure of money and time. Forest, being a relatively uniform class, was mapped the best, 93%, with water at 86%. This good classification for water was primarily due to the large difference between the water signatures and all the others present in the data scene. This classification percentage was especially good considering the fact that only one training area was used for this category. The primary reason for the relatively poor classification result obtained for abused land is the large diversity within the class and the fact that only two training areas, with relatively few points, were defined for abused land. The same reasoning applies to agricultural land. Had more training areas (and subclasses) been defined for each class, classifier performance would have increased.

In conclusion, the Skylab S190B photography was used as a very effective source of ground truth data in this project. Its resolution is ideal for use with Landsat digital data, since it is more detailed than Landsat, but not as detailed as lower level aircraft photography. Because of its very fine resolution, the latter can introduce confusion when used with Landsat data. In addition to providing accurate ground truth in such applications, the resolution of the S190B photography permits very rapid comparison and verification. The 230 mm size of photograph would be best if a zoom transfer scope is available for visual overlay of the photographs and the computer-produced maps. Topographic maps are always helpful as ground truth, but again they are very detailed and often quite out of date. Thus, Skylab S190B should be considered not only as a primary type of data, but also as an excellent source of ground truth for Landsat digital data processing.

4.0 GEOLOGIC STUDIES

One of the objectives of this study was to map lineaments on the Skylab/EREP data and to determine how well these lineaments correlated with those mapped from the Landsat-1 imagery. As a basis for correlation of the two data sources, a lineament map of Pennsylvania was produced from Landsat-1 imagery because of its complete coverage of Pennsylvania. Skylab photographs were then used to compare the distribution of visible lineaments and to help position them more accurately on larger scale maps. As a result of the comparison between Skylab and Landsat-1 lineaments, it became possible to determine the lineament sampling bias on both types of data. Considerable field work was also undertaken to determine if the lineaments delineated on the Skylab photography can be correlated with actual field conditions.

Upon completion of the lineament map, the extent of correlation of lineaments with ore deposits was determined. This necessitated the preparation of a Pennsylvania mineral deposit map. The lineaments were also related to groundwater well yields in the carbonate areas of Pennsylvania. A zone of lineation determined on Skylab photography was also used in a study to investigate the origin and extent of a thermal anomaly in central Pennsylvania.

Finally, digital wavenumber analysis (spatial filtering) was attempted to determine if it can be used to enhance certain subtle features and, in particular, to locate and verify lineaments.

4.1 LINEAMENTS (Gold and Parizek)

Lineaments have been defined as naturally occurring linear topographic and tonal features greater than 1 mile (1.6 km) in length (Lattman, 1958). Lineaments, similar to shorter linear features known as fracture traces (Lattman and Nickelson, 1958; Lattman and Matzke, 1961; Kiem, 1962; Lattman and Parizek, 1964; Wobber, 1967) appear to be the surface manifestation of nearly vertical zones of fracturing or faulting in the underlying bedrock (Parizek, 1971a; Wier, et al., 1973; Gold, et al., 1973; Gold, et al., 1974). Since the launching of Landsat-1, Gold, Parizek, and Alexander have mapped tentative groupings of lineaments, from a few to an excess of 150 km in length, on Landsat-1 MSS images. They recognize at least six scales of linear features in Pennsylvania which they believe may be genetically related. A single mechanism, possibly related to stress fields imposed on a drifting continental plate, may explain the origin of these features on all scales. It has been shown here that these fractured zones may act as conduits of increased permeability, channeling fluids in the crust.

Lineaments and fracture traces appear to be universal in their distribution. They owe their expression to aligned surface sags and depressions; gaps in ridges; tonal changes revealing variations in soil moisture; aligned springs, seeps, and perched surface ponds; alignments in vegetation, vegetation types, and height changes; straight stream and valley segments; abrupt changes in valley alignments, gully development, etc. These surface features help to reveal zones of fracture concentration within bedrock heavily mantled by soil. Lineaments and fracture traces related to bedrock fractures manifest themselves in areas with residual and transported soils with thicknesses in excess of 88 m near State College, Pennsylvania, and through similar thicknesses of glacial drift in the northwestern portions of the state.

Fracture traces and lineaments are commonly straight, unaffected by topography, and hence are considered surface manifestations of vertical to near vertical zones of fracture concentrations. In the ridge and valley province of the Appalachians, for example, lineaments have been mapped above folded bedrock where dips are vertical. There is no evidence of offset of beds on either side of a fracture trace or lineament, even when beds are thin, distinct, and relatively well exposed. The same is true where fracture zones are observed in cross-section. Parizek (1971a) and others have observed that fracture traces may be underlain by 1) relatively few closely spaced joints which cut one or more beds but not overlying or underlying beds, 2) joints which cut all beds exposed at a given location, or 3) hundreds of closely spaced fractures that give the rock a brecciated appearance.

Gold, et al (1973) reported that lineaments observed on Landsat-1 images have the same morphological characteristics as fracture traces, except they are longer, appear wider, are not at all obvious in the field, and exert a major influence on topography. Although most lineaments are straight, some appear to be gently curved. All lineaments appear to be independent of regional structural trends. The authors state that "some of the lineaments spaced about 10 miles (16 km) apart, are approximately

perpendicular to the Appalachian Mountain trend, and fan with the Appalachian orocline..." In their test area, east of Harrisburg, Pennsylvania, the intermediate and short lineaments appear to be conjugate with an angle of about 30° to a northwesterly trending axis. Likewise, these shorter lineaments cut across regional primary structure and major physiographic province boundaries. Except for lineaments coincident with known faults, their physical nature in the third dimension is not known; but by analogy with fracture traces, the authors speculate that lineaments are underlain by zones of fractured and jointed rocks and represent zones of deformation or movement between "jostling" blocks. They must be either a rejuvenated crustal fracture system impressed on the younger rocks as active crustal "joints", or they represent the deformation in response to a widespread and pervasively imposed stress field, as would be expected from a drifting North American plate.

Little has been found to alter these conclusions. On the contrary, joint spacing, breccias, fractured and slickensided surfaces in float, and base metal mineralization studied by Krohn (1975) lend support to these hypotheses. The most pronounced expressions of lineaments result from the alignment of wind and water gaps, upland sags and depressions, aligned valley segments of both tributary drainages and master streams and rivers, and aligned field and woodland boundaries which terminate along steeper valley slopes. Their analogy with fracture traces is striking with the exception that topographic features associated with lineaments are on a larger and more pronounced scale.

Fracture traces (lineaments less than 1.5 km in length) have been mapped for 17 years for purposes of locating zones of increased weathering, porosity, and permeability development within bedrock under a wide variety of geological settings (Lattman and Parizek, 1964). Fracture traces are known to reveal narrow zones (2 to 20 meters wide) suitable for groundwater prospecting, high permeability and porosity avenues 10 to 1,000 times that of adjacent strata, permitting water to escape from below dams and from settlement lagoons and reservoirs. They define flood and roof stability hazard areas within mines, tunnels and quarries; landslide prone areas; and areas of potential foundation instability.

Fracture zones form an interlaced highly transmissive network in most terranes; serve as local groundwater feeder routes from more massive blocks of rock in interfracture areas; and supply water to more regional conduits, which in turn may be localized by these same features (Figure 4-1).

Cline and Parizek (1975) have shown that fracture traces can be used to locate high capacity wells in folded siltstones, shales, and sandstones in east-central Pennsylvania. Parizek (1971b), Koppe and Thompson (1972), and Lovell and Gunnett (1974) have shown how fracture traces could be used in controlling and abating mine drainage produced from deep coal mines, and how they related to mine seals and to groundwater inflow to mines. Parizek and Voight (1970) and Parizek (1969 and 1971a) have shown that fracture traces could be used in geotechnical investigations to predict zones of increased weathering in advance of foundation exploration; areas of potential roof collapse and excess water

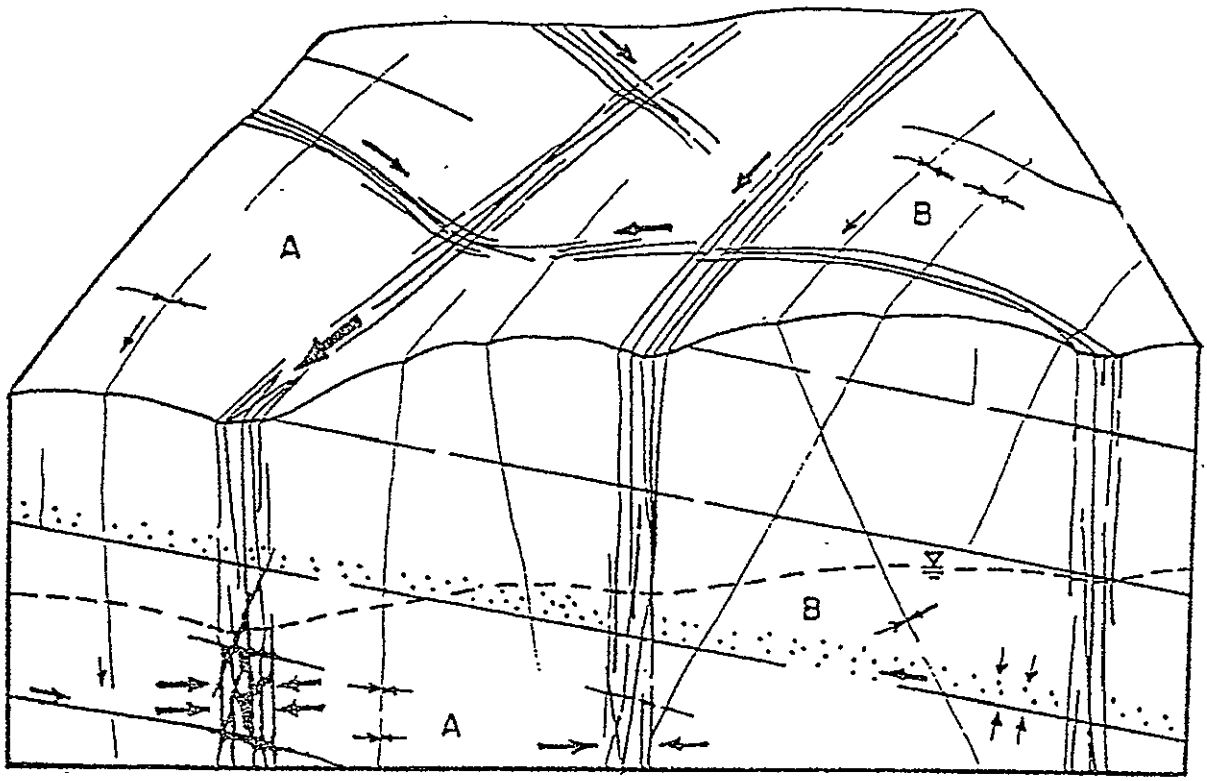

Figure 4-1: High permeability development along zones of fracture concentration in a massive block of carbonate rock. Transmission and storage properties are afforded by intergranular and vulgular openings within selected beds, bedding plane partings, joints, and fault zones. The arrows depict avenues of groundwater movement. (From Parizek, 1971a).

in mining and tunneling operations; and leakage beneath dams and into excavations within bedrock. Zones of fracture concentration also could be mapped to account for seepage pressure variations, risk of blowouts and piping, and strength variations within bedrock. Detailed knowledge of the significance and distribution of zones of fracture concentration is also useful in planning, designing, and conducting grout or cut-off wall operations, and in locating highly effective pressure and drainage wells. Studies conducted on lineaments identified on Landsat and Skylab data indicate that similar relationships exist for lineaments; however, more adequate ground truth verification must be established.

A few lineaments had been mapped prior to the availability of Landsat and Skylab images. These were interpreted from airphotos and photomosaics prepared on a county-wide scale for index purposes. Alignment of surface features such as wind gaps, water gaps, and surface sags among resistant ridges within the Appalachian mountains; straight valley and stream segments; soil tonal changes; and sinkhole, spring and seepage areas revealed lineaments from less than two to ten or more kilometers in length. Many mountain top notches and wind and water gaps are known to be underlain by closely spaced joint concentrations; however, these could not be matched with any degree of certainty across valley uplands and between mountain ridges because the orientation of the lineament could not be determined.

This problem has been all but eliminated through the Landsat and Skylab programs. Hundreds of lineaments of various lengths are now mapped for Pennsylvania where previously only a few were known (compare Kowalik, 1975 with Gold, et al., 1973 and with Koppe and Thompson 1972). Further study is needed, however, concerning the nature and significance of lineaments:

1. The nature of the structural features which underlie lineaments, their width and depth, and the genetic relation of lineaments and other structures of larger and smaller scale must be established.

2. Lineaments observed on Landsat and Skylab images must be accurately located on the ground to permit direct observation and use in field studies.

3. The significance of lineaments in geological and engineering applications must be further established under controlled conditions, rather than by inference.

A key to the solution of these problems is adequate Skylab-type coverage over areas for which controlled ground truth data are available.

The performance of water wells, foundations, tunnels, mine roofs, and similar structures, have to be determined on a case by case basis and compared with a number of similar facilities located on and off lineaments before the geological and engineering significance of lineaments can be fully evaluated. It is easy to design the necessary verification studies required; however, carrying out these studies poses a formidable challenge because good quality field data are scarce and the opportunity for repetitive observations is limited, particularly in the more humid regions, which

contain a thick soil cover and dense vegetation.

Before an accurate assessment can be made of the significance of lineaments to efforts such as groundwater and mineral prospecting and the solution of engineering problems, it is of vital concern to establish the width and depth of influence of lineaments in various terranes. Parizek (1971a) has observed the width of fracture concentrations in fracture traces, and has measured such zones from 3 to over 33.3 m wide in various rock types in the United States. In the vicinity of State College, Pennsylvania, he has found zones 2 to 20 m wide in the folded and faulted rocks of the Central Appalachian region. In siltstones and shales of northeastern Pennsylvania fracture zones vary from 3 to over 20 m wide, averaging 13.3 m, and are inclined 2 to 3 degrees from vertical. Individual joints may be closely spaced, 5 to over 60 in number, and sub-parallel to parallel. They may cut all beds equally well, or be concentrated in selected bedrock units and poorly developed to scant in number in overlying and underlying units. Five or more distinct high-angle joints have been observed under fracture traces in limestone and dolomite bedrock in the Central Appalachian area. At other sites, bedrock contains hundreds of joints which are so closely spaced and intersecting as to impart a shattered appearance to the rock (Parizek, 1971 and 1975).

The width and depth of bedrock weathering underlying fracture traces varies with rock type and regional setting. The character of drill cuttings, well-yield and caliper log data obtained from wells completed 66 to 166 m deep in interbedded dolomites and sandy dolomite of Cambrian and Ordovician age suggests that weathering may extend laterally for 66 to 93 m along bedding planes and within selected beds of some carbonate rocks. In fresh granite, metamorphic rocks, sandstone, shale, siltstone, and other rocks, weathering may extend but a few centimeters beyond the zone of fracture concentration.

In the absence of more detailed information, a width of 1 km has been assumed in many cases for structures controlling lineaments, in spite of the fact that it is highly likely that lineaments in ridges are of a different width than those in the valleys. The width of these features most likely varies with lithology and structural environment. With the availability of Skylab data, preliminary studies have been made toward determining the width of individual lineaments, as these data have, for the first time, provided a ready means to accurately locate on the ground a lineament which has been identified on satellite images.

4.2 LINEAMENT MAP OF PENNSYLVANIA (Gold and Kowalik)

Figure 4-2 represents a conservative and tentative compilation of lineaments interpreted from the best available Landsat-1 infrared (channel 7, 0.8 - 1.1 μ) positive transparent images (Kowalik and Gold, 1975). Landsat imagery was chosen because of its complete coverage of Pennsylvania. Skylab photographs in selected areas, such as shown in Figure 4-3, were used to compare the distributions of visible lineaments and to help position them more accurately on larger scale maps.

The lineaments of Figure 4-2 were mapped on individual positive transparencies in standard Landsat format and compiled in a laydown mosaic at the same scale (approximately 1:989,000). The individual frames used and their positions in the mosaic are indicated in the top center of the map.

The lineaments in both Landsat and Skylab scenes were mapped on a light table (transmitted light) and interpreted on a subjective ordinal scale of quality, linearity, and expression from one to three, where class three lineaments are the straightest and best expressed. On the map, the number symbols are represented by a dotted line (class 1), dashed line (class 2), and solid line (class 3).

In addition, each lineament was categorized by the components of its composition as: (a) straight segments of major streams, i.e., where water is visible; (b) straight segments of minor streams, particularly alignments of these segments; and (c) alignment of tonal features, e.g., swampy patches, small streams, vegetation, wind gaps. This classification is descriptive only; genetic relationships are incidental to the mapping scheme.

The overlays from each image mapped were checked against 1:250,000 topographic maps and "lineaments" clearly corresponding to cultural features such as roads, power lines, pipe lines, field boundaries, plough patterns, and trails were removed from the final compilation. Topographic features along which cultural features have been built were retained as lineaments. Lineaments along primary lithologic contacts were avoided; however, those representing secondary or imposed structures, such as the trace of dikes or faults, were included.

After the lineaments were digitized for computer processing, three FORTRAN IV programs were written to sort the data by lineament length, degree of expressions, and type (TRANSFORM and AZMAP) and to plot their orientation (ROSE) (see discussion of these results in section 4.3). In addition, two programs were written to provide Calcomp plotter line maps at desired scales. The map was enlarged by means of the Calcomp plotter, to the scale of the Stream Map of Pennsylvania[1] (1:380,160) on which all known metallic mineral localities, mineral prospects, and abandoned and working mines had been plotted.

Comparison with lineaments seen on Skylab photographs, discussed

---

[1] Published in 1965 by the College of Agriculture, The Pennsylvania State University.

Figure 4-2: Landsat-1 lineament map of Pennsylvania. The outline on this map indicates the area on which lineaments are plotted on the Skylab scene of Figure 4-3. On both scenes, lineament rankings are indicated by letters and numbers according to the legend shown on this figure.

Figure 4-3: Lineaments plotted on a Skylab scene, ranked according to the same system employed for the Landsat scene in Figure 4-2. In the upper portion of the scene, Delaware Water Gap can be seen as the prominent break in the ridge where it is transected by a long lineament. A smaller lineament localizes the gap through the ridge at Palmerton, to the left. Wind Gap can be seen in the center of the ridge. The area of this scene is outlined on Figure 4-2, on which also may be found the key to the lineament rankings (by letters and numbers) on this figure. (SL3, orbit 52, S190B, roll 87, frame 297.)

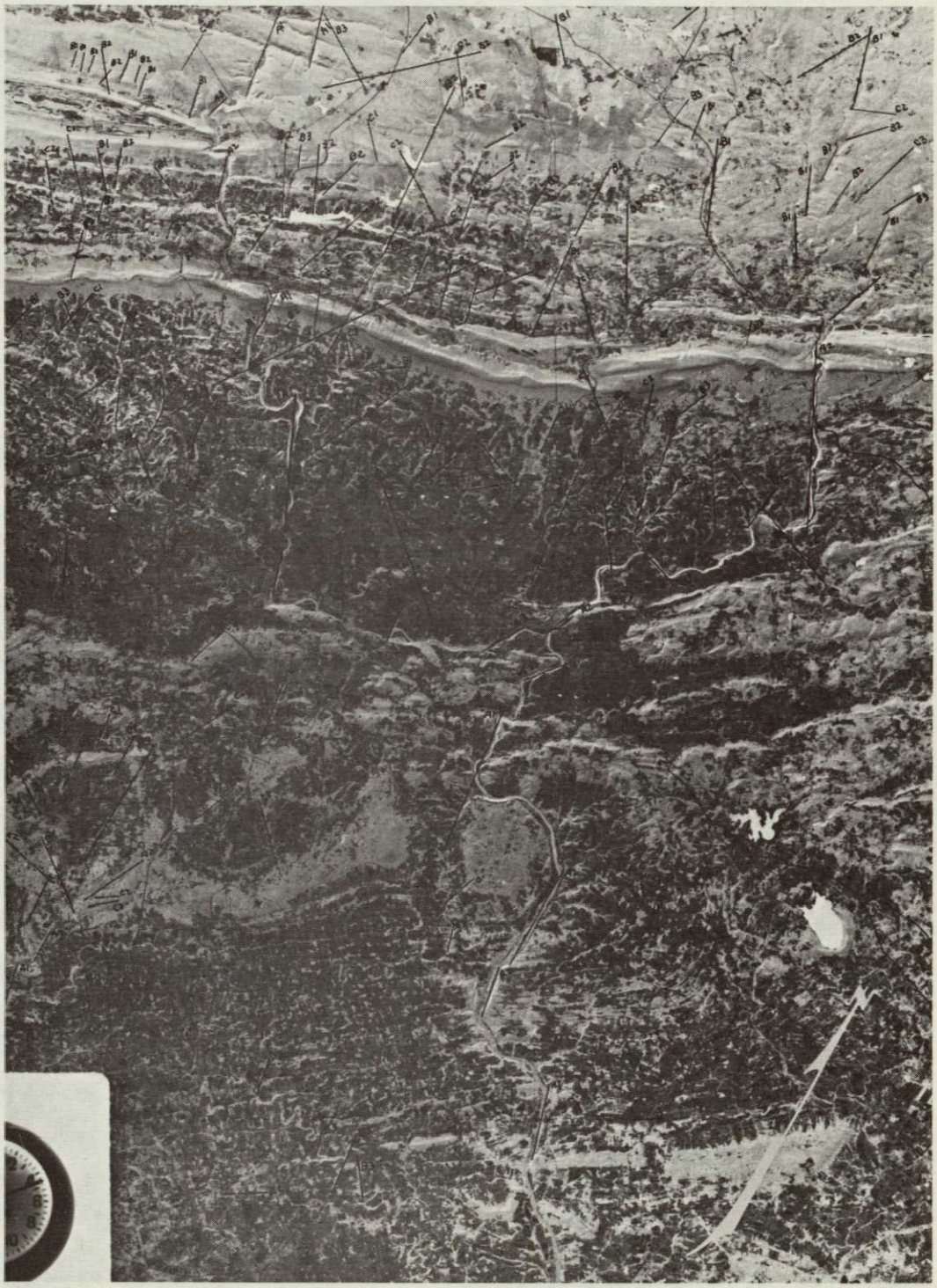

in section 4.3, indicates that a bias is present against detecting lineaments near the sun azimuth and near the scan line direction. Geologists mapping lineaments should be aware of the illumination and scan line biases prior to interpreting orientation diagrams. Images sensed at different seasons are useful for interpreting lineaments in a particular area because of the change in the sun angle. Lineament degree of expression is also somewhat dependent on these biasing factors and is not necessarily a measure of the extent of structural disturbance underlying the lineament.

4.3 LINEAMENT SAMPLING BIAS (Gold and Kowalik)

Wise (1968) has noted the lineament sampling bias caused by illumination from a point source. He showed that maximum enhancement of lineaments occurs when the incident light completely illuminates one valley wall and just grazes the opposite wall. The enhancement of any lineament is thus a function of valley wall slope and the orientation of the lineament with respect to the illumination azimuth and vertical illumination angle. The conditions for maximum enhancement are illustrated in Figure 4-4. Note that if the inclination angle exceeds the valley slope, no shadow enhancement occurs.

In order to determine lineament sampling bias on Skylab and Landsat data, the following two scenes were chosen:

Skylab 4, S190B, 4 Jan 1974, roll 91, frame 324,
Color positive, 1:517,000 scale.

Landsat-1, scene 1459-15221, 25 Oct 1973,
channel 7, 1:989,000 scale.

The study area covered approximately 5000 km^2, including portions of eight counties on the Appalachian Plateau in northcentral Pennsylvania (Figure 4-5). In this area, the steepest valley walls are close to 32°. Although outcrops of the resistant Pocono and Pottsville units approach 90° for a few meters in some of these valley walls, it is doubtful that these cliffs cause much shadow. Therefore, the lineaments enhanced to maximum visibility on the Skylab photograph (20° sun elevation), should theoretically be oriented between 40° and 90° to the illumination direction. On the Landsat image (32° sun elevation), maximum enhancement should occur for lineaments oriented approximately 90° to the illumination direction. Conversely, lineaments should be relatively obscured at angles from 0° (parallel) and up to about 40° to the sun azimuth on the Skylab photograph and at nearly all angles -- but especially parallel to the sun azimuth -- on the Landsat image.

Positive transparencies of the Landsat and Skylab images were viewed on a light table and relatively short lineaments were mapped (Figure 4-6). The length distributions of the Landsat and Skylab lineaments, shown with their means ($\bar{x}$) on Figure 4-7, are similar, except for the larger number of shorter Skylab lineaments. This indicates that essentially the same population of lineaments was sampled in each case.

The lineaments were rated on a three-class ordinal scale of degree of expression, and on a purely descriptive three-level classification of lineament type (major streams, minor streams, or tonal lineaments). The majority of lineaments are mapped from alignments of stream channel segments. The lineament orientations were summarized using modified versions of programs by Podwysocki (1974).

Figure 4-8 presents the total length-versus-orientation histograms for the Skylab and Landsat lineaments interpreted in the area. The

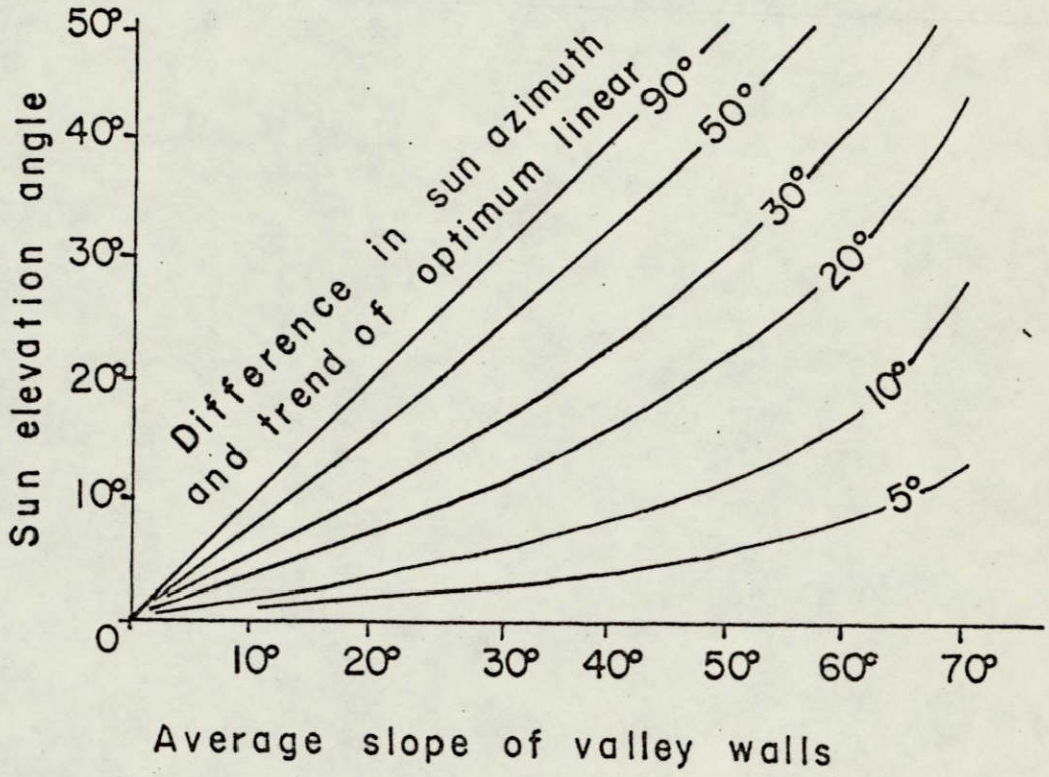

Figure 4-4: Conditions for maximum enhancement of a topographic linear feature by shadow techniques. (After Wise, 1968.)

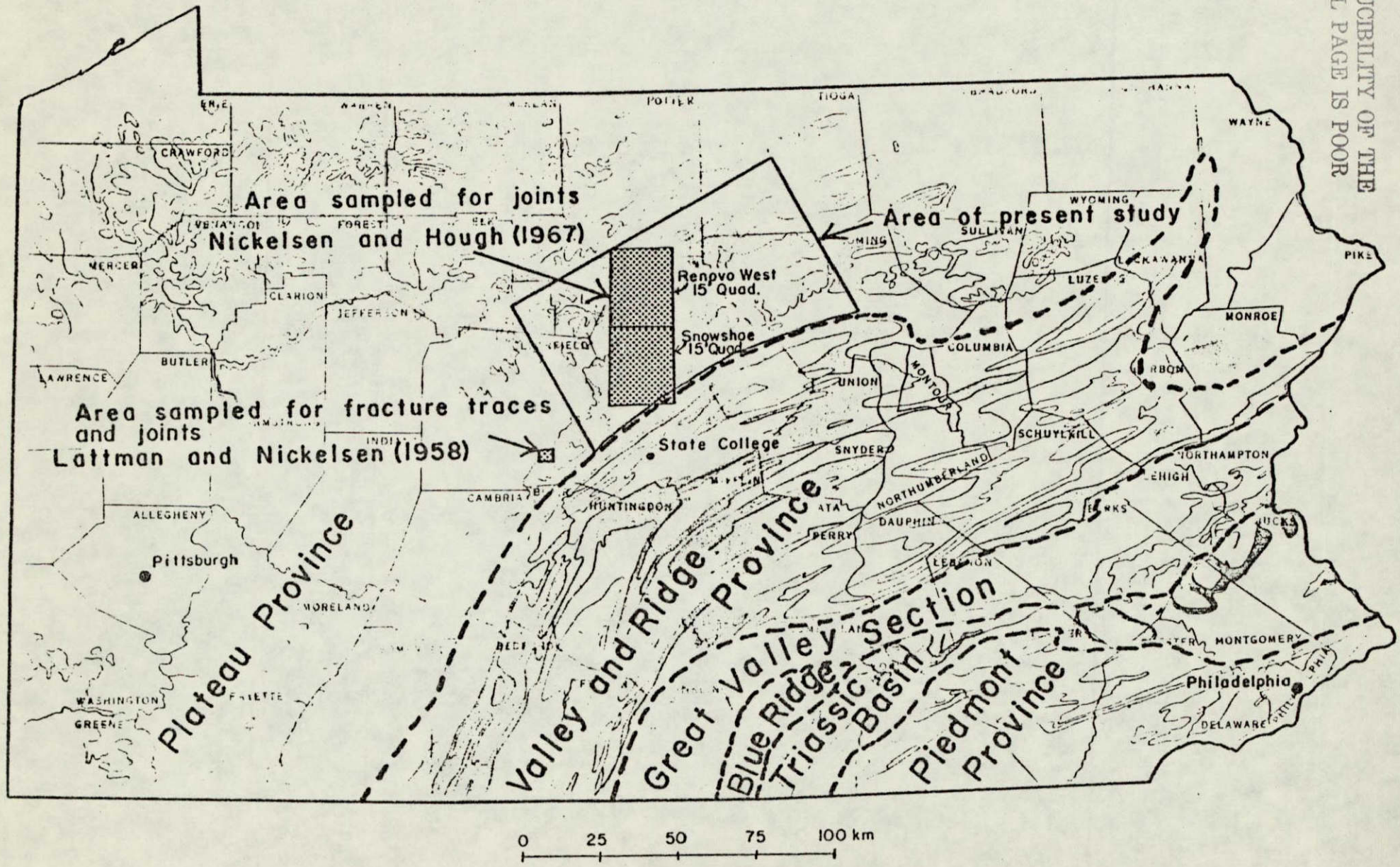

Figure 4-5: Site location map for studies discussed in sections 4.3 and 4.4. The base map is a geologic map of Pennsylvania (provided by the Pennsylvania Topographic and Geologic Survey).

Figure 4-6: Lineaments seen on Skylab and Landsat scenes, shown plotted on the Skylab scene (SL4, 4 January 1974, S190B, roll 91, frame 324). Solid lines indicate lineaments seen on both scenes. Those seen only on the Landsat image are shown as dashed lines, and those seen only on the Skylab photograph are shown as dotted lines. The Landsat lineaments (dashed and solid lines) are on the average three times longer than the Skylab lineaments (dotted and solid), and approximately 60% of the lineaments detected from Landsat have a Skylab lineament somewhere along them. The most prominent lineaments (solid) were detected from both altitudes. In the area considered here, the orientations of the lineaments determined from both scenes generally agree, with NW, N, and ENE trends predominating. (Note that the lineament plots on this scene have been offset slightly from the actual lineament in order not to obscure the linear feature on the photograph.)

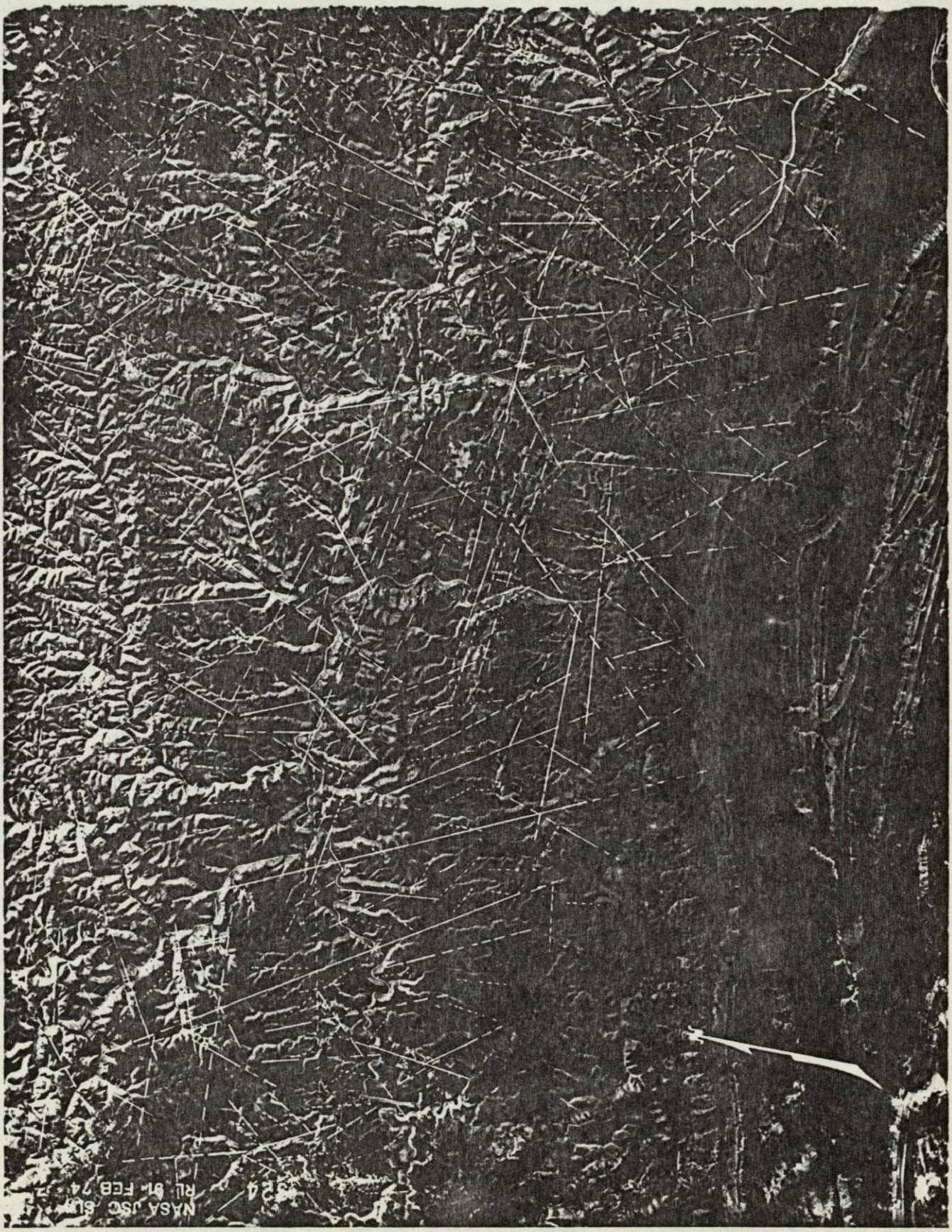

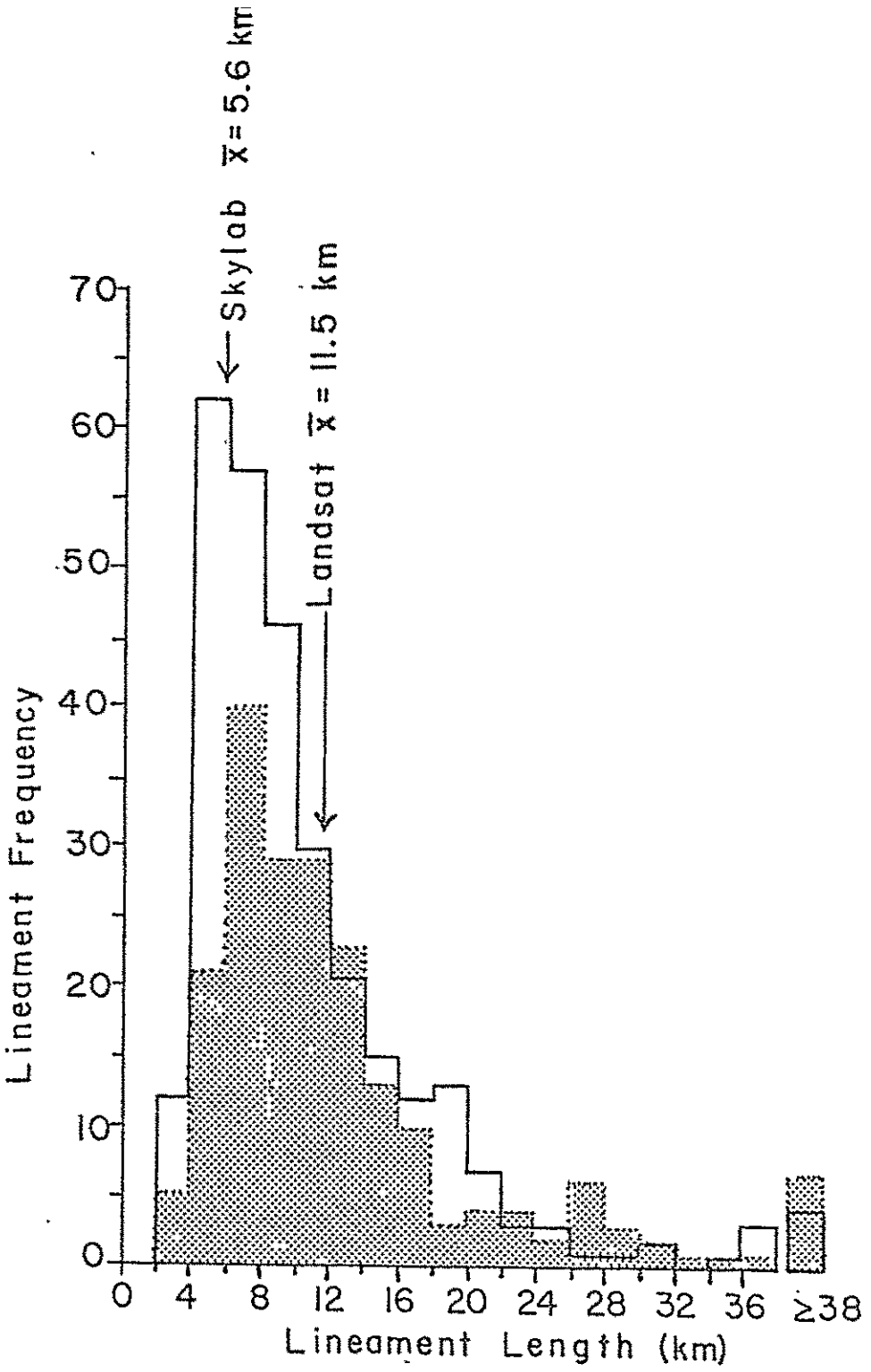

Figure 4-7: Lineament length distributions interpreted from Skylab and Landsat images. The shaded distributions are for the Landsat lineaments. Means are shown for both sets of lineaments.

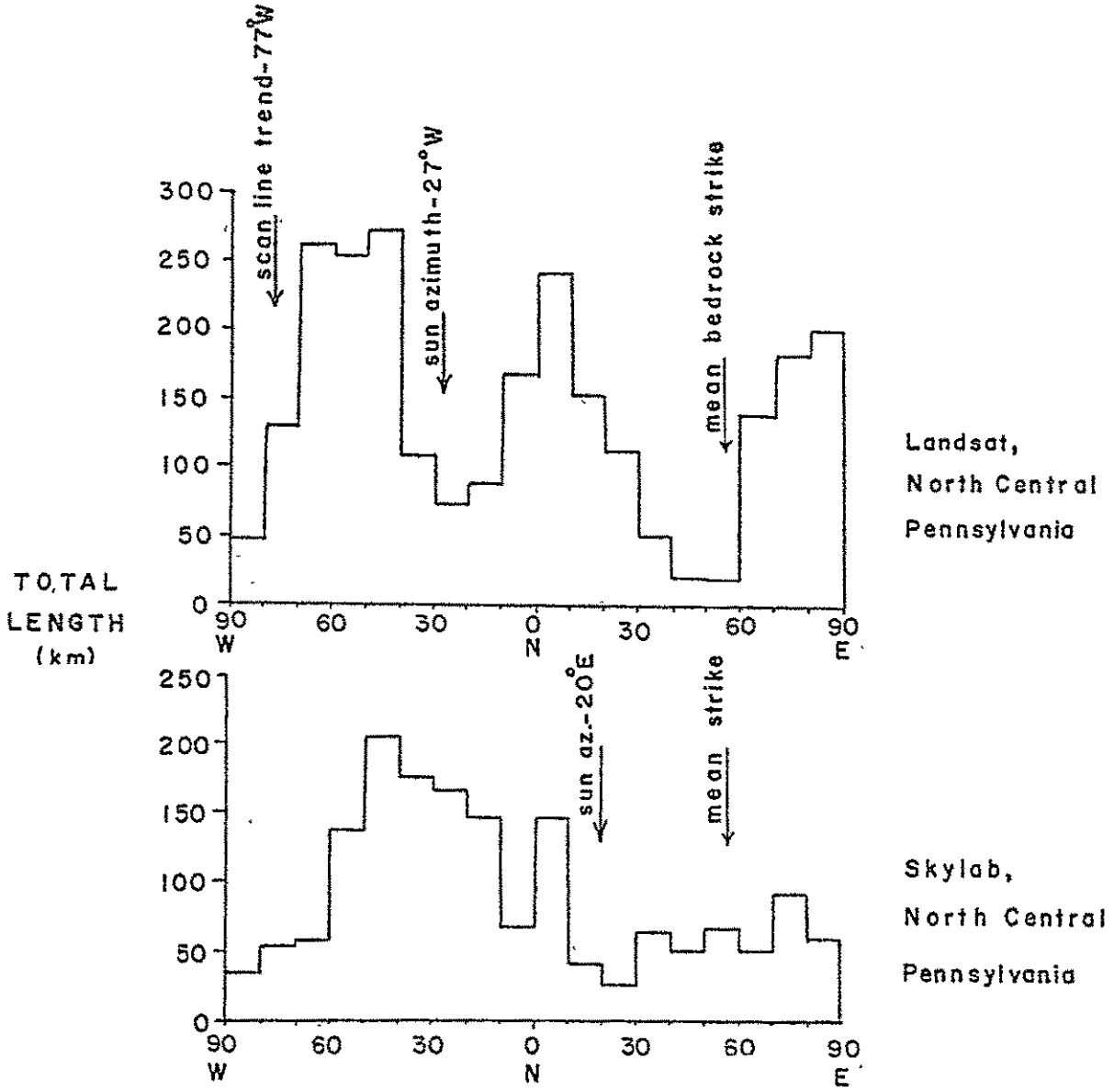

Figure 4-8: Summed length versus orientation histograms for Landsat and Skylab lineament interpretations.

Landsat histogram shows a double NW peak and the Skylab histogram shows a single broad peak at that position. The double Landsat peak appears to be primarily a function of the lack of lineaments parallel to the sun azimuth. The Skylab histogram also shows a decrease of lineaments near its sun azimuth.

The direction of maximum enhancement of the Landsat lineaments lies near the bedrock strike direction, near which lineaments were purposely not drawn. The major N-NW Skylab peak lies within the zone of optimum enhancement of lineaments on the Skylab photograph. It appears that this peak is real because the Skylab histogram does not show a symmetrical peak to the east of the mean strike direction where one might also be expected as a result of lineament enhancement.

A preliminary conclusion, therefore, might be that there is a bias against detecting lineaments parallel to the scan lines on Landsat images. However, the Skylab photograph, which lacks scan lines, also shows a paucity of lineaments parallel to the Landsat scan line direction (N77°W), and this suggests that the decrease in lineaments detected on Landsat images is not entirely artificially introduced.

The value of Skylab data is clearly demonstrated here, in that a lack of lineaments plotted in the Landsat scan line direction was thought to be entirely due to scan line bias, whereas Skylab photography has revealed it to be a combination of two factors: scan line bias and fewer actual lineaments oriented in that direction.

Sorting of lineaments by degree of expression showed that the straightest and best expressed lineaments lie between N40°W and N60°W on the Landsat image and between N10°W and N50°W on the Skylab photograph (Figure 4-9). This difference may be a result of the scale difference between Landsat and Skylab images, but the position of the respective sun azimuths suggests that the more well expressed Landsat lineaments may lie in the general trend of N30°W as they do in the Skylab photograph. It appears that if the illumination and strike biases were eliminated, the orientations would be much less peaked. However, the peak of the best expressed Landsat lineaments near the sun azimuth, where lineaments should be relatively obscured, must indicate an actual preferred orientation.

Figures 4-10 and 4-11 show rose diagrams of lineament orientation (created by means of the computer programs described in section 4.2) for Pennsylvania. In Figure 4-10, the diagrams are shown as plotted, whereas in Figure 4-11 the sun angle and scan line bias estimates have been added. The magnitude of these biases is estimated from an orientation diagram generated from lineaments mapped from Skylab photographs (Figure 4-9a), which have a different sun angle and are free of scan lines.

In summary, the Landsat lineaments, when compared with the Skylab lineaments, appear to be biased by illumination and scan line directions. While there is an illumination bias in the Skylab photograph, its direction does not coincide with the main transverse lineament trend, thus providing an independent assessment of the illumination direction bias. Skylab photography revealed that the apparent scan line bias in the Landsat lineament plots was due in part to a natural paucity of lineaments in the direction of the scan lines, and in part was an actual scan line bias.

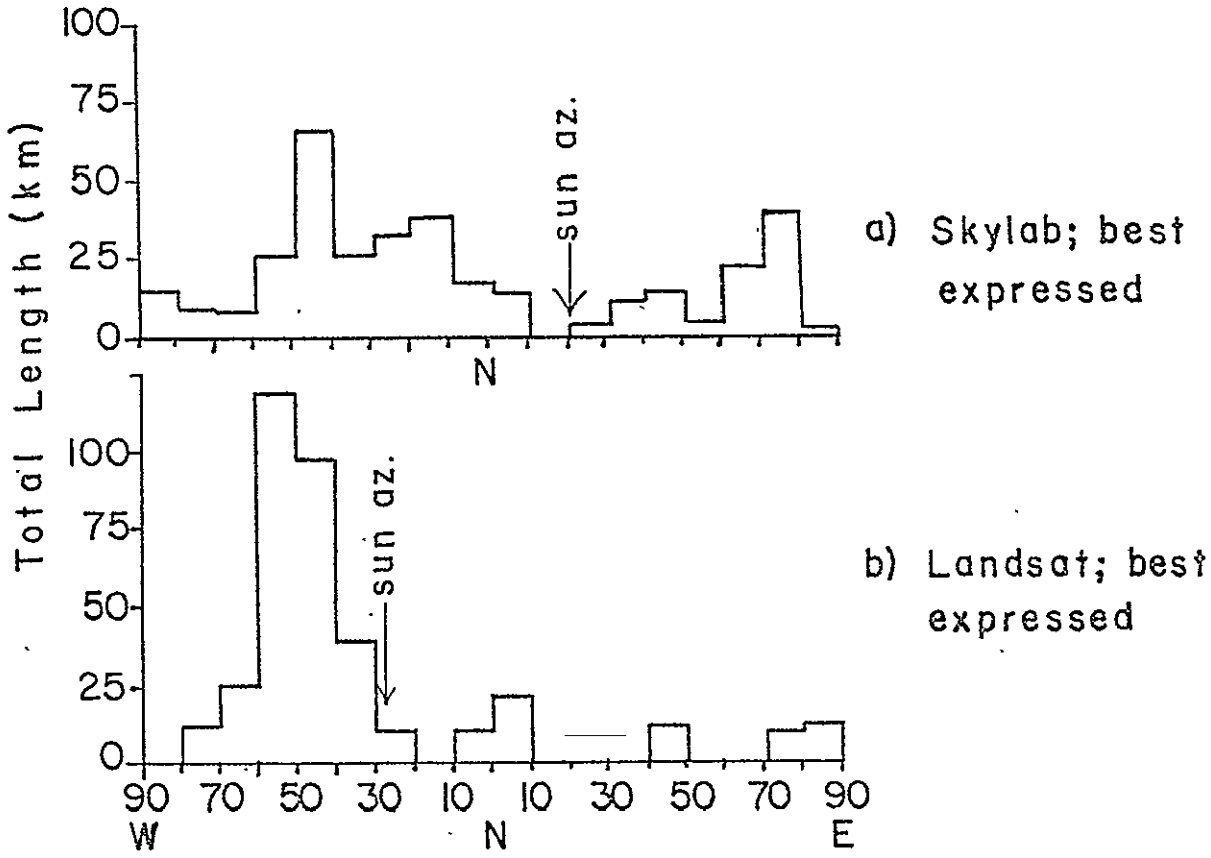

Figure 4-9: Summed length versus orientation histograms for the most linear and best expressed Skylab and Landsat lineaments.

Figure 4-10: Intermediate length lineament orientations, summarized in rose diagrams for cells (62 km by 85 km) on a grid across Pennsylvania. The scan line direction (WNW arrow), sun azimuth (two arrows for cells on overlapping images with different sun angles), and general strike of bedrock (NE arrow) are superimposed on each rose diagram. Note the general paucity of lineaments near these arrows, due to inherent biases (scan line effect and sun azimuth-shadow effects) in the system, and the artificial filtering of lineaments coinciding with bedding strike during the mapping process. The density of lineaments in each cell can be judged by the sum of their lengths, recorded in kilometers, in the lower left corner of each cell.

Figure 4-11: Orientation of intermediate length lineaments (heavy dot pattern), adjusted for possible scan line and sun angle biases (light pattern enclosed by dashed lines). The magnitude of these biases is estimated from an orientation diagram generated from lineaments mapped from Skylab photographs, which have a different sun angle and are free from scan lines, for the same test area. The estimated bias is approximately the smoothed quadrant between the peaks adjacent to the bias lines. The bedding strike bias has not been removed (see Figure 4-10).

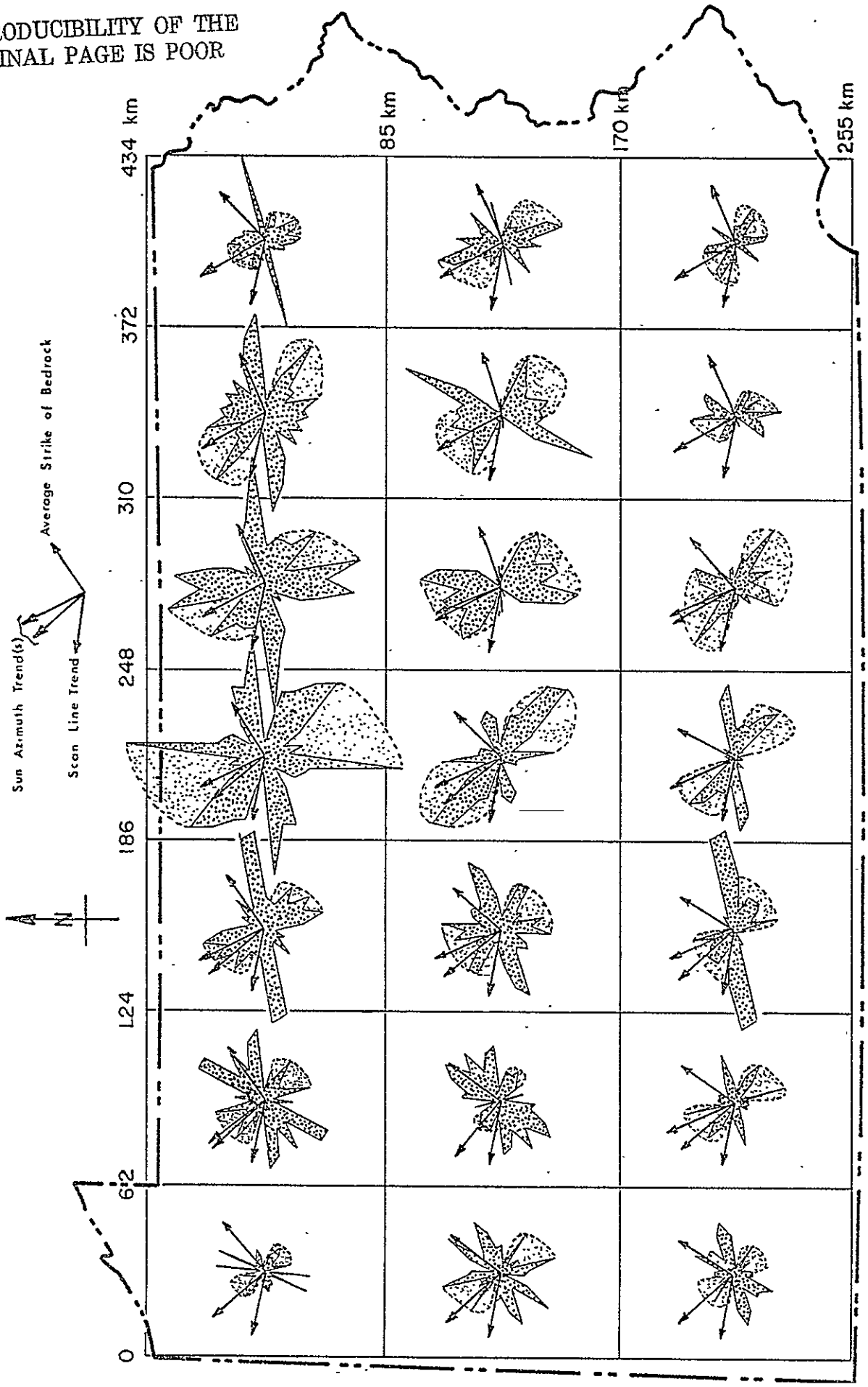

4.4 RELATIONSHIP OF LINEAMENTS TO JOINTS (Gold and Kowalik)

A geometric and/or mechanical relationship between joints, fracture traces[1], and lineaments[2] has been inferred (Gold, et al., 1973; Gol'braikh, et al., 1968; and Haman, 1964). In order to study the possible relationships between linear features at different scales, linear topographic and tonal features in parts of eight counties on the Allegheny Plateau (see Figure 4-5) were mapped and interpreted from a Skylab-4 photograph[3] and part of a Landsat-1 infrared image[4].

Immediately adjacent to the area considered here, Lattman and Nickelsen (1958) have shown that joint directions are typically subparallel to the fracture traces and that the fracture traces peak from N20°W to N45°W near Houtzdale. Elsewhere, in similarly undeformed strata, Hough (1960) and Boyer and McQueen (1964) have shown that joints lie subparallel to fracture trends on the Allegheny Plateau. Lineaments in the area studied here also lie subparallel to joints and to the fracture traces identified by Lattman and Nickelsen (1958). This subparallel orientation of joints, fracture traces, and lineaments suggests a genetic relationship for these features on the Allegheny Plateau.

The procedure for sampling the lineaments studied here is described in section 4.3. Length and orientation histograms are included in that section as well.

The major shale joint and coal cleat orientations in the Snowshoe and Renovo West Quadrangles (Nickelsen and Hough, 1967) are drawn on lineament histograms of the area in Figure 4-12. A shale joint peak at N35°W and a coal cleat peak at N25°W, both nearly perpendicular to bedrock strike, correspond with the peak of the Skylab lineaments in that direction. A poorer relationship exists between Landsat lineaments and joints. This is thought to be due to a significant illumination bias (see section 4.3) and the small sample of Landsat lineaments within the area covered by the 15-minute quadrangle maps. The histogram of all Landsat lineaments within the area (see Figure 4-12) shows the major peak near the main joint trends of N35-45°W over the entire area studied. (One may postulate that the Landsat NW peak should broaden northward and be similar to the Skylab peak if the Landsat illumination bias was not present.)

This agreement reflects the long observed and typical similarity of stream channel orientations (here largely forming the lineaments) and joint trends in undisturbed sedimentary rock (Van Hise, 1895; Hobbs, 1905;

---

[1] Linear features less than 1.6 km long (Lattman, 1958).

[2] Linear features greater than 1.6 km long (Lattman, 1958).

[3] S190B, 4 Jan 1974, roll 91, frame 324, color positive, 1:517,000 scale.

[4] Scene 1459-15221, 25 Oct 1973, channel 7, 1:989,000 scale.

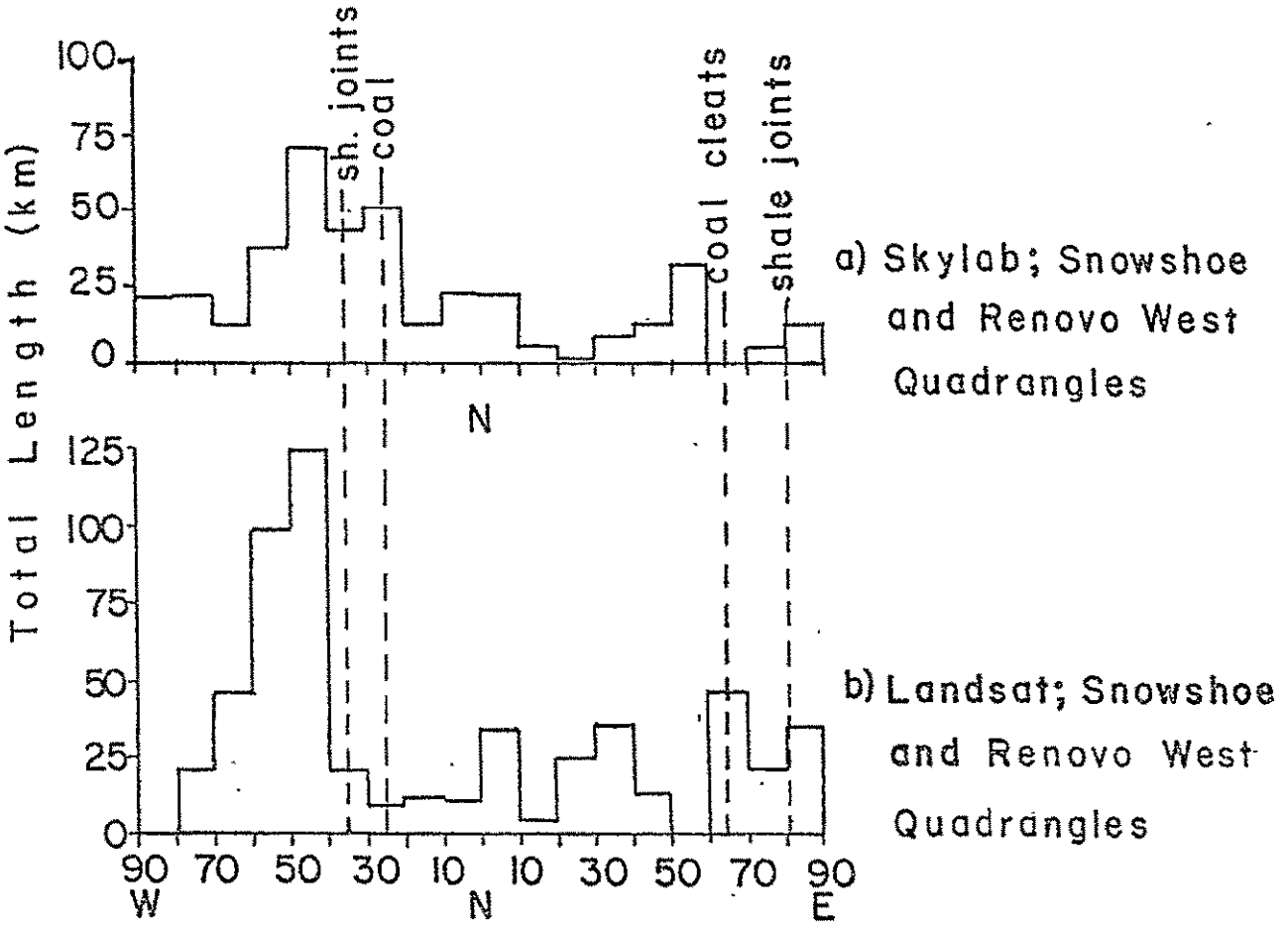

Figure 4-12: Summed length versus orientation histograms for lineaments in the Snowshoe and Renovo West 15 minute quadrangles for Skylab and Landsat data. (Joint and cleat orientations are from Nickelsen and Hough, 1967.)

Stone, 1964; and Thornbury, 1966). Because of the great scale difference between joints and lineaments, and because many lineaments cross drainage divides, the structural significance of lineaments must be more significant than simple parallelism with joints and reduced erosion resistance in the joint direction.

A second order relationship between lineaments of the size detected here and joints of lower order as envisioned by Gold, et al. (1973) would require changes in strike of 20° to 60°. Instead, joint directions tend to coincide with the strike of fracture traces and lineaments rather than lying in symmetrical peaks at acute angles to the linear topographic and tonal features. It seems likely that in undisturbed strata, joints and lineaments are differently scaled effects of a continuous range of natural linears of similar origin. It is notable that body forces have been invoked to explain the origin of joints (Hodgson, 1961), as well as of fracture traces (Blanchet, 1957) and of lineaments (Blanchet, 1957; Gold, et al., 1974). Price (1966) pointed out that several workers have noted an inverse relationship between joint frequency and bed thickness, holding other factors such as lithology and degree of tectonic deformation constant. Lineaments may be produced by body forces acting on mega-layers of the earth's crust in much the same fashion that fracture traces may be produced in structurally coherent thicknesses of strata. These same forces, at much higher frequencies, may also provide joints parallel to the larger lineaments in individual lithologic units.

In summary, the histogram peaks of lineaments mapped from the Skylab photograph at a scale of 1:517,000 lie subparallel, within 20°, to major shale joints and coal cleats in the part of the Allegheny Plateau considered here. The coincidence in direction, suggested by lineaments mapped on the Landsat images, if illumination and scan line bias derived from Skylab photographs is taken into account, indicates a geometric relationship between joints, fracture traces, and lineaments which is more consistent with a tensional model than a shear model of origin.

4.5 FIELD STUDY OF LINEAMENTS IN CROSS-SECTION (Gold and Krohn)

Construction on a portion of the Route 220 bypass at Tyrone, Pennsylvania, (Figure 4-13), revealed highly variable bedrock conditions suspected to be related, in part, to the Tyrone - Mount Union lineament transecting the ridge at the construction site. Existing geological maps are too general in scale to predict such conditions, and poor exposures in Bald Eagle Valley, especially on the lower hill slopes, render geological mapping a difficult and imprecise task. The construction site presented an excellent opportunity to study a lineament in cross-section. The lithologic exposures at the site also presented the opportunity to determine the nature of linear patterns seen parallel to the valley trend on both the Landsat Imagery (Figure 4-14) and the Skylab photography (Figure 4-15). These appeared to represent lithologic units and boundaries, and verifying these as geologic contacts in the new road cuts is important ground control for establishing their use for geological mapping from satellite data in central Pennsylvania.

The exposure at the Route 220 bypass roadcut, therefore, presented an opportunity for obtaining ground truth information for a variety of linear features seen on Skylab and Landsat scenes. A summary of the images and photographs assembled for this study is presented in Table 4-1.

The new highway along the western flank of Bald Eagle mountain and northeast of Tyrone (Figure 4-15) parallels the ridge from the village of Bald Eagle to south of Grazierville and spans three lineaments (AA, BB, CC of Figure 4-14). The road cuts were monitored during construction for rock type, lithologic contacts, and anomalous structural conditions, and selected areas were singled out for detailed mapping. These detailed observations helped establish the continuity and strike of transgressive features picked up in mapping the ridge crest and the Tyrone - Mount Union lineament along the Little Juniata River valley (studies in progress).

Structurally, the western flank of Bald Eagle ridge represents the steeply dipping northwest limb of the Sinking Valley anticline (Butts, 1939). By analogy with the overturned beds where Route 322 crosses the ridge to the northeast, the overturned beds exposed in the road cuts are not anomalous, but the degree of fracturing and faulting encountered was far greater than indicated on the geologic map by Butts (1939). As long as competent rocks were left in the road cuts, the resulting slopes should be stable, but a combination of steeply dipping beds and thin units with intercalated shale, necessitated stabilizing most of the slopes. Two zones of poorly drained and friable material were of interest because they coincide with the trace of lineaments AA and CC (DD may also be involved near its intersection with CC). The road cuts in these localities remained unstable; hill-side creep was active and small land slides developed on the graded slopes, especially during the spring thaw and runoff, and at times of heavy and prolonged precipitation. A large volume of material was excavated from the site at AA.

The excavations (Figure 4-16) about 1 km southwest of Bald Eagle village (close to the intersections of lineaments CC and DD) are important for the exposures of Helderberg limestone, Oriskany sandstone, Marcellus

Figure 4-13: C130 scene of the construction site. (Mission 230, 15 April 1973, roll 74, frame 227.)

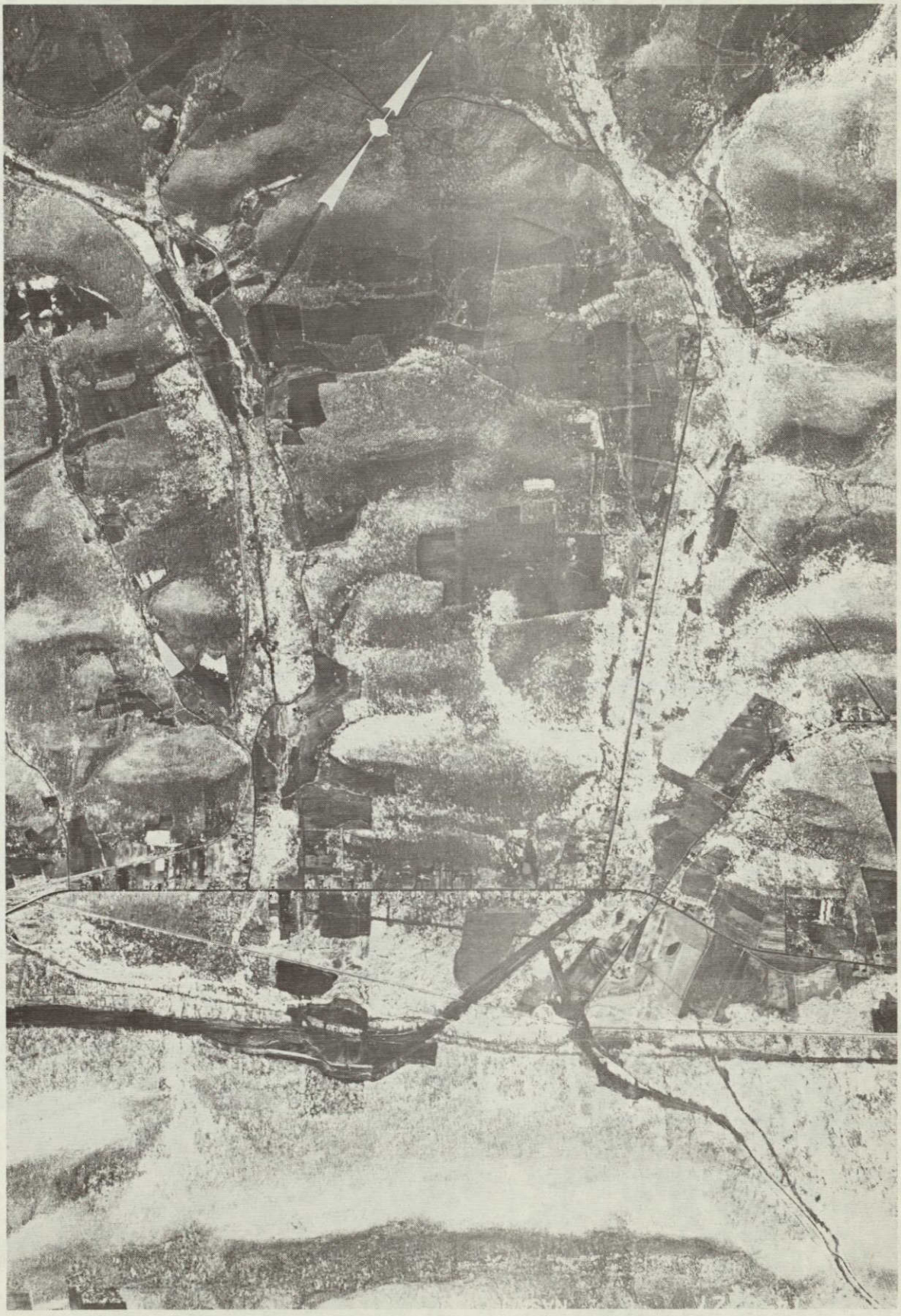

Figure 4-14: Enlargement of Landsat-1 scene with lineaments plotted across Bald Eagle Ridge. (Scene 1243-15253, channel 7.)


10
0
10
Km
N
M
O
P
K
J
I
H
G
F
E
D
C
B
A

Figure 4-15: Highway construction transverse to the Tyrone - Mount Union lineament, seen on an enlargement of the Skylab photograph. The short white arrows indicate the construction site; the black arrows show the trace of the Tyrone - Mount Union lineament. (SL3, S190A, orbit 14, roll 21, frame 192, enlarged 2X from the 230 mm photograph.)

Table 4-1: Summary of Data Used for the Lineament Cross-section Study

Source	Approx. Scale	Mission/Sensor Roll/Frame	Date	Image Type	Comments
Landsat-1	1:1,000,000	1045-15243-7	6 Sep 72	B&W 0.8-1.1μ	General physiography and structure apparent.
Landsat-1	1:250,000	1243-15253-7	23 Mar 73	B&W enlarg. 0.8-1.1μ	Image with good depth and clarity, minimum vegetation cover; base for lineament and geological mapping.
Landsat-1	1:1,000,000	1513-15220-7	18 Dec 73	B&W 0.8-1.1μ	Gross structure apparent; used for checking lineament mapping.
Skylab-3	1:700,000	Orbit 14, S190A Roll 21, fr. 191-192	5 Aug 73	Color IR 0.5-0.88μ	Complete view of the Tyrone-Mount Union lineament to South Mountain. Cloud-free.
Skylab-4	1:700,000	Orbit 73, S190A Roll 55, fr. 317	4 Jan 74	B&W 0.7-0.8μ	Scattered cloud over study area. Structure on Allegheny Plateau shows well, as does lithology in Bald Eagle Valley. Suitable base for geological mapping.
U2	1:130,000	Mis. 016, sensor 23 Fr. 6120 & 6121	5 Feb 74	B&W enlarg. of color IR 0.59-0.90μ	Shows U.S. Route 220 bypass, ridge crest offset, and lithology in Bald Eagle Valley. Useful for transferring lineaments.
U2	1:130,000	Mis. 060A, sensor 17 Fr. 8127 & 8128	25 Apr 74	B&W enlarg. of color IR 0.59-0.90μ	As above.

(Continued)

Table 4-1 (Continued)

Source	Approx. Scale	Mission/Sensor Roll/Frame	Date	Image Type	Comments
U2	1:130,000	Mis. 009, sensor 12 Fr. 80 - 82	25 Jan 73	B&W enlarg. 0.58-0.68μ	As above. Flight along the Tyrone - Mount Union lineament.
C130	1:30,000	Mis. 230, roll 74 Fr. 226 & 227	15 Apr 73	Color IR 0.5-0.9μ	Useful for positioning road cut (see inset in Figure 4-16).
USDA Aircraft	1:40,000	42013-271-86 & 87	13 Jul 74	B&W ~0.5-0.7μ	Fault and offsets not apparent. Road and construction sites show up well.
USDA Aircraft	1:20,000	AQH-6V-34 & 35	7 May 58	B&W ~0.5-0.7μ	Flown prior to road construction; useful for fracture trace mapping. Valley lithology not apparent.

Figure 4-16: Aerial view of US Route 220 bypass, 1 km southwest of the village of Bald Eagle. Lineament trace coincides with the main curved section of the exit ramp. Note the slump features.

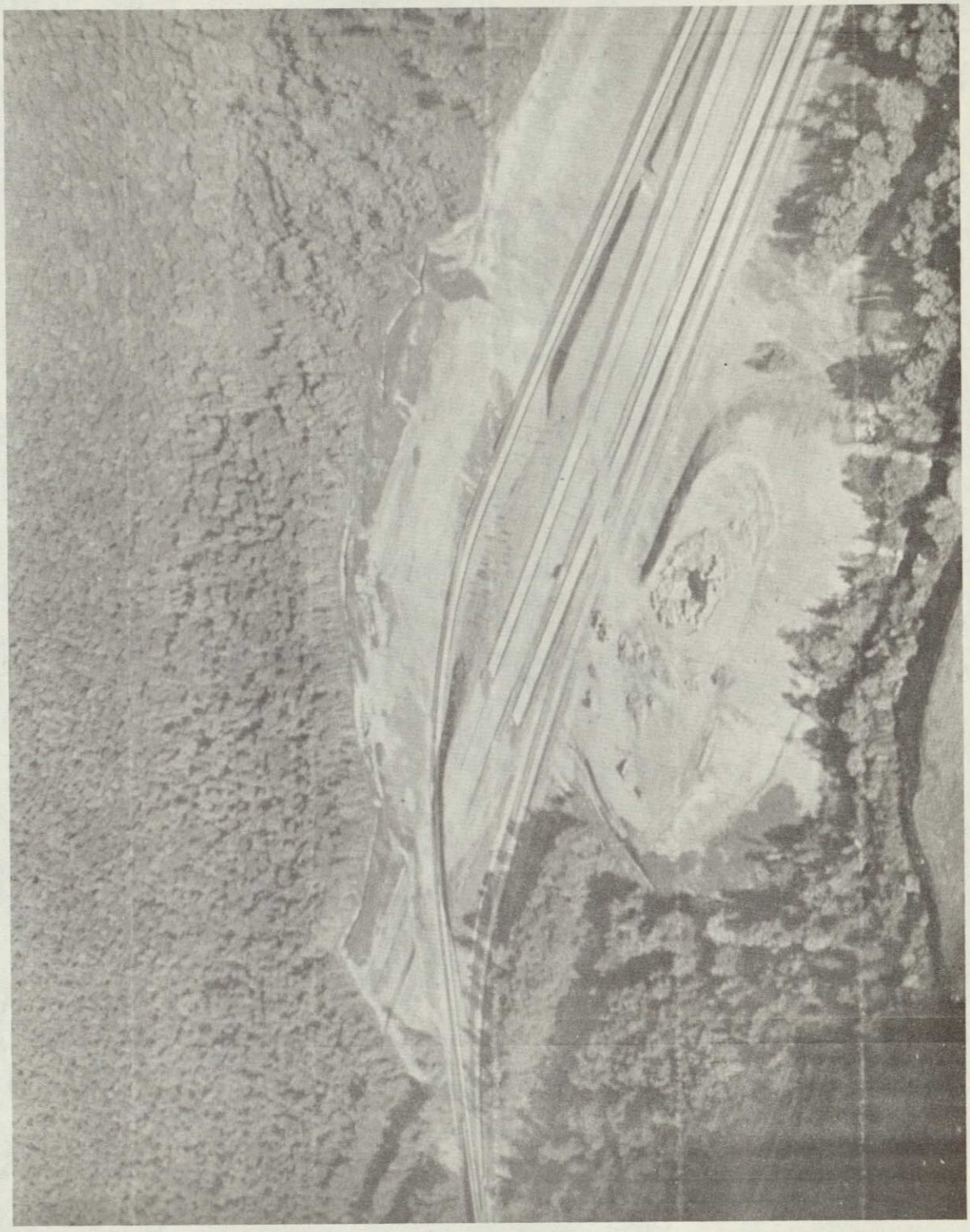

shale, a fault, and two zones of fractured rocks. The geology was mapped in a plane table survey on a scale of 1:1200 (Figure 4-17) which was updated as construction revealed new attitudes and before bedrock was excavated or contacts covered by the road bed.

Along the exit ramp, north to route 350 (see inset, Figure 4-17), the following sequence of steeply dipping to overturned beds are encountered:

1. A coarse to medium-grained sandstone, grey limestone (fragmental and fossiliferous in places).

2. A brown-weathered shale grading down-section into a black shale, and

3. A highly friable sandstone overlain by talus near the northern end of the road cut.

The sedimentary contact between the sandstone and limestone is well exposed, and these beds represent, respectively, the Oriskany and the Helderberg Formations in faulted contact with the younger Marcellus shale member of the Hamilton Formation. This fault, which strikes northeast across the road, is transverse and exhibits right lateral separation. A ridge offset to the east with the right sense of displacement is apparent on the Landsat imagery, as well as on the Skylab and U2 photographs (see Table 4-1 for frame numbers). About 200 m farther north, friable sands from the brecciated Oriskany Formation (probably the Ridgeley Sandstone member) were exposed at the base of the road cut and are overlain by a deep talus. This zone extends for about 100 m into talus near the northern end of the embankment.

In places, the sandstone was saturated with water, promoting a quick condition in some of the material. Hillside creep was active and small slumps were common (Figure 4-18). A large part of the bank was excavated during the summer of 1975, when it threatened to slide.

That this zone is a conduit for ground water was demonstrated during the spring of 1975, when the concrete road bed broke and heaved approximately 30 cm. Test holes drilled through and adjacent to the road bed showed a rise in the piezometric surface of about 1 m, and artesian water flowed through the top of the pipes (Figure 4-18).

It is concluded that the zone of fractured material represents a zone of high porosity and permeability, which is collecting and channeling ground water, resulting in the development of landslides on artificial slopes. There appears to be a good correlation of these zones with lineaments seen on Landsat and Skylab photography.

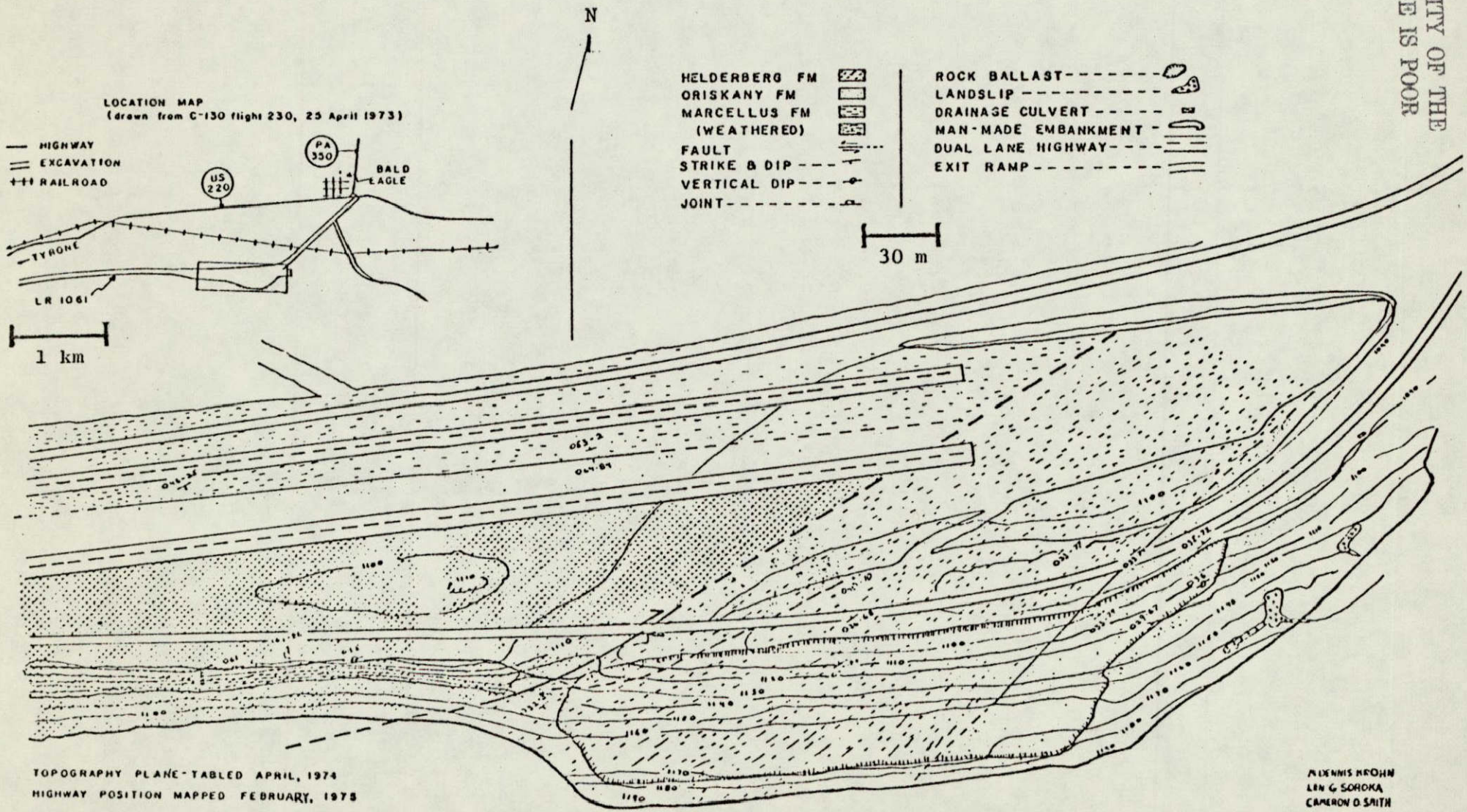

Figure 4-17: Plane-tabled geologic map of a portion of the construction site for the Route 220 bypass.

Figure 4-18: Enlarged view of a portion of the study site, showing a small landslide on the slope. Note the change in grade of the roadbed (heaved approximately 30 cm) and the artesian water flowing from the pipe in the foreground.

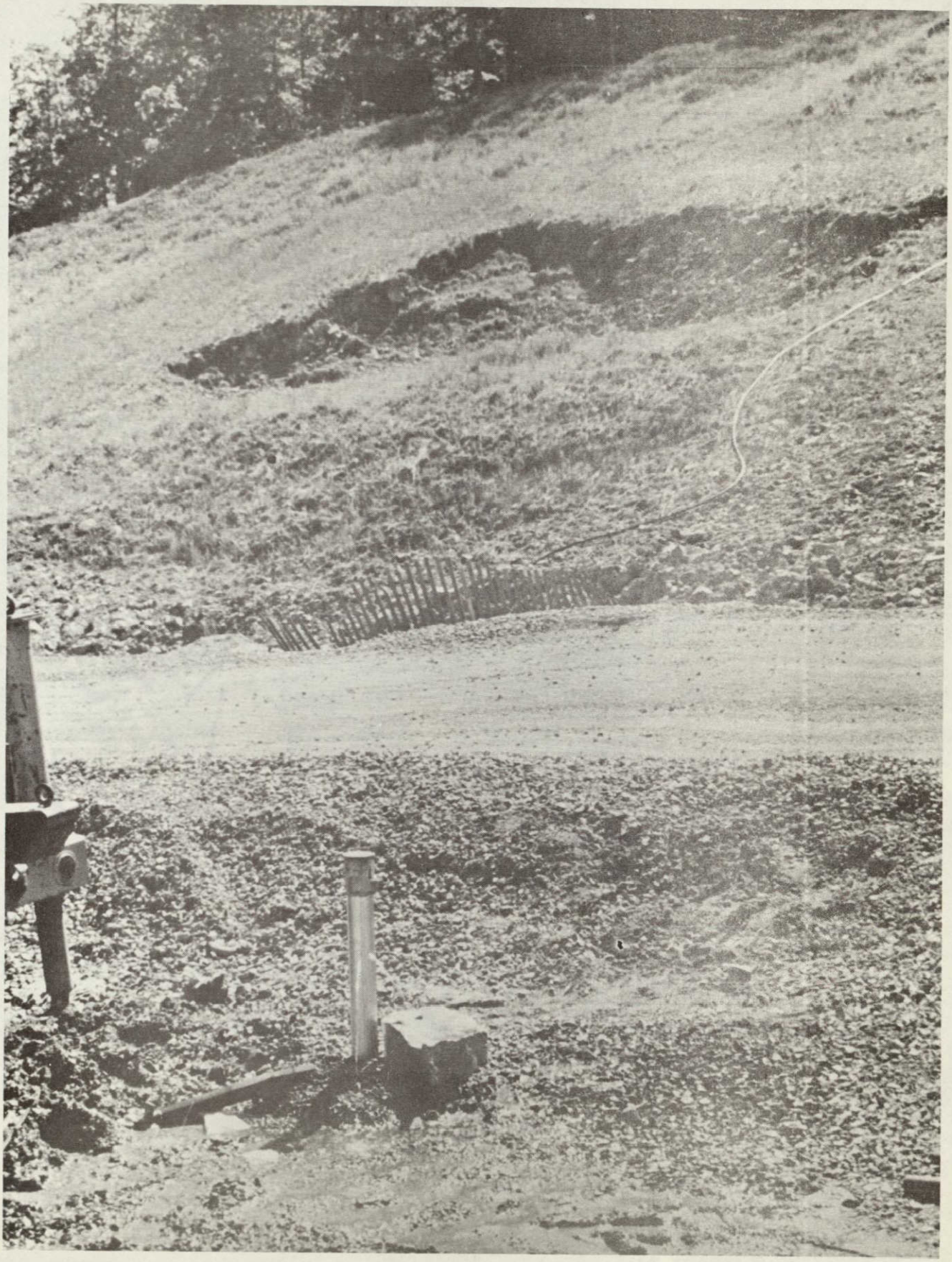

4.6 RELATION OF LINEAMENTS TO GEOLOGIC STRUCTURE (Gold and Kowalik)

Lineaments represent a significant class of structural elements. Their recently detected universal occurrence has generated a resurgence of studies of global fracture patterns which may tie into plate tectonics. Ground truth investigation (geological and geophysical probing for the three-dimensional aspect) has been aimed toward characterization of these features, to facilitate the development of genetic classification as well as to assess their economic potential and utility. The Landsat program has spurred the development of a theory (first offered by Moody and Hill, 1956) to account for the size and frequency of linear features on all scales. This theory is being refined by Gold, et al. (1973) to facilitate dynamic analyses of stress distribution. The increased detail available on Skylab photographs (see Figure 4-3 and 4-19) is of invaluable assistance in this effort.

The longest lineaments (>100 km) detected on Landsat images of Pennsylvania are probably buried tear faults, as defined by Gwinn (1964) in the Paleozoic strata overlying the basal Appalachian decollement (Figure 4-20). These may also be basement related, as they appear somwhat analogous to two lineaments described in Alabama by Drahovzal, et al. (1973), which are evidently basement controlled. One of these in Pennsylvania, the Everett Lineament (Figure 4-19), if extended across part of the Great Valley, also traverses the Blue Ridge, suggesting that the basal decollement extends below the Blue Ridge toward the east.

Most shorter lineaments are not obviously expressed as "Gwinn-Type" lineaments, which characteristically pass along the noses of plunging folds. The origin of shorter lineaments may be more consistent with a tensional than a shear model. In any event, a relationship in mechanism between joints, fracture traces, and short lineaments is suggested by the coincidence in direction, regardless of scale, of linear features studied in an area of the Allegheny Plateau in central Pennsylvania. The majority of the 2,200 lineaments mapped (see Figure 4-2) are of unknown origin but are suspected to be related to continuously operating earth body forces.

Many shorter lineaments trending across strike may be related to tears in upward splaying thrusts. The passage of many probable buried tear faults through wind and water gaps indicates that the gaps are points of structural weakness and are not randomly located, as theories of drainage superposition contend.

A preliminary examination of the relationship of lineaments observed on Skylab and Landsat scenes to such aeromagnetic intensity maps as are available for Pennsylvania, reveals a distinct difference between the correlation in the western and eastern portions of the state. In western Pennsylvania, where the lineaments appear to connect magnetic lows, the magnetic amonalies are thought to be basement controlled. In the eastern portion of the state, however, the anomalies are highly concentrated and tightly intertwined, with no visible relationship between lineaments and the magnetic patterns. The implication of these differences has not yet been studied.

Figure 4-19: Two major Pennsylvania lineaments which show clearly on both Skylab and Landsat scenes. (Shown here on SL3, orbit 14, S190A, roll 19, frame 192.) Five Pb-Zn occurrences are associated with the Tyrone - Mount Union lineament. Both features are probably buried tear faults (see Figure 4-20), as defined by Gwinn (1964), and are suspected to be associated with the basal Appalachian decollement.

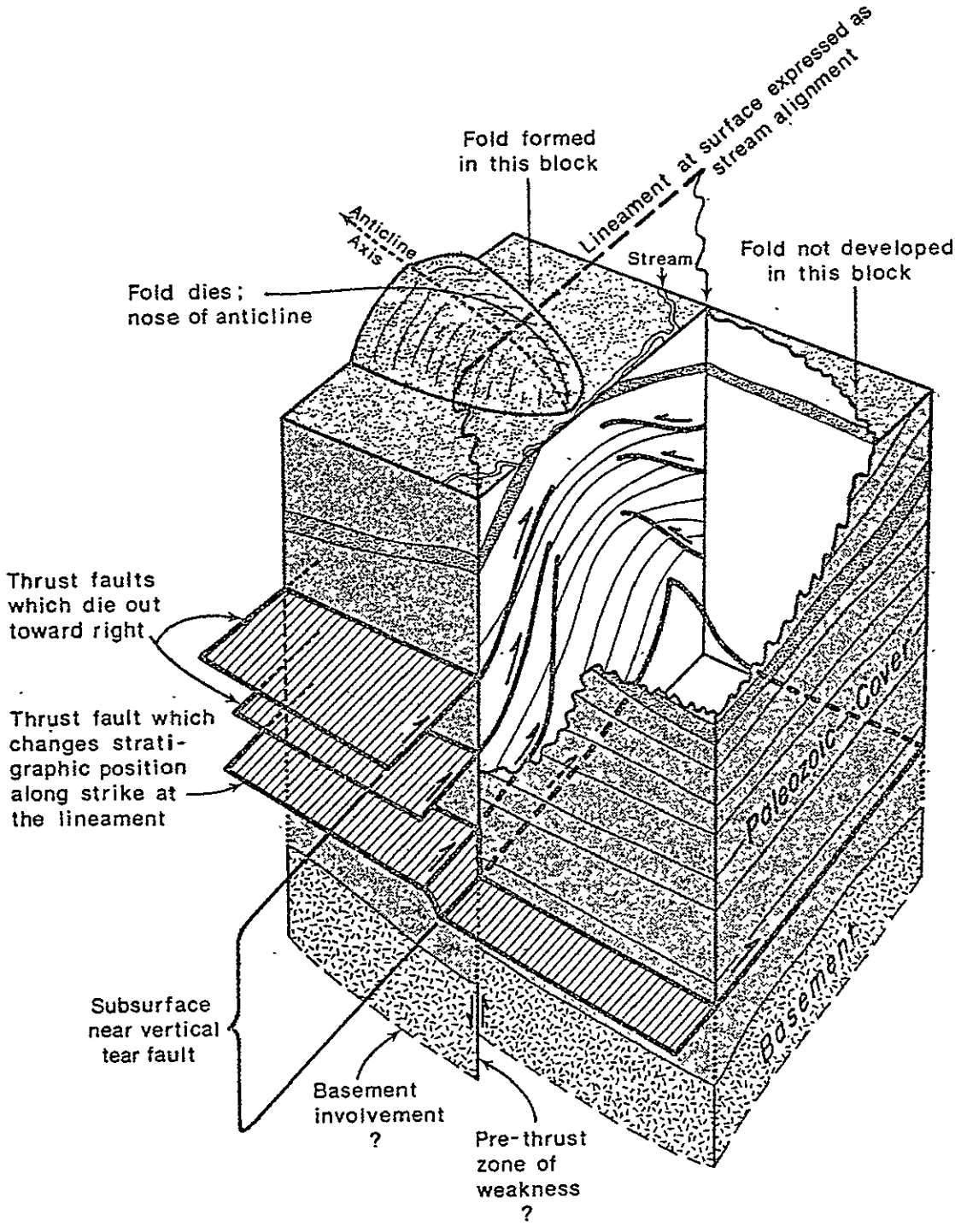

Figure 4-20: Idealized block diagram showing the postulated third dimensional structure of a "Gwinn-type" lineament (Gwinn, 1968). These lineaments are thought to represent the boundary between semi-independent thrust blocks.

There is no doubt that continuing studies of these features are greatly assisted by data at the Skylab scale, for the key to both their origin and their economic significance lies in being able to relate lineaments to mesoscopic structural elements on the ground. On Landsat images, the information is generalized, and in generalizing one can be misled in both location and interpretation. These preliminary studies of the Skylab data available for Pennsylvania have shown that a high level of accuracy in location can be obtained from the data. Hence, ground truth correlation is greatly facilitated.

Some specific advantages of Skylab photography for geologic mapping are listed below:

Regional Color Contrast: The color photographs (both S190A and S190B) covering large areas made it possible to identify rock units by virtue of their color and areal extent. This is a distinct advantage over Landsat images, where the natural color and adequate resolution is lacking; and over aerial photography, where the coverage is not sufficiently extensive in a single scene. Skylab photography was of great assistance in mapping red beds of large areal extent.

Improved Resolution: The Skylab color transparencies exhibited greater resolution and detail than the Landsat color composites, with only about a 25% difference in scale. Valley floors and tributary streams are seen on the Skylab S190A and S190B visible color and color IR photography not only with greater clarity than on the Landsat scenes, but also free from scan bias, and the ground locations of the features seen are established far more accurately. The black and white S190A Skylab photography studied by ORSER was not as good as the best Landsat images, being rather flat and having less contrast than the Landsat black and white images. However, only the available Skylab photography was compared with the best available Landsat imagery of the same area, and the option of optimum seasonal coverage was not available. Thus, atmospheric haze on the particular day of the Skylab pass could have been the source of the difficulty. Another possible explanation could be differences in the gray scales of the Skylab and Landsat black and white photographs, because the Skylab color transparencies were clearly better than the Landsat color composites or black and white images. For lineament mapping purposes, the winter scenes were the best.

4.7 LINEAMENTS AND MINERAL OCCURRENCES (Gold and Kowalik)

Smith, et al. (1971), Drahovzal (1973), and Krohn and Gold (1975), have cited possible genetic associations of lineaments and mineral occurrences in the Appalachians. Other workers have noted an association between the increased density of lineament intersections and major mining districts in Nevada and Colorado (Levandowski, et al., 1973; Jensen, 1973; and Nicolais, 1973).

Preliminary work with the Tyrone - Mount Union Lineament (see Figure 4-15 and 4-19) identified by ORSER geologists from Landsat imagery, which has several mineral deposits along it, indicated the possible significance of further work in establishing the extent of correlation of lineaments with ore deposits. Skylab photography, with resolution improved over that of Landsat imagery, has been of great assistance in this effort, limited only by its restricted coverage of Pennsylvania and cloud and snow cover on pass 73 of Skylab-4, the only pass over the central portion of the state.

4.7.1 The Mineral Deposit Map

As part of the program to study possible relationships between the occurrence of base metal deposits and structural features identified from satellite imagery, a library search was initiated for reports on base metals and kimberlite intrusions in Pennsylvania. Fortunately, most of the earlier reports had been culled and the results tabulated by Rose (1970; reprinted in 1973) as Part 3 of the "Atlas of Pennsylvania's Mineral Resources." The pre-1968 literature is listed by Rose and cross-indexed by county and locality in his report. Post-1968 sources used in completion of the map in Figure 4-21 are listed separately in ORSER-SSEL Technical Report 14-75: "Lineaments and Mineral Occurrences in Pennsylvania," by Kowalik and Gold (1975). Because of the small scale of the map, reference to the original sources should be made for the detailed location of each site.

All of the metal mines, base metal occurrences, and kimberlite dikes reported in Pennsylvania have been plotted on Figure 4-21, an updated version of the map accompanying the Atlas of Pennsylvania's Mineral Resources (Rose, 1970). This plot was originally made at the scale of 1:250,000. Using the classification proposed by Rose (1970), the base metal occurrences were plotted as symbols according to relative size (or dollar value of production) and by letter designating one of 22 different types, based on structural setting, composition, and age of host rock. The details of the classification scheme are given in Table 4-2, which also serves as the legend and the key to the types of deposits in Figure 4-21. The kimberlite localities have been included in this study because they indicate regions of crustal tension at the time of emplacement (Gold, 1973).

4.7.2 Mineral Deposits and Lineament Association

Although plotting of the base metal localities was accomplished best on a large scale map (1:250,000), the accuracy of transferring linear

Figure 4-21: Mineral deposit map of Pennsylvania. The key to the symbols used on this map may be found in Table 4-2.

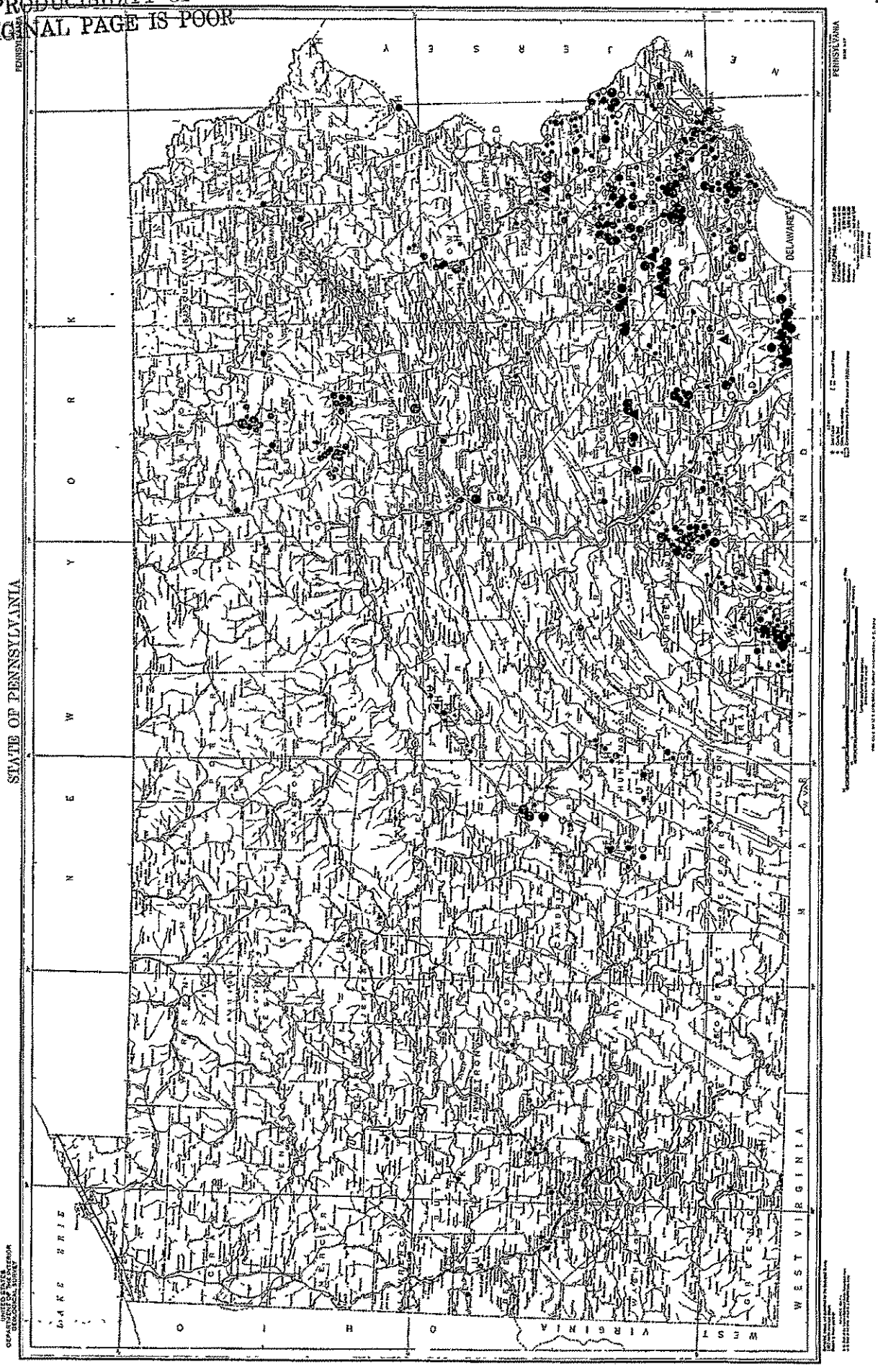

Table 4-2: Metallic Mineral Occurrences in Pennsylvania[a]

VALUE OF MINERAL OCCURRENCE

- ▲ COMMERCIAL DEPOSITS HAVING PRODUCED MORE THAN $1,000,000 IN VALUE
- ◉ COMMERCIAL DEPOSITS HAVING PRODUCED LESS THAN $1,000,000 IN VALUE
- ⊙ MINERAL PROSPECTS
- • MINERAL LOCALITIES; —◈— KIMBERLITE DIKE LOCALITIES

TYPE OF MINERAL OCCURRENCE

PRECAMBRIAN AND PIEDMONT HOST ROCK GROUP

- TYPE A: CR WITH MINOR NI, CU, AND FE, ASSOCIATED WITH ULTRAMAFIC ROCKS
- B: NI AND CU SULFIDES WITH MAFIC TO ULTRAMAFIC ROCKS (GAP NICKEL)
- C: MO, CU, U AND OTHER ELEMENTS IN PEGMATITES, OR ASSOCIATED WITH PEGMATITES
- D: CU AND OTHER ELEMENTS IN GNIESS, SCHIST, METAGABBRO AND RELATED ROCKS
- E: NATIVE CU AND CU SULFIDES IN METABASALT (LAKE SUPERIOR TYPE)

PALEOZOIC HOST ROCK GROUP

- F: APPALACHIAN-TYPE ZN-PB DEPOSITS IN CAMBRO-ORDOVICIAN LIMESTONE
- G: ZN-PB SULFIDES IN HELDERBERG-TONOLOWAY LIMESTONES
- H: OTHER ZN-PB IN SEDIMENTARY ROCKS
- I: BARITE IN LIMESTONE
- J: ZN-PB-CU SULFIDES AS FRACTURE FILLINGS AND VEINS IN LIMESTONE
- K: WURTZITE AND OTHER SULFIDES IN NODULES
- L: SANDSTONE-TYPE CU-U, U, AND CU DEPOSITS

TRIASSIC HOST ROCK GROUP

- M: CU, AU, AND OTHER ELEMENTS IN TRIASSIC DIABASE
- N: CORNWALL-TYPE MAGNETITE-CUPPER DEPOSITS
- O: CU IN TRIASSIC SEDIMENTS ADJACENT TO DIABASE, AND RELATED DEPOSITS
- P: CU IN TRIASSIC SEDIMENTS DISTANT FROM DIABASE
- Q: ZN-PB-CU IN QUARTZ VEINS CUTTING TRIASSIC AND PRECAMBRIAN ROCKS
- R: U IN TRIASSIC SEDIMENTS

UNCLASSIFIED GROUP

- S: OTHER CU
- T: OTHER NI
- U: OTHER BARITE
- V: PLACER DEPOSITS
- W: MISCELLANEOUS

[a]From Rose (1970)

features mapped on standard size Landsat and Skylab scenes declines with increasing scale. Except for the original lineament plots, therefore, the lineament map was produced by the CalComp plotter from the digitized data at the intermediate scale of 1:380,160 (the scale of the Stream Map of Pennsylvania) as a compromise in scale suitable for merging of the two sets of data.

Typical widths and the subsurface nature of lineaments are poorly known or understood. Recent sampling by Krohn and Gold (1975) along the crest of Bald Eagle Mountain suggests that lineaments transecting the ridge are underlain by a disturbed zone with anomalous faulting, jointing, and brecciation averaging 1 km wide and ranging from 0.65 to 2 km in width. Assuming this applies to the valleys as well as to the quartzite ridge crest, and to the remainder of the state as well as to Bald Eagle Mountain, the 1 km wide zone is accepted here as a practical working width for the anomalous bedrock fracturing of a lineament. This width was used here in deciding whether a particular mineral occurrence is on or off a lineament.

Figure 4-22 shows the lineament map of Pennsylvania with lineaments associated with mineral localities numbered (Kowalik and Gold 1975). Lineaments are approximated on the figure by straight lines, and mineral occurrences are represented by circular dots. In reality, lineaments may vary in linearity (when viewed at larger scales), in width, in origin, and in the type and intensity of fracturing. Similarly, the shape of the mineral occurrences varies. Despite these approximations, this lineament - mineral occurrence comparison provides a first order measure of the association of mineralized areas with the lineaments mapped.

Tables of mineral occurrences lying on 1 km wide lineaments are given in Kowalik and Gold (1975). Each table lists, by host rock age, the lineament class and type, and the type of mineralization, the county-number identification code devised by Rose (1970), the name of the occurrence, and the known value contracted from the occurrence. It should be remembered, however, that these lists of mineral occurrences coincident with lineaments do not necessarily imply of themselves a genetic relationship, for several reasons: 1) the large numbers of lineaments and mineral occurrences makes chance associations inevitable; 2) lineaments frequently lie along major valleys, the walls of which are commonly the most favorable site of outcrops and, therefore, of mineral discovery; and 3) in a soil-and-vegetation covered area such as Pennsylvania, the chances of discovering a mineral locality in an inter-lineament area is probably lower than average -- again, because of the paucity of outcrops.

It is not possible to identify and isolate these sources of bias at this stage of investigation. However, the fact that of 383 known mineral occurrences, 116 show a geographical association with lineaments and another 25 lie at intersections of two lineaments, strongly suggests that a genetic relationship is present -- particularly where large numbers of mineral occurrences lie along a single lineament.

Two lineaments in Pennsylvania are notable here. The Tyrone - Mount Union lineament (Gold, et al., 1973; Krohn, 1975) in central Pennsylvania

Figure 4-22: Lineament map of Pennsylvania with lineaments associated with mineral localities numbered. The localities are shown by dots.

ERTS-I LINEAMENT MAP OF PENNSYLVANIA

(see Figure 4-15) passes through three major water gaps along the Little Juniata River in crossing the Valley and Ridge Province from the southeast toward the Allegheny Plateau, where its trace coincides with a strike slip fault (Gray, et al., 1960). Previously mined Pb-Zn veins in Ordovician limestones lie on its trace at the town of Birmingham. Five Pb-Zn occurrences lie on lesser lineaments adjacent to the main lineament along the northwest trending zone described by Smith, et al. (1971). The Perkiomen Creek lineament (Figure 4-23) trends north across the Triassic Basin in southeastern Pennsylvania. Nine Cu-Fe mineralized areas are distributed along its length. Sanders (1963) noted a period of late Triassic northeast and north trending fracturing accompanied by the main Triassic mineralization. The Perkiomen Creek lineament may be the surface expression of a major zone of late Triassic fractures and may have controlled the locations of the mineralization at that time.

4.7.3 Conclusions

The tables and figures presented here should provide users with clues to possible controls of metallic mineralization in Pennsylvania. The Tyrone - Mount Union lineament complex and the Perkiomen Creek lineament are the most strongly associated with mineralization in Pennsylvania. Other unnamed lineaments shown on Figure 4-22 are geographically associated with 3, 4, and 5 mineral occurrences each. (See lineaments 1, 2, 10, 12, 15, 29, 47, 58, 60, 65, 83, 88, and 95, in the report by Kowalik and Gold (1975).)

Further work with surface and subsurface structural expression of lineaments will be necessary to define and separate lineaments genetically, and to sort out those most likely to be mineralized. The present study will hopefully encourage further field study of lineaments in varied terranes across the state. Such studies, combined with more accurate lineament plots, such as would be available from future Skylab-type data, should result in a map which would be a valuable prospecting tool.

Figure 4-23: Perkiomen Creek lineament with known mineral deposits along its length. The lineament, as shown here, extends from just east of Phoenixville north to Perkiomenville. Allentown is located at the right-angle bend in the Lehigh River, to the northeast. (SL3, S190B, orbit 44, roll 87, frame 296).

▩ Mineral localities or prospects

✲ Abandoned mines

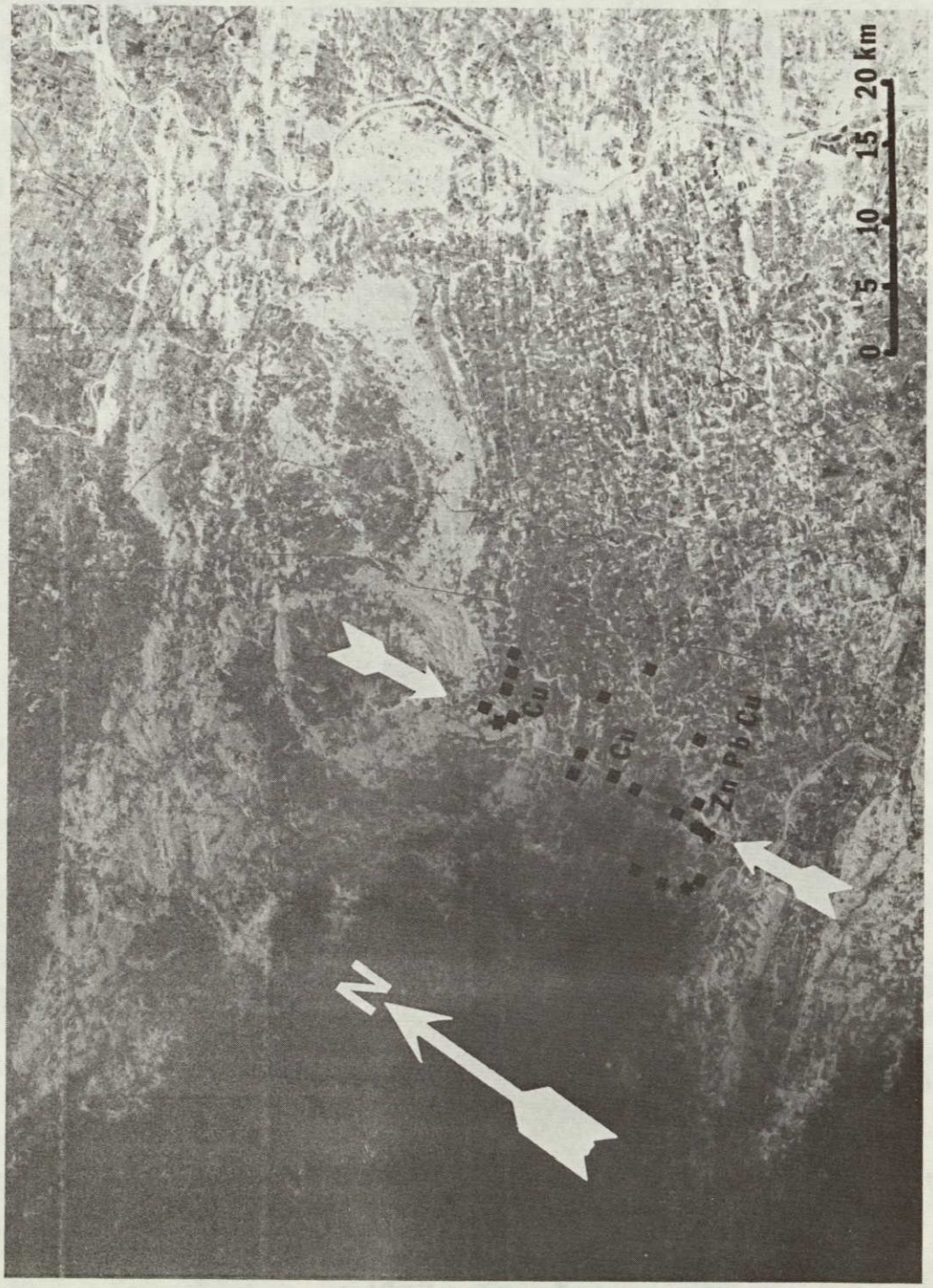

4.8 LINEAMENTS AND GROUNDWATER (Parizek)

A considerable amount of work has been done over the last 17 years to establish the nature and significance of fracture traces and to apply this knowledge to groundwater and engineering exploration. These investigations have been reviewed by Siddiqui (1969), Parizek (1971a), and Parizek (1975). Since data have been available from Landsat and Skylab, analogies have been noted between fracture traces and lineaments and it has been concluded that structures which underlie lineaments tend to permanently fix master drainages in a vertical plane (Gold, Parizek, and Alexander, 1973). Parizek (1975) has cited as a basic principle that valley environments, whether or not they are controlled by fracture zones, favor increased local and regional permeability development in a wide variety of carbonate and other terranes and represent excellent sites for potentially high capacity wells. Well yield data presented by various workers support this conclusion, as does information on cave distribution, theoretical ground-water flow data obtained from an electric analog model showing convergent flow adjacent to groundwater discharge areas, observations on the distribution and topographic control on springs in carbonate rocks located down valley from underdrained valleys, and water table maps showing troughs parallel to and below karst valleys. The realization that joints, zones of fracture concentration and fault zones localize valley development and, therefore, contribute to initial secondary permeability and porosity development also supports this conclusion. The chemical character of spring water discharged from some conduits located below underdrained valleys shows that rapid recharge and through flow occurs within these conduits when compared to springs draining more distant uplands, where diffuse flow dominates.

Many factors, however, combine to influence well yields at a particular location (well radius, well depth and diameter, casing length, method of drilling, degree of well development, depth to water table, presence of various changes of rock type, dip of beds, topographic setting, rock type, type of fold structure, presence and type of joints, faults, number and type of zones of fracture concentration, etc.). Comparison of yields of but a few wells and springs on or off a lineament will not suffice to establish a significant relationship, even though a strong inference may have been established. Similar variables influence depth and extent of weathering and permeability development, factors which are of importance in engineering foundation studies, mine and tunnel roof stability analyses, and similar investigations.

To date, more than 2,000 water wells, which lend themselves to analysis, have been inventoried, by various workers, within Pennsylvania. This has resulted in no more than 800 wells being available at which to conduct controlled pumping tests. These data points have been compiled and reviewed for use in the analysis of well yields to determine the significance of lineaments. These data have been obtained under similar pumping test conditions and under known field conditions. Data points have been ranked by topographic and geologic setting, well radius, depth, duration of testing, etc. Yields are being standardized to a common well radius, depth of penetration and pumping duration.

To date, not all these control points have been classified according to their location on or off lineaments mapped on Landsat or Skylab scenes. The resolution of the Landsat imagery, for which the best geographical coverage is available, is inadequate to allow a transfer of lineaments to a precise field location. Well control points for selected test areas covered by Skylab photography have been ranked according to their location on or off lineaments (assuming a 1 km width of influence) and according to their location on fracture traces, at fracture trace intersections, or off fracture traces, as mapped on underflight photography and examined in the field.

4.8.1 General Study Procedure

A number of conditions must be satisfied to conclusively prove a relationship between lineaments and permeability development because of the many factors which influence well yields within a given rock unit where secondary permeability and porosity predominate.

One method of study is to use for analysis all wells available within a given region for which construction details are known and the wells can be tested for yield under controlled conditions. Here one relies upon the probability that as the number of well control points increases the likelihood also increases that wells will fall within all combinations of conditions which influence permeability development. Unfortunately, a number of well points must fall within each combination of conditions being tested for significance before one can conclusively prove which of many possible factors influence well yields and the extent to which each contributes. Study results using this approach have not yet been completed.

A more efficient method of study is to keep as many variables constant as possible, thereby reducing the number of data points required in the analysis. Ideally, wells should be drilled, completed, and developed under identical conditions, and located all within a single rock type and under one topographic setting. Only the lineament/nonlineament variable should be allowed to vary. This experimental design could not be strictly adopted because existing well control data had to be relied upon in the study. At best, yields were tested for wells on and off lineaments and either within a single rock type or within a series of associated rock types with all other factors, such as well depth, diameter, and topography, permitted to vary.

The best geological and well control data were available in the Nittany Valley area of central Pennsylvania, where lineaments had been detected on Landsat-1 images. Unfortunately, initial Skylab data (SL3) did not cover the area; and later data (SL4), which did cover Nittany Valley, contained 40 to 60% cloud and cloud-shadow cover. The extent of Skylab coverage was not completely known until a considerable amount of a new field work had already been done in the area, thus a test area based on Skylab data coverage could not be chosen. Nevertheless, Skylab S190A and S190B photographs were used, where available, to improve the resolution of lineaments originally mapped on Landsat-1 channel 7 images of the Nittany Valley region. The Skylab photos were especially helpful

in precisely locating wells on single formations, yielding positive results in the final analysis of this study. To broaden the conclusions which might be drawn, other test areas were selected where the Skylab S190A coverage was known to be adequate. This included an area of folded siltstone, shale, and sandstone beds of Devonian age in Northumberland and Schuylkill counties. Additional areas were examined but the well-yield data base was inadequate.

4.8.2 Well Yields and Lineaments in a Single Rock Type

Well yield data were obtained from the Upper Sandy Dolomite Member of the Gatesburg Formation of Late Cambrian Age, in the area in Nittany Valley shown in Figure 4-24. The data for wells on lineaments (Table 4-3) and off lineaments (Table 4-4) were obtained under controlled conditions for locations on fracture traces, at fracture trace intersections and remote from fracture traces; within beds with various dips (0 to 35°); and for wells within valley bottom, valley wall and upland settings. These similarities in hydrogeologic setting allowed for the positive conclusions drawn. The well-yield data, adjusted for depth of saturated rock penetrated or saturated rock exposed below the well casing, are given as "productivity" in units of liters per second per meter of drawdown per meter of saturated rock penetrated (ℓ/sec/m/m). Wells were considered as on lineaments if they fell within a 1 km wide belt, as defined from the Landsat and/or Skylab scene and off lineaments if they fell beyond this assumed width. (Landsat scene 1045-15243, 6 Sept 1972 and Skylab-4 S190B photograph from roll 91, frame 323 were used.) Both generations of images were required because of the partial cloud cover on the Skylab scenes over the area where the well yield data base was best developed. The probability distributions of the well yield data are plotted in Figure 4-25. The maximum, minimum, and 50% productivity values were 6.3, 0.001, and 0.2 ℓ/sec/m/m for lineament wells compared with 1.5, 0.002, and 0.05 ℓ/sec/m/m for non-lineament wells.

It is apparent that some wells were highly productive regardless of whether they were on or off lineaments. In both cases, nearly all of the more productive wells were located on fracture traces or fracture trace intersections; hence, they derived the benefit of penetrating narrow (1.5 to 20 m in width) zones of fracture concentration. The slope of the line for wells considered to be on lineaments (whether on or off fracture traces) is less steep than the slope defined by wells remote from lineaments. This implies that wells will be more consistent in their yield, and display less variability, when located on both lineaments and fracture traces and in favorable topographic and bedrock settings. It may be concluded from this study that, when selecting water well sites, a positive benefit can be derived by combining both fracture traces and their intersections with lineaments and lineament intersections wherever possible.

4.8.3 Well Yields and Lineaments in Folded and Faulted Sandstone, Shale, and Siltstone

This project, a comparison study to that reported upon by Siddiqui

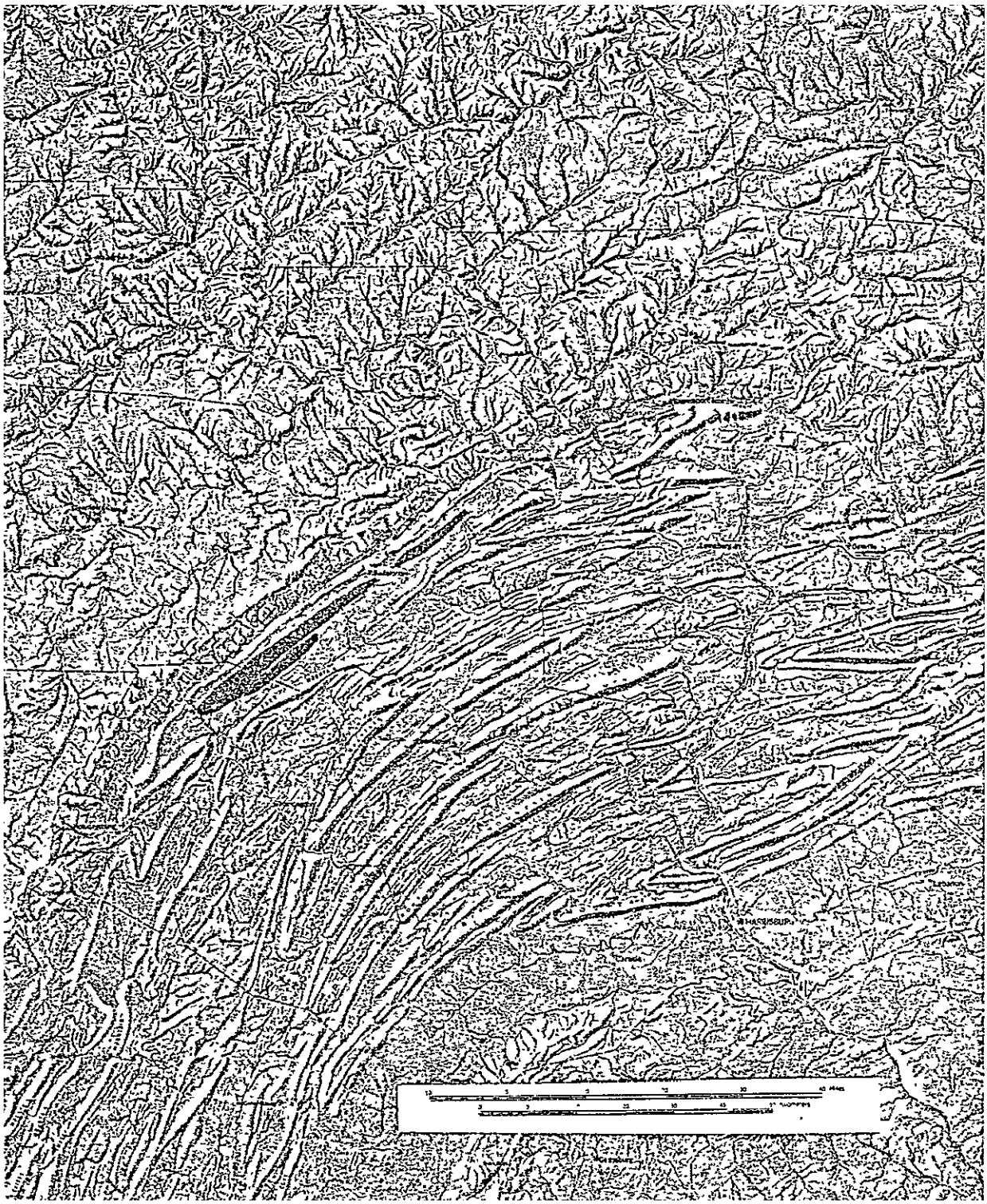

Figure 4-24: Physiographic map of central Pennsylvania showing the outcrop area of the Gatesburg Dolomite of Late Cambrian age.

Table 4-3: Wells Completed on Lineaments in the Gatesburg Formation[a]

Well	Casing[b] Length (m)	Well Depth (m)	Well Diameter (cm)	Pumping Rate (ℓ/sec)	Productivity (ℓ/sec/m/m)
INTERFRACTURE TRACE AREA					
UN-20	9.75	121.9	30.5		0.00098
SINGLE FRACTURE TRACES					
UN-2	11.4	99.1	30.5		0.084
UN-3	14.5	87.8	17.8	33.2	0.011
UN-16	19.2	138.1	25.4	17.5	0.025
FC-BSH-1	10.3[c]	38.1	38.1	49.2	0.828
FC-BSH-1	10.3[c]	38.1	38.1	126.2	0.706
FC-BSH-2	10.7[c]	42.7	38.1-317.5	126.2	0.360
FRACTURE TRACE INTERSECTIONS					
415	86.7	90.8	25.4		0.631
UN-17	9.5	57.3	32.5	42.9	0.077-0.085
UN-25					0.020
UN-24[d]	7.0	91.4	30.5	33.1	0.115-0.122
UN-26	12.2	121.9	30.5		0.081
FC-1	3.7	44.8	[e]	53.0	0.233
FC-2[a]	5.3	44.5	30.5	68.2	0.183
FC-2[b]	5.3	44.5	30.5	103.5	0.197
FC-3	11.6	45.7	33.0	116.7	0.316
393	7.4	95.4	15.2		0.023
SC-18	109.4	152.4	25.4		1.080

(Continued)

[a] Lineaments are assumed to be 1 km wide. Wells are located in valley bottoms, on valley walls, and on uplands. Dips ranged from 0 to 45°.

[b] Casing diameter equals well diameter, unless otherwise noted.

[c] Casing diameter = 40.6 cm.

[d] Screened for 30.5 meters.

[e] 30.5 cm diameter to 10.4 m, then 20.3 cm to 44.8 m.

Table 4-3 (continued)

Well	Casing Length (m)	Well Depth (m)	Well Diameter (cm)	Pumping Rate (ℓ/sec)	Productivity (ℓ/sec/m/m)
SC-19	132.3	143.3	35.6		0.252
Imbt Quarry	50.0	92.7	20.0	37.9	0.068
Imbt Quarry	50.0	92.7	20.0	63.1	0.046
FC-LSH-2	11.6[f]	45.7	33.7	113.6	
FC-LSH-2	11.6[f]	45.7	33.7	116.7	0.306
FC-USH-1	10.9	30.5	45.7[g]	101.0	0.422
FC-USH-1	10.9	h	35.6	101.0	6.314
FC-USH-2	7.5[i]	30.5	43.2	116.7	0.614

[f] 35.6 cm casing.

[g] Outer diameter

[h] Caved at 12.2 m.

[i] 45.7 cm outer diameter.

Table 4-4: Wells Completed Remote from Lineaments in the Gatesburg Formation[a]

Well	Casing[b] Length (m)	Well Depth (m)	Well Diameter (cm)	Pumping Rate (ℓ/sec)	Productivity (ℓ/sec/m/m)
INTERFRACTURE TRACE AREA					
Donsborough	39.6	59.4	15.2	0.4	0.019
L.G. Appt.	115.2	125.3	21.9	3.8	0.011
I-80 #31	72.1	96.3	15.2	3.8	0.033
I-80 #31	72.1	96.3	15.2	2.7	0.057
SINGLE FRACTURE TRACES					
UN-22	29.0	104.6	15.2		0.021
408	8.5	51.8	15.2		0.002
P.G.C.[c]	54.6	154.2	d	32.2	0.229
FRACTURE TRACE INTERSECTIONS					
UN-23	31.2	82.3	15.2	1.7	0.082/0.102
UN-14	15.2	65.5	30.5		0.117
SC-16	87.1	138.1	20.3		1.125
SC-15	110.0	139.6	30.5		0.019
SC-5	117.0	111.3	25.4		1.496
SC-17	90.5	137.2	25.4		0.002
UN-14	15.2	65.5	30.5		0.117
G-10	88.1	97.5	15.2		0.320
409	22.6	60.1	15.2		0.046

[a]Wells are located in valley bottoms, on valley walls, and on uplands. Dips range from 0 to 45°.

[b]Casing diameter equals well diameter, unless otherwise noted.

[c]20.3 cm screen from 54.6 to 127.6 m.

[d]30.5 cm diameter to 127.6 m, then 20.3 cm to 154.5 m.

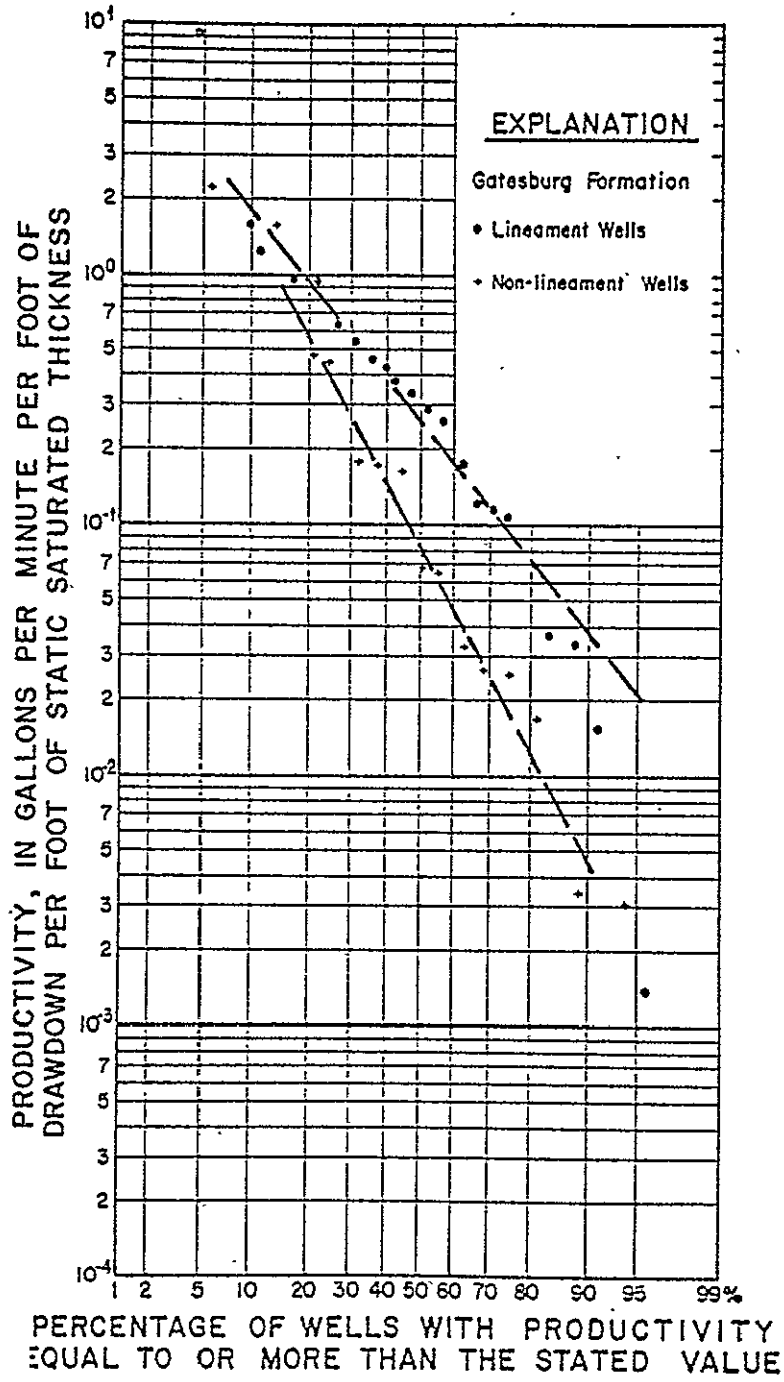

Figure 4-25: Comparison of productivity frequency graphs for wells located on and off lineaments. All wells are located in the Gatesburg Formation of Late Cambrian age and under similar topographic, fracture trace, and non-fracture trace settings. (Lineaments are assumed to be 1 km wide. Productivity in gpm/ft/ft x 0.679 equals productivity in ℓ/sec/m/m.)

and Parizek (1971a and b) for Northumberland and Schuylkill Counties of east central Pennsylvania, incorporates the more recent data available from the Skylab and Landsat satellites. Fifty-nine controlled pumping tests were conducted on domestic and farm wells within a 155 km^2 test area in the Valley and Ridge province. Wells were completed in the partially folded and faulted rocks of either the Trimmers Rock Sandstone or Catskill Formation, of Devonian age. The wells penetrated either sandstone, siltstone, shale, or interbedded siltstone and shale beds.

4.8.3.1 Study Procedure

This study involved the correlation of many variables other than well placement with respect to lineaments and fracture traces. The various phases of the project are outlined below. Those portions of the study relating to lineaments and the use of satellite data are then described in detail. However, detailed discussions of the other sections (marked with an asterisk below) are not included here.

1. Well-yield data were obtained under controlled testing conditions and adjusted to a common well radius, depth, and duration of testing.

2. Assuming a fracture trace width of 13.3 m, the wells were ranked as on or off a fracture trace and their yields compared.

3. Assuming a fracture trace width of 10.3 m, the original wells were ranked as above. Ten intentional fracture trace wells were also drilled, tested for yield, and included in the new analysis. (A correlation was obtained.)

4. The wells were ranked by topography, according to whether they occurred on uplands, valley walls, and valley bottoms, and their yields were compared. (A correlation was obtained.)

5. The wells were ranked according to rock type -- sandstone, shale, siltstone, and interbedded siltstone and shale -- and their yields compared. (A correlation was obtained.)

*6. The wells were ranked by well depth, depth to water table, and other relevant characteristics.

*7. The wells were ranked by dip of beds and type of fold structure.

8. Wells representing the same combination of rock types, topography, and location with respect to fracture traces (on or off), were ranked as on or off lineaments at the Klingerstown water gap site. (A correlation was obtained.)

The wells were first located and tested for yield (Cline and Parizek, 1975). The areas in which the wells were located were then marked on aerial photographs at a scale of 1:10,000. All obvious fracture traces were mapped independently, without prior knowledge of the location or yield of wells. This procedure was followed to avoid the strong temptation of including high-yielding wells on subtle lineations which had not previously been mapped as fracture traces. (From previous experience, it was realized that a number of lineations which are quite faint and less than 333 or so meters in length can often be seen on photographs. These may be underlain by individual joints, by less fractured bedrock overlying more intensively fractured bedrock, or by less well developed zones of fracture concentration. Minor lineations normally are not included as fracture traces when more obvious features are being mapped. The usefulness of these minor lineations to determine permeability and porosity distribution has not been demonstrated to date.)

Comparison of early well-yield probability plots revealed that there appeared to be no significant difference between yields of wells classified as on one or more fracture traces and those classified as off fracture traces. It was concluded from these findings (Cline, 1968) that fracture traces in this sandstone-siltstone-shale sequence of rocks are underlain by zones of fracture concentration less than 13.3 m wide, or that some of the wells considered to be on fracture traces probably missed zones of fracture concentration entirely, or that fracture traces are not useful guides in prospecting for water in this terrane.

As a further test of the fracture trace hypothesis, three studies were initiated:

1. Well sites were selected on some of the most obvious fracture traces and 10 test wells were purposely drilled and tested for yield. These wells ranged in depth from 16.6 to 23.3 m and averaged 17.7 meters. Wells were located in valley bottom settings to minimize the total footage of drilling required and to obtain additional well-yield data in the valley bottom environment. Well sites were carefully selected after fracture traces were located in the field to minimize chances of missing fracture zones.

2. Zones of fracture concentration exposed on bedrock escarpments 95 to 120 km to the east were mapped and the width of fracture concentrations measured at 9 stations. The average width was found to be 10.3 m, or 3.0 m less than originally assumed.

3. Based on these measurements, a new average width of 10.3 m was assumed for zones of fracture concentration and each well rated as on a fracture trace, on this basis, was field checked. The location of the center line was estimated in the field and the perpendicular distance to the well was measured. Several wells originally included in the fracture-trace category were eliminated by this procedure. The 10 new intentionally located test wells and the remaining reclassified fracture-trace wells were replotted. This followup study reversed the initial conclusion; i.e., fracture traces can be used to delineate zones of increased permeability and porosity.

(Structure, bedrock lithology, depth of well, depth to water table and other factors were also included as geologic variables, but these will not be reported upon here.)

In siltstones, shales, and sandstones with low intergranular permeabilities, wells must directly penetrate zones of fracture concentration to show increases in yield. An incorrect assessment of width will lead to a negative conclusion in a statistical analysis of well-yield data. In carbonate rocks, wells that just miss zones of fracture concentration may still show increased yields because solution openings frequently extend along bedding planes, individual joints, and selected beds on either side of the zones of fracture concentration. Hence, insofar as they influence well yields, fracture traces in carbonate rocks have a greater "apparent width" than they do in sandstones, siltstones, and shales; or in igneous and metamorphic rocks.

4.8.3.2 Influence of Topographic Setting

Topography was the first geologic factor considered. The region was subdivided into upland, valley wall, and valley bottom settings and well yields were compared within each setting. At least two distinct plots were obtained indicating that wells located in valley bottoms have significantly higher yields than wells located in valley wall or upland settings, and that valley bottom wells have more variable yields than wells for the other two settings. Upland wells are as consistent as valley wall wells but are slightly less productive.

A lineament valley appears to be one of the factors which was responsible for a distinct change in slope observed on the probability frequency plots (when wells were ranked by rock type or other settings) for valley bottom wells. These plots (Figure 4-26) show that there was a second distinct population present. These more productive wells, therefore, were removed from subsequent probability plots and treated separately. Segments of most valleys in the research area define fracture traces; hence, the valleys must be largely structurally controlled. Joints, plus weathering along these joints, probably are much more extensive and better developed in valley bottoms, resulting in greater flow of water to wells. Other factors, discussed earlier, undoubtedly also contribute to higher well yields in the valley environment.

Lithologic variations were tested by grouping well-yield data into sandstone, siltstone, siltstone-shale, and shale categories according to well location. The original plots of these data showed significant breaks in slope when variations in topographic settings were ignored. Because it had already been established that valley bottom wells were significantly more productive, it was reasoned that these wells may be accounting for the break in slope noted in the original plot. All valley bottom wells were eliminated and the data replotted in an attempt to stablize control points so that the various lithologic categories could be evaluated independent of topography. The resulting plots were greatly improved. This procedure of segregating wells by topography and one additional geologic variable was followed in all subsequent tests.

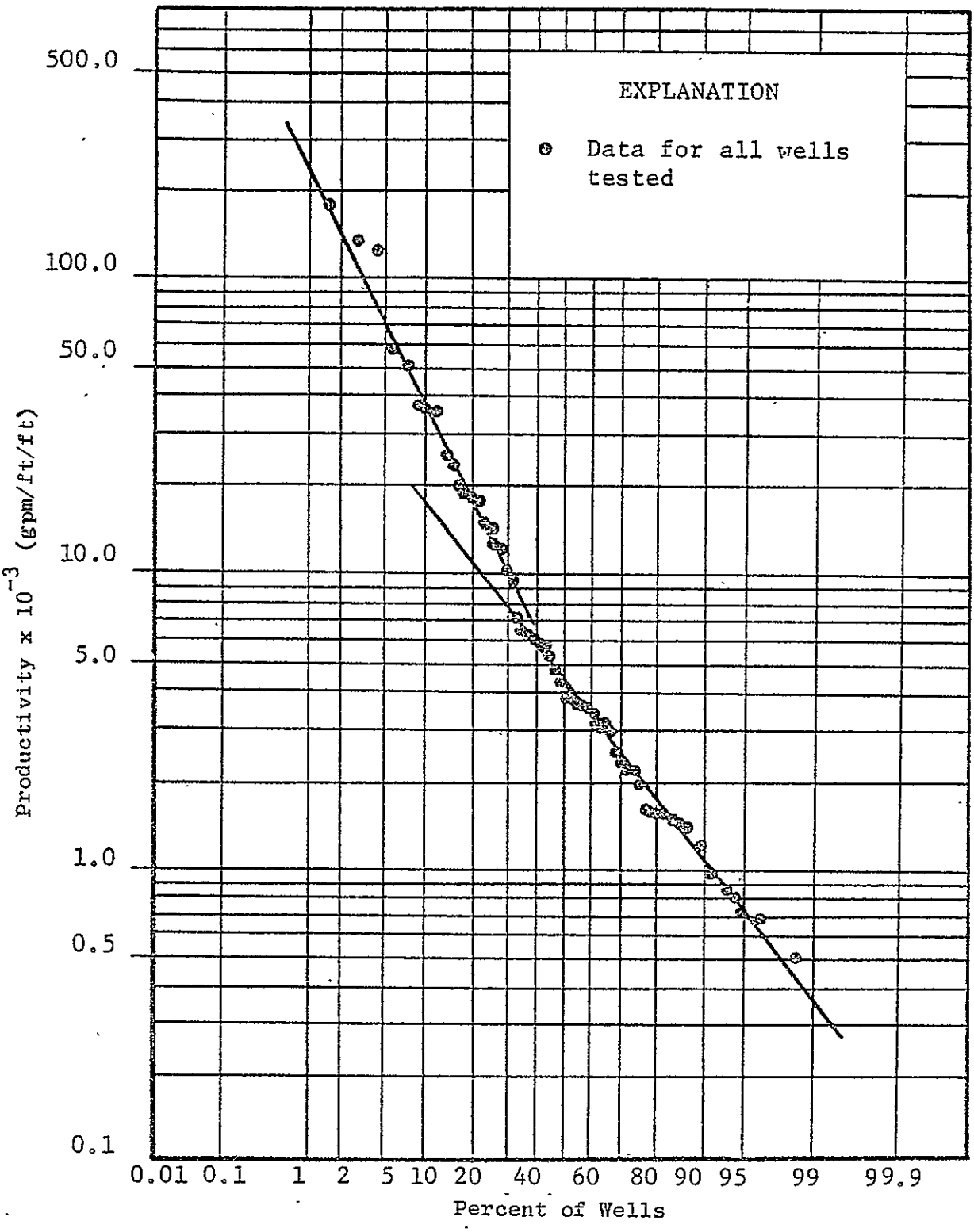

Figure 4-26: Productivity frequency graph for 59 wells located in folded shale, siltstone, and interbedded shale and sandstone of Devonian age. The break in slope reveals that two distinct populations are being sampled. Nearly all wells which define the high-yield population are located on one of two lineaments at Klingerstown, Pennsylvania. (Productivity in ℓ/sec/m/m may be obtained by multiplying gpm/ft/ft by 0.679.)

4.8.3.3 Influence of Fracture Zones

Yields of ten intentionally located fracture trace wells were combined with yields of wells reclassified as on fracture traces, using an average width for fracture zones of 10.3 meters. These were compared with yields of wells which are located adjacent to or remote from fracture traces (Figure 4-27). There is a difference between yields of wells in the two categories. The productivity equalled or exceeded 50% or more of the time in the on-fracture trace category was 0.0065 ℓ/sec/m/m, whereas the 50% value was 0.0031 ℓ/sec/m/m for the off-fracture trace category.

Other comparisons were made to determine the influence fracture traces have on well yields. For instance, valley bottom wells located on fracture traces were compared with valley bottom wells located adjacent to or remote from fracture traces. The graphs revealed that valley bottom wells off fracture traces appeared to be more productive than valley bottom wells located on fracture traces. This contradiction brought to light another important influence on well yields. Most of the high well yields or upper points on the graph which fell within the off fracture trace category and lead to this interpretation are from wells located opposite a mountain water gap at Klingerstown and in a valley with a large floodplain. The yields of these wells undoubtedly were influenced by a combination of geologic factors other than fracture traces, as discussed previously. The lines of best fit for data points displayed for all probability graphs that included the Klingerstown Gap wells showed breaks in slope, or two distinct populations. All data from wells located opposite the water gap were eliminated and a new plot was constructed which compared valley bottom wells located on and off fracture traces for regions remote from the water gap. Average yields for wells located on and off fracture traces determined from the new graphs probably are more representative of the study as a whole. For wells located on fracture traces, the productivity ranged from 0.00033 to 0.0344 ℓ/sec/m/m, and equalled or exceeded 0.0057 ℓ/sec/m/m 50% of the time. For wells located off fracture traces, the productivity ranged from 0.00089 to 0.0120 ℓ/sec/m/m, and equalled or exceeded 0.0026 ℓ/sec/m/m 50% of the time.

A number of explanations have been offered to account for the higher yield from wells located on a floodplain, as was found within the water gap (Parizek 1975). Somewhat permeable and saturated floodplain sediments are known to occur in the vicinity of Klingerstown. These can serve as a source of vertical recharge to underlying joints and fractures supplying water to wells cased into bedrock and tested for yield in this setting. Induced streambed infiltration, diversion of water from natural discharge and from water-loving vegetation are not likely to be responsible for the higher yields created in this setting, however, when compared to adjacent areas, because all pumping tests were of short duration and these influences should not have been brought into play.

A more appealing explanation, one that is relevant to this study, is the fact that the Klingerstown wells are located opposite a water gap controlled by a zone of shear, or more regional zone of fracture concentration, revealed by lineaments mapped on Landsat and Skylab images. The presence of zones of shear or fracture concentrations within the folded

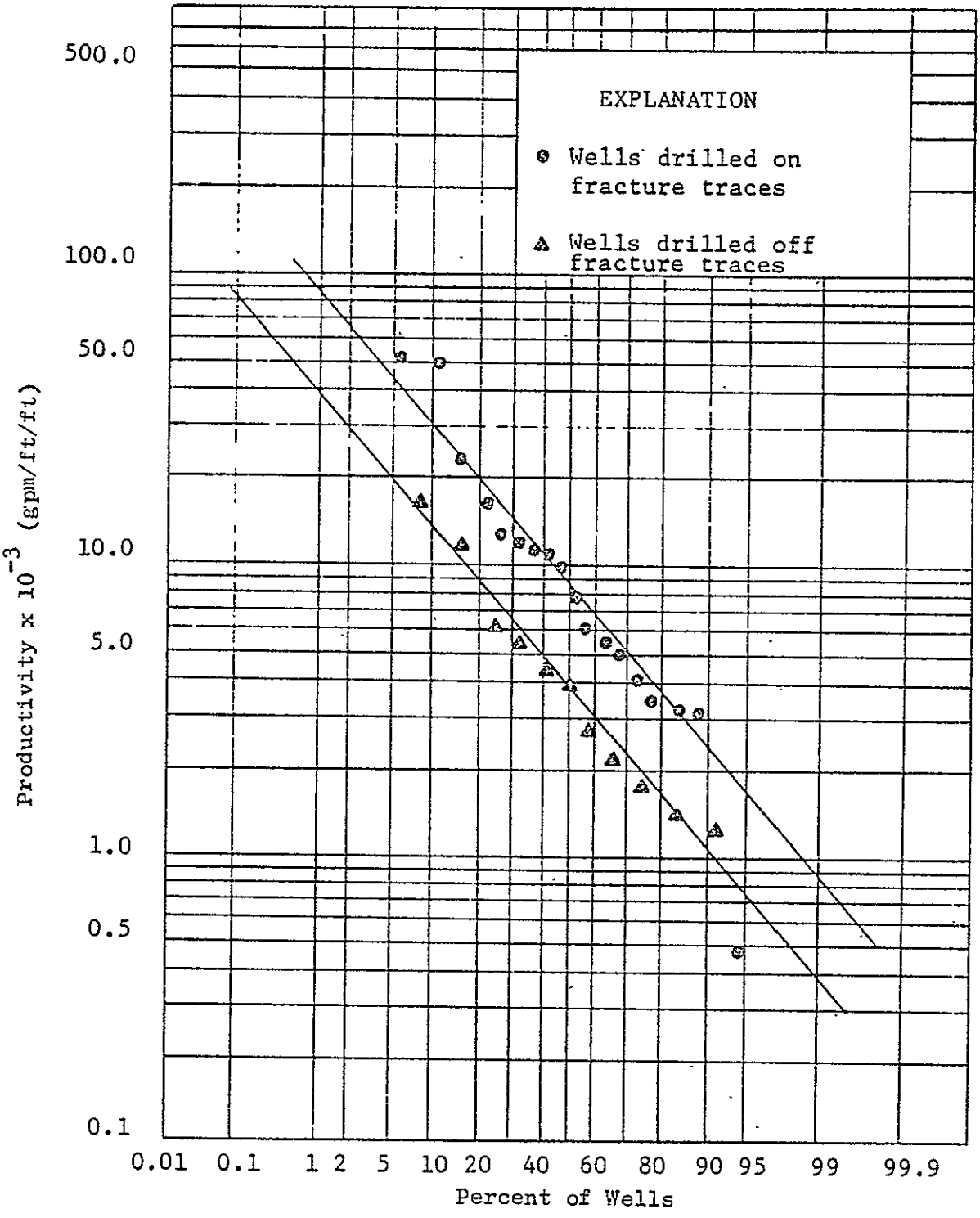

Figure 4-27: Productivity of wells grouped by location on or off fracture traces at Klingerstown, Pennsylvania. (Productivity in ℓ/sec/m/m may be obtained by multiplying gpm/ft/ft by 0.679.)

Appalachians is reasonable, in view of the work by Gwinn (1964), Wise (1968), Gold, et al. (1973), and others. Alignment of the Klingerstown water gap with segments of adjacent tributaries and the master stream, and topographic breaks in the adjacent uplands and mountain ridges, reveal structural controls on the water gap. The width of these structures and the exact position of the lineaments with respect to the wells for which yield data have been collected are not precisely known, but a zone 1 km wide would encompass all the wells studied in the gap.

It is significant that the wells located near Klingerstown are among the most productive wells within this folded sequence of sandstones, shales, and siltstones tested for yield in the study area, and that the lineaments were recognized by independent operators on the Skylab S190B photograph (SL3, orbit 44, roll 88, frame 067).

4.8.3.4 Well Yields Adjacent to Other Water Gaps

Further data in support of the significance of lineaments in groundwater prospecting can be made for scant well-yield data obtained opposite or within other water gaps. Two wells were drilled at Spring Bank, Centre County, Pennsylvania, just upstream from a water gap controlled by a lineament and its associated structures. The relatively obvious lineament had been recognized earlier on oblique low altitude aircraft photography and later verified on Skylab photography (SL4, orbit 73, roll 91, frame 324).

The first well was drilled in rocks of the Colburn-Salona Formations, which are among the poorest producing strata encountered in central Pennsylvania. The second well has started in this same formation but may have extended into underlying, more productive, limestone before being terminated. Drill cuttings and fluids were not circulated during the bottom drilling of the second well because a shallow, dry, uncased void had been encountered during drilling and cuttings were not returned. Both wells were caliper logged and are among the most productive Salona-Colburn wells tested for yield. Both wells are ranked as lineament wells, in view of their close proximity to the known lineament mapped for this water gap, and would be rated as lineament wells even for a lineament width of 0.5 km.

Several wells were drilled in Potters Mills (SL4, S190B, orbit 73, roll 91, frame 323), opposite a water gap developed in Tussey Mountain, Centre County, Pennsylvania, to replace shallow domestic wells polluted by an unprotected stockpile of road salt. These wells were drilled and tested for yield under controlled conditions. They penetrated the Salona-Colburn Formations and again showed comparatively high yields when compared to other wells drilled into the same formation remote from this or other gaps not controlled by lineament-related structures. The gaps at Spring Bank and Potters Mills both contain permanent streams and it may be argued that the above average well yields observed in these settings are due to induced streambed infiltration rather than to structural controls. Both Spring Bank wells were located on fracture trace intersections.

A more spectacular example is cited for an underdrained valley oriented transverse to bedrock strike and lacking a permanent stream. A

gap is developed in a mountain ridge underlain by resistant sandstones and quartzite (Tussey Mountain near Shingletown, Centre County, Pennsylvania) at the head of the valley. The regional trend of this youthful karst valley was known to be linear and related to the gap at Shingletown. A new well field was recommended for the lower reach of this valley because:

1. It would be in close proximity to existing wells (the Thomas Well Field) and to pipe and power lines.

2. Bedrock was gently dipping and among the most productive dolomites available in the area.

3. A valley bottom setting was available which would increase permeability development and high rates of seasonal recharge following snow melt.

4. The field would be close to the confluence of a small stream which would further augment recharge.

5. Water levels were expected to be shallow.

6. A zig-zag offsetting the regional valley alignment assured that well-developed fracture traces were available to pinpoint high capacity test well sites favorably clustered on a single property available for purchase. No major pollution threats existed in the immediate area.

Prospecting was guided by the favorable combination of factors listed above and by a knowledge of the optimum set of field conditions which favor permeability development. That is, the best targets in the area were at fracture trace intersections, within the Upper Sandy Dolomite Member of the Gatesbury Formation (Late Cambrian Age) or the Nittany Dolomite, on crests of anticlines or at least in beds with less than 15° dips, where water tables are shallow but in carbonates, and within valley bottoms. Most of these conditions were satisfied at the proposed site. The poorest sites were expected within interfracture trace areas, on uplands, on synclinal troughs, where bedrock dips were in excess of 30°, where the water table is deep, in shales, and where the Bellefonte Dolomite or selected limestone units were exposed.

The combination of stratigraphic, structural, and topographic conditions which favor the best and poorest permeability development for the study area are summarized in Table 4-5. Although the ranking of the individually named stratigraphic units is unique to this study area, this is not true of their petrographic properties, which control primary and secondary intergranular permeability and porosity development and preservation. Controls influenced by topographic and structural settings should have more nearly universal application when prospecting for groundwater in both carbonate and noncarbonate rocks.

Test wells (25, 26, and 27 of Table 4-6) were drilled at high priority fracture intersection test sites, using air rotary and cable tool methods of drilling, and developed and tested by pumping. These were completed as final production wells and were among the most productive

Table 4-5: Guide to Groundwater Prospecting Within the Folded and Faulted Carbonate Rocks of the Central Appalachian Type (Aquifers are listed from the best to the poorest.)

Rock Type	Structure	Topographic Setting
Nealmont Formation Center Hall Member Rodman Member	Fracture trace intersection combined with lineament intersection.	Valley bottoms opposite wind and water gaps controlled by zones of fracture concentration and faults.
Benner Formation Valentine Member Valley View Member Oak Hall Member Stover Member	Normal and thrust faults.	Valley bottoms with rivers and creeks, shallow water tables and saturated overburden deposits.
Hatler Formation Graiser Member	Anticlinal crests.	Base of mountain slopes favoring high rates of recharge and conduit development.
Gatesburg Formation Upper Sandy Dolomite Member Nittany Dolomite	Beds with dips of <15°	Underdrained valleys.
Other Limestones Axmann Stonehenge Worrior	Synclinal troughs.	Valley walls.
Bellefonte Dolomite	Beds with dips >15° to 90°.	Uplands
Reedsville and Antes Shale		
Coburn-Salona Limestones		

Table 4-6: Lineament and Non-Lineament Wells in the Nittany Dolomite

Well	Casing[a] Length (m)	Well Depth (m)	Well Diameter (cm)	Pumping Rate (ℓ/sec)	Specific Capacity (ℓ/sec/m)	Productivity (ℓ/sec/m/m)
ON A LINEAMENT AND AT FRACTURE TRACE INTERSECTIONS (Harner Farm Wells) (All wells have 40.6 cm diameter screens for 12.2 m.)						
25	18.6	69.5[b]	50.8	138.3	41.4	0.81
26	19.2	85.3	c	138.3	82.8-103.5	2.315-2.893
27	18.9	79.3[d]	e	138.3	108.7	1.77
ADJACENT TO A LINEAMENT AND ON A FRACTURE TRACE OR AT FRACTURE TRACE INTERSECTIONS (Thomas Farm Wells) (Wells not screened.)						
7	21.0	50.3	30.5	63.1	29.56	1.032
8	21.5	50.3	30.5	50.5	23.66	0.835
11	24.8	47.2	34.9	104.1	48.79	2.220
14	25.0	43.3	30.5		28.21	1.541

[a] Casing diameter equals well diameter.

[b] Caved to 39.9 m.

[c] 50.8 cm diameter to 32.3 m, then 27.9 cm to 85.3 m.

[d] Caved to 73.9 m.

[e] 50.8 cm diameter to 32.0 m, then 27.9 cm to 79.3 m.

wells ever drilled in the region (Figure 4-28). On the average, the specific capacity values for these wells on the lineament and fracture trace intersections (25, 26, and 27) are considerably higher than for wells located adjacent to the lineament (7, 8, 11, and 14) but within the same rock type, with the same dip, and in a valley bottom setting, just over 1 km away. Wells 7 and 8 are on single fracture traces by chance, and wells 11 and 14 are at fracture trace intersections (11 by chance, 14 by design). Productivity values adjusted for depth of saturated rock penetrated appear less conclusive because the non-lineament wells were all shallower and, hence, their value was not diminished by extension into less productive rock. Study of driller's and caliper logs of these wells revealed that cavity distribution diminished markedly within the lower 30.5 m of each well. Although wells 25 and 27 were found to be caved and filled above their original depths following pumping (Table 4-6), the depth of saturated rock penetrated was assumed to be the initial drilled depth; hence, productivity values appear lower than they otherwise would have been. The specific capacity values alone, however, should provide convincing evidence of the added significance of the lineament present. Wells 25, 26, and 27 were drilled by air rotary and cable tool methods and were developed more extensively than wells 7, 8, 11, or 14. However, the former are screened and gravel packed, which reduces their efficiency significantly compared to unscreened rock wells.

Landsat-1 and Skylab images became available after the well field was located. A comparatively minor lineament, when compared to more obvious longer lineaments, was mapped for this water gap and aligned valley, verifying what had been suspected from analysis of conventional photographs. This lineament was identified by independent operators, as were those in the other two areas. Thus, multiple operators agree on lineaments being present for those areas for which we have the well-yield data.

A more complete well-yield data array for this and other settings will be required to meet the objections of skeptics, and these will soon be forthcoming. But in the interim, lineaments and lineament intersections combined with fracture trace intersections should be added to the list of conditions favoring increased well yields in a wide range of rock types.

From average well-yield data collected by the State Geological Survey for the Altoona, Hollidaysburg, and Tyrone area in Pennsylvania, for instance -- for 58 wells in three formations -- one would get the impression that groundwater resources are very poor (average productivity of 0.611 ℓ/sec.) However, yields from 12 intentionally located fracture trace wells in these same formations had an average yield of 868 ℓ/sec. Hence, when a drilling site can be pinpointed from a study of Skylab and aircraft data combined, the status of a very poorly regarded aquifer can be raised to that of a high priority aquifer. Here, the formational units and structural setting differ from those cited in Table 4-5, but once again the fundamental principles apply when defining optimum permeability and porosity development. The same combination of topographic and structural factors may be used to locate areas with favorable permeability development even when well-yield data are scant and not revealing of the true potential of the aquifer.

Figure 4-28: Site of a three-well, 23 million liters a day, well field in gently dipping dolomite. The wells are located at fracture trace intersections on a lineament assumed to be 1 km wide. Dashed lines show the fracture traces and the arrows indicate the trace of the lineament (not readily apparent on aerial photographs). The wells are shown as asterisks.

4.8.4 Operational Procedure for Lineament Detection and Field Location

Studies conducted at the sites described above indicate the essential nature of Skylab S190B data in the study of lineaments related to groundwater resources. We believe that current coverage of Pennsylvania in the form of Landsat and aircraft data is adequate for geologic purposes. What is needed is the intermediate resolution of Skylab data, preferably that from the S190B sensor. For ultimate accuracy, Skylab coverage for the entire state, for probably two seasons at intervals of 5 to 10 years, would be adequate.

Seasonal coverage is important from the standpoint of changes in sun angle and ground cover (such as bare fields vs. various crops). Coverage repeated over intervals of several years may reveal lineaments in areas such as those which have been reforested after logging or fire. This has been found to be true for fracture traces on aircraft photography.

These data should then be studied by several operators to create a lineament map of Pennsylvania not only highly useful for groundwater prospecting, but also for mineral prospecting, foundation studies, and the other applications discussed elsewhere in this report.

The importance of constructing an accurate lineament map of this or any other state in the near future should be emphasized. Criteria for the recognition of fracture traces and possibly lineaments are readily obscured by even minor changes in landscape, and it is important to protect potential high-capacity well sites in advance of urban and industrial sprawl. Needless to say, knowledge of zones of fracture concentration in areas of proposed construction is also important.

Landsat MSS images show a great number of long lineaments. On Skylab photographs, these are revealed to consist of shorter segments which may differ in orientation somewhat from the mean orientation of the long lineament seen on the Landsat image. On a Landsat image, field location of a lineament is a highly subjective procedure, whereas at the Skylab resolution (particularly on the S190B photography) details such as roads, buildings, and fields are of great value in establishing the field location of a lineament. Thus, the actual zones of fracture along the lineament can be accurately located on the Skylab S190B photography, whereas only the general location can be seen on Landsat images. This fact has been verified by several different operators working in the same areas.

The Landsat-derived lineament map shows an uneven distribution of lineaments for various sections of the state. In particular, fewer lineaments are seen in the southeastern and northwestern areas than other regions of the state. These variations may be more a function of operator bias than of geological causes, particularly in the case of interpretation of culture of features in more densely populated regions. For this reason, multiple operators should be used to increase the chances of detecting more subtle lineaments. It is also important to obtain more Skylab-type photography as soon as possible, because cultural changes probably will obscure, to some extent, the traces of lineaments which may later prove

critical to mineral and groundwater exploration, foundation engineering, and pollution control studies. (Cultural features have definitely been shown to obscure fracture traces on aircraft photography.)

Figures 4-29a through d illustrate how lineaments initially mapped on a Landsat mosaic can be verified in ground location through the use of Skylab and aircraft photography. It is through this procedure -- in which Skylab photography is a vital link -- that accurate lineament widths in various lithologies and terranes will eventually be established, making possible close correlation of these features with terrane characteristics such as well yield, topography, foundation stability, and mineralization.

Figure 4-29: Operational procedure for locating lineaments and fracture traces on the ground from remote sensing data.

a) Megalineaments mapped on a Landsat-1 mosaic of channel 7 images. The dashed lines represent known faults which exhibit displacements on this scale. The physiographic provinces -- the Allegheny plateau to the north and west, the curved Appalachian folded belt through the central section, and the Piedmont to the southeast -- show up well. The dark crescent-like area in the northeastern part of the state is the "anthracite coal basin around Scranton and Wilkes-Barre. (Somewhat more detailed lineament mapping can be done by enlarging segments of Landsat-1 images.) The rectangle defines the area shown in the Skylab photography of b.

b) Skylab scene of the area outlined in the Landsat mosaic of a. Here, many shorter lineaments have been mapped, and it can be seen that lineaments mapped as single features on the Landsat scene (shown here by arrows) transect concentrations of shorter lineaments mapped on the Skylab photo. This is especially true where the Landsat lineaments intersect. The field location of lineaments is enhanced by landmarks obvious at the Skylab scale but not visible at the Landsat scale. The rectangle on this scene defines the area shown on the C130 photograph of c. (SL3, S190B, orbit 44, roll 88, frame 069.)

c) Several fracture traces mapped at the C130 aircraft scale in the area of the rectangle on the Skylab scene of b. Several shorter lineaments from the Skylab scene have been transferred to this photo. It can be seen that these lineaments are clearly defined on the Skylab photo and segments of them are seen on the C130 photo, showing that Skylab photography is far more accurate than Landsat imagery for location of linear features in the field. (Mission 258, roll 56, frame 205.)

d) A typical fracture trace/lineament cross section as seen in the field. Note the massive rock present on both sides of the fractured zone, and the weathering which has taken place along the fractures.

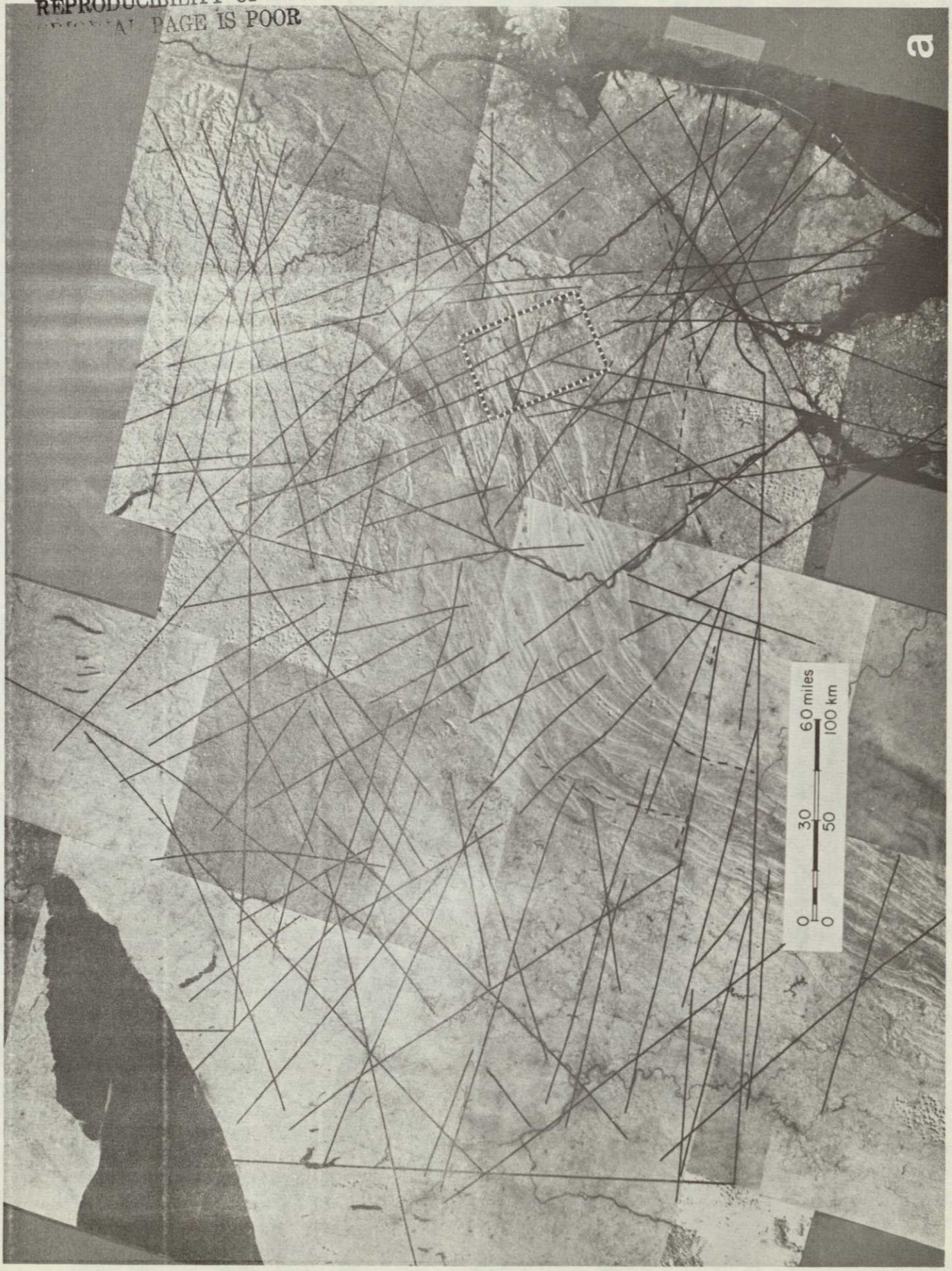


b


56-0205
NASA JSC 258 FEB 74
N

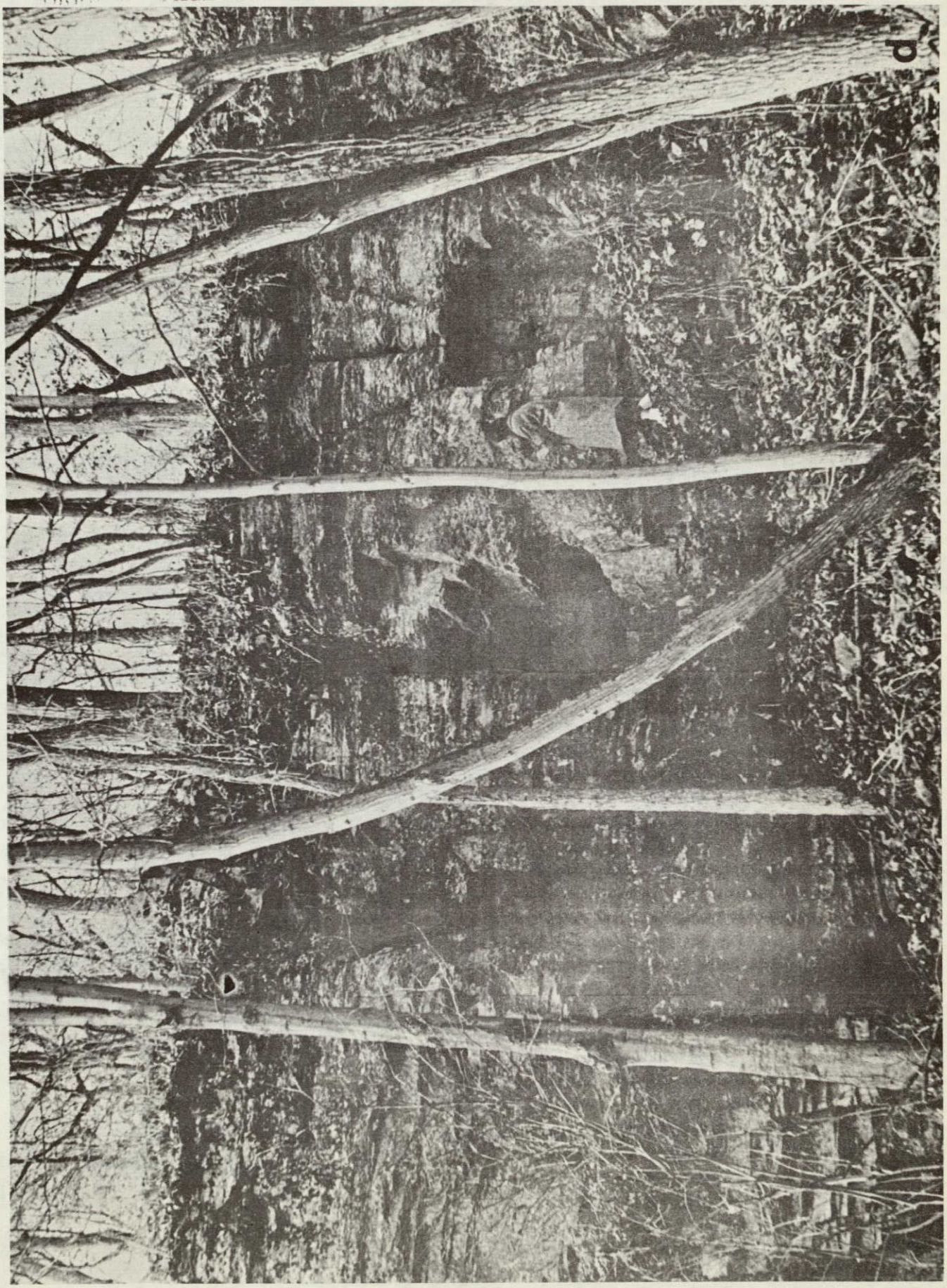

4.9 THERMAL SPRINGS AND LINEAMENTS (Alexander and Weinman)

With energy shortages becoming increasingly acute, and fossil fuel prices at record levels, interest is being shown in more unconventional forms of energy--one of these being geothermal. The State of Pennsylvania has only one known thermal anomaly, Warm Springs, Shermansdale, Pennsylvania. A study was initiated to investigate the origin and extent of this feature and to assess the potential effectiveness of various techniques in exploring for other geothermal anomalies.

Though little likelihood was held for an economically important thermal anomaly to show up at Shermansdale, its origin and relation to local geologic features was not known and the only previous measurements in the area consisted of a rudimentary chemical and temperature check on the water flowing from the spring. Further impetus for the study was provided when it was realized that a large aeromagnetic anomaly (some 500 gammas) centered over this area and that satellite imagery from Skylab and Landsat-1 showed the location of the Warm Springs to be on the edge of a large doming structure and on a prominent lineament (Figure 4-30).

Field investigation has shown that the Warm Springs issue along an outcrop of the Ridgely sandstone, a formation which is interbedded with shales and limestones in a synclinal trough (see Figures 4-31 and 4-32). The occurrence of a cold spring (11.5°C) in the same geologic outcrop 1 km away further complicates the geologic explanation of the thermal springs in this area.

The focus of this investigation was to ascertain the thermal source of these springs and determine if its hydrologic history is related to fractured permeable beds along a synclinal flow path or if a more vertical fault-fracture (lineament) flow path need be invoked.

4.9.1 Remote Sensing Data

Remote sensing data were available for this area from three different altitudes: Landsat-1 (900 km), Skylab (385 km) and aircraft (1220 m). Each supplied important information on the Warm Springs area. In combination, they helped delineate associated, or possibly associated, geologic structures and to define the spatial extent of the thermal anomaly in the area. The imagery at different scales also helped in the interpretation of ground-based measurements and aeromagnetic maps. In this section, we briefly discuss these three types of data and the relevant features which can be seen on images of the Warm Springs area.

4.9.1.1 Landsat-1 Data

Figure 4-30 shows a channel 7 Landsat-1 image (1243-15253) of central Pennsylvania, covering a portion of the Valley and Ridge province of the Appalachian Mountains. The arrow indicates the approximate location of Warm Springs; the Susquehanna River and the city of Harrisburg are directly east (right) of the Springs. The exact location of Warm Springs could not be seen on the Landsat scene due to the shadowing effect of

Figure 4-30: A portion of a Landsat-1 scene, covering the Warm Springs area. The dome structure north of the Springs is outlined and the three prominent lineaments are shown. The curved white arrow shows the approximate location of Warm Springs. (Channel 7 scene 1243-15253.)

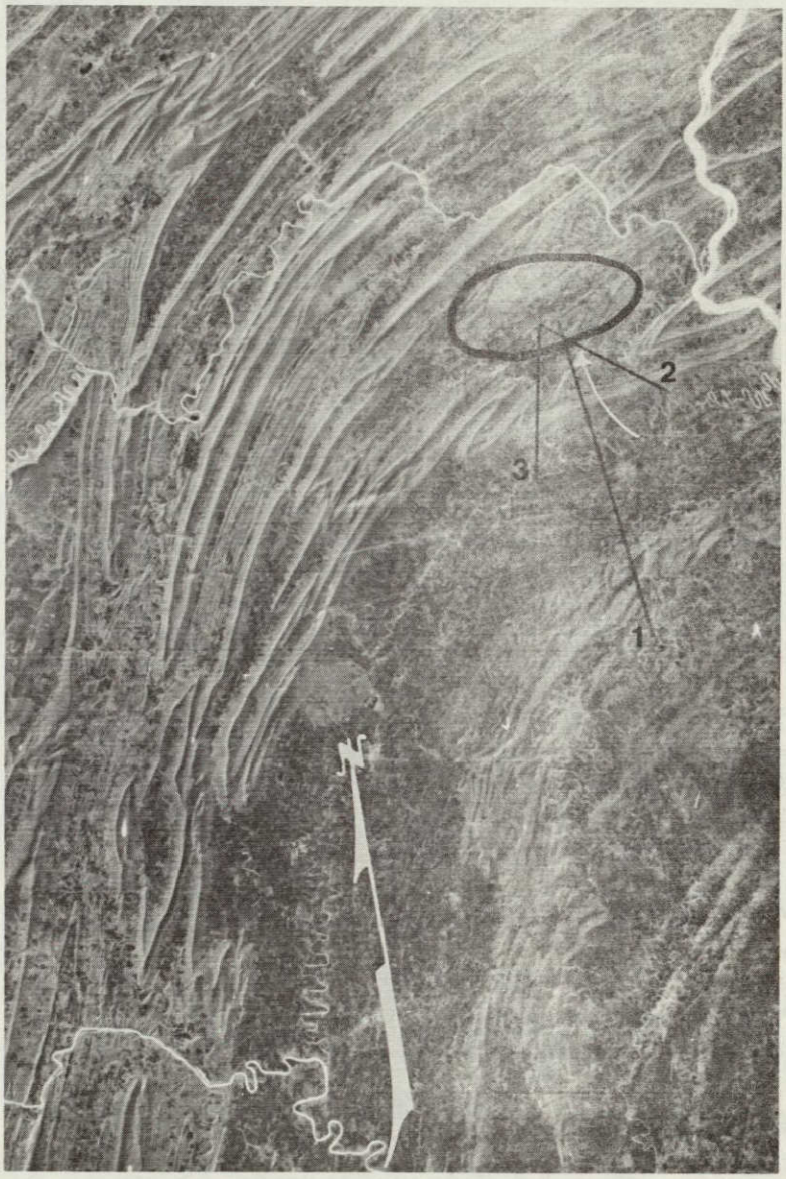
2
3
1
N

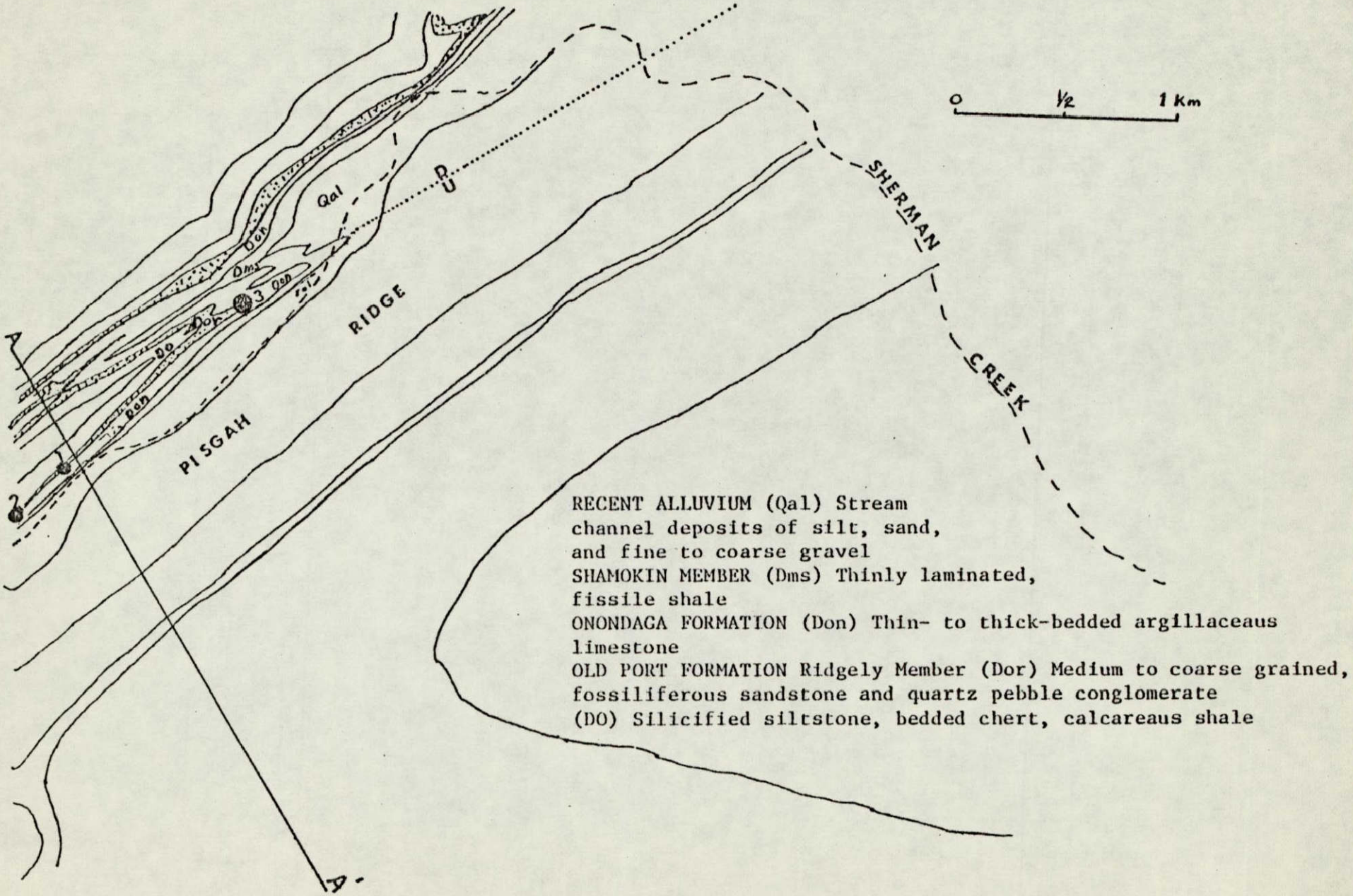

Figure 4-31: Geologic map of the Warm Springs area. Cross-section A-A' is shown in Figure 4-32. Points 1, 2, and 3 correspond to the springs shown on Figure 4-34.

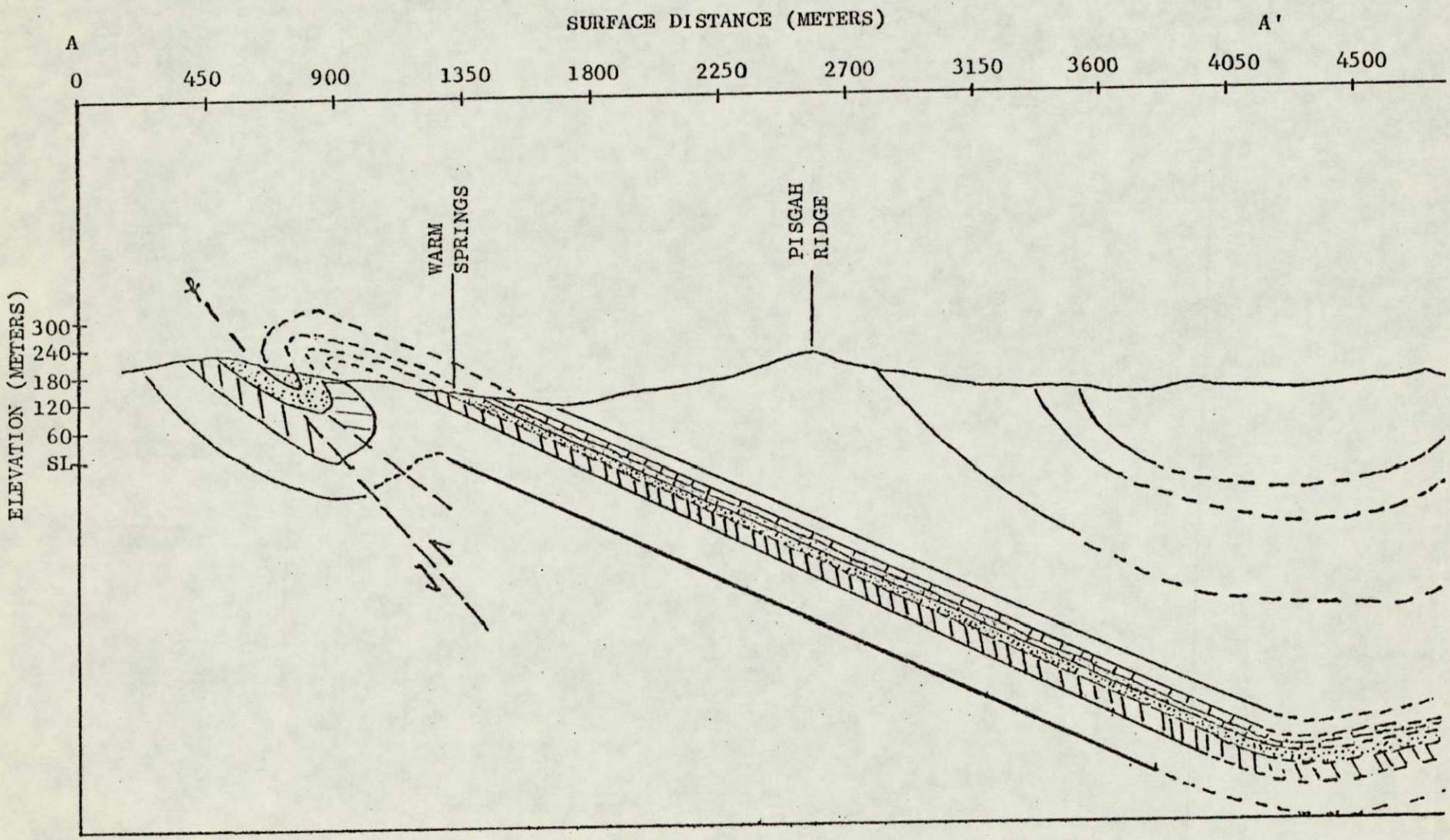

Figure 4-32: Cross-section of Warm Springs area indicated on Figure 4-31.

Pisgah Ridge to the east which rises 123 m higher than the elevation of Warm Springs (see Figure 4-32).

Observation of Figure 4-30 reveals that north of Warm Springs is the outline of a doming structure approximately 20 km in diameter. If this is an expression of uplift, normal faulting may have occurred; which, in turn, may provide a mechanism whereby down-going ground water is heated by the earth's thermal gradient and returned quickly to the surface along fracture zones. This structure, however, is more likely to be the surface expression of a basement intrusion in pre-Cambrian time. Its differing mechanical properties and topographic relief at depth could produce an observable effect in the subsequently developed overlying folded sediments.

Further support that this doming structure may represent the near surface topographic expression of a basement intrusive comes from geophysical data. Analysis of a 475 gamma magnetic anomaly extending some 70 km across and located on the dome yields a depth-to-basement estimate of 14 km. An independent interpretation of gravity and magnetic data in this area by Fleming (1975) resulted in a model of northwesterly trending slab 7 km thick, 25 km wide, with a depth-to-basement of 20 km.

Of more interest are the lineament zones crossing the Warm Springs region. Three definable zones of lineation are present and two intersect near the location of the Warm Springs (Figure 4-30). In general, these linear transgressive features show up photographically as narrow bands of contrasting tone and topography or zones that displace areas of similar tone or pattern. Investigations conducted at Penn State by Gold, Alexander, and Parizek (1974), have shown these features are expressed morphologically as water gaps and the surface expression of dikes, faults, and zones of fracture concentration. If these lineaments overlie fracture zones and extend to depths proportional to the order of their length, then they would be expected to influence ground water flow in the Warm Springs area -- providing not only deep circulation paths for ground water, but exercising control over the discharge location of springs.

4.9.1.2 Skylab Data

In an effort to locate more exactly the zones of lineation shown by Landsat-1, photographic data from Skylab were used. The large doming structure apparent on the Landsat scene of Figure 3-30 is not included in the field of view of the Skylab scene in Figure 4-33. However, a more accurate placement of lineaments from the Skylab data than from Landsat data is possible. Examination of the figure shows that the three lineaments originally observed on the Landsat scene have been relocated by use of Skylab data. Lineaments 2 and 3, which are the easiest to locate on the Landsat scene proved to be more subjective on Skylab photographs, while lineament 1 (most subjective on Landsat) was the most prominent on Skylab.

Figure 4-33: Skylab scene of the Warm Springs area. A more accurate plot of lineament 1 is seen here. The dome structure seen on the Landsat image is out of the field of view in this Skylab photo. The curved arrow indicates the location of Warm Springs. (SL3, S190B, roll 88, frame 66.)

The exact location of the Warm Springs was not discernible from Landsat imagery due to limited resolution and the shadowing effect from Pisgah Ridge on the valley below where the thermal springs discharged. Observation of the Skylab photograph with a microscope, however, revealed the exact location of the Warm Springs. This is important because linear zones of concentrated fracturing should exercise control on ground water flow patterns in this region, and the Warm Springs spatial relationship to the fracture zones may be related to these flow patterns.

Digital analysis of multispectral scanner (MSS) data from Landsat imagery was attempted for the Warm Springs area. This effort failed, probably due to the limited spatial resolution and the shadowing effects from Pisgah Ridge. No digital data were available for the Warm Springs area from Skylab, but if MSS data had been available, it is believed that a successful classification system could have been devised which would show the effects of the thermal springs region. Evidence for this was that under microscopic examination of Figure 4-33, an increase in water reflectivity appears to occur at approximately the intersection of the thermal springs effluent and Shermans Creek.

Thus, observation of Skylab photographs has revealed important spatial relationships between the Warm Springs and lineaments in the region and provided a vital scale of coverage. Combined use of the Skylab data, Landsat imagery and underflights offers the best chance of relating geologic structures to thermal anomalies.

4.9.1.3 Thermal IR Data

In an effort to map the Warm Springs and define their thermal extent and influence over the immediate region, and to locate any new areas of undiscovered thermal activity, a thermal infrared survey was undertaken with the assistance of HRB-Singer, Inc. The aerial IR coverage was flown on 5 April, 1975 at 18:00 hours EDST. Figure 4-34 shows a segment of the thermal infrared scanner data covering an area of approximately 2 km^2. Point 1 on this figure is the site of the Warm Springs (19.5°C). Point 2 is a previously unknown thermal spring (17.0°C) and point 3, although showing up as thermally warm, was, in fact, a cold spring (11.5°C). This spring emptied into a large shallow, stagnant pond which was subsequently solar heated and thus showed up as a thermal anomaly. A sinuous stream between points 1 and 2 appears to have thermal seeps, and to the left of 1 are two small thermal springs which are barely detectable. Also noticeable is the greater brightness of the dirt road boarding Sherman Creek. Because the flight was conducted at 18:00 hours (shortly after sundown), the earth thermal cross-over point has not yet occurred. Further, the fact that the Warm Springs region as a whole does not appear as a region of higher luminosity suggests that the thermal source is either far removed from the spring or weak.

It is noteworthy that these springs, warm and cold, appear to lie on a straight line. A check of the geologic map (see Figure 4-31) and subsequent field observation have shown that this alignment coincides with the outcropping of the Ridgely sandstone.

Figure 4-34: Thermal IR image for the Warm Springs area. Point 1 is the site of Warm Springs, point 2 is a previously unknown thermal spring, and point 3 is a cold spring which feeds a shallow stagnant pond warmed by the sun.

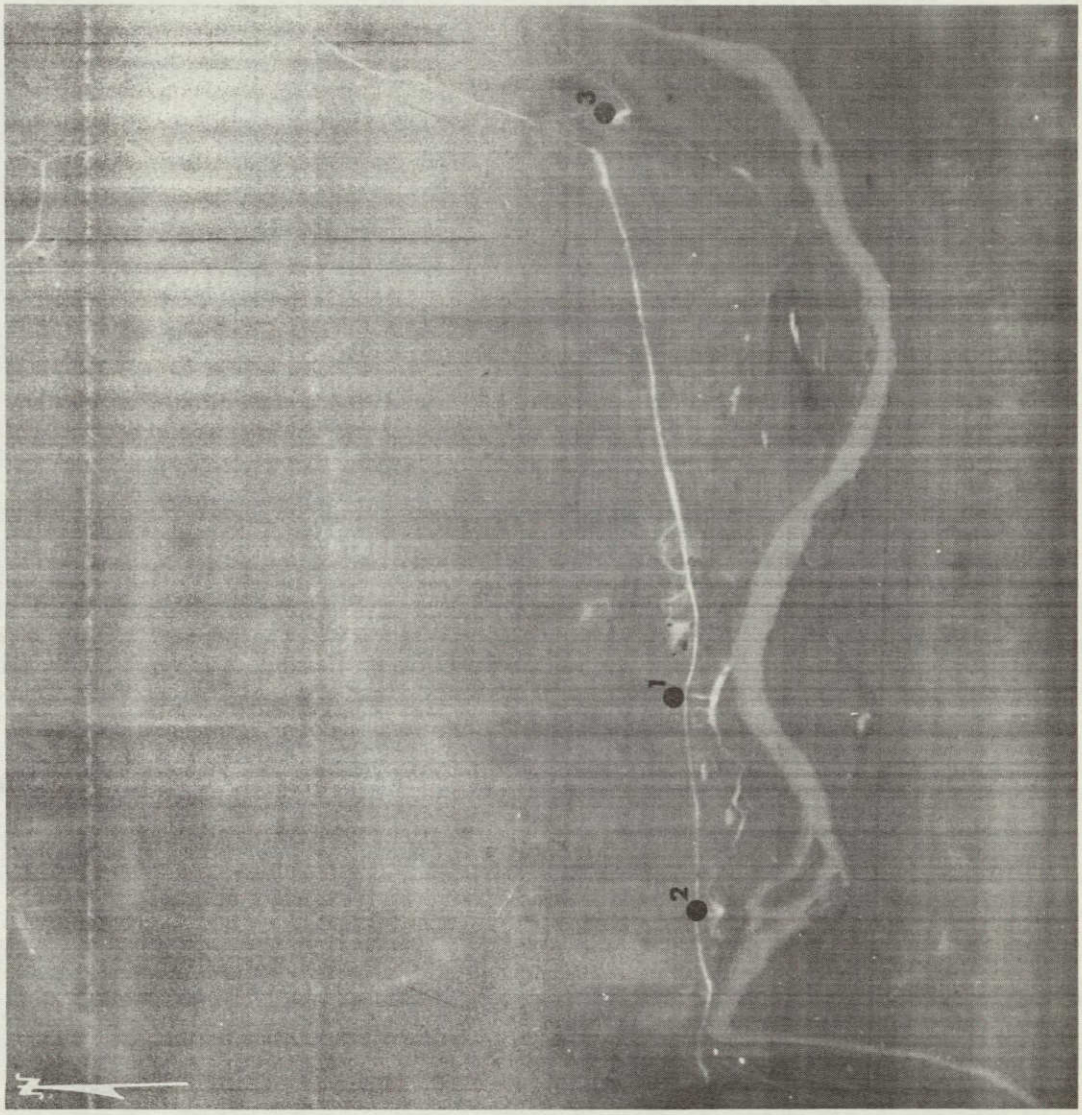
3
1
2

4.9.1.4 Conclusions

A variety of forms of remote sensing data (Landsat, Skylab, and aircraft) in combination helped delineate associated geologic structures and helped to define the spatial extent of the thermal anomaly. Landsat and Skylab provided valuable data on lineament zones in the Warm Springs region which bear a direct relation to ground water flow patterns. Thermal IR data provided information on the detailed thermal regime of the area and the associated lithologic formations where the springs discharge.

4.9.2 Associated Studies

Temperature monitoring conducted during this study indicates that the maximum range of temperatures taken on by the ground water occur during the time period of late February to middle September (Figure 4-35). It was also observed that no significant time lag is present between seasonal surface water temperature changes and the Warm Springs temperature fluctuations. It may be concluded, therefore, that a deeper, thermal water source is mixing with shallow ground water. The fact that a cold spring is located in the same geologic outcrop 1 km away may indicate that, in the area of the Warm Springs, this zone is more fractured and permits intermixing. O^{18}/O^{16} isotopic measurements indicate that at no time was the water in Warm Springs exposed to high temperatures for prolonged periods.

A fault zone, shown on the geologic map (Figure 4-31) appears to be directly in line with the outcropping sandstone, but it is located 1 km east of the Warm Springs. Two electrical resistivity surveys were conducted in the area to ascertain if the fault continued into the Warm Springs area and thereby exercised control over water flow paths. Both surveys showed no evidence of a fault zone continuing into the sandstone.

4.9.3 Numerical Model

As discussed previously, the Warm Springs may have a synclinal trough as their controlling flow path. To determine if such a geothermal syncline could exist, with the required permeability for water flow rates through its beds, a numerical model was devised giving the temperature history of the water as it flowed upward in a synclinal trough. Using Darcy's Law and a standard expression for mass flow between parallel plates, an expression for mass flow in permeable beds can be obtained:

$$q = \frac{Qd^3}{24kA} \quad \text{gm/cm-sec}$$

where q = mass flow
Q = discharge rate of spring
d = diameter of crack
k = permeability of bed
A = cross-sectional area of bed

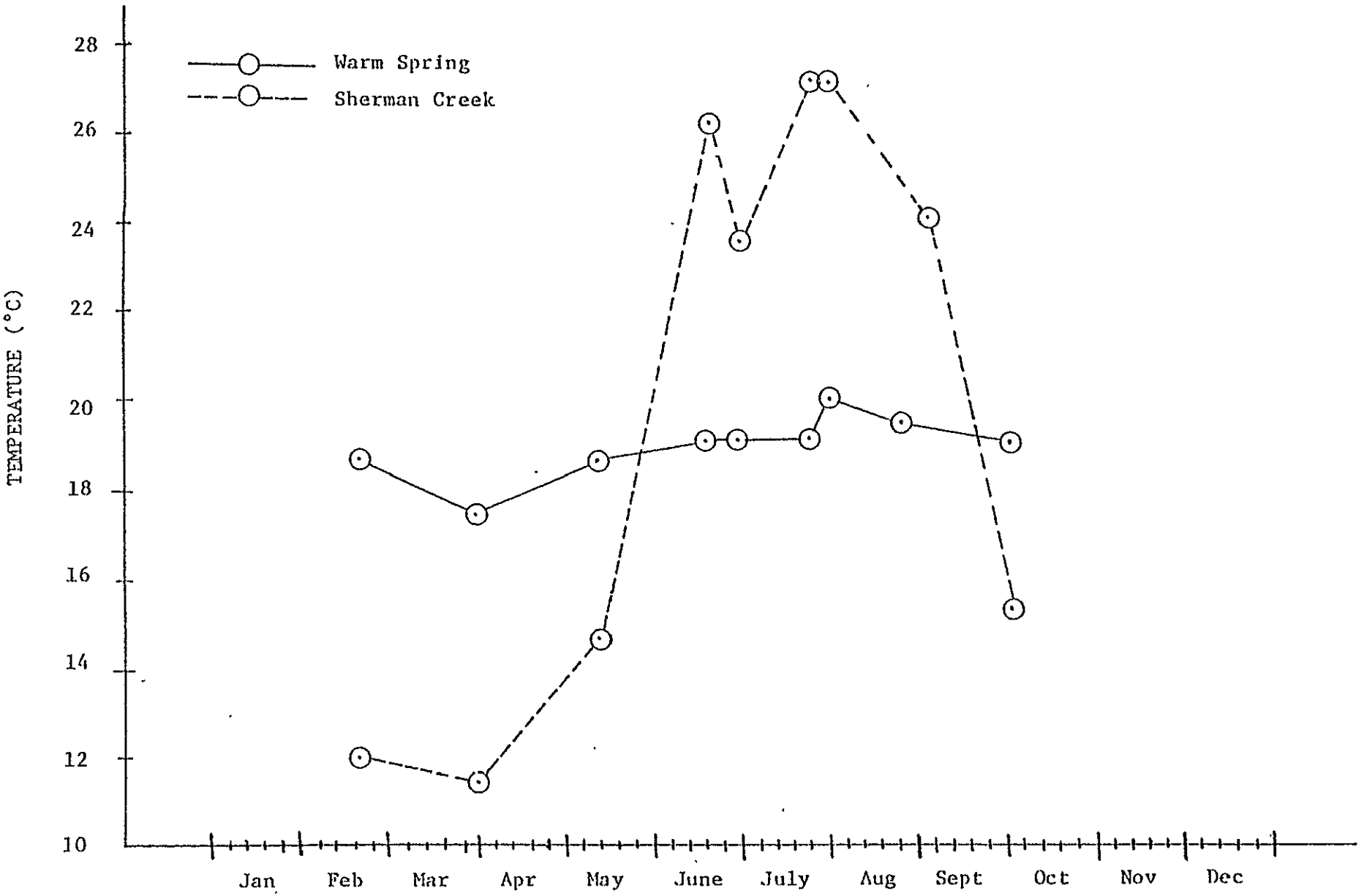

Figure 4-35: Seasonal changes in temperature for the Warm Springs and Shermans Creek.

Using the observed discharge rate of the spring of 455,000 ℓ/day, a 0.001 cm crack, and permeability equal to 400 md, this equation yields a mass flow of 0.06 gm/cm-sec.

Using the differential equation describing heat flow at a convecting boundary:

$$sq \frac{dT}{dx} = \frac{K}{L} (T-T_{\infty})$$

where s = specific heat of the liquid
T = temperature
x = surface distance
K = thermal conductivity
L = contact resistance (length)

then, considering that a syncline of any form can be described as sinusodal with wavelength λ, and using the central difference scheme, the following numerical expression can be derived:

$$T_{n+1} = T_{n-1} + 2\Delta x \frac{K}{sqL} \{1+(Z_o w)^2 \sin^2 wx\}^{1/2} \{\beta Z_o \cos wx - Tn\}$$

where

$$w = \frac{2\pi}{\lambda}$$

Z_o = max. depth of syncline

β = geothermal gradient

Figure 4-36 shows the results of various mass flow rates and their temperature history. It is found for a half-kilometer deep syncline of wavelength λ equal to that of the Warm Springs syncline and a mass flow of q = 0.01 the observed water temperature of the Warm Springs (19.5°C) is matched to within good agreement.

The numerical model shows that geothermal synclines can exist given the required permeability for its beds. The synclinal trough for the Warm Springs consists of interbedded shales, limestones, and sandstone. It is well known that such an arrangement can give rise to selective fracturing. Increased fracturing can change permeability from millidarcys to darcys. The numerical model requires a minimum permeability of 3 darcys to obtain the necessary flow rates. Whether interbedding alone can give rise to the required permeability is in doubt. If, as shown by the Landsat and Skylab imagery, zones of lineation cross this area, increased fracturing is expected. These zones would further select the water flow paths, controlling the issuing point for the thermal springs. This may

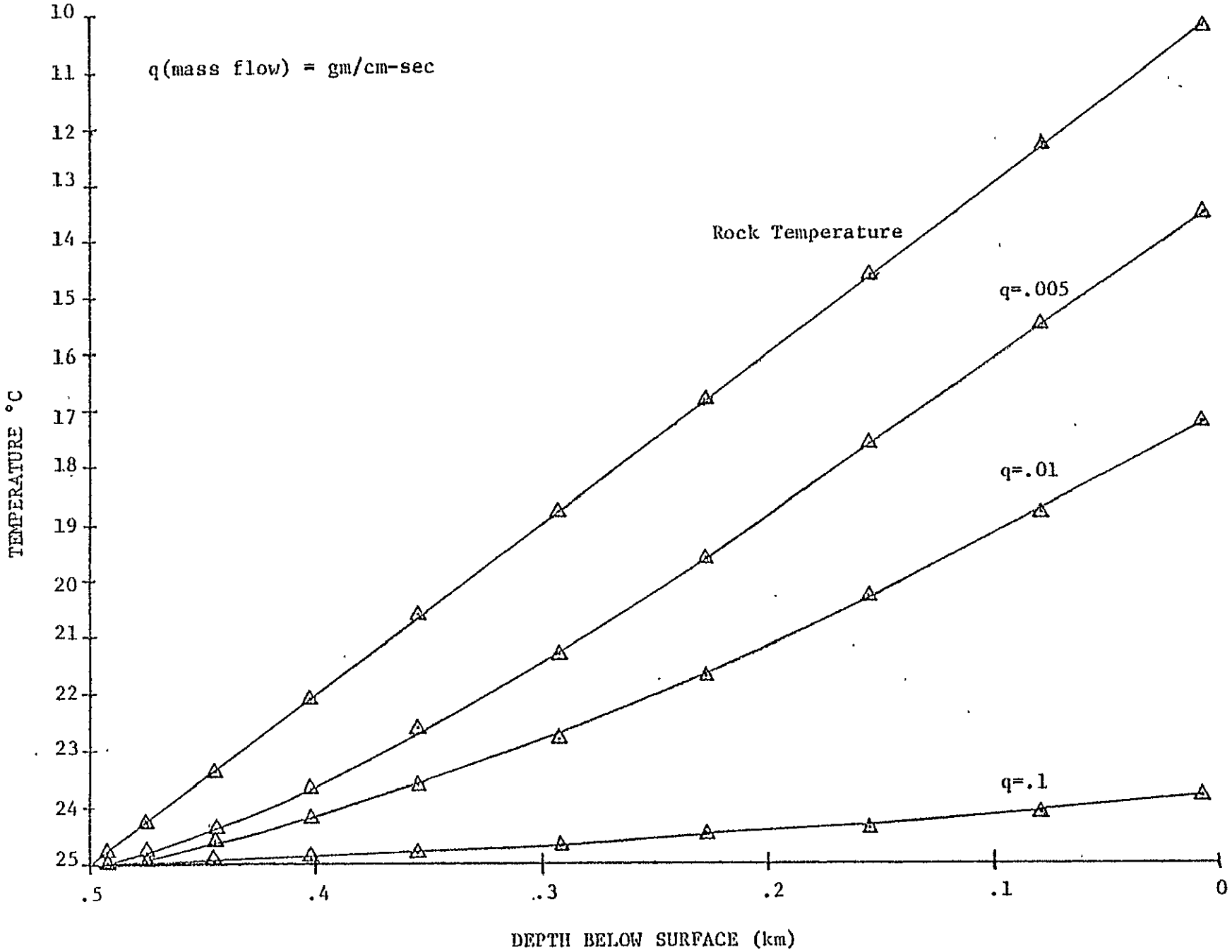

Figure 4-36: Groundwater temperature history for the Warm Springs geothermal syncline.

provide an explanation for the occurrence of cold and thermal springs within 1 km of each other in the same geologic outcrop -- the thermal springs subsurface flow path being controlled by a zone of increased fracturing, most likely from lineament number 2, seen in the Skylab data (Figure 4-33).

4.10 APPLICABILITY OF WAVENUMBER ANALYSIS TO THE INTERPRETATION OF SKYLAB MSS DIGITAL DATA (Alexander and Baumgardt)

Wavenumber analysis of spatially sampled two-dimensional data arrays has seen wide application in various scientific and engineering problems. Since multispectral scanners on the Skylab and Landsat satellites provide spectral intensity data for pixels arranged on a regular square grid spatially, it is apparent that such data easily lends itself to wavenumber analysis. The determination of spatial wavenumber signatures with these methods, along with the electromagnetic spectral signatures[1] obtained from statistical classification algorithms, provides a potentially powerful quantitative tool for interpreting satellite data, particularly in cases where the spatial periodicity of intensity is important to the problem at hand.

In the wave number approach to analysis of digital imagery, the two-dimensional spatial pattern of an image is represented as a double Fourier series in which the image is obtained by summing, with the appropriate weights, periodic components (sines and cosines) representing different spatial wavelength contributions. Mathematically, this is simply the Fourier transform of the image, namely:

$$f(x,y) = \frac{1}{(4\pi)^2} \int_{-\infty}^{\infty} \int_{-\infty}^{\infty} F(K_x,K_y) e^{iK_xX} e^{iK_yY} dK_x dK_y$$

where f is the intensity of the image at map point (x,y) and

$K_x = 2\pi/\lambda_x$, with λ_x = spatial wavelength in the x direction

$K_y = 2\pi/\lambda_y$, with λ_y = spatial wavelength in the y direction

$F(K_x,K_y)$ = wavenumber spectrum representing the contribution of each spatial wavelength to the total image; the phase of this complex-valued function carries the information on how to shift the maxima and minima of the periodic components in order to build observed map features at their proper positions upon summing over all wavelengths.

As an example of the application of wave number analysis to MSS data, the wavenumber spectrum $F(K_x,K_y)$ of the folded Appalachians should

[1] It is important to distinguish the spatial wavelengths discussed here that refer to the dimensions of features on the ground from the electromagnetic wavelengths (of light) that define the spectral bands for each channel of scanner data.

have a large value for the wavenumbers corresponding to the spatial wavelength of the folds (i.e., the distance interval between the mountain peaks). In more complicated, less obvious cases, where features of several different dimensions are present, the wavenumber spectrum gives a quantitative estimate of the dominant spacing and orientation of intensity variations on the image.

It is possible to design filters which will either selectively keep or reject contributions of a given range of spatial wavelengths to the image. Moreover, contributions can be selectively kept or rejected in a given strike direction on the image. This capability is especially useful in geologic applications to remove or subdue dominant but unwanted spatial features, such as the folded Appalachian trends, in order to look for the dominant dimension and orientation of more subtle features. Thus, in the study of various geologic structures, such as surface folds and periodically spaced fractures, Fourier analysis and digital filter processing can be applied to digital pictures of these features for the purpose of enhancing, classifying, and interpreting them.

The importance of the periodic properties of folds to their origin and structure has been pointed out previously by Hudleston (1973). He showed that the amplitudes of the different Fourier components for folds can be related systematically to the relative viscosities of the stratigraphic layers in the fold structure and to the stress field which produced the fold. Corrêa and Lyon (1974) have carried out a study of geologic lineaments using analog (rather than digital) Fourier analysis, where they took advantage of the fact that the Fourier transform of a spatial function is optically the Fraunhofer diffraction pattern of the function. Therefore, when a laser-produced light beam is passed through a transparent image and projected on a screen, the projection is the Fourier transform. Horning and Smith (1973) did a similar experiment on model apertures and also used a Fast Fourier Transform (FFT) algorithm to obtain digital Fourier transforms of Landsat-1 images. However, they were primarily interested in non-geologic pattern recognition.

The use of digital filter processing has usually been limited to image enhancement. These techniques have been used for diverse applications such as enhancement of television images from space probes (Billingsley, 1970) and biomedical pictures (Selzer, 1968). The application of filter processing to remote sensing data has been discussed by Maul, et al. (1974).

In this section, computer programs developed for Fourier analysis and spatial filtering of digital remote sensing data are discussed. The relation of the wavenumber domain to the spatial domain has been studied for artificial test cases, as well as for real data, with emphasis placed on ground features of geologic interest. Also, the applications of these techniques in the study of various ground features are given. The data used in this study were obtained from Skylab digital tapes, although the methods discussed are of general applicability.

4.10.1 Computer Programs

Computer programs were written to compute the wavenumber spectrum of the spatial intensity output from an image for a single channel. Also, filter programs were written to produce the lowpass, highpass, bandpass and strike select (or reject) filter responses for each image.

4.10.1.1 Fourier Transform Program

The Fourier transform program uses the Fast Fourier Transform (FFT) algorithm developed by Cooley and Tukey (1965). Our program uses the IBM subroutine HARM (IBM Corp., 1966). This method cuts down the computing time from being proportional to N^2 for the direct method to being proportional to $N \log_2 N$ for the FFT, where N is the number of transform points. Hence, the number of points to be transformed must be a power of 2. In the examples discussed below, 32 x 32 arrays were transformed using this program.

The output from a two-dimensional FFT consists of four quadrants of numbers in wavenumber space, where the axes dividing the quadrants extend from $+K_{XN}$ to $-K_{XN}$ horizontally and $+K_{YN}$ to $-K_{YN}$ vertically, where $\pm K_{XN}$ and $\pm K_{YN}$ are the maximum resolvable (Nyquist) wavenumbers in the X and Y directions respectively, namely $\pi/\Delta X$ and $\pi/\Delta Y$ with ΔX and ΔY the ground distance between pixel centers. Because of symmetry, two of the four quadrants are redundant. Hence, in the computer plots of the wavenumber spectrum, only two quadrants are displayed. Examples of wavenumber spectra of Skylab channels will be presented in a later section.

4.10.1.2 Filter Programs

Two-dimensional spatial filters have been used extensively in geophysics in the interpretation of gravity, magnetic, and seismic array data. The theory of two-dimensional filters for gravity data was reviewed by DeMeyer (1970). Selzer (1968) presents a number of examples of the application of two-dimensional filters to visual imagery. Such filters may be implemented either by convolution in the spatial domain or multiplication in the wavenumber domain. In order to take advantage of the speed of the FFT, our programs use the latter approach.

Three different programs were developed. One program implements a two-dimensional band-pass filter, which is trapezoidal or triangular in shape, as a function of wavenumber K. The filter transfer function is multiplied by the Fourier transform of each scan line intensity in the data block, and the product is then transformed back to the spatial domain. This generates the filtered response of the data along scan lines. The data block is then transposed and the above procedure is repeated. This effectively filters the data block along element lines completing the two-dimensional filtering operation on the entire block or image. This type of filter has the disadvantage of being square symmetric, and, therefore, diagonal directions are filtered with a somewhat different

band-pass. However, this program is still useful, particularly if the periodic topographic features strike along or perpendicular to scan lines.

A second program is available which is circularly symmetric and does not suffer from the disadvantages of the previous filter program. The filter coefficients are computed in polar co-ordinates for wavenumber space by tapering a sharp wavenumber cutoff with a Bessel function of zero order. The theory for the calculation of this low pass filter was given by Lavin and Devane (1970). A high pass, band pass, or band reject filter may be obtained from this low pass filter algorithm by the method described by Selzer (1968).

The third program implements a strike select (strike reject) filter. Embree, et al. (1963) introduced this filter technique to seismology where it was applied to one-dimensional spatial seismic data to enhance (or eliminate) waves propagating at particular velocities across an array of receivers. The filter coefficients were computed for applying the filter in the frequency-wavenumber domain. Fuller (1967) gave the coefficients for this type of filter in the two-dimensional wavenumber domain. In both cases, the filter function is applied by convolution with the data set. Our program for rejecting wavenumber contributions within a certain azimuthal wedge (strike reject filter) simply puts in zeroes within the wedge and leaves the rest of the wavenumber spectrum unchanged. The edges of the wedge are smoothed by applying a cosine taper along scan lines and element lines. Transformation back to the spatial domain then produces a map with features striking in the specified azimuthal wedge eliminated. Limits in wavenumber can be read-in in order to produce a low pass, high pass, or band-pass, strike-select filter using the same program. This permits control of the scale (wavelength) of features rejected or selected in the azimuthal wedge (strike direction). More complete descriptions of these programs and examples of their use can be found in ORSER-SSEL Technical Report 3-76.

Subroutines were also written to generate artificial data for experimental purposes and to verify that our programs were working properly. The Skylab digital data were taken from the original NASA tapes for a selected smaller training area by subsetting the data for the training area onto another tape using the ORSER program SUBSET[1]. An intensity map of the area was obtained by using the NMAP program developed previously by ORSER. A contour subroutine was also used to print maps as contours of intensity before and after filtering and also to plot the wavenumber spectrum.

4.10.2 Applications

4.10.2.1 Wavenumber Spectra

Simulated imagery. Three sets of simulated data were Fourier

[1]ORSER programs are briefly described in section 5.1.

transformed using the FFT program: a single lineament; multiple lineaments spaced apart at periodic intervals; and a lineament with peaks in intensity, or spikes, placed at a small number of points along the lineament. These cases are of geologic interest because many lineaments, some of which are parallel or sub-parallel to one another, have been found on satellite imagery. The FFT of other types of features, such as rectangles, squares, and circles, have been presented by Horning and Smith (1973). As mentioned above, our contour plots represent two quadrants of the wavenumber spectrum, with the horizontal direction going from K = 0 to $-K_{YN}$ increasing downward. The Nyquist wavenumber in the X and Y directions is defined as $1/(2\Delta s) = 0.5$ samples per data interval, where Δs, the data interval, is the distance between the centers of two pixels. On all the plots to be presented, the wavenumber coordinates are normalized by the respective Nyquist wavenumbers in the X and Y directions. This was done for convenience in applying the filter programs and to keep the results general for any scale of digital imagery.

The FFT of a lineament extending from the upper left to the lower right produces a lineament in the wavenumber domain trending perpendicular to the strike in the spatial domain as seen in Figure 4-37a and b. The plot shows the lineament projecting from K = 0 to the lower left (the direction perpendicular to the lineament strike), as expected (Figure 4-37b). For multiple parallel lineaments, the FFT produces a set of cluster points lining up perpendicular to the strike of the lineaments as illustrated in Figure 4-38a and b. The clusters consist of a set of main lobes and a set of smaller amplitude side lobes in the wavenumber spectrum. The spacing of the lobes is controlled by the spatial frequency (spacing) of the lineaments, and the amplitudes and shapes of the lobes are controlled by the number and intensity of the individual lineaments. In this example, there are 7 parallel lineaments spaced by data intervals of approximately 4 (perpendicular distance between lineaments); hence, in wavenumber space, the main lobes are spaced by 0.25 samples per data interval (Figure 4-38b). In a comparison of the case of 7 lineaments with a case of 5 parallel lineaments, the lobe shapes and intensities were found to be different, as expected. These results agree with those of Corrêa and Lyon (1974, Fig. 1).

As a final test example, we consider the case of a lineament trending from upper left to lower right, as before, but this time with 6 spires, or sharp intensity peaks, superimposed at spaced intervals along the lineament as shown in Figure 4-39a. The resultant wavenumber spectrum consists of a number of parallel maxima (Figure 4-39b). The primary maximum response goes from K = 0 diagonally to the lower left and is associated with the main lineament in the spatial domain. The other parallel maxima in the wavenumber domain are produced by the spires. No attempt was made to space the spires periodically, hence their irregular spacing in the wave number domain.

Skylab data. The Skylab data used in this study were obtained from mission 3, orbit 14, 30 August 1974. The data on the 9-track NASA tape had been line straightened. For the purposes of this study, two training areas near Bedford, Pennsylvania were subset. The first is about 6 kilometers east of the northern tip of the Wills anticlinorium. The subset line and column numbers for these two areas are:

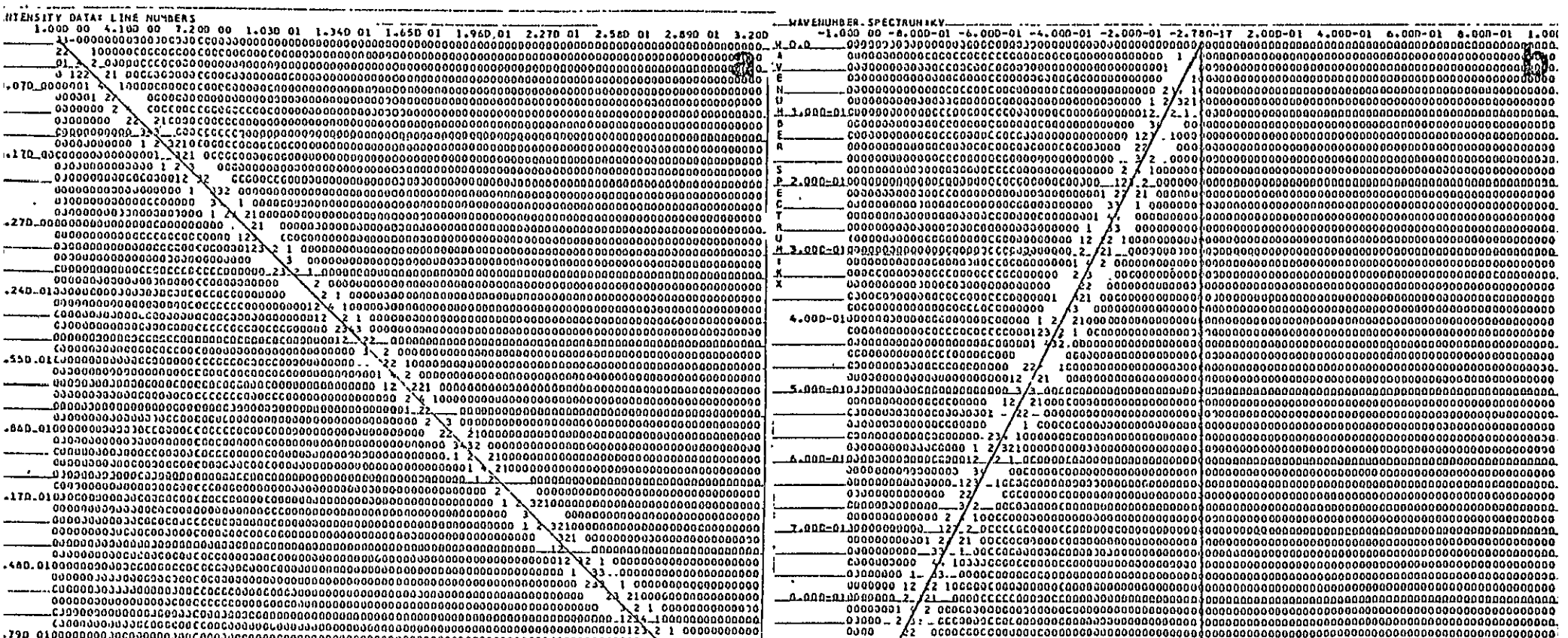

Figure 4-37: a) Contour plot of a simulated lineament trending NW-SE. b) Contour plot of the FFT wavenumber spectrum of the simulated lineament. The vertical line denotes the $K_X = 0$ axis. The +Ky axis is increasing down from this point. The spectrum is a line in wavenumber space perpendicular to the strike of the lineament in the spatial domain.

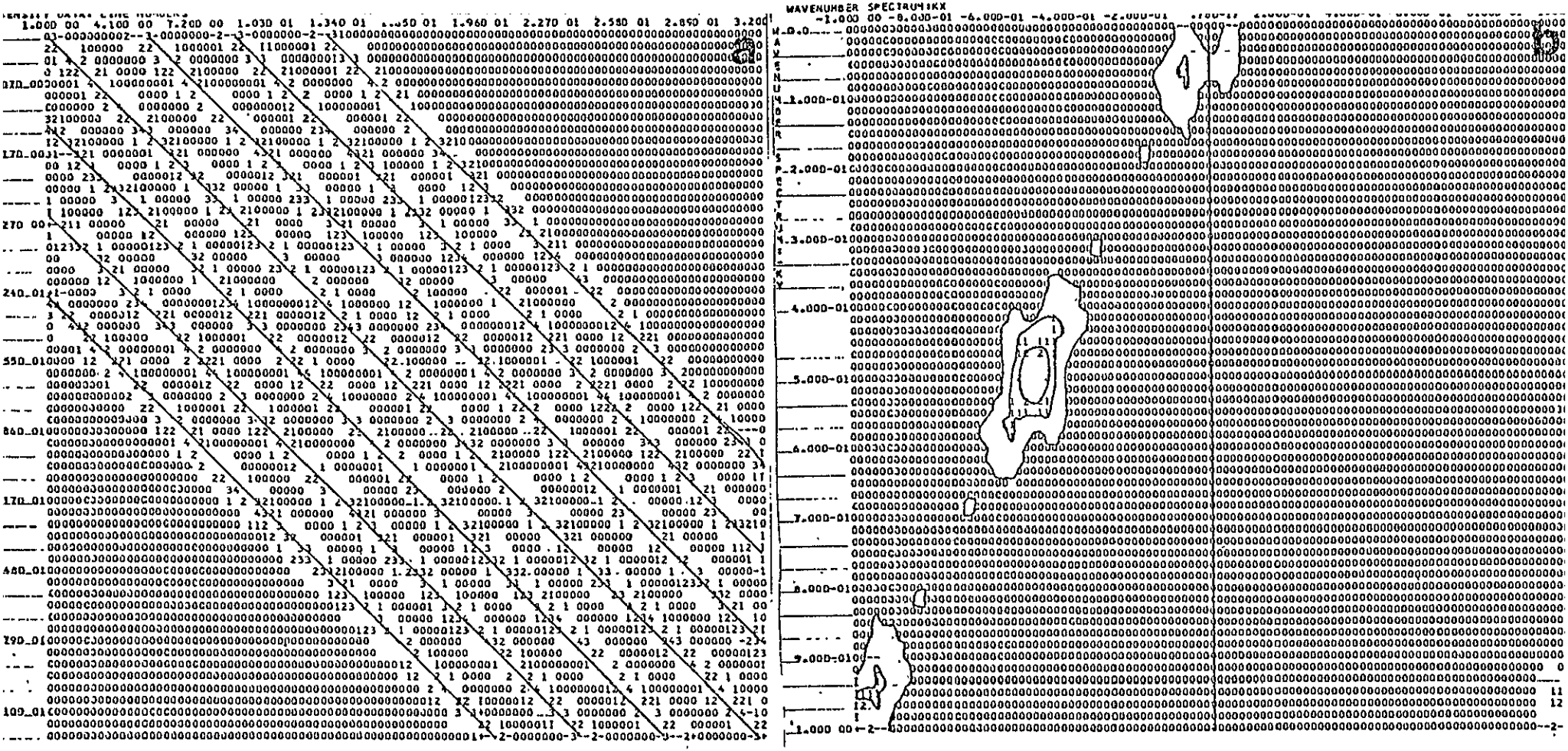

Figure 4-38: a) Contour plot of seven simulated lineaments trending NW-SE. b) Contour plot of the FFT wavenumber spectrum of the seven simulated lineaments. The peaks of intensity in wavenumber space line up perpendicular to the strike of the lineament in the spatial domain. The spacing of the peaks is determined by the spacing of the lineaments.

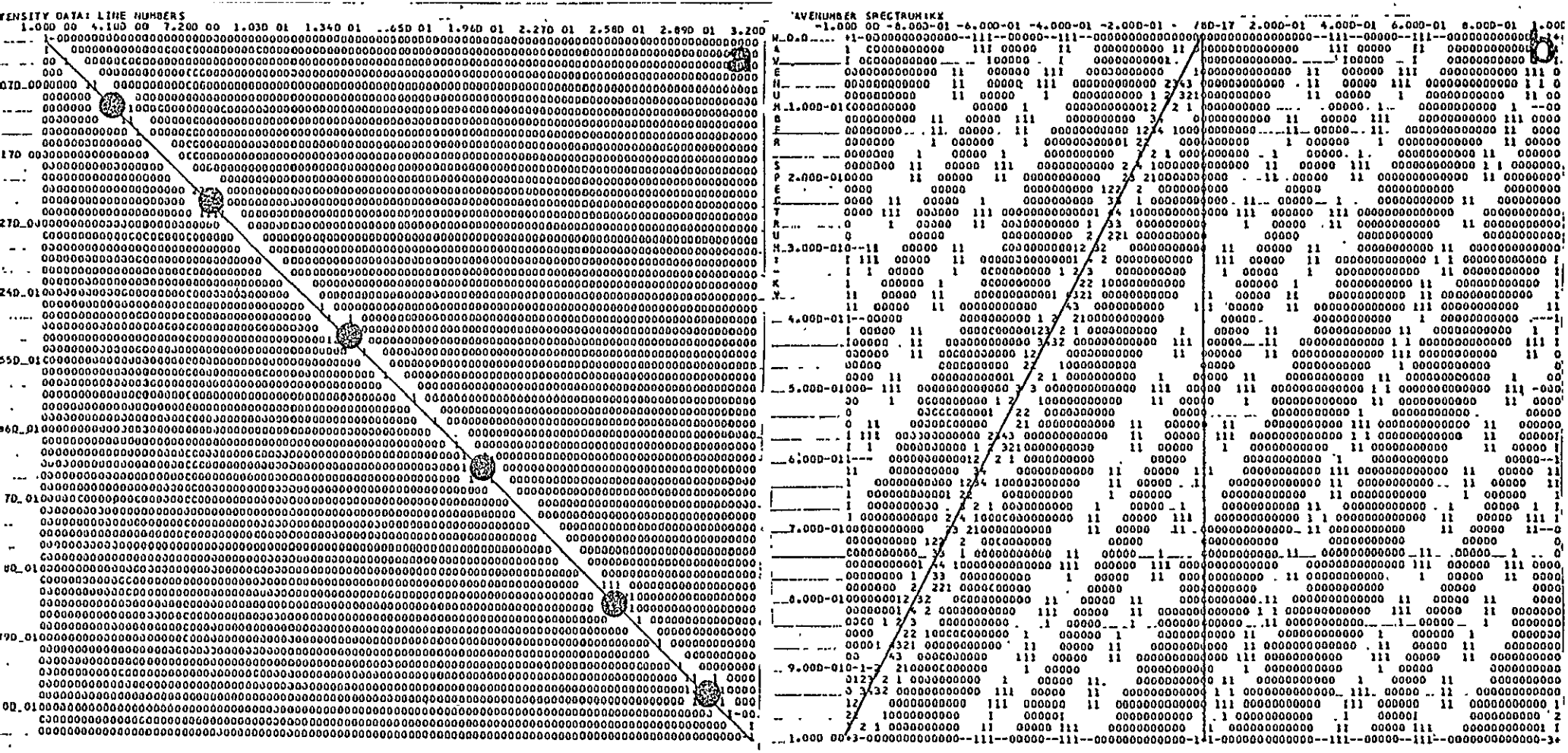

Figure 4-39: a) Contour plot of a simulated lineament with six spires, or spikes, in intensity along its length. No attempt was made to space the spires periodically. (The spires are indicated by black dots.) b) Contour plot of the FFT wavenumber spectrum of the simulated lineament with six spires. The lineament extending from K = 0 to the corner of the left quadrant, denoted by the dark line, is produced from the original lineament. The other parallel lineaments, represented by 1's, are produced by the six spires. The spacing of these lineaments is determined by the spacing of the spires.

Northern Area (A)		Southern Area (B)	
Line	335 - 336	Line	524 - 555
Column	781 -812	Column	490 - 521

These subsets (A and B) are shown in Figure 4-40, along with the entire swath of ground area covered by the MSS data on this tape. We selected this area because the Everett lineament strikes east-west across the southeastern half of Pennsylvania and apparently crosses the tip of the Wills mountain. Results that isolate this lineament conclusively are not presented here, but the wavenumber properties of the dominant linear features in this area are discussed.

The wavenumber spectra of the two subset training areas mentioned above were obtained. In Figures 4-41 and 4-42 we compare contour plots of the wavenumber spectra of channels 15 (10.20-12.50 μ) and 17 (1.20-1.30 μ), respectively, for the two areas indicated in Figure 4-40. Figures 4-41 and 4-42 each consists of the response of a single channel, so that the two training areas can be compared. In both areas, the flight path of spacecraft is such that the vertical axis in the space domain and the K_Y axis in the wavenumber domain both point N-NW (see Figure 4-40).

An examination of these four wavenumber spectra (Figures 4-41 and 4-42) reveals that not only are the responses different for the two areas in the same channel but there are significant differences in the wavenumber spectra for two different channels of the same area (compare Figures 4-41a with 4-42a and 4-41b with 4-42b), indicating different dominant scale features and feature periodicities in the images for different channels.

Other MSS channels were also analyzed in this manner and more complete discussion of these wavenumber spectra can be found in ORSER Technical Report 3-76.

In the northern area, the main topographic feature is Evitts mountain, which strikes N-NE and, therefore, almost at an angle of 45 to the vertical on the Skylab imagery. On the wavenumber spectra for the 7 channels of the northern area (Figures 4-41a and 4-42a), it can be seen that dominant wavenumber contributions project into the bottom right quadrant, or perpendicular to the strike of the ridge. In both cases, the dominant wavenumber intensities cluster about low wavenumbers (i.e., relatively large scale ground feature periodicities). The contour plots of the wavenumber spectra also reveal a distinctive wavenumber signature for each channel. Channel 15, which is in the middle of the emissive infrared band, produces a broad spectrum with higher wavenumbers and channel response intensities than the other channels.

The higher wavenumber content of this band of the electromagnetic spectrum indicates more sharply contrasting linear features and, therefore, more detailed imagery. Channel 17, which is the upper part of the infrared and is of narrower bandwidth than channel 15, does not show the same breadth of wavenumbers as channel 15 but still contains large contributions in the high wavenumbers. Also channel 17 shows side-lobe features along

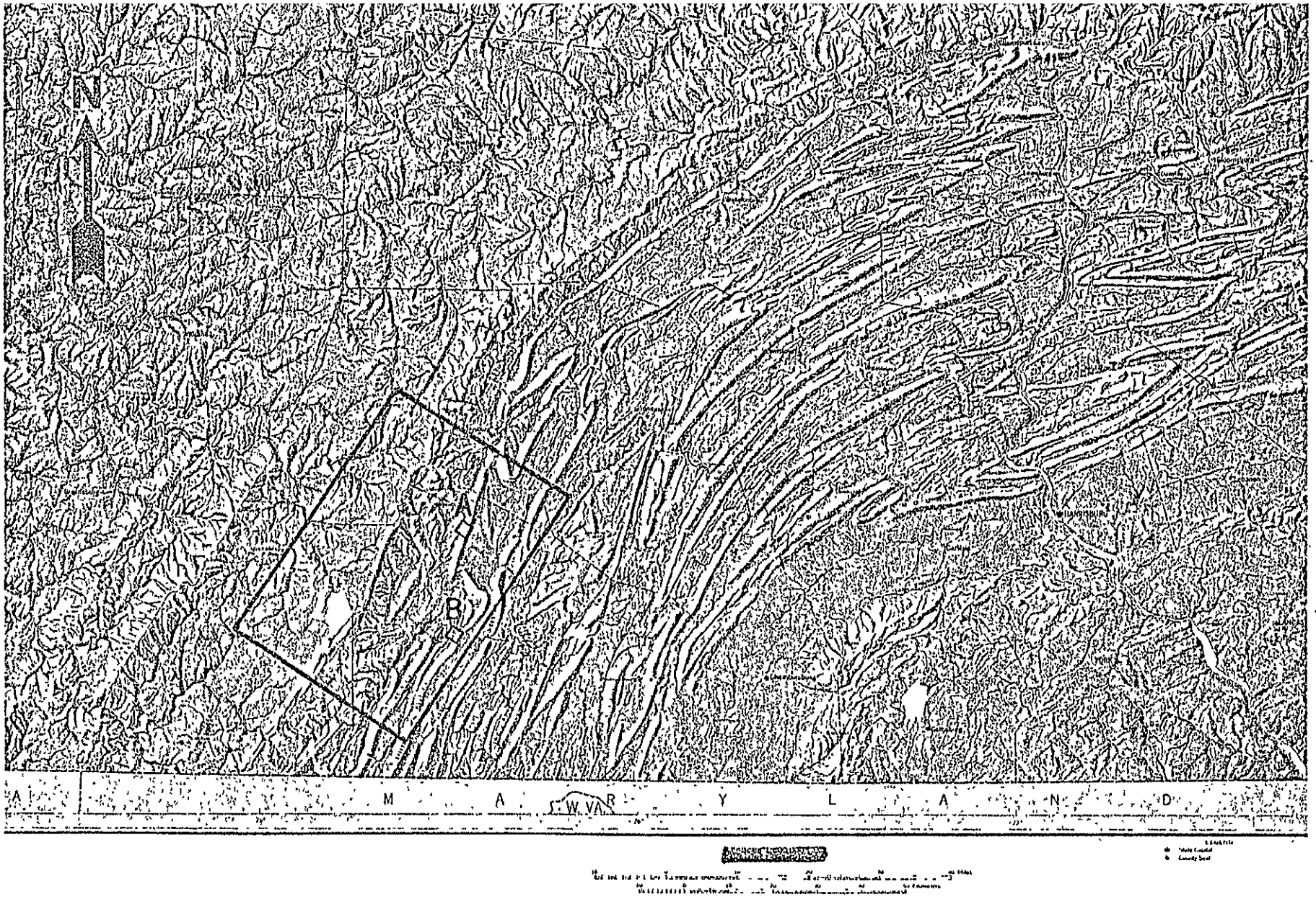

Figure 4-40: Physiographic base map of a portion of Pennsylvania showing the ground surface covered by the Skylab digital tape data (SL3, orbit 14) and the two training areas (A and B). The trace of the Everett lineament is indicated by white arrows.

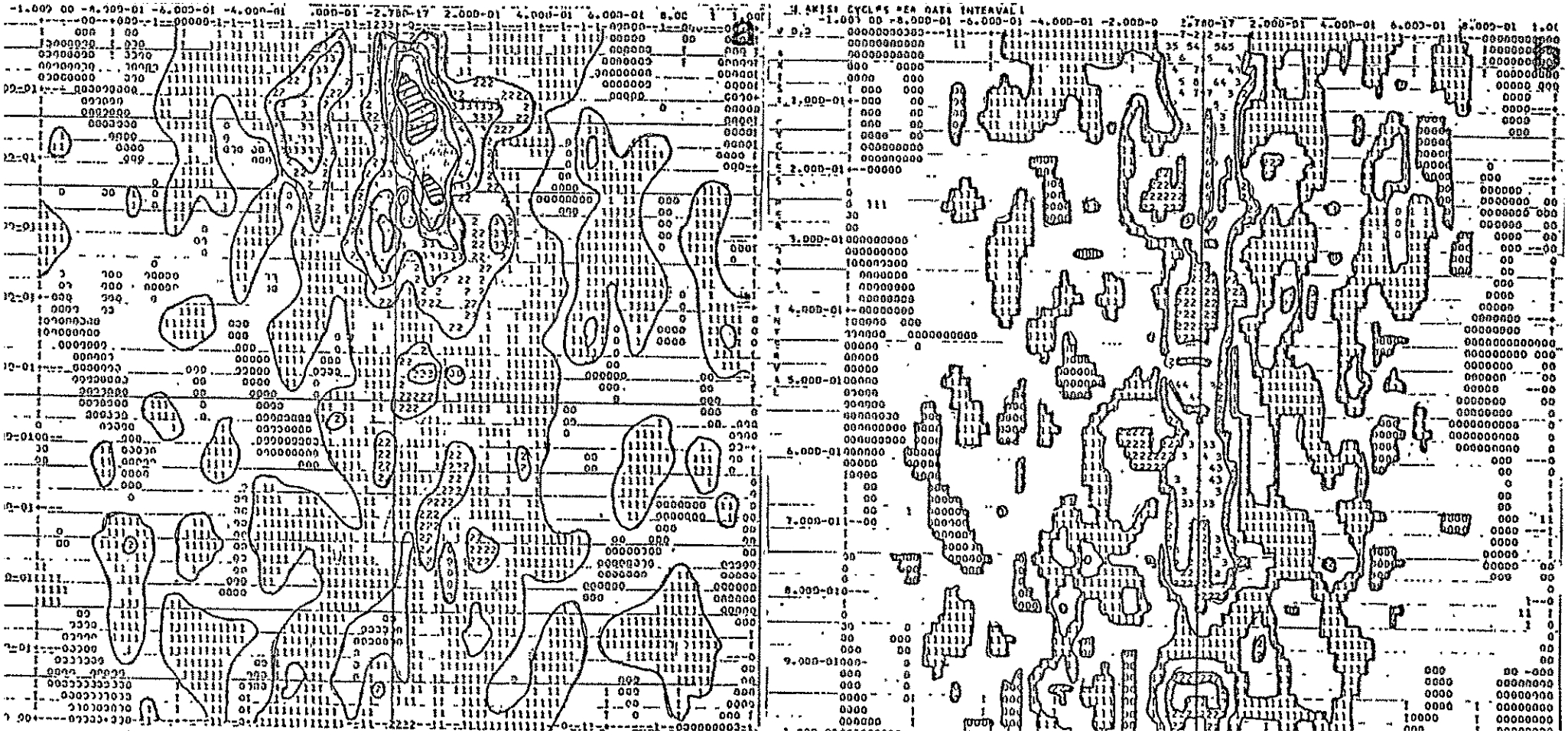

Figure 4-41: a) Contour plot of the wavenumber spectrum of the northern area (area A on Figure 4-40) for channel 15 (10.20-12.50 μ). b) Contour plot of the wavenumber spectrum of the southern area (B) for channel 15.

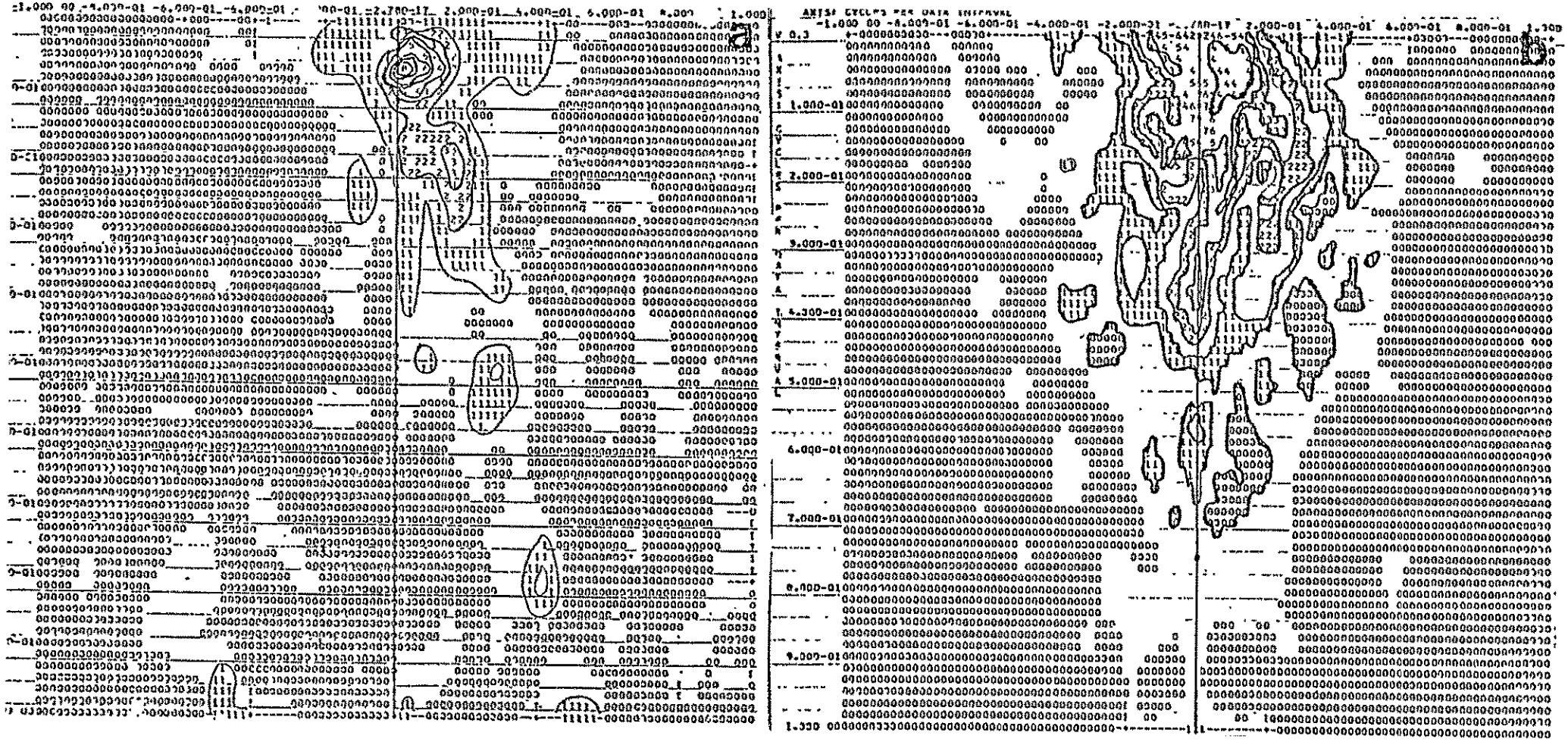

Figure 4-42: a) Contour plot of the wavenumber spectrum of the northern area (area A on Figure 4-40) for channel 17 (1.20 - 1.30 μ). b) Contour plot of the wavenumber spectrum of the southern area (B) for channel 17.

the prevailing strike direction out to the Nyquist wavenumber characteristic of a multiple lineament. This is due to the fact that there is another ridge adjacent to Evitts mountain, as can be seen on the digital NMAP. These side lobes are suggested in the other channels as well, but their relative intensities are not as pronounced as in the infrared channel. This suggests that contrasting features not easily seen in the visible band, such as varying degrees of shadow produced by a double ridge, would be more pronounced in the thermal IR because of its strong dependence on the thermal properties of the ground.

In the southern area, the southern extension of Evitts mountain trends more toward the NE-SW direction and, hence, is almost horizontal on the Skylab image (i.e., perpendicular to the track direction). The block input into the FFT program contains the portion of the ridge that is cut by a gorge through which pass both the Raystown Branch of the Juniata River and the Pennsylvania Turnpike. On the wavenumber spectra for this area, the high intensities are concentrated in the low wavenumbers controlled by the mountain. The wavenumbers are more spread out about the ridge strike feature than in the northern area, because the ridge is arcuate and convex toward the northwest. This causes the wavenumber response from this ridge feature to spread fan-like about the $K_X = 0$ axis.

The IR channel (15) again reveals a more detailed wavenumber spectrum than the other channels. The side-lobe feature produced by multiple ridge shadows is apparent on the ridge strike feature. Also, a linear feature can be seen projecting into the lower right quadrant. This lineation, is produced by the river and highway which cut through the gorge. Also, in channel 15, a lineation can be seen extending into the lower left quadrant at about a 20° angle with the $K_X = 0$ axis. This feature is also suggested in channel 13 but is not obvious on the other channels. We believe this may be the Everett lineament, which would produce a strike feature in this direction.

4.10.2.2 Filter Analysis

Trapezoidal Band-Pass Digital Filter. To test the trapezoidal filter program, the impulse response of the bandpass filter was obtained by filtering the data block with two single-point intensity spikes. The filter is triangular in shape, with low cutoff of 0.5, high cutoff of 0.875, and center wavelength of 0.6875. The actual wavenumbers in cycles per data interval would be these numbers divided by two. The filter response is peaked at the positions of the two spikes and the sidelobes extend in the K_X and K_Y directions until wavenumbers equal those in the filter passband.

This filter was applied to the two Skylab training areas discussed before. In both cases, the outputs show clusters of points at locations where the passband wavenumbers are produced. Since the filter is essentially highpass (short wave length) and the ridges contribute principally to the low wavenumbers (long wave length) the ridges are completely removed by the filter. No significant differences can be seen between the two filter outputs.

Strike select filter. To test the strike select (strike reject) filter program, an attempt was made to remove a NW-SE trending lineament by applying the azimuthal reject filter to the experimental data. With angles measured from the $-K_y$ axis, with negative signs in the left quadrant and positive signs in the right quadrant, the range of angles to be rejected are -20° to -60°. This filter effectively removed the NW-SE lineament.

Another interesting example is the case of a lineament with local spires (Figures 4-39a and b). By applying the same fan angles to this case the strike feature in the wavenumber spectrum is removed leaving the parallel features produced by the spires. On inverse transforming, the spires remain and are lined up along the strike of the original lineament.

The strike selective filter was then applied to the southern training area for channel 20 (1.09-1.19 μ). In this channel, the river and highway which cut through the gorge form a straight linear feature on the image. This shows up as an alignment of 1's, 2's, and 3's between the two dotted lines in Figure 4-43a. By passing the data block through the band reject filter with azimuthal limits of 30° and 75°, this linear feature was removed, producing the contour plot in Figure 4-43b, where the previous alignment of numbers between the dotted line has been removed.

Another run was made on channel 15 where the FFT produced a possible strike feature for the Everett lineament. The filter was designed to remove the dominant wavenumbers of the ridge and leave the lineament feature. Although the ridge was removed, no resulting lineament feature was evident in the spatial domain. This means that even with the ridge effects removed, the lineament in this area did not manifest itself strongly enough to be distinguished from other local features.

Also, visual inspection of the imagery for this small area does not reveal any obvious indication of the lineament in the area analyzed; the inference that it actually passes through this area comes from examining a much larger area and connecting places where the feature is clearly evident. Limits on the data block size (ground area) that can be analyzed in the present computer programs preclude the analysis of areas from Skylab imagery large enough to include a complete major lineament (e.g., 150 km x 150 km). However, it is anticipated that a re-structuring of the program to use temporary disk storage more fully, as well as program overlay features of the IBM 370 computer, would permit analysis of significantly larger ground areas. This effort now seems justified, based on the examples and results presented here.

4.10.3 Conclusions and Recommendations

4.10.3.1 Conclusions

As a result of studying the spatial wavenumber spectrum of the individual Skylab channels, it has been shown that each channel provides

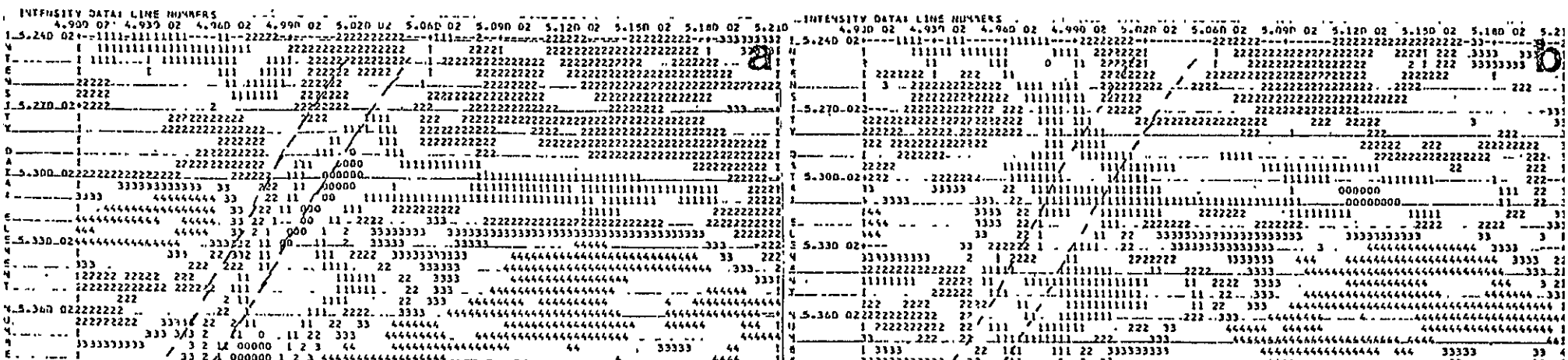

Figure 4-43: a) Contour plot of the southern area (B on Figure 4-40) for channel 20 (1.09-1.19). The highway which cuts through the gorge in Evitts mountain is enclosed in the two black dotted lines. Notice the alignment of 3's, 2's, and 1's parallel to these lines.
b) Contour plot of the scene after the application of the strike select (band reject) filter with angles 30° and 75°. Notice that the lineations between the two dashed lines have been removed.

unique wavenumber information about a particular scene. The peaks and troughs produced in the wavenumber domain by a scene are shaped differently in different channels, and the separations of the intensities of peaks and troughs vary for different channels. The most detailed wavenumber spectrum is produced by the thermal IR channel (15) which has higher intensities in higher wavenumbers than the other channels. The channels in the IR and near IR show a relatively distinct wavenumber signature for the dominant periodic feature in the scene. The channels in the visible range have a flatter wavenumber response, and the wavenumber signature associated with the dominant scale feature is not as sharp and as well defined as in the IR channels.

Wavenumber analysis is very helpful for quantitatively studying geologic structures, particularly folds and fracture traces. It also has potential application in quantitatively studying and enhancing the lineaments and other subtle features which have been observed on satellite imagery. If the lineaments appear as a line of discontinuous line segments or peaks in intensity relative to the intensity of the surroundings, they will exhibit the distinctive wavenumber response of the analogous test case presented (Figure 4-39). Indeed, because of the distinctive patterns found, it may be useful to search for lineaments in the wavenumber domain rather than in the spatial domain.

Filter analysis has a number of applications in remote sensing. In geology, the strike selective filter can be used to verify lineaments observed by photo-interpretive methods. For instance, if a lineament is suspected on the basis of the alignment of streams or lakes, it may be desirable to see if the higher resolution of the digital data would show supporting evidence for the lineament. One could use a strike selective filter for the expected strike feature of the lineament. If the lineament exists, it will be enhanced on the filtered image. This type of filter may also be used in conjunction with various other kinds of feature enhancement filters similar to those described by Selzer (1968, p. 827).

Another type of filter which has potential is a derivative operator. This operator works in the wavenumber domain and returns the spatial derivative operator. This operator works in the wavenumber domain and returns the spatial derivative of the data. The derivation of these operators is described by Fuller (1967). If sharp spatial contrasts in intensity appear in the scene, such as a lineament, the derivative operator will give a large output where these rapid changes in intensity occur.

Filter analysis may also be used in conjunction with existing cluster analysis programs to set up data in a form that contains only information for the scale feature (spatial wavelength range) of interest. For example, if one wishes to classify features associated with cities which may consist mainly of high wavenumbers (small-scale features), a high pass or high wavenumber filter may be applied to the data before classification. Related to this, filter analysis can be used to aid in deciding which channels to use for studying a particular problem. This may be done by filtering more than one channel to see which ones give the highest response in the spatial wavelength band of interest. Also, comparing the wavenumber spectrum of different channels would reveal redundancy and help in the selection of the optimum spectral bands.

This also may be important in selecting a small number of channels for color displays for the particular problem at hand or to limit the amount of data collected.

All the above applications of wavenumber analysis have been for multispectral intensity data for particular channels. It should be emphasized that these techniques can be applied to any set of data which can be represented as a two-dimensional array of points. For example, data in the form of the norm of intensities from different channels, ratios of intensities of different channels, or data classification associated with classification of points into clusters can also be analyzed with these techniques.

4.10.3.2 Recommendations

As a result of this preliminary study, the following recommendations are made:

1. Wavenumber analysis should be used in conjunction with other techniques, such as canonical analysis, in assessing which channels contain the optimal amount of information for a particular application and in removing channels which contain redundant information.

2. Wavenumber analysis can be used in improving classification maps by filtering out unwanted (perhaps major) contributions to the spectral signatures. This would be particularly useful in unsupervised classification techniques, such as cluster analysis, where only a small number of signature classes condensed from all the signatures present in an image can be represented by symbols on a map.

3. Enhancement of more subtle features on an image can be accomplished by rejecting the prevailing unwanted wavenumbers or by strike-selective, band-pass filtering to retain only the subtle features of interest oriented in a preferred strike direction.

4. Since periodic ground features, such as folds and multiple lineaments, are of interest geologically, channels containing a great amount of wavenumber character (after system noise has been filtered out) would be desirable for geological studies. We, therefore, recommend that thermal infrared channels be included on future geological remote sensing missions since the Skylab thermal channel consistently produced a wavenumber spectrum with contributions in all wavenumbers.

5. To realize the full potential of wavenumber analysis in remote sensing and geologic applications, programs must be developed which are capable of operating on large data blocks representing ground areas of the order of 1 to 4 x 10^4 km^2. Basically, the area considered must be large enough to contain the salient shape characteristics of the feature(s) of interest.

4.11 SUMMARY AND CONCLUSIONS OF GEOLOGIC STUDIES

4.11.1 Summary

One of the objectives of this study was to map lineaments on the Skylab/EREP data and to determine how well these lineaments correlated with those mapped from the Landsat-1 imagery. As a basis for correlation of the two data sources, a lineament map of Pennsylvania was produced from Landsat-1 imagery because of its complete coverage of Pennsylvania. Skylab photographs were then used to compare the distribution of visible lineaments and to help position them more accurately on larger scale maps. As a result of the comparison between Skylab and Landsat-1 lineaments, it became possible to determine the lineament sampling bias on both types of data. Considerable field work was also undertaken to determine if the lineaments delineated on the Skylab photography can be correlated with actual field conditions.

Upon completion of the lineament map, the extent of correlation of lineaments with ore deposits was determined. This necessitated the preparation of a Pennsylvania mineral deposit map. The lineaments were also related to groundwater well yields in the carbonate areas of Pennsylvania. A zone of lineation determined on Skylab photography was also used in a study to investigate the origin and extent of a thermal anomaly in central Pennsylvania.

Finally, digital wavenumber analysis (spatial filtering) was attempted to determine if it can be used to enhance certain subtle features and, in particular, to locate and verify lineaments.

4.11.2 Conclusions

Based upon the analysis performed in this investigation on the use of Skylab data for geologic purposes, the following conclusions are drawn:

1. Skylab photography is superior to both Landsat imagery and high altitude aircraft (U2 or RB57) photography in the accurate location of lineaments initially detected on Landsat imagery.

2. With the better resolution of Skylab photography, it has been determined that a number of long lineaments originally mapped on Landsat images are actually made up of several shorter segments. These segments may differ in orientation by several degrees from the mean orientation of the long lineament originally plotted from the Landsat data.

3. A comparison of lineaments plotted on Skylab scenes with those plotted on Landsat images has revealed that the Landsat plots suffer from a significant bias by illumination and scan line directions. While there is an illumination bias in the Skylab photograph, its direction does not coincide with the main transverse lineament trend, thus providing an independent assessment of the illumination direction bias.

4. Yield data presented in this report establishes the fact that lineaments can be used with advantage in groundwater prospecting to increase the chance of obtaining maximum well yields available within a given terrane. Lineaments will have far broader application to groundwater prospecting throughout the nation and world than many hydrogeologists still realize. All sedimentary rocks, even with moderate-to-limited amounts of cement, will yield increased amounts of water when fractured. For metamorphic and igneous rocks, zones of fracture concentration offer the best hope of obtaining maximum well yields at the least economic risk. However, test well sites must be selected to take into consideration other geological controls that favor groundwater occurrence; i.e., rock type, topographic setting, dip of beds, existing and possible future pollution potential and other factors.

5. Based upon relations observed between the mineral deposit map prepared for Pennsylvania and structural features identified from satellite imagery, there appears to be an indication that lineaments provide clues to possible controls of metallic mineralization in Pennsylvania. The Tyrone-Mount Union lineament complex and the Perkiomen Creek lineament are the most strongly associated with mineralization in Pennsylvania. Several other unnamed lineaments were geographically associated with mineral occurrences.

6. Combined use of the Skylab photography, Landsat imagery, and aircraft photography, and thermal IR data were used to delineate associated geologic structures and to define the spatial extent of a thermal anomaly. Landsat and Skylab provided valuable data on lineament zones in the Warm Springs region which bear a direct relation to ground water flow patterns. Thermal IR data provided information on the detailed thermal regime of the area and the associated lithologic formations where the springs discharge.

7. There is still a problem in determining the width of structures that underlie lineaments and the affective depth of permeability development along these structures. Width data for various rock types transected by the same lineament are unknown. Skylab is clearly of assistance in this width determination work, but our present assumption of a 1 km width must be refined by more ground control obtained through adequately spaced well yield information added to direct observation of bedrock at natural and man-made exposures that transect lineaments.

8. Lineaments are underlain by structural features that increase the physical and chemical weathering of bedrock of all types. The damage caused by improper waste management along lineaments is likely to cause more regional groundwater pollution than for adjacent areas where bedrock is less permeable. Lineament mapping, therefore, will be of significance in planning waste treatment and management facilities and monitoring water quality changes below and adjacent to such facilities.

9. Sinkholes, swallow holes, cave entrances, influence streams, and land subsidence occur along lineaments and at lineament intersections in carbonate terranes. These structures combined with other details such as depth of water table, seasonal variation in water table position with

respect to residual and transported soils, distribution of surface water, groundwater development, details of rock type, and other structural features combine to define hazardous, subsidence and leakage areas. Lineament maps will help to delineate risk areas for various structures although they cannot be used independently to predict precisely when and where subsidence and cave-ins and severe leakage are going to occur. However, they can be used to flag areas where caution should be exercised in land use planning and where more detailed test drilling and foundation exploration work are justified.

10. The utility of seasonal coverage of Skylab images for lineaments work has not been adequately evaluated. Repetitive coverage is lacking for most areas. Also, scenes with a snow cover, or partial cloud cover, appear to have lineaments obscured.

11. The lineament map shows an uneven distribution of lineaments for sections of the state. In particular, southeastern and northwestern Pennsylvania have fewer lineaments than other regions of the state. These variations may be more due to operator bias than due to geological causes and subject to operator interpretation and cultural features in more densely populated regions. For this reason, multiple operators should be used to increase the chances of detecting more subtle lineaments.

12. The best operational procedure for lineament mapping appears to be one that combines available Landsat and Skylab images for the same area. Following an initial mapping on each set of imagery, lineaments should be transferred to Skylab level B (S190B) quality images to allow field detection of their location. Individual fields, field borders, contour cropping patterns, minor roads, bridges, individual homes and woodlots show adequately enough to allow rather accurate location of lineaments even if the width of their underlying structure is not known. Often the transfer can be made directly to 7 1/2-minute quadrangle maps where topographic features are distinct.

13. Some specific advantages of Skylab photography for geologic mapping are listed below:

a. Scale: There is no doubt that continuing studies of geologic features are greatly assisted by data at the Skylab scale, for the key to both the origin and economic significance of these features lies in being able to relate lineaments to megascopic structural elements on the ground. On Landsat images, the information is generalized and, in generalizing, one can be misled in both location and interpretation. These studies of the data available for Pennsylvania have shown that a high level of accuracy in location can be obtained from the Skylab data. Hence, ground truth correlation is greatly facilitated. Skylab photography appears to be superior to U2 or RB57 photography for mapping lineaments, as high altitude photography is of too large a scale to reveal most lineaments, yet too small a scale on which to locate fracture traces. Skylab level of coverage does not, however, supersede the need for underflight black and white or colored photographs for stereo investigation of fracture traces, rock type, dip of beds and related geological observations.

Fracture traces are essentially not mappable on Skylab images at the standard scale. In fact, their resolution is reduced even on aerial photographs at a 1:40,000 or smaller scale for all but the most skilled investigator. At the U2 level of observation, more lineaments can be detected than can be seen on stereo-paired USDA high altitude photographs available at a 1:20,000 scale.

b. Regional Color Contrast: The color photographs (both S190A and S190B) covering large areas make it possible to identify rock units by virtue of their color and areal extent. This is a distinct advantage over Landsat images, where the natural color and adequate resolution is lacking; and over aerial photography, where the coverage is not sufficiently extensive in a single scene. Skylab photography was of great assistance in mapping red beds of large areal extent.

c. Improved Resolution: The Skylab color transparencies exhibit greater resolution and detail than the Landsat color composites. Valley floors and tributary streams are seen on the Skylab S190A and S190B visible color and color IR photography not only with greater clarity than on the Landsat scenes, but also free from scan bias, and the ground locations of the features seen are established far more accurately. The black and white S190A Skylab photography studied by ORSER was not as good as the best Landsat images, being rather flat and having less contrast than the Landsat black and white images. However, only the available Skylab photography was compared with the best available Landsat imagery of the same area, and the option of optimum seasonal coverage was not available. Thus, atmospheric haze on the particular day of the Skylab pass could have been the source of the difficulty. Another possible explanation could be differences in the grey scales of the Skylab and Landsat black and white photographs, because the Skylab color transparencies were clearly better than the Landsat color composites or black and white images. For lineament mapping purposes, the winter scenes were the best.

14. As a result of studying the wavenumber spectrum of the individual Skylab channels, it is concluded that each channel provides unique wavenumber information about a particular scene. The peaks and troughs produced in the wavenumber domain by a scene are shaped differently in different channels, and the separations of the intensities of peaks and troughs vary for different channels. The most detailed wavenumber spectrum is produced by the thermal IR which has higher intensities in higher wavenumbers than the other channels. The channels in the IR and near IR show a relatively distinct wavenumber signature for the dominant periodic feature in the scene. The channels in the visible range have a flatter wavenumber response, and the wavenumber signature associated with the dominant feature is not as sharp and as well defined as in the IR channels.

4.11.3 Recommendations

Based upon the results of ORSER's analysis of the use of Skylab data for geologic purposes, the following suggestions are recommended for serious consideration:

1. Skylab photography, or imagery at that scale and resolution, should be obtained on a seasonal basis and over major geographical areas for continued lineaments work. Repetitive Skylab coverage is lacking for most areas, and some areas are not covered at all. Stereo coverage would also be recommended on future flights.

2. Investigation should be continued into the effects of operator, scan line, and illumination bias on Skylab and Landsat photography and imagery. Multiple operators should be used to increase the probability of detecting more subtle lineaments.

3. There should be an investigation to determine from ground-based observations the nature of the structural features which underlie lineaments and to determine the nature and tectonic significance of well known major lineaments to establish their relationship to less prominent surrounding lineaments.

4. An accurate lineament map of the Commonwealth of Pennsylvania should be prepared using Skylab-type data and evaluated for its use in groundwater and mineral prospecting, siting of proposed construction, and pollution.

5. It is recommended that thermal infrared channels be included on future geological remote sensing missions since the Skylab thermal channel consistently produced a wavenumber spectrum with contributions in all wavenumbers, with a greater intensity in the higher wavenumbers than in the other channels. Since periodic ground features, such as folds and multiple lineaments, are of interest geologically, channels containing a great amount of wavenumber character would be desirable for geological studies.

6. To realize the full potential of wavenumber analysis in remote sensing and geologic applications, computer programs must be developed which are capable of operating on large data blocks representing ground areas of the order of 1 to 4 x 10^4 km^2. Basically, the area considered must be large enough to contain the salient shape characteristics of the feature(s) of interest.

5.0 DIGITAL MSS PROCESSING

Processing of S192 (MSS) digital data was accomplished relatively late in the project using the ORSER digital data processing system. Because of the considerable experience of ORSER in processing Landsat digital MSS data, it was natural to compare spectral signatures of common targets, or categories, as measured by the S192 and Landsat.

The major digital processing effort was directed toward the evaluation of S192 channels. Specifically, the objectives were to determine the redundancy and the discriminatory information content in the various channels. The procedures involved the visual observation of individual channel imagery, discriminatory analysis by the use of canonical analysis and principal components, and statistical comparisons using correlation techniques and, finally, evaluation of classification mapping results.

Since ORSER had opportunities to display results at various stages of classification on several types of display systems, a section has also been included which summarizes the ORSER experiences with several color displays.

5.1 THE ORSER DIGITAL DATA PROCESSING SYSTEM

The ORSER system for processing MSS digital tapes was developed for use by a wide variety of researchers working in remote sensing. These users represent many disciplines and have a wide range of experience and skill in photointerpretation and computer usage. Interpretive techniques which are used in the system include computer processing, visual image interpretation, and a hybrid technique which closely integrates photo-interpretive techniques with computer analytic procedures.

Automatic data processing equipment utilized in the ORSER system is primarily located at The Pennsylvania State University Computation Center. The principal computer is the IBM System 370 Model 168 consisting of a main frame and attached devices for input and on-line storage. Users may have access to the computer in any of three ways:

1) central and remote high speed dispatch points operated by the Computation Center,

2) slow speed Remote Job Entry (RJE) terminals using IBM 2741, Tektronix 4010, or similar remote terminals supported by the user or by the Computation Center, and

3) intermediate speed remote batch terminals, such as the IBM 2780, supported by the user or the Computation Center. The ORSER processing system for MSS data was developed for use with any of these entry points.

ORSER has installed a RAMTEK color TV display system interfaced with a Tektronix 4010 terminal and the RJE system to the Computation Center By means of this system, ORSER investigators are able to display their results in color at all stages of analysis. Non-University users, as well as Penn State users, may join the system. Any compatible terminal may be used to process data via the RJE system, including equipment at Non-University Park locations tied in by long distance telephone connections.

ORSER investigators use RJE terminals for most developmental work. Bulk output for final runs is directed from an RJE terminal to any of the high speed terminal sites. No programs card decks need to be input, as the MSS data processing programs are kept in library files. Files for building control information or for storing output are available to the user. MSS data is input from magnetic tapes which, along with user-owned working tapes, are managed by the Computation Center.

A standard digital tape format was designed within which all known MSS sources can conveniently be placed. The system is couched in a multivariate framework, e.g., each observation, identifiable by scan line and element number, consists of a vector with as many components as there are channels.

A user's guide to the ORSER MSS digital data processing system, updated yearly (Borden, et al. 1975), provides program descriptions and instructions for processing of data and for use of all programs in the ORSER system. Programs in current use by ORSER include:

TPINFO	obtains information about tape contents from the internal label.
SUBSET	subsets satellite data onto a working tape, in ORSER format.
SUBAIR	subsets aircraft data onto a working tape, in ORSER format.
SUBTRAN	reformats to Landsat (ERTS) format data in various other formats and performs additional selected data manipulations.
NMAP	creates a brightness map from digital data.
UMAP	creates a uniformity map from digital data.
STATS & STCLASS	obtain basic statistics for user-defined small blocks of data.
PPD	classifies according to the parallelepiped method.
CANAL	uses the method of canonical analysis to derive an orthogonal transformation which maximizes category separability on as few axes as possible.
RATIO	performs classification and mapping based on the ratio of two selected channels of data.
MERGE	merges data from two different passes of Landsat over the same area.
MAPCOMP	compares, element by element, two digital classification maps of the same ground area.
GMCLASS	makes geometric and scaling corrections to classified data and generates gray-scale or color printer output.
CLASS & MINDIS	supervised parametric classifiers which classify data from a set of user-specified spectral signatures according to the angle or distance of separation.
CLUS	unsupervised classifier which develops a set of spectral signatures using a clustering algorithm.

NPAR	non-parametric classifier employing the linear discriminant function.
QUADNPAR	non-parametric classifier employing the quadratic discriminant function.
PARAM	parametric classifier based on the maximum likelihood decision rule.
LMAP	outputs a black and white line map scaled to user specifications on either a Cal-Comp 564 plotter or a Tektronix 4010 CRT terminal.

5.2 COMPARISON OF SKYLAB AND LANDSAT SIGNATURE RESPONSE FOR COMPARABLE CHANNEL WAVELENGTHS AND SCENES (Alexander and Baumgardt)

A comparison was made between the Skylab and Landsat multispectral scanner (MSS) signatures for the same ground area in SW Pennsylvania at about the same time of the year. Signatures were obtained by using the unsupervised cluster analysis program, DCLUS, to classify data from Skylab and Landsat channels from approximately the same wavelength bands. Seven Skylab channels are needed to span the spectral interval covered by the four Landsat channels.

The Skylab and Landsat images also differ in their orientation and scale. The Skylab pass was NW-SE whereas the Landsat pass was NNE-SSW. Hence, the Landsat image must be rotated about 74° clockwise for it to match the Skylab image. Because Skylab was at a lower altitude than Landsat and used a different sensor package, the Skylab image covers a somewhat smaller area than the Landsat image. Also, for a given size ground area, a larger number of distinctive classifications from Skylab imagery are obtained than from Landsat imagery, due to the greater spatial resolution of the Skylab observations.

The area studied in detail was a small region centered approximately 5 km east of Bedford, Pennsylvania (area B in Figure 4-40). This area was chosen for its variety of features, facilitating comparison and orientation. Skylab orbit 14 data covering this area were obtained on 5 August 1973. The Landsat scene used was 1405-15235 from 1 September 1973. Data for both scenes were collected in the mid-morning, and obtained less than a month apart.

The cluster classification maps of the area from Skylab and Landsat data are shown in Figure 5-1a and b, respectively. Four signatures were matched with ground features seen on the S190B photography (roll 21, frame 192). Three "ridge" signatures mapped the forest on Evitts mountain and one signature mapped the gorge through the ridge. The plots of these spectral signatures for the Skylab and Landsat data are presented in Figures 5-2 and 5-3, respectively.

Comparing the signatures from the two data sets, the intensities appear to differ, but only because the Skylab and Landsat channels are calibrated differently as discussed below. In the visible part of the spectrum, from 0.5 to 0.8 μ, the spectral shapes of the four signatures are very similar for both Skylab and Landsat data. The differences in shape are due largely to the fact that the channel band widths differ for the two satellites. If one were to average the intensities of the Skylab channels over the same spectral band widths as the Landsat channels, the match between the visible spectral signatures would be very close.

On Figures 5-2 and 5-3, it can also be seen that there is an apparent difference between the shape of Skylab and Landsat signatures in the near infrared channels, from about 0.8 to 1.2 μ. This is largely a function of the difference in intensity scaling between the Skylab and Landsat scanners for these channels. The range in intensity values for

Figure 5-1: Comparison of DCLUS classification maps from the Skylab (a) and Landsat (b) data. The solid lines outline the ridge and the dashed lines outline the gorge on both maps.

Legend:

Feature	Map a	Map b
Forest (ridge in shadow)	Z	+
Forest (sunlit ridge)	M	-
Forest (ridge)	*	X
Gorge (river and highway)	+	Z

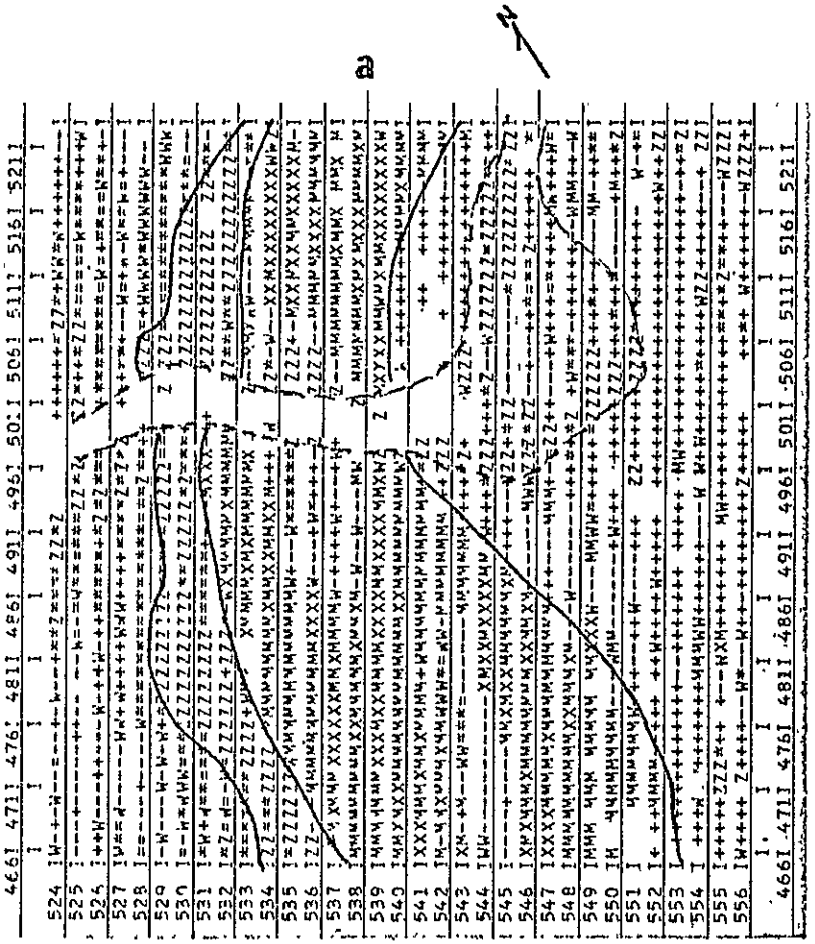

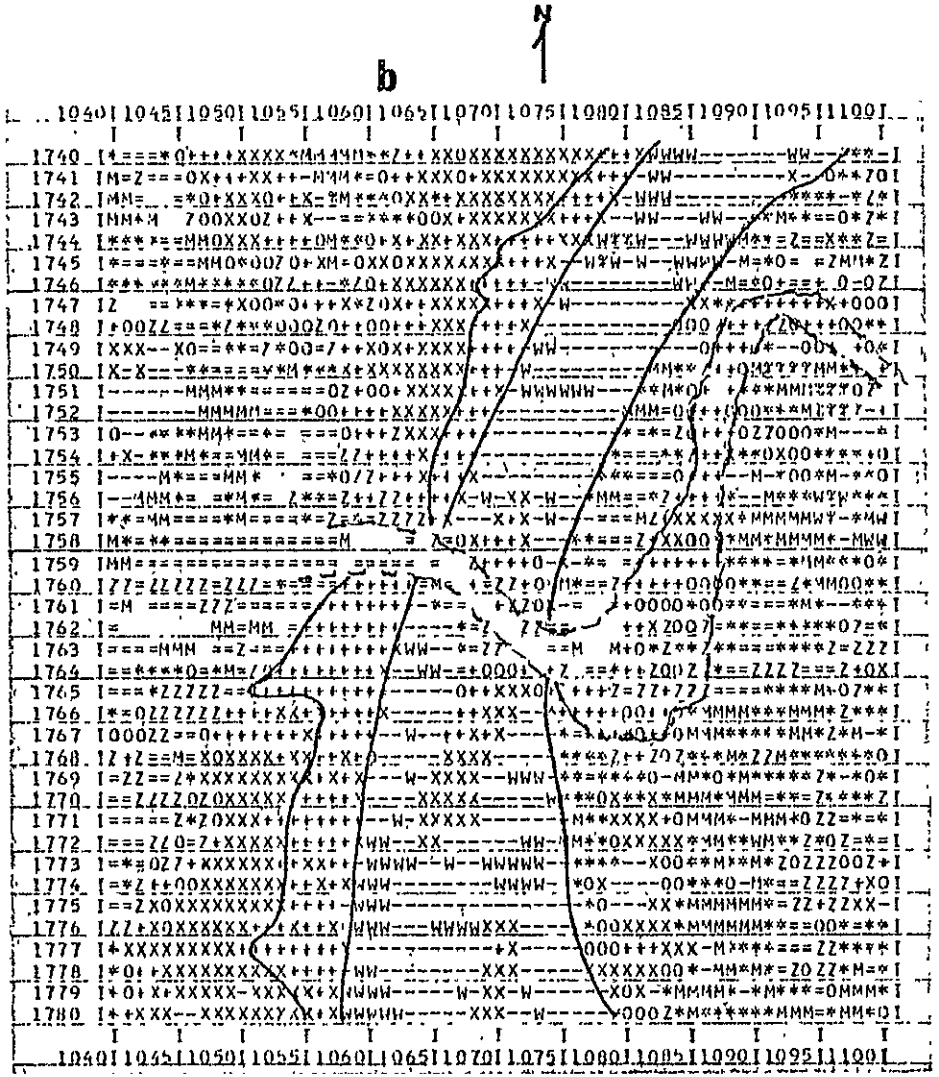

Figure 5-2: Plot of the four Skylab signatures. The heavy solid line is the forest (sunlit ridge) signature from the Landsat classification, provided for the purpose of comparison.

Legend:

Forest (ridge in shadow)	—·—·—·—·—
Forest (sunlit ridge)	————————
Forest (ridge)	- - - - - -
Gorge (river and highway)	· · · · · ·

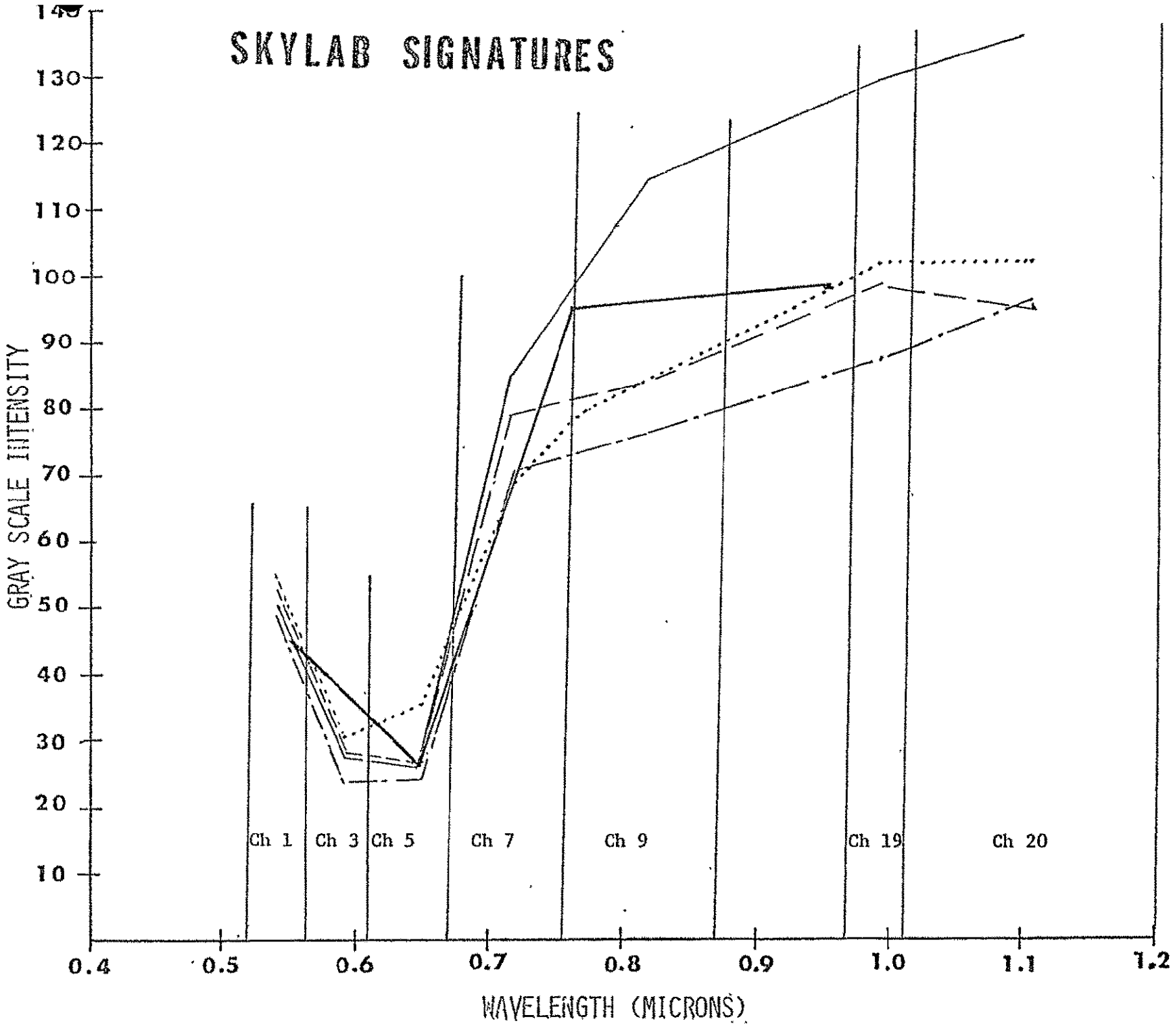
SKYLAB SIGNATURES
GRAY SCALE INTENSITY
140
130
120
110
100
90
80
70
60
50
40
30
20
10
Ch 1
Ch 3
Ch 5
Ch 7
Ch 9
Ch 19
Ch 20
0.4
0.5
0.6
0.7
0.8
0.9
1.0
1.1
1.2
WAVELENGTH (MICRONS)

Figure 5-3: Plot of the four Landsat signatures. Note that the intensity scale is half that for the Skylab signatures in Figure 5-2, and that the uncorrected and corrected signatures for channel 7 are indicated on the plot.

Legend:

Forest (ridge in shadow)	—·—·—·—·—
Forest (sunlit ridge)	————————
Forest (ridge)	- - - - - -
Gorge (river and highway)	. . . . .

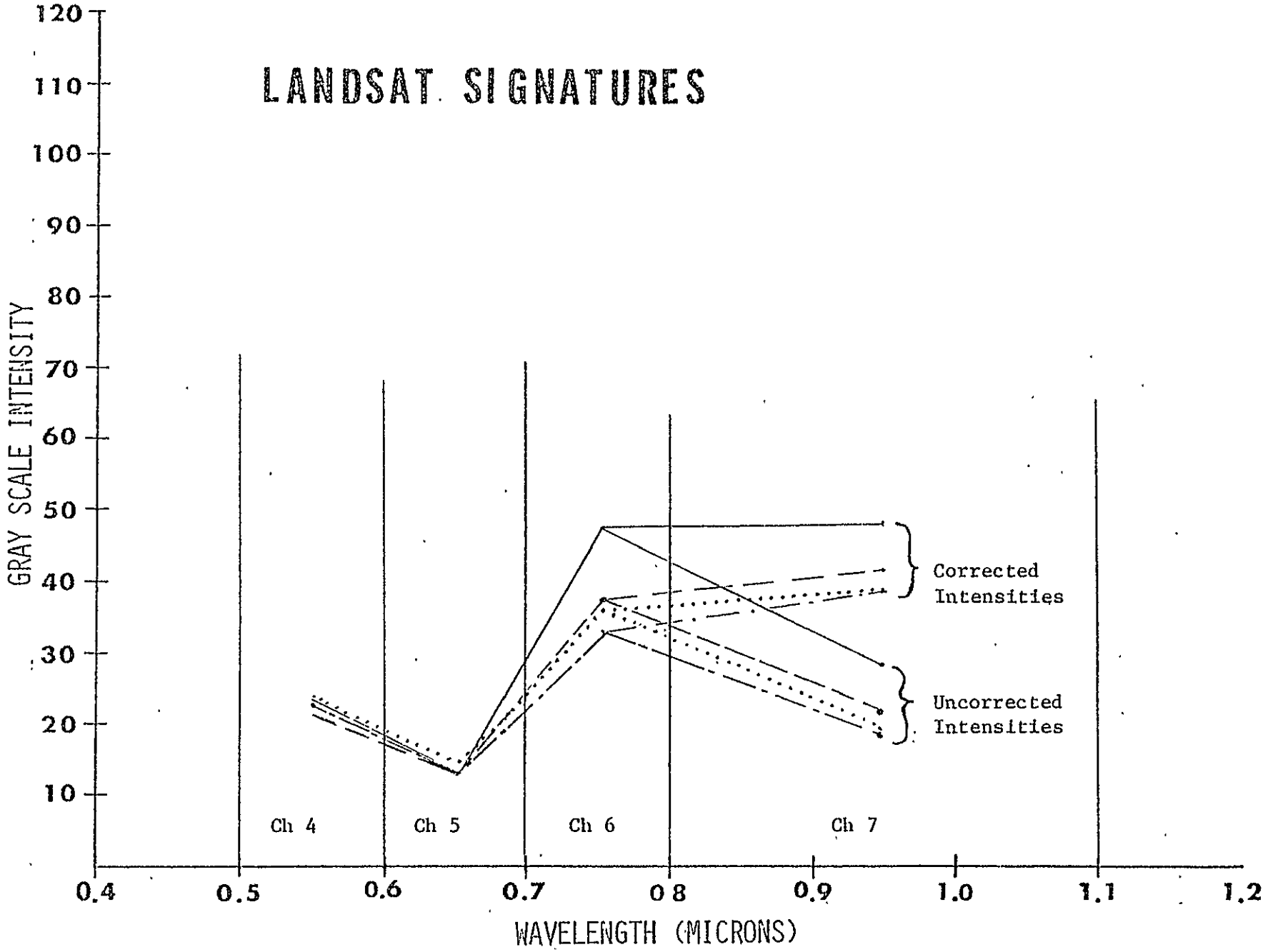
LANDSAT SIGNATURES
GRAY SCALE INTENSITY
120
110
100
90
80
70
60
50
40
30
20
10
Ch 4
Ch 5
Ch 6
Ch 7
Corrected Intensities
Uncorrected Intensities
0.4
0.5
0.6
0.7
0 8
0.9
1.0
1.1
1.2
WAVELENGTH (MICRONS)

the Landsat bands is 0 to 127 for channels 1 through 3, and 0 to 63 for channel 4. The Skylab intensity values are scaled 0 through 255 for all channels. If corrections are made for this difference in scaling, the signatures become remarkably similar. This is shown in Figure 5-2 in which the corrected Landsat signature for sunlit ridge forest (solid line map symbol) was plotted for comparison with the four Skylab signatures. It can be seen that this signature is almost exactly the same as the corresponding Skylab signature for sunlit ridge forest, except in the thermal infrared region. The Skylab near-infrared channel responses are still somewhat higher than the Landsat near-infrared channel responses. This may be partially due to the differences in channel band widths, and partially due to temporal differences in atmospheric and ground conditions. Over a period of a month, the moisture content, temperature, and vegetative conditions in the scene may change substantially, and the near infrared channel signatures are very sensitive to these changes. Nevertheless, the spectral signatures compare remarkably closely in level and shape as recorded on Landsat and Skylab imagery.

As a result of this comparison, the following conclusions can be made:

1. To equalize the intensity scales for comparing Skylab and Landsat spectral signatures, the intensity values for the first three Landsat channels (4, 5, 6) should be multiplied by a factor of 2 and channel 7 should be multiplied by a factor of 4, which in effect places all channels on an intensity scale ranging from 0 to 255.

2. In the classification of a given area using cluster analysis for Skylab and Landsat categories, there is generally a larger number of distinctive categories found from Skylab imagery than from Landsat when identical variances for categories are specified. This results from the better spatial resolution of a Skylab pixel compared to a Landsat pixel. The close correspondence found in spectral signatures between Skylab and Landsat imagery for rather homogeneous forested areas indicates a comparable response for the two scanning systems. Therefore, any differences in spectral signatures which are seen for less homogeneous areas will most probably represent real differences in resolution and local spectral reflectance signatures. One should expect such differences to become pronounced when ground features can be resolved at the Skylab scale of viewing but not at the Landsat scale; in such a case, the Skylab signatures would be more reliable.

5.3 S192 CHANNEL EVALUATION BY ANALYSIS OF DIGITAL DATA (Borden, Barr, and Applegate)

5.3.1 Organization of the Research

The objective of the investigation of the S192 digital data was to evaluate the various spectral bands for classification and thematic mapping. In order to meet the objective, it was necessary to produce satisfactory classifications and thematic maps according to the resolution of the S192. This was the most difficult and time-consuming phase of the task, but once it was completed the spectral band evaluation was then relatively simple.

Prior to the classification and mapping phase, an initial screening evaluation of the channels was made in order to delete obviously poor channels and to reduce the number of channels from the original 22 to 16. The ORSER system was used for the data processing. Although the programs in the ORSER system were designed for 24 channels, some could accommodate only 16 channels of S192 data at the time they were used because of array size limitations on the total number of bytes in a scan line.

During the classification and mapping phase, a number of color map display devices were available for use by the investigators. The digital analysis of MSS data is dominated by the spectral characteristics of the pixels, with little or no analytical value placed on the spatial relationships among pixels. To judge classification and mapping results, not only must the spectral analysis results be considered but, of equal importance, the spatial patterns of pixel classification must be considered. Color display is superior to print-character or grey-scale computer printer maps because of the better visual interpretation afforded to the eye by color. A comparative evaluation of color display devices which were used was made in connection with the mapping requirements of the investigation.

Subsequent to the classification and mapping phase, analyses for channel evaluation were performed based on statistics previously generated by the ORSER programs used during classification. Since the terminology and methods may not be familiar to non-statisticians and since the evaluation discussions must rely on the technical interpretations of the statistics, a section describing the techniques and terminology has been included.

The report of S192 channel evaluation has been organized according to this preliminary discussion into five major parts, each covering one of the phases as defined by tasks, presented in order as follows:

1) reduce the number of channels for analysis to 16 by screening out the poorest and most redundant,

2) classify and map categories based on the selected channels,

3) define specific statistical methods and the conceptual framework in which they are applied,

4) evaluate channels on the basis of statistics and interpretations resulting from classification and mapping, and

5) evaluate color displays and their products based on their use in classification and mapping.

5.3.2 Methods for Channel Evaluation

A number of ways exist or can be conjectured for evaluating the utility of channels. Five were considered for the S192 data:

1) comparison of separate channel imagery,

2) evaluation of channels for redundancy,

3) evaluation of each channel for its contribution to the total information content of a scene,

4) evaluation of each channel for its contribution to the discriminatory information content of a scene composed of a number of categories, and

5) comparison of classification and map results for channels and channel combinations.

Of these five ways, four were deemed feasible. The last one, comparison of classification and map results, was not considered to be feasible for the following reasons. First, a comprehensive ground truth data base would be required to form a common basis for comparisons. This did not exist for the area under investigation. Second, in order to compare all combinations of 16 channels, the number of comparisons of classification maps would be:

$$\sum_{i=1}^{16} \frac{16!}{(16 - i)!\, i!} = 41{,}225$$

Even though many combinations could be eliminated *a priori*, the number of combinations would still be very large for a comprehensive evaluation. The amount of time and computing expense for this method would be exorbitant.

Each of the other four methods listed above was employed. Comparison of separate channel images can be used successfully for a crude evaluation of channels. Its main drawback, and the reason it is useless for other than identifying very poor channels, is that it does not take into account the combined effects of two or more channels. Combinations of three

channels at a time could be done by using color composites or color additive viewing instruments. However, for 16 channels, 560 color composites would be required for a complete comparison, in that

$$\frac{16!}{13!\ 3!} = 560$$

Although many combinations could be eliminated a priori, the situation is still very similar to the method previously discussed, and for this reason the method was not used comprehensively.

Evaluating channels for redundancy based on simple correlations of the digital data is limited to the identification of highly redundant channels. This method was used as the basis for initially eliminating some channels given the knowledge that the eliminated ones had one or more spectral bands identical with channels not eliminated. For instance, on Table 5-1, channels 9 and 10 have a 0.95 correlation, which indicates a large measure of redundancy. One is essentially useless in the presence of the other. This conclusion is further confirmed when the correlations of these two channels with other channels are compared. Compare each pair of values across the lines for channels 9 and 10 in the table. The very close similarity of each pair indicates that not only are the two channels strongly correlated, but each is correlated in the same way to each of the other channels. The criteria which were employed to identify strongly redundant channels were a high correlation between the two channels, and a very similar pattern of correlations of each with the other channels. The limitation of this method of channel evaluation is that it is useful only in identifying pairs of channels which are redundant. The method does not help in determining the comparative value of channels for recognition of land features.

The method of channel evaluation based on the contribution of each channel to the total information content of a scene uses a principal components analysis of data for a scene or a representative sample thereof. The main and secondary dimensions (axes) existing in the data can be found from principal components analysis, and this can then be followed by the determination of the correlation of each channel with each of the axes. Channels which are strongly correlated with the important axes are, therefore, important in contributing to the total information content of the data. In this method, however, channel redundancy is not taken into account.

To evaluate channels regarding their contribution to discriminatory information content, canonical analysis was used. After recognizing the predominant categories in a scene, canonical analysis identifies the discriminatory dimensions (axes) among categories. Correlations of channels with the important discriminatory axes then can be used to identify the importance of each channel for discrimination among the various categories. As with the prior method, channel redundancy is not considered. Furthermore, the success of the method is contingent upon satisfactorily identifying and defining the predominant categories in the scene.

Table 5-1: Correlation Matrix for Selected S192 Bands Computed from Test Block 4

Band Number	Wave-length(μ)	Channel Number	Band Number (Channel Number) 3(1)	3(2)	4(3)	4(4)	5(5)	5(6)	6(7)	6(8)	7(9)	7(10)	8(19)	9(20)	11(11)	11(12)	12(13)	12(14)
3	0.52-0.56	1	1.00															
3	0.52-0.56	2	0.87	1.00														
4	0.56-0.61	3	0.80	0.74	1.00													
4	0.56-0.61	4	0.76	0.79	0.88	1.00												
5	0.62-0.67	5	0.69	0.64	0.74	0.70	1.00											
5	0.62-0.67	6	0.65	0.69	0.67	0.74	0.85	1.00										
6	0.68-0.76	7	0.49	0.50	0.50	0.49	0.44	0.44	1.00									
6	0.68-0.76	8	0.47	0.51	0.47	0.50	0.42	0.45	0.97	1.00								
7	0.78-0.88	9	0.14	0.14	0.16	0.16	0.15	0.15	0.77	0.77	1.00							
7	0.78-0.88	10	0.13	0.14	0.15	0.16	0.14	0.15	0.74	0.77	0.95	1.00						
8	0.98-1.03	19	0.14	0.15	0.16	0.14	0.15	0.14	0.76	0.72	0.88	0.80	1.00					
9	1.09-1.19	20	0.17	0.18	0.18	0.18	0.17	0.18	0.82	0.81	0.94	0.90	0.91	1.00				
11	1.55-1.75	11	0.60	0.60	0.60	0.59	0.54	0.53	0.85	0.84	0.66	0.65	0.66	0.73	1.00			
11	1.55-1.75	12	0.58	0.61	0.57	0.60	0.51	0.54	0.83	0.85	0.65	0.66	0.63	0.71	0.97	1.00		
12	2.10-2.35	13	0.69	0.68	0.68	0.66	0.61	0.59	0.65	0.64	0.34	0.34	0.37	0.41	0.81	0.79	1.00	
12	2.10-2.35	14	0.66	0.70	0.64	0.68	0.58	0.61	0.64	0.65	0.34	0.34	0.36	0.41	0.79	0.81	0.91	1.00

Each of the methods has advantages and disadvantages, so that no one method could be singled out for exclusive use with complete success as the anticipated result. The various methods, therefore, were used in a complementary fashion and the combined interpretation of results was used as the basis for final channel evaluations.

The selection of these methods and the results of their use have a strong and intended orientation toward land use classification and mapping. The methods and resultant channel evaluations must be considered in this context. These methods do not lend themselves to direct use for identifying channels which measure subtle phenomena dispersed over large areas, such as certain geologic or phenologic expressions. In addition, the methods as used were not oriented toward discovering channels which would precisely identify any specific category against a background of other undifferentiated categories. It must be kept in mind that the results of the study are for the general mix of land use patterns existing in the growing season for an area representative of western Pennsylvania. It would be conjectural to extrapolate the results to other substantially different climatic areas, such as semi-arid ones, or to another very different season of the year, such as winter. Although the methodology would be expected to be as satisfactory in channel evaluation under other conditions, the specific results might very well be quite different.

5.3.3 Data Specifications

S192 digital data were taken from the line-straightened data file specified as SL3, orbit 14, 5 August 1975, tape 933847. Of the total of about 500 scan lines in the file, five blocks of data were chosen each of which was 112 lines by 116 elements. The blocks, identified as test blocks 1-5, were non-overlapping and randomly located across the scan lines. In test block 4, the town of Freeport, Pennsylvania, and the Allegheny River were easily identified, providing a suitable reference pattern in the data. This block contained the complete mix of target types and was, therefore, used predominantly for signature extraction and channel evaluation. Scan line and element coordinates of the test blocks are given in Table 5-2.

Table 5-2: Specifications of Test Blocks

Test Block	Beginning Scan Line	Ending Scan Line	Beginning Element	Ending Element
1	1	112	879	994
2	113	224	364	479
3	225	336	243	358
4	337	448	460	575
5	449	560	659	774

5.3.4 Calibration

Uncalibrated data were used. It was decided that data calibration would be attempted only if the uncalibrated data were found to be otherwise not useful. Radiometric striping, seen in the images from some of the channels, is the appearance of differences in adjacent scan lines carried over the whole scan line length. It is apparent when gains and offsets of the sensor electronics are consistent from scan line to scan line. It is also apparent when calibration is incorrect or inadequate. For example, radiometric striping is apparent in some scenes of Landsat data even though the data were calibrated. Although radiometric striping was detectable in images of some channels, it was not seen at any stage of the Skylab digital analysis.

Calibration is seldom an easy task and would not necessarily be justified if the sensor systems were quite stable over a scene. Calibration to achieve linearization and particular units of measure are of no consequence in classification and mapping. In view of the above factors, calibration was deemed unnecessary considering the time and expense the development of calibration programs would have required.

5.3.5 Initial Channel Evaluation and Selection

5.3.5.1 Image Evaluation

Imagery and data tapes were received late in February 1975. Because of the lateness of the receipt of materials and the scheduled project termination date of June 30, 1975, a detailed visual analysis of the channel imagery was not conducted. The channel imagery was visually evaluated solely for the purpose of determining the adequacy of the digital data for processing. The quality of the imagery for photo-interpretation was not under investigation in this phase of the total project. Annotation on the imagery indicated that each image was composed of a single channel. One image from each band was furnished. Comparisons between two sensors covering the same spectral band, therefore, could not be made.

In the rating of each band, the following questions were posed: Are land features or use patterns discernible? How much contrast do the patterns show against the background? Does the image contain apparent striping and, if so, how serious is it compared with discernible patterns? Does the image contain random noise, evidenced by erratic grey level changes, not associated with any discernible patterns? To what extent does the image show non-random noise such as gaps in scan lines? Based on the overall answers to these questions, the band was rated as good, fair, poor, or bad. The results of the evaluation are given in Table 5-3. During the evaluation, it was understood and taken into consideration that the kinds of patterns in an image are dependent upon the wavelength limits of the band. For example, patterns of vegetation were not expected in band 1 (0.41-0.46 μ), whereas patterns of man-made features were anticipated.

Table 5-3: Visual Band Ratings for S192 Data

Channel	Band	Rating	Wavelength (μ)
22	1	Bad	0.41-0.46
18	2	Bad	0.46-0.51
1	3	Good	0.52-0.56
3	4	Fair	0.56-0.61
5	5	Poor	0.62-0.67
7	6	Fair	0.68-0.76
9	7	Good	0.78-0.88
19	8	Fair	0.98-1.03
20	9	Good	1.09-1.19
17	10	Good	1.20-1.30
11	11	Good	1.55-1.75
13	12	Fair	2.10-2.35
21	13	Poor	10.20-12.50

Specific characteristics of each band are given in the following: (Channel numbers are given in parentheses.)

1) bands 1 (22) and 2 (18) both lacked patterns of land use, although in band 2 (18), urban areas were vaguely expressed. Both bands indicated "memory" (poor sensor recovery) from one element to the next. This was evidenced by the elongated smear after the trailing edges of sensed clouds,

2) bands 3 (1) and 4 (3) lacked sharpness, but vegetation patterns showed,

3) the band 5 (5) image appeared to have uniformly poor quality which could have been caused by a film production problem,

4) band 6 (7) showed better resolution, particularly for water; the river patterns were well defined. Resolution and pattern definition, particularly for water, were of good quality in band 7 (9), and strip mine patterns were apparent in the image,

5) in band 8 (19) urban, water, and strip mine patterns were well defined, but the overall quality, compared with band 7 (9), was fair,

6) bands 9 (20), 10 (17), and 11 (11) were of better overall quality than band 8 (19),

7) in band 10 (17) and 11 (11), vegetation patterns were apparent but urban patterns were not as well expressed,

8) in bands 12 (13) and 13 (21), various patterns were visible but resolution was only fair. Radiometric striping was apparent, but not strongly, in some images. Such striping did not appear when multiple channels were used in the digital processing, hence, it was judged to be of no serious consequence.

Although this method of channel evaluation yielded an expectation for the utility of each band in digital processing, it was not felt that the evaluation gave sufficient justification for deleting specific bands from further study.

5.3.5.2 Preliminary Evaluation of Digital Data

The ORSER system was designed to process remote sensor digital data from a variety of sources, many of which were undefined at the time the system was designed. The key to this feature is that source data are first reformatted into the ORSER format which can then be used for all ORSER programs. As for other new source data formats, it was necessary only to write two subroutines to input and unpack S192 data for the SUBSET program. These routines had been written and tested prior to the arrival of the S192 data.

Because of the length of the scan lines, combined with the number of channels (~23,000 bytes per scan line), it was not possible to retain all of the data in each scan line. This constraint was imposed by array size and storage limitations in the SUBSET program which can accommodate 3692 bytes per scan line. It was decided to meet the constraint by retaining all channels but to correspondingly reduce the scan line length. Five blocks were defined as specified in Table 5-2, each containing 112 sequential scan lines, 116 sequential elements, and all 22 channels. The blocks were chosen not to have overlapping line numbers and, in total, to cover the full length of the scene. The beginning element for each block was randomly selected to avoid biasing the samples. This sampling scheme was adopted instead of periodic sampling of elements in the scan lines in order to avoid the apparent loss of resolution caused by periodic sampling.

The reformatting and subsetting was accomplished in one operation with the SUBSET program. The subset tape, in ORSER format and containing the five blocks of data, was kept for subsequent processing.

Once the subset was achieved, the inspection of the channels was continued using the NMAP program. This program is designed to produce a printer output map according to grey levels, along with other tabular information concerning distribution of grey levels and including minimum and maximum responses for the specified channel. For use in this task, the program required an initial run excluding the map to obtain the table of the distributions. Then, after selecting the limits for each grey level to be mapped, the program was rerun to produce the map. The limits for the grey levels to be mapped were set according to the distribution of responses in the channel to give the greatest opportunity for spatial patterns to register. The block which was used

extensively, but not exclusively, for this purpose was test block 4, which contained the Allegheny River, in the town of Freeport, and both forested and agricultural land.

The data for each channel were processed separately in the above way. The map for each channel was evaluated in the same way as for the imagery. The questions considered in that section were asked of the single channel maps, hence, they are not repeated here.

The results of the investigation substantiated the findings of the preview of the imagery. For the most part, on the basis of this admittedly unrefined evaluation, all channels of the same band were of similar quality.

At this point in the analysis, it was necessary to select channels to reduce the number from 22 to 16 in order to meet restrictions in some programs which were to be used. Only the channels which seemed to be of no value at all were considered for elimination. Channels which may have shown evidence of radiometric striping, but otherwise showed patterns fairly well were rated as questionable but were kept. In other words, only the very worst channels were considered for deletion. Table 5-4 presents the evaluation results with the preliminary decision to keep or delete each channel.

The decision was made to drop both of the bad channels and also the two channels of band 13 which were poor. The third channel of band 13 was kept because it appeared to have the best quality of the three and it was desirable to include at least one channel in the thermal infrared range for further investigation. This left a total of 18 channels; therefore, 2 more had to be dropped. In order to assist in making the decision, a table of channel-to-channel correlations was produced (Table 5-1). This showed that the highest correlation, 0.97, of a channel to its partner channel of the same band was for band 6 (channels 7 and 8) and band 11 (channels 11 and 12). Therefore, it was decided to drop channel 7 of band 6 and channel 11 of band 11 because it was felt the data in each of these channels were probably very closely duplicated in the partner channel. This left a total of 16 channels in 12 bands.

Having made the final channel selections, the five random blocks were resubset, but only with those selected channels. Having now reduced the number of channels to 16, it would have been possible to increase the number of elements per block. It was decided, however, to stay with the original 116-element blocks to avoid additional computer processing expense and because the variety of targets within these blocks was sufficient.

5.3.6 Interpretation of Principal Components and Canonical Analyses

Canonical analysis and principal components analysis are generally presented with emphasis on the statistical and mathematical aspects, which form the basis for discussions of their use and interpretation. These methods will be discussed with the minimum possible technical orientation

Table 5-4: Evaluation Results with Preliminary Decision to Keep or Delete Channels

Channel	Band	Quality	Decision
1	3	Good	Kept
2	3	Good	Kept
3	4	Good	Kept
4	4	Good	Kept
5	5	Questionable	Kept
6	5	Questionable	Kept
7	6	Good	Kept
8	6	Good	Kept
9	7	Good	Kept
10	7	Good	Kept
11	11	Good	Kept
12	11	Good	Kept
13	12	Questionable	Kept
14	12	Questionable	Kept
15	13	Poor	Dropped
16	13	Poor	Dropped
17	10	Good	Kept
18	2	Bad	Dropped
19	8	Good	Kept
20	9	Good	Kept
21	13	Questionable	Kept
22	1	Bad	Dropped

and with major emphasis on the interpretation of results. The level of technical detail presented is that which is necessary to understand and interpret the statistical discussion and the tables in this report. Simplified examples which can be geometrically represented will be used to assist in the understanding of the technical concepts. The technical aspects for three concepts must be developed as the basis for discussion:

1) the observational vector, mean vector, covariance matrix, and total variance which constitute the concept of the organization and presentation of data and results;

2) the linear transformation as the concept of data manipulation; and

3) the correlation coefficient as the concept of a basic interpretive measure.

5.3.6.1 Data Representation and Statistics

An observation corresponding to a pixel, obtained from a multispectral scanner (MSS) is composed of p values, one for each of the p spectral channels sensed by the MSS. For the examples below, p is four, yielding four values for each observation. Let X represent an observation and have the structure of a vector, so that for p = 4,

$$X \doteq \begin{bmatrix} x_1 \\ x_2 \\ x_3 \\ x_4 \end{bmatrix}$$

where x_1 through x_4 are the values for the first through fourth MSS spectral channels, respectively. For an observed ground area sensed by 100 scan lines and 100 elements per scan line of a four-channel MSS, 10^4 X 's (or observation vectors) would result, with each X composed of four values organized as above. The location of each X is usually specified by subscripts on X indicating scan line and element. However, since the location of X's is not pertinent to this discussion, this kind of subscripting will not be employed here. Subscripting will be used for other purposes.

Although a four-element vector cannot be presented graphically, a vector of two elements can, as shown in Figure 5-4. The vector corresponds to a pixel of a two-channel MSS, where x_1 and x_2 are, respectively, channels 1 and 2. In the figure, the vector, 0-A is defined by the coordinates $x_1 = 50$, $x_2 = 75$, or

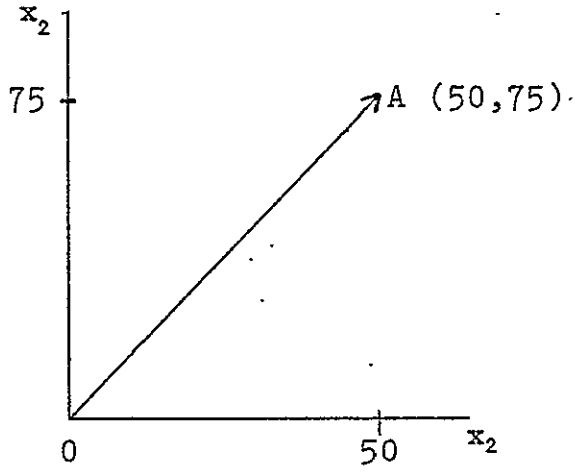

Figure 5-4: Geometric representation of a two-channel MSS observation.

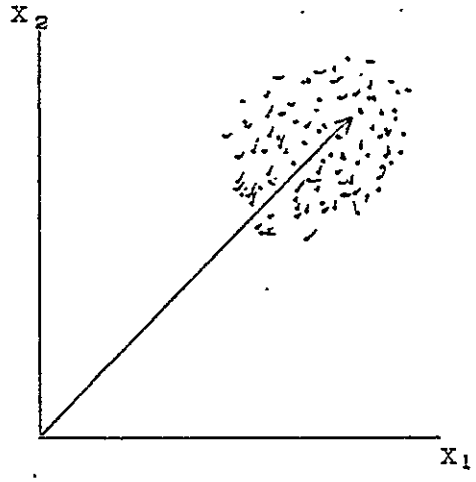

Figure 5-5: Mean vector for a category with sample points showing dispersion.

$$X = \begin{bmatrix} 50 \\ 75 \end{bmatrix}$$

Consider a target which represents a category of interest, say water, composed of a number of observations by a p-channel MSS. To estimate the spectral signature of the category as sensed by the p-channel MSS, a sample of the observations would be taken and the average value for each channel computed. In other words, the mean vector, with the same structure as an observational vector but with channel averages instead of raw data, would be computed from the observational vectors. The mean vector is the estimate of the p-channel spectral signature for the category.

Geometrically, the mean vector, or spectral signature, of a category in a two-channel MSS system can be shown as in Figure 5-5. The scatter of points represents the pixels of the training sample for the category. The graphed vector represents the mean vector, the coordinates of which are the average values for channels 1 and 2 of the pixels in the sample.

The measure of the dispersion, or scatter, of the points about the endpoint of the mean vector, as shown in Figure 5-5, is the covariance matrix. In addition to the mean vector, certain analyses require the sample covariance matrix. This can be computed using the same sample data as for the mean vector. In a very general sense, the covariance matrix is composed of the measures of inter-and-intra channel data dispersion about the spectral signature. Using W to symbolize the matrix, for p = 4 the matrix is structured as:

$$W = \begin{bmatrix} s_{11} & s_{12} & s_{13} & s_{14} \\ s_{21} & s_{22} & s_{23} & s_{24} \\ s_{31} & s_{32} & s_{33} & s_{34} \\ s_{41} & s_{42} & s_{43} & s_{44} \end{bmatrix}$$

The s's are variance and covariance values computed from the sample observational vectors. The subscripts identify the row and column positions, respectively; e.g., s_{34} is in the third row, fourth column position. The subscripts also identify the channels contributing to the term; e.g., s_{12} is the covariance of channels one and two. The covariance of channel one with channel two is identical in definition and value to the covariance of channel two with channel one, $s_{12} = s_{21}$. The same is true for all other pairs of channels; e.g., $s_{13} = s_{31}$, $s_{23} = s_{32}$, etc. The terms on the matrix

diagonal, s_{11}, s_{22}, s_{33}, and s_{44}, are the channel variances; e.g., s_{11} is channel one variance, s_{22} is channel two variance, etc. The variance is a measure of the dispersion of values about the mean value for a channel: the greater the variance, the greater the dispersion. For a given category, the variances give an indication of the spectral heterogeneity within the category. The greater the variances, the greater the heterogeneity. The total variance is simply the sum of the variances. In reference to the covariance matrix, W, the total variance is the sum of the diagonal terms; i.e., $s_{11} + s_{22} + s_{33} + s_{44}$.

For simplicity, the examples given herein are for four-channel MSS data rather than for the Skylab S192 sensor, which has numerous channels. Specifications of the scene, targets, etc. are unimportant for this discussion, and, therefore, will be omitted. Extensions of the concepts from the four-channel examples to larger MSS systems such as the S192 are direct. Although the interpretations may be quite different for a larger number of channels, the concepts are completely general. For a sampled category of four-channel data, the following mean vector and covariance matrix were computed:

$$X = \begin{bmatrix} 24.5 \\ 12.4 \\ 7.4 \\ 1.3 \end{bmatrix} \qquad W = \begin{bmatrix} 0.69 & -0.13 & -0.16 & -0.14 \\ -0.13 & 0.44 & 0.12 & 0.01 \\ -0.16 & 0.12 & 0.88 & 0.17 \\ -0.14 & 0.01 & 0.17 & 0.40 \end{bmatrix}$$

The mean vector represents the spectral signature for the category (which happens to be water), based on the MSS system used for measurement. For this category, the total variance is 2.41 found by the sum of 0.69 + 0.44 + 0.88 + 0.40. It can be seen that channel three is the most variable. Its within-channel variability about the mean (0.88) represents 37% of the total variance. The least variable channel is channel four, with a variance of 0.40.

5.3.6.2 Linear Transformations

For principal components and canonical analyses, as well as numerous other data manipulation and analysis methods, the use of linear transformations is fundamental. A linear transformation equation is of the form:

$$y = c_1x_1 + c_2x_2 + \ldots + c_px_p$$

In the equation, y is the transformed variable, the x's are the original or untransformed variables, and the c's are the transformation coefficients. A number of y's can be found at once from each set of x's by using different sets of c's. For example, two simultaneous linear transformation equations can be written as:

$$y_1 = c_{11}x_1 + c_{12}\,x_2 + \ldots + c_{1p}\,x_p$$

$$y_2 = c_{21}x_1 + c_{22}\,x_2 + \ldots + c_{2p}\,x_p$$

where the subscripts can be seen to identify the equation number, the variable number, and the coefficients by equation and variable number. The number of simultaneous linear transformation equations can be extended indefinitely but are cumbersome in this form. A preferred form is that of linear algebra. In the above case, for example,

$$Y = CX, \text{ where } Y = \begin{bmatrix} y_1 \\ y_2 \end{bmatrix},$$

$$C = \begin{bmatrix} c_{11} & c_{12} & \cdots & c_{1p} \\ c_{21} & c_{22} & \cdots & c_{2p} \end{bmatrix}$$

and

$$X = \begin{bmatrix} x_1 \\ x_2 \\ \vdots \\ x_p \end{bmatrix}$$

The matrix, C, is the linear transformation matrix. The linear algebraic equation, Y = CX, applies generally by simply specifying C as a (qxp) matrix, where p is the number of x variables and q is the number of y variables or equations. Because of the geometrical relationships shown below, the commonly used nomenclature is to refer to each y variable as an axis.

From the geometric point of view, consider an idealized situation where two channels are perfectly correlated, as shown in Figure 5-6. Since the pixels all fall on a line, if one is given the x_2 value for a pixel, the x_1 is perfectly predictable simply by using the equation for the line; i.e., $x_1 = a + bx_2$. In this case, only one variable would be needed to carry all of the information available in x_1 and x_2. The new variable, y, can be found by translation and rotation of axes as shown in Figure 5-7. The translation was made from $x_1 = 0$, $x_2 = 0$ to $x_1 = \bar{x}_1$, $x_2 = \bar{x}_2$. Rotation was made by the angle θ so that the new $\bar{y}_1$ axis passes through all points and has a mean value, $y_1 = 0$. Axis y_2,

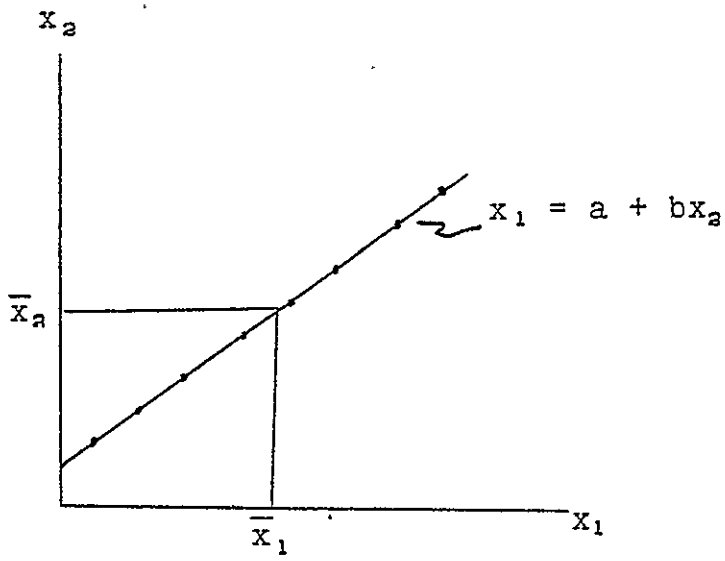

Figure 5-6: Perfectly correlated channels defining a straight line.

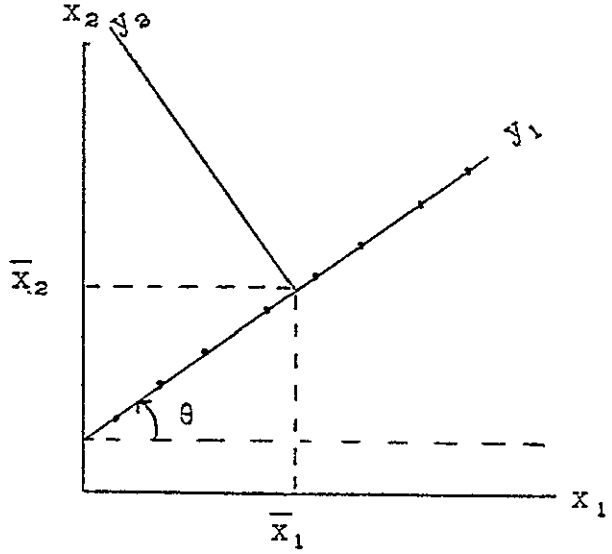

Figure 5-7: Rotation and translation transformation of axes by principal components criteria.

in this case, is not needed since, for all pixels, $y_2 = 0$. In most real-life cases, channels are not perfectly correlated and pixel patterns are often elliptical in two dimensions or ellipsoidal for greater than two dimensions. For elliptical patterns, the rotation places the y_1 axis along the principal axis of the ellipse and y_2, perpendicular to y_1, along the secondary axis of the ellipse (Figure 5-8). Notice that the pixels have not been moved at all; only the axes have been changed. Each pixel originally defined by a vector

$$X = \begin{bmatrix} x_1 \\ x_2 \end{bmatrix}$$

now can be equivalently defined by a vector

$$Y = \begin{bmatrix} y_1 \\ y_2 \end{bmatrix}$$

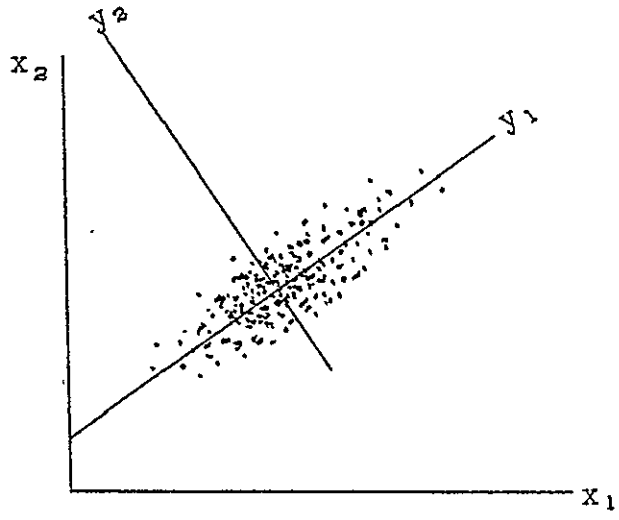

Figure 5-8: Elliptical scatter pattern of observations with rotation and translation transformation by principal components criteria.

The rotation transformation can be expressed as:

$$y_1 = c_{11} x_1 + c_{12} x_2$$

$$y_2 = c_{21} x_1 + c_{22} x_2$$

or in linear algebra, as before,

$$Y = CX$$

where

$$C = \begin{bmatrix} c_{11} & c_{12} \\ c_{21} & c_{22} \end{bmatrix}$$

The c's can be computed from the original sample of pixels, depending upon the desired transformation. To obtain the translation as well as rotation, the following equations, which have the translation factors of x_1 and x_2, can be applied.

$$y_1 = c_{11} (x_1 - \overline{x}_1) + c_{12} (x_2 - \overline{x}_2)$$

$$y_2 = c_{21} (x_1 - \overline{x}_1) + c_{22} (x_2 - \overline{x}_2)$$

In matrix form, this can also be written as $Y = C (x - \overline{x})$ or $Y = CX - D$

where $\overline{x} = \begin{bmatrix} \overline{x}_1 \\ \overline{x}_2 \end{bmatrix}$ and $D = C\overline{x}$.

Translation is optional and, therefore, is not always done.

In the preceding numerical example, the corresponding transformation matrix for the principal components solution is:

$$C = \begin{bmatrix} 0.50 & -0.25 & -0.77 & -0.29 \\ -0.78 & 0.20 & -0.59 & 0.04 \\ 0.16 & 0.84 & 0.03 & -0.51 \\ 0.32 & 0.44 & -0.23 & 0.81 \end{bmatrix}$$

which yields the following equations which could be used to produce transformed data from the raw data:

$$y_1 = 0.50x_1 - 0.25x_2 - 0.77x_3 - 0.29x_4$$

$$y_2 = -0.78x_1 + 0.20x_2 - 0.59x_3 + 0.04x_4$$

$$y_3 = 0.16x_1 + 0.84x_2 + 0.03x_3 - 0.51x_4$$

$$y_4 = 0.32x_1 + 0.44x_2 - 0.23x_3 + 0.81x_4$$

5.3.6.3 Correlations

The covariance of two variables, although it has statistically desirable characteristics, does not have interpretively desirable characteristics. Its magnitude is influenced by the units of measure, even if unknown, of the two variables and its possible range is a function of the variances of the two variables. The correlation coefficient, r, corresponding to a covariance, is much more desirable for interpretive uses and can be found as:

$$r_{ij} = \frac{s_{ij}}{\sqrt{s_{ii}\, s_{jj}}}$$

from terms in the covariance matrix. In this case, r_{ij} is the correlation coefficient of the ith and jth variables. The range of r is from -1 to +1. A perfect positive correlation is +1, which indicates that as one variable increases, the other increases in a perfectly predictable way. A perfect negative correlation is -1, but in this case, as one variable increases, the other decreases in a perfectly predictable way. Consider two original raw data variables. In the cases that r = +1 or r = -1, the two variables are statistically completely superfluous or redundant; e.g., there is no gain in information by keeping the second variable. A correlation of zero indicates a complete absence of relationship between two variables; i.e., complete statistical independence and zero redundancy.

For the four-channel covariance matrix of x-variables in the example, the corresponding correlation matrix is:

$$R = \begin{bmatrix} 1.00 & -0.23 & -0.21 & -0.26 \\ -0.23 & 1.00 & 0.19 & 0.01 \\ -0.21 & 0.19 & 1.00 & 0.29 \\ -0.26 & 0.01 & 0.29 & 1.00 \end{bmatrix}$$

Interpretation of these values shows that no pair of channels is strongly correlated; the strongest correlation is between channels 3 and 4, with a value of 0.29. Channels 2 and 4 are essentially independent because the correlation between them is only 0.01. With MSS systems having many channels, such as the S192 system, strong correlations are frequently found.

So far only the correlations between pairs of x-variables have been considered. Correlations are highly valuable in other contexts as well. For a linear transformation using a set of x-variables to produce a y-variable, a correlation coefficient can be found for each x-variable with the y-variable. The interpretation of these correlations is that x-variables which are strongly correlated with a y-variable are the main contributors to the y-variable, and x-variables weakly correlated with the y-variable are of little or no consequence in contributing to the y-variable. If all important correlations have the same sign, they are mutually additive in their contribution to the y-variable. This is so even if the signs are all negative. If all important correlations do not have the same sign, then those with positive correlations are contrasted against those with negative correlations in their contributions to the y-variable.

5.3.6.4 Principal Components Analysis

The geometric explanation of the principal components transformation has already been considered in part with regard to Figure 5-8. However, the covariance matrix for the original x-variables is now the total covariance matrix output from the sample observational vectors from all categories (not just from a single category). The transformation is made so that the y-variables are not correlated, even though the total variance is preserved. The variance for y_1 is the greatest possible for any axis rotation and the variance for y_2 is the greatest for any axis rotation yielding zero correlation with the y_1 axis. These last statements can be generalized, and are more meaningful if one considers more than two dimensions. The only advantage for the transformation so far shown is that the resulting y-variables are uncorrelated. This advantage is important for interpretive purposes, as will be shown later.

In the general case of a principal components analysis, a transformation matrix is found which preserves the total variance, produces transformed variables which are uncorrelated, and assigns the largest possible variance to the first transformed variable, the largest possible variance of the remaining variance to the second transformed variable, and so on. The covariance matrix for the p y-variables will have the same total variance as for the original p x-variables. If, as in the case for typical MSS data, many x-variables are strongly correlated, some of the y-variables will have very small or zero variance. This means that effectively all of the total variance for p x-variables can be preserved in q y-variables where q is smaller than p.

For instance, assume that the numerical four-channel example presented in section 5.3.6.1 represented a total covariance matrix instead of just the covariance matrix for a single category. Then the covariance matrix of the y-variables resulting from a principal components transformation is:

$$\Lambda = \begin{bmatrix} 1.08 & 0 & 0 & 0 \\ 0 & 0.61 & 0 & 0 \\ 0 & 0 & 0.42 & 0 \\ 0 & 0 & 0 & 0.30 \end{bmatrix}$$

The sum of the diagonal elements, the variances, is equal to the sum of the diagonal elements of the original covariance matrix presented earlier; e.g., the total variance, 2.41, in W equals the total variance, 2.41, in Λ. But, when each variance in Λ is shown as the percentage of the total variance, 45% of the total variance can be recovered by the transformation in only the first y-variable. Compare this with 37% for channel 3, the one with the largest variance in W. For MSS systems with more channels, the difference is typically very much greater. Notice the off-diagonal or covariance terms are zero in Λ, indicating zero correlation and statistical independence among the y-variables.

For MSS systems with many channels, such as the S192, many correlations between pairs of channels are strong. As a result, it is frequently possible to bring about a large reduction in the dimensionality of the data without significant loss of information by making the principal components transformation. A reduction, for instance, from 16 x-variables to 3 y-variables with a preservation of over 95% of the original total variance would not be uncommon. Such a reduction in dimensionality of the data rendered by the principal components transformation can lead to substantial computer processing savings. It is also particularly important when the dimensionality can be reduced to 3, since the transformed data can be displayed in color while retaining essentially all of the original information. With each variable assigned a different color, images much like Landsat-1 three-channel color composite images can be produced.

Correlations of the x-variables with the y-variables can be computed and these then can be used to interpret the contribution of each spectral band to each transformed variable. From the matrix, it can be seen that the first y-variable has the greatest explanatory power for the combined set of x-variables by reason that its variance is the greatest possible component of the total variance. The first y-variable then can be considered as the strongest descriptor, albeit abstract, of the data. The interpretation of the correlations of the x-variables with this y-variable then leads to an identification of those channels which are most important in defining the nature of the data and the spectral character of the targets they represent. The most important channels are identified as those for which the x-variables are most strongly correlated with the y-variable. Similar arguments can be followed for the second y-variable, and so on.

For example, if the correlations of channels 1 through 4 with the first y-variable are 0.63, -0.39, -0.86, and -0.48, the interpretation is that channel 3 makes the greatest contribution to the first y-variable, with a moderate contribution from channel 1 and the least, though not negligible, contributions from channels 2 and 4. Considering the signs, the y-variable represents the contrast of channel 1 against channels 2, 3, and 4.

5.3.6.5 Canonical Analysis

The covariance matrix of the x-variables for principal components is composed of two parts which are not separated in that analysis; i.e., the covariance matrix is the total covariance matrix. The two parts which are additive to make the total covariance matrix are the within-category and the among-category covariance matrices. Canonical analysis is addressed to the analysis of these two matrices and, as such, requires the data to be aggregated into categories.

In canonical analysis, the linear transformation is found so that transformed variables are independent and so that each axis contains the maximum possible percentage of the total among-category variance. In addition, the within-category variance of each transformed variable is unity.

Now consider the geometric interpretation of a canonical transformation. In Figure 5-9, four categories are shown with ellipses diagrammed to indicate the pattern of pixel scattering in each category. In canonical analysis, an axis rotation θ, is found so that the sum of squares of distances between category mean values on the new axis is maximized (Figure 5-10). A second axis is found, orthogonal to the first, which maximizes the remaining sum of squared distances among categories. In the case of only two axes, the second is automatically fixed as perpendicular to the first axis. In cases with more than two axes, the orthogonality and maximization criteria are simultaneously applied.

Translation is also made in canonical analysis to the overall mean values of the x-variables. In addition to translation and rotation, the y axes are scaled so that the ellipses are transformed to circles (ellipsoids to spheres for more than two dimensions) (Figure 5-11). In the axis scaling, the variance for each y-variable within each category becomes unity.

Canonical analysis, geometrically then, is a method to find a transformation for translation, rotation, and scaling of axes to maximize the separability among categories on the transformation axes.

Whereas large variances in within-category covariance matrices indicate spectral heterogeneity within the categories, large variances in among-category covariance matrices indicate large differences among spectral signatures for the categories. In an among-category covariance

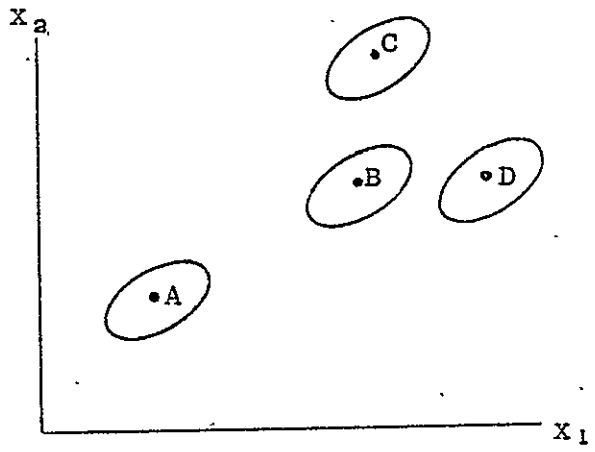

Figure 5-9: Mean values and elliptical density contours for categories A, B, C, and D.

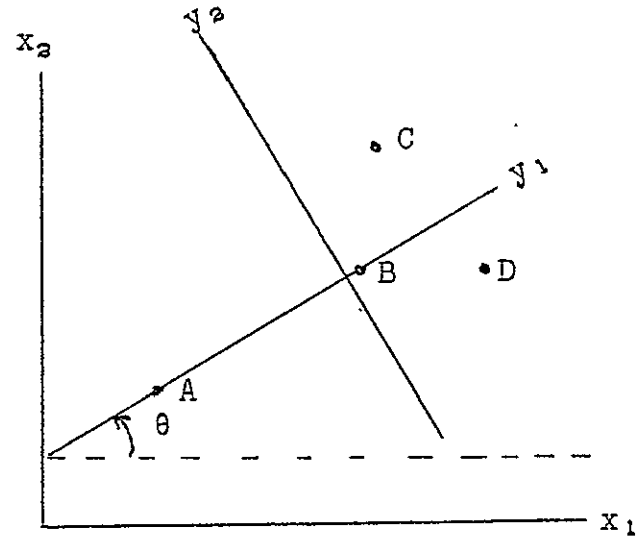

Figure 5-10: Canonical rotation and translation transformation for categories A, B, C, and D.

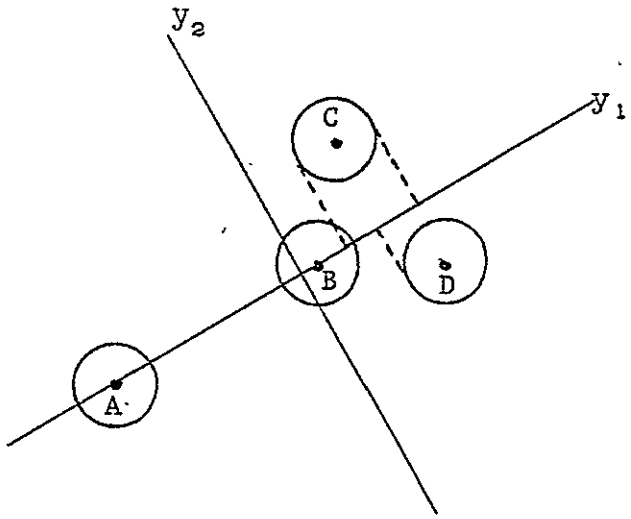

Figure 5-11: Canonical rotation, translation, and scaling transformation showing separabilities among categories A, B, C, and D.

matrix, the sum of the diagonal terms represents the total among-category variance. For the transformed variables, their among-category covariance matrix for four axes is:

$$\Lambda = \begin{bmatrix} \lambda_1 & 0 & 0 & 0 \\ 0 & \lambda_2 & 0 & 0 \\ 0 & 0 & \lambda_3 & 0 \\ 0 & 0 & 0 & \lambda_4 \end{bmatrix}$$

The sum of the λ's is equal to the total among category-variance of the x-variables and the λ's are found in order from the largest to smallest. Frequently, a large portion of the among-category variance is recovered in only a few axes.

The among-category variances are measures of the discriminatory information among categories. For the x-variables, because channels are correlated among categories, as well as within categories, some redundancy among channels exists. There is no such redundancy in the transformed variables, since they are independent, and a reduction can be made from the original number, p, of channels to a smaller number, q, of axes, where the q axes represent a concentration of the discriminatory information. When the resulting axes are three or less, the discriminatory information can be displayed in color by assigning a color to each axis

in the same way Landsat-1 color composite images of three channels are compared.

Correlations of the channels with the axes can be produced and represent the basis for interpretation of the degree of importance of each channel in the ability to discriminate among categories. Those channels which have weak correlations for all important axes are of little value in discrimination. On the other hand, those which have strong correlations with one or more important axes are valuable in discriminations. In classification of untransformed data, if an unknown pixel were to fall in an ellipse (Figure 5-9), it would be classified as belonging to that category. If it did not fall in any ellipse, it would be classified as "other." In this context, the ellipses can be considered as classification boundaries. Computations to determine whether a pixel falls within elliptical boundaries are complicated and time-consuming. This is particularly so if the number of channels is large.

These elliptical classification boundaries become circles when translated and scaled by canonical transformation (Figure 5-11). Computations are simple to determine if a transformed pixel falls within or outside a circle. In addition, if the number of y-variables is much smaller than the number of x-variables, the computational efficiency is again much increased. Referring again to Figure 5-11, if the circles are projected to the y_1 axis, these become classification bands. In Figure 5-11, on axis 1, category A is separable from categories B, C, and D; B is separable from D but not C, and C and D are not separable. On axis 2, A, B and D are not separable but A, B and D are separable from C. These separability relations are no different for the original untransformed data shown in Figure 5-9. However, in reality, with many x-variables, it is quite common to need only a few y-variables to achieve the same separability as with many x-variables.

This entire discussion on classification must be considered to be superficially explanatory. There are a number of aspects which have been intentionally overlooked. For example, the situation where two categories have overlapping classification bounds has not been considered. For further in-depth discussions of classification, reference should be made to the body of literature on multivariate statistical classification and pattern recognition.

5.3.7 Classification and Mapping

Satisfactory classification and mapping were required in order to obtain a basis for evaluation of S192 channels. The only sources of ground truth for the area covered by the S192 data sent to ORSER were USGS topographic maps and Skylab photography. These sources were adequate for checking prominent features against mapping results. However, for small scattered low-contrast features, the Skylab photography was of limited utility as ground truth. For example, it was not usually possible to delineate boundaries separating the various forest and non-forest vegetation categories which could be identified as the result of processing

S192 data. Topographic maps are even more limited because the majority of spectrally distinguishable features are not shown. In other investigations, low-altitude (4500 m) and high altitude (20000 m) photography have been found to be extremely beneficial in map verification for data in the scale of Landsat and the S192. Such photography was not available for the S192 test area.

Verification of signatures and mapping success relied mostly on the interpretation of the results of analysis. The ground truth sources were used only in a general way. Supervised and unsupervised methods were used in signature extraction. Specific algorithms based on the two approaches are common to all MSS data processing systems. Usually the supervised method algorithms require that first a known ground target, say a corn field, be located in the data. A polygon is defined in the data to enclose the MSS observations for the target. From this training area, statistics such as the mean vector (spectral signature) and covariance matrix are computed. The same is done with known ground targets for all categories of interest and then the statistics for the complete set of categories are submitted to a classification and mapping program. In this supervised method, it is generally necessary to identify ground targets by site visitation or ground truth interpretation.

An alternative to this procedure, particularly useful where ground truth is minimal and site visitation is not feasible, has been developed in the ORSER system. In this supervised method, the data are first analyzed and mapped according to areas of local spectral homogeneity. An area of local spectral homogeneity indicates the existence of a target which is the spectral equivalent of a training area in the previously discussed method. The differences between this method and the first method are that:

1) the identity of the spectrally homogeneous area may not be known, whereas it is known for a training area based on ground truth; and

2) the training area found on the basis of ground truth may not be spectrally homogeneous, whereas it is for an area defined by homogeneity.

5.3.7.1 Supervised Analysis

The scheme of supervised analysis is described in McMurtry, et al. (1974) and the details of use of the ORSER system in this method are covered in Borden, et al. (1976). In the S192 data analysis, spectrally homogeneous areas were defined as training areas and the statistics were computed for each one. The mean vectors were used in a minimum euclidean distance classifier described in detail in Borden, et al. (1976). The classification algorithm is geometrically presented in the following.

The spectral signatures for two categories, A and B, for a two-channel MSS system are graphed as vectors in Figure 5-12. Euclidean distance is the distance between the endpoints of a pair of vectors, shown as d_1 through d_4 in Figure 5-12. For an observation, U_1, to be

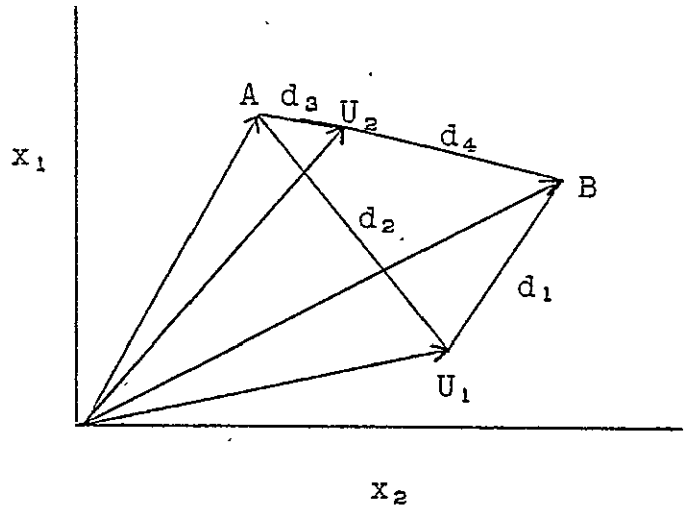

Figure 5-12: Mean vectors for two categories, A and B, and two observational vectors, U_1 and U_2, showing the euclidean distances, d_1, d_2, d_3, and d_4.

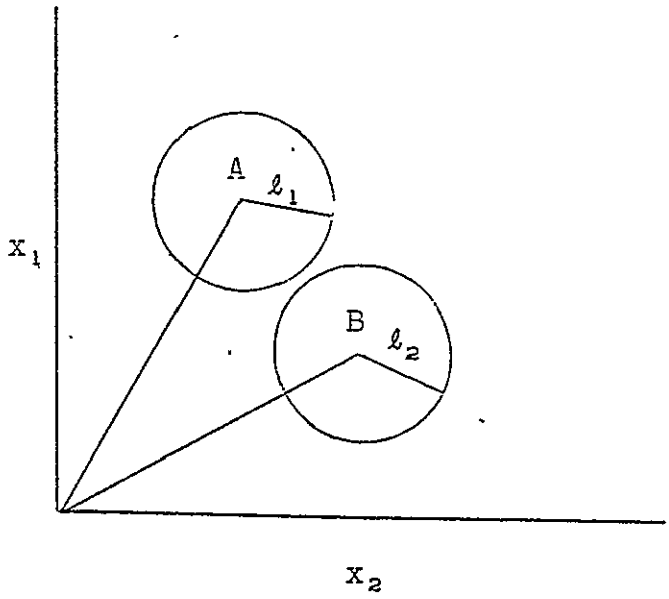

Figure 5-13: Mean vectors for two categories, A and B, showing the limits, ℓ_1 and ℓ_2, and the classification regions.

classified as belonging to either category A or B, the minimum euclidean distance (in this case d_1) of a choice between d_1 or d_2 indicates U_1 will be classified as category B. Similarly, U_2 will be classified as category A since d_3 is smaller than d_4. The advantage of this classifier is that it is very rapid compared with other multivariate classifiers. Its disadvantage is that on statistical grounds it does not consider the effect of dispersion of data in each category in the classification. Experience has shown that this last point is not of important consequence in thematic mapping. In the scheme shown in Figure 5-12, no possibility exists for observations to remain unclassified, i.e., for observations belonging to none of the specified categories to be classed as "other." The algorithm accommodates the "other" classification by using a classification limit or critical value for each specified category. In Figure 5-13, the limits for two categories are shown. A limit defines the radius of a circle (a sphere in over two dimensions) which in turn defines a classification region for the category as shown in Figure 5-13. If an observation does not fall within any classification region, it would be classed as "other." If the classification regions overlap, an observation within the regions would be classified into the category for which the minimum euclidean distance is found.

In addition to its use for classification, the euclidean distance is useful in judging the separability of categories. For a pair of categories which have a relatively large euclidean distance of separation between their mean vectors, confusion in classification between the two categories will be small. Conversely, a relatively small euclidean distance of separation between two mean spectral signatures indicates that classification confusion between the categories will possibly be large.

By the supervised method, 12 spectral signatures were initially defined. Of these, four pairs were found to be duplicates based on their very small euclidean distances of separation. Corresponding duplicate samples were combined, resulting in 8 spectral signatures. Classification limits were adjusted to obtain dense classification patterns in the sample areas. As expected, mapping with the 8 categories classified large areas as "other." No additional signatures were defined by the supervised method. In the strategy for signature extraction commonly used by ORSER, as defined by McMurtry, et al, (1974), further signatures were found by an unsupervised method (Turner, 1974).

5.3.7.2 Unsupervised Analysis

Unsupervised methods, as a class, are called cluster analysis. The steps of the cluster analysis algorithm used here will be presented only in gross generality. In a block of sample data, observations are grouped according to spectral similarity into clusters. The grouping is made without regard to the spatial locations of observations in the sample block. Spectral similarity is defined on the basis of the euclidean distance in spectral terms between pairs of observations. The distance is small for spectrally similar observations and great for dissimilar observations. A classification map is produced for the sample block for each cluster analysis. The mean vector for clusters which show

a meaningful spatial pattern are selected and those without a meaningful spatial pattern, such as random scatter patterns, are rejected. Meaningful patterns are determined on the basis of interpretation of the maps by the analyst, using whatever ground truth is available. Meaningful patterns, such as meandering streams, forest stands, and farm fields, are often quite obvious, even without ground truth. Sample blocks are usually small, seldom exceeding a few thousand pixels, and are defined to enclose areas previously classified as "other." Spectral signatures and their statistics found acceptable by the unsupervised method are added to the bank of spectral signatures. Classification and mapping then follow and the cycle is repeated until the area mapped has an acceptably small number of "other" classifications. Duplicate signatures, judged as before, are eliminated when they appear.

5.3.7.3 Classification Refinement

In the S192 data analysis, 14 spectral signatures, found by cluster analysis, were added to the 8 found by the supervised method to yield a total of 22 separate categories or targets. The identification of the targets which were represented by the spectral signatures was not simple or reliable in all cases, even with the Skylab photography for reference. In fact, some were not identified correctly until the final stages of the project, when color displays were used to present classification results. Some were easily identified, such as water, some urban, and some forest targets. A number of signatures for forest, non-forest vegetation and urban targets were not positively identified at this point.

Two steps in signature refinement were made to investigate the stability of the classification. Each refinement was made, using test block 4, by recomputing the spectral signature of each category on the basis of all the pixels classified into the category. After the second refinement, the classification was judged to be adequately stable. The final signature set is given in Table 5-5. Only 21 signatures are shown since signature 15 was eliminated because of the small number of pixels in that category. The distances of separation between categories are presented in Table 5-6. In general, it can be seen that signatures of the same category type, for example forest, have smaller distances of separation than signatures of different category types; for example, forest and water. The smallest separation distance, 12.3, is between signatures 1 and 6. In Table 5-7, the distances of separation from the signatures obtained originally and after each refinement are given. For example, in category 1, separation distance of the original signature, set 1, from the signature for the same category refined once, set 2, is 5.3. Such change was, in most cases, small from the first to the second refinement relative to the minimum separation distance between categories, namely, 12.3. In Table 5-8, the pixel count is given for classification using each of the three signature sets. Pixel counts in a category did not change appreciably from set 2 to set 3. Where the changes do not appear to be trivially small, the pixels were classified into another category of the same class; for example, from one forest to another forest category. It can be seen by referring to Tables 5-7 and 5-8 that the categories with the largest separation distance change from set 2 to set 3 were ones which had fairly small pixel counts. Therefore, even though

Table 5-5: Untransformed Data Category Specifications

Signature Number	Critical Distance	Channels 1	2	3	4	5	6	8	9	10	19	20	12	13	14	21	17
1	35	65.21	65.11	37.26	37.28	39.18	38.90	86.78	90.47	90.70	104.70	104.31	55.57	28.78	28.49	150.86	99.42
2	25	68.53	68.57	39.62	39.55	41.28	41.18	87.19	83.24	83.36	97.17	97.57	60.26	33.53	33.71	153.17	95.63
3	20	63.77	63.96	35.35	35.37	36.11	36.12	91.18	98.11	98.08	110.40	109.06	52.62	25.04	25.02	146.74	103.57
4	20	59.46	59.82	30.80	30.89	31.02	30.93	70.12	75.97	76.12	85.77	84.56	39.42	18.65	18.61	145.40	80.30
5	20	63.89	64.13	36.12	36.20	38.38	38.55	82.68	96.15	96.40	105.78	104.89	48.88	23.13	22.35	147.64	98.82
6	20	64.49	64.65	36.05	36.18	37.26	37.37	83.13	87.38	87.43	98.82	99.42	51.98	26.76	27.08	151.93	93.93
7	30	59.69	59.81	31.40	31.38	30.49	30.57	77.30	86.86	86.91	97.58	96.51	43.55	20.24	20.11	144.79	90.19
8	25	62.05	62.11	33.68	33.79	34.45	34.83	76.11	80.96	81.31	91.46	90.98	45.62	24.13	24.16	147.07	86.34
9	20	60.43	60.35	32.19	32.08	32.75	32.56	78.95	92.36	92.06	103.45	102.34	45.62	21.10	21.16	145.24	95.89
10	70	60.31	60.30	31.31	31.28	31.11	30.52	51.63	42.58	46.08	47.13	48.31	23.31	10.11	11.43	145.83	41.23
11	80	60.33	60.65	32.06	32.05	31.96	32.09	40.78	28.53	29.29	24.97	27.32	12.64	8.24	8.45	146.63	20.23
12	35	63.28	63.39	35.56	35.73	35.61	35.87	90.73	105.89	105.20	119.13	116.27	53.15	24.99	25.10	147.63	110.81
13	40	69.31	69.88	41.49	41.67	40.63	41.00	101.57	113.80	113.71	131.76	131.02	72.94	34.43	35.61	158.94	131.12
14	30	67.84	67.87	40.44	40.00	41.60	40.94	77.98	71.55	72.07	80.36	79.87	48.93	30.63	30.46	156.91	76.08
16	60	70.82	70.96	43.01	43.18	46.19	46.13	74.62	57.81	59.29	60.97	64.26	47.21	34.85	34.98	164.51	60.53
17	50	60.60	61.03	32.44	33.04	32.56	32.85	71.66	75.05	77.80	67.04	77.96	39.65	18.85	19.27	146.24	62.40
18	40	62.01	62.26	33.36	33.55	33.13	33.57	64.80	62.14	61.16	72.20	68.07	35.67	20.65	21.09	148.77	66.36
19	50	74.52	74.96	47.69	48.12	54.12	54.53	94.07	79.38	79.44	92.49	95.36	72.38	47.60	48.25	158.90	96.87
20	25	68.62	69.21	40.38	40.66	41.86	42.05	93.41	95.62	95.57	110.14	110.49	63.39	34.70	34.84	154.65	108.41
21	40	65.67	65.30	36.94	36.80	40.03	40.28	60.23	45.49	46.33	49.70	51.16	33.83	26.28	25.71	169.38	45.67
22	35	66.22	66.39	38.16	38.19	40.38	40.49	82.26	79.29	80.01	89.97	90.60	52.50	29.04	28.96	153.91	88.03

Table 5-6: Euclidean Distances of Separation for Categories

Signature Number	Signature Numbers 1	2	3	4	5	6	7	8	9	10	11	12	13	14	16	17	18	19	20	21	22
1	0.0	18.5	16.9	50.8	14.6	12.3	30.2	32.5	22.5	131.6	176.5	31.9	65.4	51.4	88.3	68.8	79.1	50.1	21.5	119.4	28.7
2	18.5	0.0	34.7	49.0	31.2	17.5	37.2	31.1	35.6	123.1	167.0	49.4	76.5	38.6	73.6	63.2	70.9	35.4	29.3	107.4	18.1
3	16.9	34.7	0.0	59.6	13.4	25.6	34.7	43.0	22.9	142.5	187.8	17.1	57.0	66.2	103.3	78.5	90.7	63.7	24.2	133.1	43.7
4	50.8	49.0	59.6	0.0	49.7	39.1	26.3	18.8	39.2	84.1	129.7	74.9	114.7	34.6	63.4	27.2	34.2	78.4	71.7	81.0	33.5
5	14.6	31.2	13.4	49.7	0.0	18.1	26.0	33.5	14.7	132.1	177.3	27.1	67.2	57.4	94.5	68.5	80.7	62.7	30.3	123.1	35.8
6	12.3	17.5	25.6	39.1	18.1	0.0	21.3	20.7	19.0	119.7	164.6	41.6	77.1	41.3	78.5	56.9	67.2	52.2	32.9	108.1	18.9
7	30.2	37.2	34.7	26.3	26.0	21.3	0.0	15.7	13.3	110.2	155.7	49.2	90.5	46.2	82.0	48.4	59.7	71.8	51.1	105.2	30.3
8	32.5	31.1	43.0	18.8	33.5	20.7	15.7	0.0	25.7	100.2	145.5	59.0	97.2	31.0	66.8	38.8	48.1	62.8	53.2	92.0	18.2
9	22.5	35.6	22.9	39.2	14.7	19.0	13.3	25.7	0.0	123.0	168.5	36.2	78.2	54.6	91.5	60.4	72.2	70.1	41.7	116.8	34.9
10	131.6	123.1	142.5	84.1	132.1	119.7	110.2	100.2	123.0	0.0	45.8	158.4	196.5	87.0	69.4	67.8	53.2	138.0	150.9	39.2	105.8
11	176.5	167.0	187.8	129.7	177.3	164.6	155.7	145.5	168.5	45.8	0.0	203.7	241.4	129.7	104.8	112.0	98.0	178.2	195.3	67.8	149.9
12	31.9	49.4	17.1	74.9	27.1	41.6	49.2	59.0	36.2	158.4	203.7	0.0	44.3	82.4	119.4	94.3	106.7	74.3	29.3	149.2	59.9
13	65.4	76.5	57.0	114.7	67.2	77.1	90.5	97.2	78.2	196.5	241.4	44.3	0.0	114.0	148.4	132.8	144.0	85.0	47.4	182.2	92.2
14	51.4	38.6	66.2	34.6	57.4	41.3	46.2	31.0	54.6	87.0	129.7	82.4	114.0	0.0	37.5	35.7	37.3	53.9	67.0	69.3	23.1
16	88.3	73.6	103.3	63.4	94.5	78.5	82.0	66.8	91.5	69.4	104.8	119.4	148.4	37.5	0.0	191.4	189.0	199.7	221.9	187.8	201.0
17	68.8	63.2	78.5	27.2	68.5	56.9	48.4	38.8	60.4	67.8	112.0	94.3	132.8	35.7	50.5	0.0	25.8	85.7	88.3	64.4	46.2
18	79.1	70.9	90.7	34.2	80.7	67.2	59.7	48.1	72.2	53.2	98.0	106.7	144.0	37.3	41.7	25.8	0.0	90.0	98.3	48.6	53.6
19	50.1	35.4	63.7	78.4	62.7	52.2	71.8	62.8	70.1	138.0	178.2	74.3	85.0	53.9	75.8	85.7	90.0	0.0	46.1	114.8	45.8
20	21.5	29.3	24.2	71.7	30.3	32.9	51.1	53.2	41.7	150.9	195.3	29.3	47.4	67.0	101.8	88.3	98.3	46.1	0.0	135.8	45.5
21	119.4	107.4	133.1	81.0	123.1	108.1	105.2	92.0	116.8	39.2	67.8	149.2	182.2	69.3	40.2	64.4	48.6	114.8	135.8	0.0	91.3
22	28.7	18.1	43.7	33.5	35.8	18.9	30.3	18.2	34.9	105.8	149.9	59.9	92.2	23.1	60.1	46.2	53.6	45.8	45.5	91.3	0.0

Table 5-7: Euclidean Distance Change in the Mean Vectors for Three Signature Sets

Signature Number	Change Between Set 1 & Set 2	Change Between Set 2 & Set 3	Change Between Set 3 & Set 1
1	5.3	6.0	8.8
2	8.1	3.5	10.2
3	5.7	4.7	9.3
4	7.8	2.0	8.9
5	4.5	3.4	6.8
6	2.7	2.0	3.9
7	6.0	2.9	7.5
8	2.6	2.4	4.4
9	3.9	4.0	7.3
10	19.4	6.2	23.2
11	8.9	2.3	10.9
12	14.0	14.2	28.1
13	5.8	2.1	5.8
14	6.4	4.8	7.6
15	5.3	--	--
16	19.1	18.0	12.1
17	20.3	16.3	34.8
18	17.1	15.3	31.2
19	20.7	6.1	16.8
20	6.1	4.4	7.9
21	14.1	15.7	15.4
22	8.6	3.7	9.0

Table 5-8: Pixel Count for Each Category on Test Block 4 Using Three Progressive Signature Sets

Signature Number	Category	Set 1	Set 2	Set 3
1	Non-forest vegetation	1697	1239	1287
2	Non-forest vegetation	849	995	1031
3	Forest	502	549	489
4	Forest	880	679	677
5	Forest	605	700	649
6	Non-forest vegetation	999	934	915
7	Forest	1369	1405	1460
8	Forest	1262	1446	1390
9	Forest	1208	1025	891
10	Water	292	264	280
11	Water	331	353	356
12	Forest	181	278	328
13	Grassy	50	68	98
14	Urban	190	239	269
15	Urban	27	31	---
16	Urban	101	84	78
17	Forest	149	249	199
18	Forest	80	190	307
19	Urban	405	636	568
20	Non-forest vegetation	448	521	682
21	Urban	87	114	46
22	Non-forest vegetation	926	854	892
Other	Unclassified	354	139	100
	Totals	12,992	12,992	12,992

the separation distances were greater than 10, the smallness of the category made these differences inconsequential. Because of the small size of category 15, the signature was deleted, reducing the number of categories to the final 21 for this stage of the classification.

5.3.7.4 Canonical Analysis

Canonical analysis was performed at this point, using the 21 signatures and their covariance matrices. A large block of data containing all five test blocks was then transformed using the first three canonical axes. During the transformation, the resulting values were translated and scaled to fall in the range from 0 through 255 to meet display device requirements. A tape was also produced in the format for the Dicomed film recorder, discussed in the section on color displays. The transformation reduced the data dimensionality from 16 to 3. The 21 spectral signatures were also transformed, translated, and scaled in the same way as the data.

Transformed data may be analyzed in the same way as untransformed data. The five test blocks were all mapped to investigate the spatial extensibility of the signatures. Classification was satisfactory, except that a number of areas were mapped as "other." This was expected, at least for strip mine targets, of which there were none in test block 4. The unsupervised method was used to extract 9 additional signatures; e.g., 4 strip mine, 2 additional forest, 1 additional urban, and 2 cloud signatures. The full set of transformed signatures is given in Table 5-9. Category 19 was deleted because of the very small number of pixels classified into these categories. When it was deleted, its pixels were classified just as well into other categories.

Map products were generated using the complete signature set. These are presented in the section on color displays and will not be discussed here.

5.3.7.5 Evaluation of Classification Results

Classification of the S192 was successful for the intended purpose; namely, for support in channel evaluation. The final classification maps were correct to the level of detail afforded by the ground truth. The test areas, typical of Pennsylvania, are composed of a variety of land uses, and spatial patterns of land use are intricate and small. Visual interpretation of the color displays indicated no major discrepancies in classification.

Two kinds of confusion occurred, but not to a degree to influence adversely the overall success. One of these was the confusion between urban and certain strip mine categories. This confusion is caused by the combined effect of general similarity of spectral characteristics and high target variability over short distances. The same problem has been encountered with Landsat data in every scene which contains urban and strip mine targets. The second kind of confusion was among non-forest vegetation categories and some forest categories. Agricultural land falls

Table 5-9: Transformed Mean Vectors, Target Identifications, and Classification Limits for the Final Signature Set

Signature Number	Classification	Limit	Axis 1	Axis 2	Axis 3
1	Non-forest vegetation	25.5	181.577	109.845	52.241
2	Non-forest vegetation	25.5	170.396	121.293	48.585
3	Forest	25.5	188.184	89.730	53.492
4	Forest	25.5	135.296	85.903	50.496
5	Forest	25.5	177.819	87.263	55.114
6	Non-forest vegetation	25.5	168.142	101.365	54.982
7	Forest	25.5	158.726	81.393	52.309
8	Forest	25.5	150.427	94.603	50.967
9	Forest	25.5	169.908	80.647	53.250
10	Water	35.0	60.253	93.739	47.982
11	Water	50.0	18.671	97.514	50.100
12	Forest	25.5	201.462	83.265	57.657
13	Non-forest vegetation	25.5	237.075	110.094	58.957
14	Urban	25.5	135.466	120.270	57.931
16	Urban	25.5	107.617	139.905	63.371
17	Forest	25.5	121.928	89.990	51.714
18	Forest	25.5	106.789	99.931	52.572
20	Non-forest vegetation	25.5	195.489	115.691	53.767
21	Urban	25.5	74.437	127.081	73.405
22	Non-forest vegetation	25.5	154.608	113.270	53.452
23	Strip mine	40.0	199.500	189.330	36.830
24	Strip mine	40.0	159.140	180.290	53.570
25	Strip mine	25.5	137.160	148.800	54.360
26	Forest	25.5	124.060	86.760	53.550
27	Forest	25.5	115.890	96.890	59.220
28	Residential urban	25.5	93.000	146.500	44.000
29	Cloud	80.0	255.000	255.000	2.900
30	Cloud	35.0	235.000	187.000	25.000
31	Strip mine	25.5	138.430	176.140	44.140

in this kind of confusion. As with Landsat data, this confusion is brought about by the intricacy of agricultural land use patterns, as well as the variety of pure and mixed spectral responses. Purity here means a single spectral feature in a pixel, such as would be obtained in pixels sensed in the middle of a corn field. Mixed, as used here, means different spectral features, each partially sensed in a pixel, such as occurs with field borders.

As with Landsat data collected from Pennsylvania, an area with a large variety of land use targets and mixed spectral responses, the number of signatures required to map an area is fairly large. Thirty or more signatures has been the rule rather than the exception with Landsat data. The same situation occurred with the S192 data.

5.3.8 Principal Components Analysis Results

In the evaluation of the contribution of each channel to the total information content of the data, a principal components analysis was made for test block 4. The general mix of categories was well represented in this block, as determined by the classification and mapping results.

In Table 5-10, for the first 3 axes, the percentage of the total variance and the correlations of the channels with the axes are given. Of the total variance, 90% was recovered in the first 3 axes and 10% was distributed over the remaining 13 axes. A loss of 10% of the total variance would not be tolerable if further analyses for classification and mapping based on 3 axes were to be done. However, the first 3 axes were considered adequate for channel evaluation for the following reasons:

1) the percentage of total variance for each axis after the third was quite small and decreased slowly with each additional axis; and

2) beyond the third axis, the correlations of channels with axes were usually small and, therefore, not useful for interpretation.

For the first axis, which accounted for 71.5% of the total variance, all channels covering the spectrum from 0.68 through 1.75 μ were important. These channels cover a small portion of the long wavelengths of the visible spectrum and extend just beyond the photographic IR wavelengths. The correlations for these channels with the axis were all greater than 0.80. Channels which were of little importance in the first axis were in the visible spectrum up to the red wavelength (0.52-0.67 μ), and the thermal IR band (10.20-12.50 μ). Their correlations with the axis were all 0.30 or less. The non-photographic IR band, from 2.10-2.35 μ, was intermediate but not interpreted as important.

The second axis accounted for 14.4% of the total variance or about 20% the amount recovered in the first axis. Those channels which were not important in the first axis were important in the second axis, with the exception of the thermal IR channel. The thermal IR was of questionable importance in axis two and of inconsequential importance in

Table 5-10: Percent of Total Variance for Three Axes, and Correlations of Channels with Axes for Principal Components Analysis of Test Block 4

		Correlations		
		Axis 1	Axis 2	Axis 3
Channel Number	Wavelength (μ)			
1	0.52-0.56	0.30	-0.79[a]	0.04
2	0.52-0.56	0.31	-0.79[a]	0.00
3	0.56-0.61	0.31	-0.78[a]	0.02
4	0.56-0.61	0.31	-0.80[a]	-0.04
5	0.62-0.67	0.29	-0.75[a]	0.01
6	0.62-0.67	0.30	-0.76[a]	-0.03
8	0.68-0.76	0.87[a]	-0.29	-0.19
9	0.78-0.88	0.94[a]	0.20	-0.18
10	0.78-0.88	0.91[a]	0.18	-0.34[a]
19	0.98-1.03	0.93[a]	0.20	0.23[a]
20	1.09-1.19	0.97[a]	0.15	-0.06
17	1.20-1.30	0.95[a]	0.07	0.25[a]
12	1.55-1.75	0.81[a]	-0.48	-0.07
13	2.10-2.35	0.54	-0.72[a]	0.10
14	2.10-2.35	0.53	-0.72[a]	0.04
21	10.20-12.50	0.16	-0.51	0.11
Total Variance[b]		71.5%	14.4%	3.8%

[a]Strongest correlations of channel to axis.

[b]89.7 percent of the total variance accounted for by axes 1-3.

axis one. The important channels for axis two covered the visible spectrum, from 0.52-0.67 μ, and the IR wavelengths, from 2.10-2.35 μ. The correlations were all greater than 0.70 in absolute value. The correlation of -0.48 for the 1.55-1.75 μ band was considered marginal, relative to the other large correlations. In axis three, which recovered only 3.8% of the total variance, correlations were all much lower than for the first two axes. Only three channels were considered to be of relative importance, namely those for the 0.78-0.88, 0.98-1.03 and 1.20-1.30 μ bands. These are a repetitious subset of the important channels in axis one, although the transformation vector, of course, is not the same.

The conclusions from this phase of the channel evaluation are that the most important channels in defining total information content cover the long visible through short IR wavelengths (0.68-1.75 μ); the next most important channels defining total information content cover almost all of the sensed visible wavelengths (0.52-0.67 μ) in addition to the long reflected IR band from 2.10-2.35 μ; and, finally, the least important, but not useless, band is the thermal IR band (10.20-12.50 μ).

5.3.9 Canonical Analysis Results

The total among-category variance for a number of categories defines an upper bound on the amount of discriminatory information available in a data set. This variance will be called the discriminatory variance for the purposes of this report. Canonical analysis finds the fewest linear transformations which maximize the recovery of the discriminatory variance. Using the 29 categories which map all but an inconsequentially small area of the scene sensed by the S192, the correlation aspects of canonical analysis then would give a reliable basis to evaluate channels with respect to their contribution to the discriminatory power of the data for the scene. This point is important, because if only a few categories were used and they comprised only a small part of the scene, it could be questioned whether the canonical analysis results would be applicable to the full set of categories or to the full scene.

Table 5-11 presents the canonical analysis results for the first three axes. In these three axes, nearly 99% of the discriminatory variance was recovered with almost 84% recovered in the first axis alone. The third axis is of little consequence, except for the existence of the strong correlation of the thermal IR channel with the axis. Table 5-12 presents the variances for the 16 transformed variables, and Table 5-13 presents the transformation matrix for the first three of these variables.

In axis one, the bands from the long visible through short IR wavelengths (0.68-1.75 μ) are important. The bands from 0.52-0.67 μ, as well as the thermal IR, are definitely not important, since their correlations are all less than 0.08. The 2.10-2.35 μ band is of dubious importance, with a correlation for these two channels of 0.20.

In the second axis, the bands covering 1.55-2.35 μ are important,

Table 5-11: Percent of Total Among Category Variance and Correlations of Channels with Axes for the First Three Canonical Analyses

		Correlations		
		Axis 1	Axis 2	Axis 3
Channel Number	Wavelength (μ)			
1	0.52-0.56	0.07	0.48[a]	0.07
2	0.52-0.56	0.07	0.48[a]	0.03
3	0.56-0.61	0.07	0.46[a]	0.05
4	0.56-0.61	0.07	0.46[a]	0.03
5	0.62-0.67	0.06	0.43[a]	0.00
6	0.62-0.67	0.06	0.44[a]	0.00
8	0.68-0.76	0.42[a]	0.26	0.05
9	0.78-0.88	0.67[a]	-0.32	0.17
10	0.78-0.88	0.61[a]	-0.29	0.17
19	0.98-1.03	0.62[a]	-0.21	0.04
20	1.09-1.19	0.75[a]	-0.18	-0.02
17	1.20-1.30	0.60[a]	-0.03	-0.13
12	1.55-1.75	0.49[a]	-0.62[a]	-0.29
13	2.10-2.35	0.20	0.60[a]	0.06
14	2.10-2.35	0.20	0.60[a]	0.00
21	10.20-12.50	0.01	0.35	0.85[a]
Total Variance[b]		83.61%	14.49%	0.72%

[a]Strongest correlations of channel to axis.

[b]1.17 percent of total variance not accounted for by axes 1-3.

Table 5-12 Variances for 16 Canonical Axes

Axis	Variance	Percentage of Total Variance
1	1.5×10^5	83.61
2	2.6×10^4	14.49
3	1.3×10^3	0.72
4	6.6×10^2	0.37
5	5.4×10^2	0.30
6	3.7×10^2	0.20
7	2.3×10^2	0.13
8	1.1×10^2	0.06
9	7.2×10^1	0.04
10	4.2×10^1	0.02
11	2.6×10^1	0.01
12	2.2×10^1	0.01
13	1.3×10^1	0.01
14	6.7×10^0	0.00
15	5.5×10^0	0.00
16	1.1×10^0	0.00

Table 5-13: Transformation Matrix Derived from Canonical Analysis

	Ch 1	Ch 2	Ch 3	Ch 4	Ch 5	Ch 6	Ch 8	Ch 9	Ch 10	Ch 19	Ch 20	Ch 17	Ch 12	Ch 13	Ch 14	Ch 21
Wavelength (μ)	0.52-0.56	0.52-0.56	0.56-0.61	0.56-0.61	0.62-0.67	0.62-0.67	0.68-0.76	0.78-0.88	0.78-0.88	0.98-1.03	1.09-1.19	1.20-1.30	1.55-1.75	2.10-2.35	2.10-2.35	10.20-12.50
Axis 1	0.001	-0.002	0.003	-0.010	-0.002	-0.002	0.029	0.031	0.048	0.042	0.054	0.029	0.058	0.020	0.002	0.002
Axis 2	0.020	0.036	0.035	-0.008	0.024	0.023	0.018	-0.033	-0.057	-0.018	-0.004	0.006	0.100	0.040	0.032	0.037
Axis 3	0.012	-0.015	-0.026	0.027	-0.020	-0.002	0.017	0.028	0.036	0.034	-0.026	-0.025	-0.105	0.020	0.022	0.150

with correlations of 0.60 or greater. The bands covering the visible spectrum from 0.52-0.67 are important, but less so than for the 2.10-2.35 μ bands. It is difficult to make a firm statement about the bands covering 0.68-1.19 μ and 10.20-12.50 μ, but these were judged to be relatively unimportant. Judgments concerning these correlations are difficult because no sharp distinctions are evident. It should be noted that a statistical test is of no value since, because of the large number of observations, a correlation coefficient as low as 0.03 is significantly different from 0 at the 95% probability level. Similarly, two correlations differing by only 0.03 are significantly different.

In axis three only the thermal IR is of obvious importance, with a correlation of 0.85 with the axis, while the next most important, the 2.10-2.35 μ channel, is of dubious value with a -0.29 correlation value. All others are definitely unimportant in this axis.

In considering the percentage of discriminatory variance recovered for each axis, as well as the correlations of channels with each axis, the conclusion can be drawn that the channels in the short wavelength IR region, from 0.68 through 1.75 μ, are most important in category discrimination. The second conclusion is that longer wavelength IR (but not thermal IR), 2.10-2.35 μ, and to a lesser degree visible bands from 0.52-0.67 μ, are secondary and of lesser importance in category discrimination. The third conclusion is that the thermal IR 10.20-12.50 μ band is of little importance in category discrimination.

5.3.10 Comparison of Principal Components and Canonical Analyses Results

The channels which contributed the most information to the first two axes of the principal components analysis are essentially the same as those which contributed the most to the first two axes of the canonical analysis. In each analysis for the first axis, the short wavelength IR bands from 0.68-1.75 μ were important, and the visible channels from 0.52-0.67 μ were not important. In addition, the thermal IR band from 10.20-12.50 μ was not important. In each analysis, the second axis was substantially less important than the first axis in the recovery of variance. In these second axes, the visible channels from 0.52-0.67 μ were important, in addition to the long reflected IR channel from 2.10-2.35 μ. Comparing the first with the second axes, the important channels in the first axes were unimportant in the second axes, and vice versa. In neither the first nor second axes was the thermal IR channel of consequential importance.

The third axis for each kind of analysis did not agree; however, the third axis in each case was of minor importance compared with the first two axes. It is likely that the third axis found in canonical analysis, in which the thermal IR was important, would match one of the axes beyond the third axis of the principal components analysis.

Overall, the principal components analysis shows that, in the first two axes, the recovery of the total variance was dominated by discriminatory information. This is inferred by the close agreement in these

two axes between the principal components and canonical analyses.

5.3.11 Comprehensive Evaluation of Channels and Bands

5.3.11.1 Comprehensive Evaluation of Channels Within Bands

In this evaluation, the objective is to determine if there is an identifiable "best" channel for each band which has multiple channels.

A preliminary evaluation of channels within bands was conducted early in the project to select channels for analysis. It was not done comprehensively, nor for the same reasons as in the evaluation discussed here.

In order to determine if any difference existed between pairs of channels in the same band, correlations between all pairs of channels were computed using approximately 11,000 observations in test block 4. The results for selected bands are shown in Table 5-14. For bands 6, 7, and 11, with correlations of 0.96 or 0.97, the pairs are almost perfect duplicates. For bands 3, 4, 5, and 12, correlations range from 0.85 to 0.91, and since they are so strongly correlated, they may be considered to be effective duplicates. Correlations among the pairs of the thermal IR channels, band 13, are not strong enough to be considered as duplicates. It should be remembered that uncalibrated data were used and it is possible that calibration of these channels could improve the correlation.

In addition to the comparison of correlations, the within category variances can be used for comparison. The within category variances are measures of the variability within channels, or channel noise relative to thematic mapping of the categories. For two channels in the same band which are essentially duplicates, the channel with the smallest within category variance is preferred because it is least noisy for thematic mapping purposes. Classification based on that channel, instead of others in the same band, would be more precise. Among and within category variances are shown for bands 3, 4, 5, 7, and 12 in Table 5-15. The among category variance is a measure of the spectral differences of a channel among categories. The ability to distinguish among categories in general is dependent upon the relative differences between the among and within category variances for the aggregate of channels. The ratios of among to within category variances for all channels in Table 5-15 ranges in order of magnitude from approximately 10^3 to 10^4. These are very large ratios, indicating that the ratio of discriminatory information to noise is very large.

On the other hand, the pairwise comparison of channels in the same band shows that the within category variances are all essentially the same. That is to say, for any pair of channels in the same band, there is no practical difference in noise level for bands 3, 4, 5, 7, or 12.

Table 5-14: Correlations Between Pairs of Channels in the Same Band

Band	Channels	Correlation
3	1, 2	0.87
4	3, 4	0.88
5	5, 6	0.85
6	7, 8	0.97
7	9, 10	0.96
11	11, 12	0.97
12	13, 14	0.91
13	15, 16	0.64
13	15, 21	0.49
13	16, 21	0.47

Table 5-15: Among and Within Category Variances for Pairs of Channels in the Same Band

Band	Channel	Among Category Variance	Within Category Variance
3	1	86×10^3	11
	2	89×10^3	11
4	3	10×10^4	14
	4	10×10^4	14
5	5	18×10^4	29
	6	19×10^4	29
7	9	18×10^5	27
	10	18×10^5	33
12	13	40×10^4	23
	14	40×10^4	24

Combining the interpretations of the correlation with those of the within category variances, the following can be concluded. Paired channels in bands 3, 4, 5, 7, and 12 are duplicates with respect to thematic mapping. Because of the nearly perfect correlations between pairs in bands 6 and 12, as shown in Table 5-14, these can be considered duplicates. For bands 3, 4, 5, 6, 7, 11, and 12, therefore, the choice of the best sensor in each band should be determined by other factors, such as cost, design and reliability.

5.3.11.2 Evaluation of All Bands

With the aim of selecting the minimum number of bands which could be used effectively to support thematic mapping at the same level as the S192, correlations between all pairs of bands were computed. Table 5-16 presents the results. The correlations were averaged for bands with duplicate channels. Two groups of associations emerged from interpretation of the table. These have been enclosed by lines in the table and are labeled A and B for the two associations. In each of these associations, the correlations are generally quite strong. For bands 1 and 2, the correlations with all other bands are relatively small indicating independence not only between the two bands but also between these and all other bands. Whatever information is contained in these bands is not redundant with that of any other bands. Therefore, if either band contained discriminatory information for thematic mapping, it would have to be retained. Since such was not the case, as shown above in section 5.3.8 - 5.3.10, it can be concluded that neither has to be retained.

Band 13, for example, is marginally independent. The correlations are not particularly strong with the other bands but correlations with bands 3, 4, 5, 6, 11, and 12 indicate some redundancy with these bands. Because of this, and because of the prior finding of the possible importance of a band 13 channel in the third canonical axis, band 13 cannot be eliminated.

Bands 3, 4, 5, 6, 11, and 12, which form association group A in Table 5-16, are all mutually correlated in a fairly strong way. Except for bands 6 and 11, they are only weakly correlated with bands in association group B. Bands 6 and 11 appear to be intermediate but with a stronger association with group B than group A. Because of their mutually strong correlations, it would seem that only one of bands 3, 4, 5, and 12 would have to be retained. The choice would be band 12 inasmuch as it had the strongest correlation, 0.60, with the second canonical axis.

Bands 6, 7, 8, 9, 10, and 11, composing association group B in Table 5-16, are mutually strongly correlated. For the same reasons as given for group A, it is likely only one band would be needed. Of this group, band 9 would be slightly preferred because it has the highest correlation, 0.75, with the first canonical axis.

Table 5-16: Correlations Between Pairs of Bands

Band	Wavelength (μ)	1	2	3	4	5	6	7	8	9	10	11	12	13
1	0.41-0.46	1.00												
2	0.46-0.51	0.05	1.00											
3	0.52-0.56	0.26	0.14	1.00										
4	0.56-0.61	0.29	0.15	0.78	1.00									
5	0.62-0.67	0.30	0.14	0.68	0.72	1.00								
6	0.68-0.76	0.20	0.06	0.49	0.49	0.45	1.00							
7	0.78-0.88	0.13	-0.03	0.16	0.17	0.16	0.78	1.00						
8	0.98-1.03	0.12	-0.02	0.15	0.16	0.16	0.75	0.86	1.00					
9	1.09-1.19	0.13	-0.02	0.18	0.19	0.19	0.83	0.93	0.91	1.00				
10	1.20-1.30	0.12	-0.01	0.24	0.25	0.23	0.79	0.85	0.94	0.92	1.00			
11	1.55-1.75	0.22	0.07	0.59	0.59	0.53	0.85	0.68	0.67	0.74	0.75	1.00		
12	2.10-2.35	0.23	0.12	0.68	0.66	0.61	0.66	0.37	0.39	0.44	0.48	0.80	1.00	
13	10.20-12.50	0.10	0.09	0.45	0.37	0.32	0.21	0.04	0.0	0.05	0.09	0.45	0.35	1.00

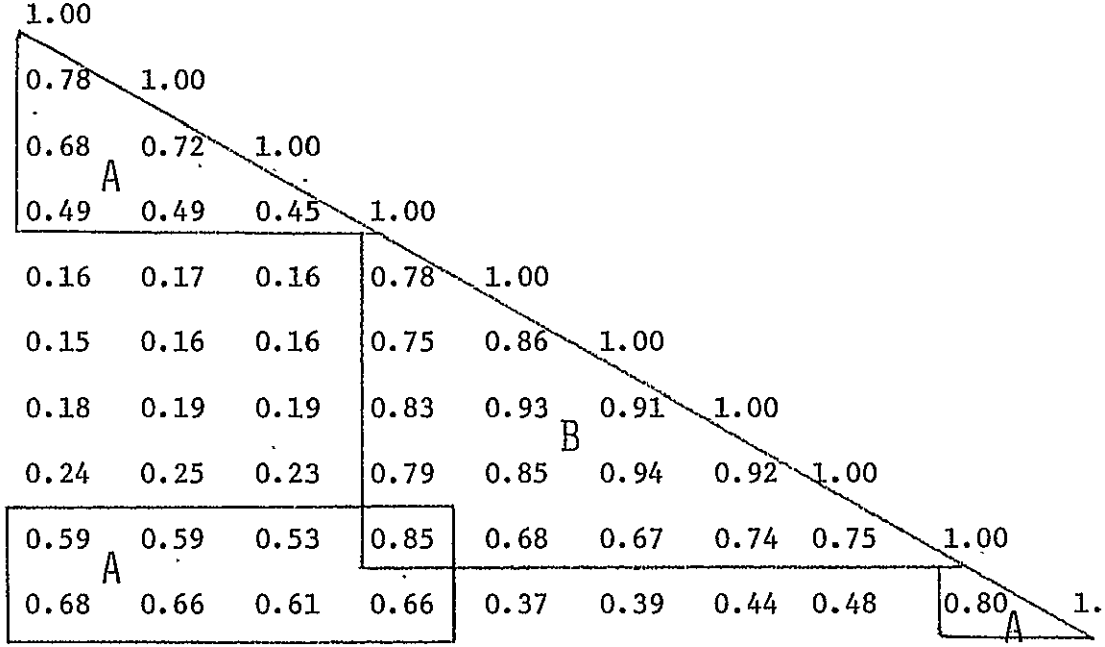

To summarize these interpretations, on the basis of parsimonious selection of existing bands, three would be the minimum to achieve thematic mapping results consistent with the use of all bands. These three would be bands 9, 12, and 13, representing 1.08-1.19 μ, 2.10-2.35 μ, and 10.2-12.5 μ, respectively. Alternate bands to these which would do just about as well would be bands 6, 7, 8, or 10 for band 9 and bands 3, 4, 5, or 11 for band 12. No alternates exist for band 13.

From an entirely different point of view, consider how an MSS might be designed to accomplish similar results to the 13 bands of the S192. Three or four bands would seem to be necessary. (To avoid confusion with S192 bands, these will be given Roman numerals.) Band I would be designed to cover the spectrum from 0.5 to 0.7 μ, corresponding to S192 bands 3, 4, 5, and the short wavelength part of 6. Band II would be from 0.7 to 1.3, corresponding to S192 bands 7, 8, 9, 10, and the long wavelength part of 6. Band III would be from 1.5 to 2.5 μ, corresponding to S192 bands 11 and 12, the second part of the association group A bands. Band IV would be from 10.0 to 12.5 μ, corresponding to S192 band 13. The question immediately occurs, how do these bands relate to the four Landsat bands (0.5-0.6, 0.6-0.7, 0.7-0.8, and 0.8-1.1 μ). For the hypothetical bands, band I covers the first two Landsat bands and band II covers the second two Landsat bands. Band III does not correspond to any Landsat band, being in the longer reflected IR range. Band IV is equivalent (i.e., thermal IR) to a future Landsat band.

5.3.12 Color Displays

5.3.12.1 Comparison of Color Displays With Standard Printer Maps

Although there are numerous advantages in using a large computer for MSS data analysis, if the computer has only printer output for map displays, the final product is often disappointing even to the point of becoming a disadvantage. Printer maps are composed of print characters designating map category classifications, or of overprinted characters to achieve pseudo-grey levels. For small areas composed of 100 or so lines and elements, such map displays are completely satisfactory for work copy and have the distinct advantage of being inexpensive to produce. For large areas, however, particularly when many different symbols or grey levels are used, printer maps are grossly inferior to other display media. First, they are often difficult to interpret because of the diversity of characters used and, second, the scale is limited to the neighborhood of the printer scale of the data; i.e., each pixel mapped in a 1/10" by 1/6" print position. Output for large areas is, therefore, bulky as well as difficult to interpret.

Other display media which use color and have more versatile scale control are much more useful for displaying large-area classification results, particularly if there are a large number of categories. Such display media, however, usually have the disadvantages of greater expense

and time for production compared to the generation of printer maps. For these reasons, such media are inappropriate for use in all but the later stages of MSS data analysis. For preliminary maps and during most of the signature development stages, printer maps are strongly preferred. Usually only small areas need to be displayed to evaluate progress and, for such small areas, interpretations are not difficult. During the later stages of signature extraction and classification evaluation, other display media assume greater value. Large areas are involved in evaluating signature extendability and overall classification success.

For final display products, particularly for large areas, media other than printer output are preferable in most cases even though each has certain disadvantages. For a final map in the scale vicinity of 1:24,000, S192 and Landsat data can adequately be done by printer output if the number of map categories is not large. Data from these sources are in this scale range. Use of colored ribbons to produce multicolored printer maps frequently improves the quality, but production time and reproduction present problems.

Final products in the scale range of 1:50,000 to 1:1,000,000 based on S192 or Landsat data are most satisfactory if generated by other than a printer. Usually, a large number of signatures and map categories are involved. In these stages, it is strongly desirable to see the "big picture" in order to make the refinements for final classification and map processing.

On this Skylab project, in addition to the standard printer, four color display means for map production were used in the later stages of the S192 analysis and for final product generation. Their characteristics are compared in the following section. In section 5.3.12.3, specific display products are shown and discussed in terms of their use in the analysis.

5.3.12.2 Comparison of Color Display Devices

Four color display devices were used to their maximum existing capabilities frequently enough in this and other projects so that they are well understood and familiar to project investigators. It is certain, however, that improvements in performance and extensions of capabilities will take place for the devices. Therefore, the evaluation and comparison of the devices apply only to their present (November 1975) state of development. The comparison is also based on their specific use by ORSER personnel and some comparative statements will not necessarily apply to other users. The four devices are described briefly in the following:

The IBM 1401 computing system with an IBM 1403, 600-line-per-minute printer was used with a special program (refer to ORSER/SSEL Technical Report 1-76) and four color ribbons. Color maps were generated by passing the printer paper four times through the printer, once for each color ribbon. Up to six tones were achieved with each color by overprinting with different print-character combinations, thus, yielding a capability to print out up to 25 different categories (including one represented by a blank). The system is located at The Pennsylvania State University Computation Center.

The General Electric Image 100 system, located at Beltsville, Maryland, was used for color display by post-processing data after analysis into a format acceptable by the machine. The analysis capability of the Image 100 was not used; the machine was used only for color display. It was used by ORSER personnel under the same policy and operating conditions which apply to other Image 100 users.

The Dicomed film recorder system for color photograph generation from digital data was used by post-processing data in the same way as for the Image 100. The data tapes were then mailed for processing at its location at NASA/GSFC in Greenbelt, Maryland. Photographs were returned by mail.

The Ramtek system which has a color cathode ray tube display resides at ORSER. It has been interfaced with an Alpha LSI mini-computer, a Tektronix 4010 graphics computer terminal, and a Vadic 1200 baud modem which can support communication to ORSER programs operating at the main computer at The Pennsylvania State University Computation Center.

Comparative characteristics are presented in Table 5-17. Underlining has been used to indicate the advantages of each machine. In some cases, different characteristics, such as the coverage area appropriate to each display, are advantageous for all devices when the requirements of display match the characteristic.

5.3.12.3 Color Display Products and Their Use

An example of a color printout using the IBM 1401 is presented in Figure 5-14. The map was actually produced using canonically transformed data, but it shows the usefulness and ability of such a map in enhancing patterns and showing the spatial relationships of the categories.

The categories mapped were water, forest, open vegetation, low grass, central urban, residential urban, strip mine, and a combined category of factories and bare soil. The latter category represents a sharing of mapping symbols because of the maximum number (13) of signatures which can be displayed as discussed below. These two categories were chosen for sharing since it was felt that any confusion between them could be resolved on the basis of their contextual location within the scene.

The categories shown in this map were produced after canonically transforming the data onto three axes. The transformed data was then classified using the standard ORSER minimum distance classifier.

Table 5-17: Characteristics of Color Display Devices as Used by ORSER

Characteristic	Display Device Characteristics[a]			
	1401	Image 100	Dicomed	Ramtek
Access	local	650 km trip[b]	mail	local
Control	ORSER	G.E.	NASA/GSFC	ORSER
Cost	low	high[c]	unknown	low
Turn-around time	1-12 hrs.	indefinite[d]	1-2 wks.	1-2 hrs
Operator support required	no	yes	yes	no
User manual available	yes	no	yes	yes
Product medium	printer paper	35 mm slide[e]	230 mm color print	35 mm slide[e]
Quality	low[f]	moderate[g]	high	high
Coverage area	small	med. to large	med. to large	small to medium
Scale of display[h]	1:24,000	1:250,000	1:250,000	1:50,000
Scale of product[h]	1:24,000	(i)	1:250,000	(i)
Input medium	tape	tape	tape	phone line[j]
Preview capability	no	yes	no	yes
Interactive display	no	yes	no	yes
No. of selectable colors	4	8	256^3	16^3
No. of simultaneously Displayable colors	4	8	256^3	16

[a]Underlined characteristics signify device advantages.

[b]On-site visit required.

[c]Processing cost high plus travel expenses for on-site visit.

[d]Time must be scheduled for on-site visit.

[e]Any camera photographic recording possible; 35 mm slide common.

[f]Overprinted printer characters do not yield solid colors and present blocky appearance.

[g]Available colors do not record well in photographs.

[h]General representative magnitude of scale.

[i]Scale dependent on photographic means

[j]Direct phone line communication with main computer.

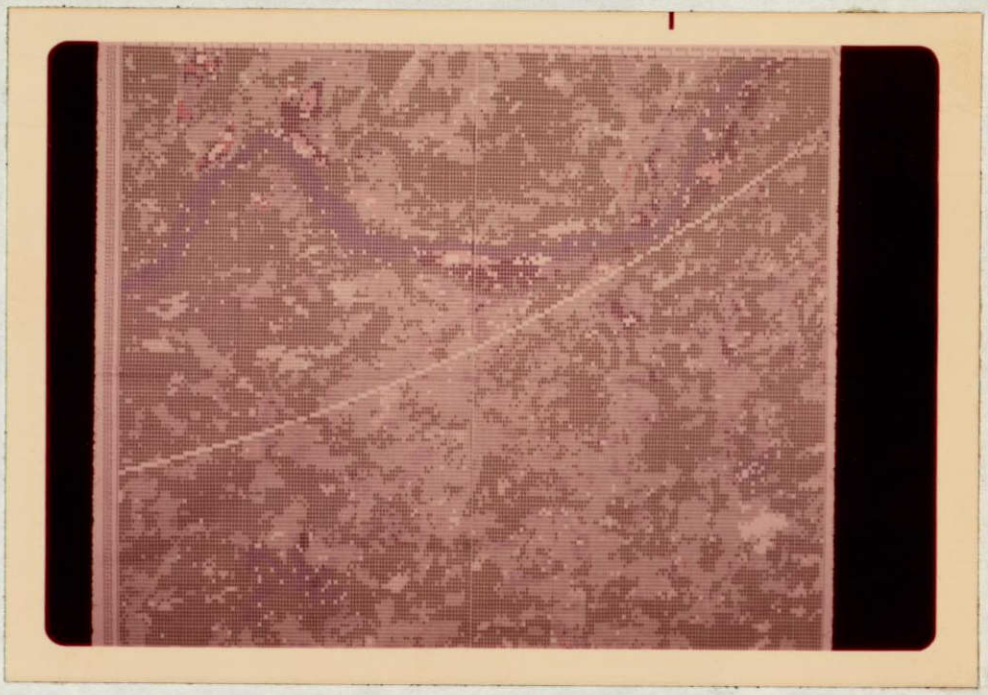

Figure 5-14: Printer output color-coded and overprinted (Classified S192 data from SL3, orbit 14, tape 933847 of 5 August 1975)

Dark Blue	(▓) -	Water
Dark Green	(▓) -	Forested
Medium Green	(X) -	Open vegetation
Light Green	(·) -	Low grass
Dark Black	(▓) -	Central urban
Medium Black	(X) -	Residential urban
Dark Red	(▓) -	Strip mine
Medium Red	(X) -	Factories and bare soil

The map is not of the final classification results but shows the status of classification at the stage where most signatures had been obtained. A shortcoming of this display medium is that it is limited to four colors and only six tone levels in each color. It is difficult to distinguish more than three tone levels in each color so only 13 (3 tones in each of 4 colors plus no color) map categories are displayed at one time. If there are over 12 signatures (plus a category for "other"), some must share the same mapping category. No problem exists if there is no question about which signatures belong in each map category. For example, referring to the above map categories, does a specific signature belong to the open vegetation or low grass category? This problem did exist for the S192 data analysis and was caused by having over 20 signatures and inadequate ground truth for classification verification. The problem of proper assignment of signatures to map categories could not be resolved by this display medium. In spite of this limitation, some major classification problems were identified leading then to their resolution in later steps.

A particularly useful product was generated by the Dicomed film recorder. Canonically transformed data for three axes (y-variables) were used in the display. In these three axes the majority of the discriminatory information was recovered from the 16 channels of S192 data which were used. The film recorder functions in essentially the same way that Landsat image-generating equipment functions. The three y-variables can be thought of as corresponding to the three Landsat MSS data channels which are used to produce color composite imagery. Each variable, or axis, is assigned one of the three film colors. In this case, red was assigned to y_1, green to y_2, and blue to y_3. Since the range of the y-variables did not correspond to the range of the film recorder, the y-variables had to be translated and scaled. This was done, as well as formatting the output for the film recorder, by the SUBTRAN program (ORSER Technical Report 1-76). The translation and scaling was done in the following way:

For a y-variable, let a and b be the lower and upper limits of the y-variable. For each data value, y, the properly translated and scaled value, z, was computed by $z = [(y - a)/(b - a)]\ 256$. The range of z values is thus 0-255, and this meets the requirements of the film recorder.

Reproductions of the color print generated by the film recorder are shown in Figures 5-15 and 5-16. Table 5-18 gives the category types, signature numbers, reference point numbers, and the color of the targets. The overlay in Figure 5-15 outlines various target areas. Figure 5-16 is of the same area, but without the overlay. The color tones are useful in the interpretation of the degree of importance of each axis in discriminating each category. For example, urban areas have a high response in axis three (blue), but little response in the first two axes (red and green) as shown in the urbanized area along the Allegheny River. This product was the first output produced using transformed data and proved to be quite helpful in the evaluation of confusion between various target types. It also aided in determining the ability of each axis to discriminate among different targets.

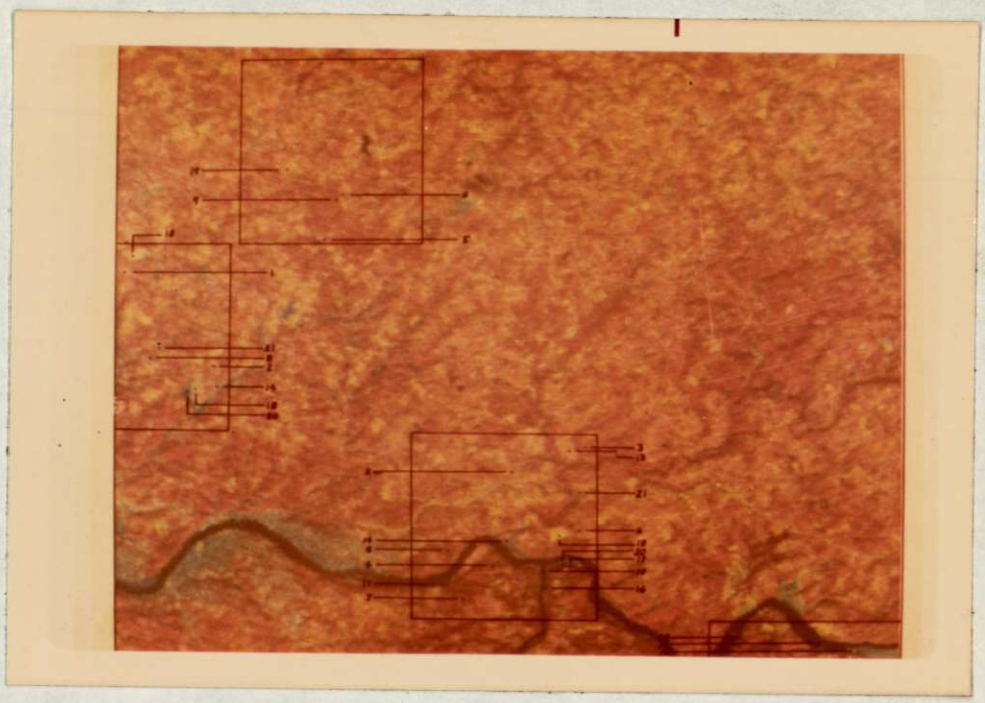

Figure 5-15: Dicomed film recorder display of three canonically transformed axes of S192 data. Outlined areas are, from top to bottom: Test area 2, part of test area 3, test area 4, and part of test area 5. See Table 5-18 for color key.

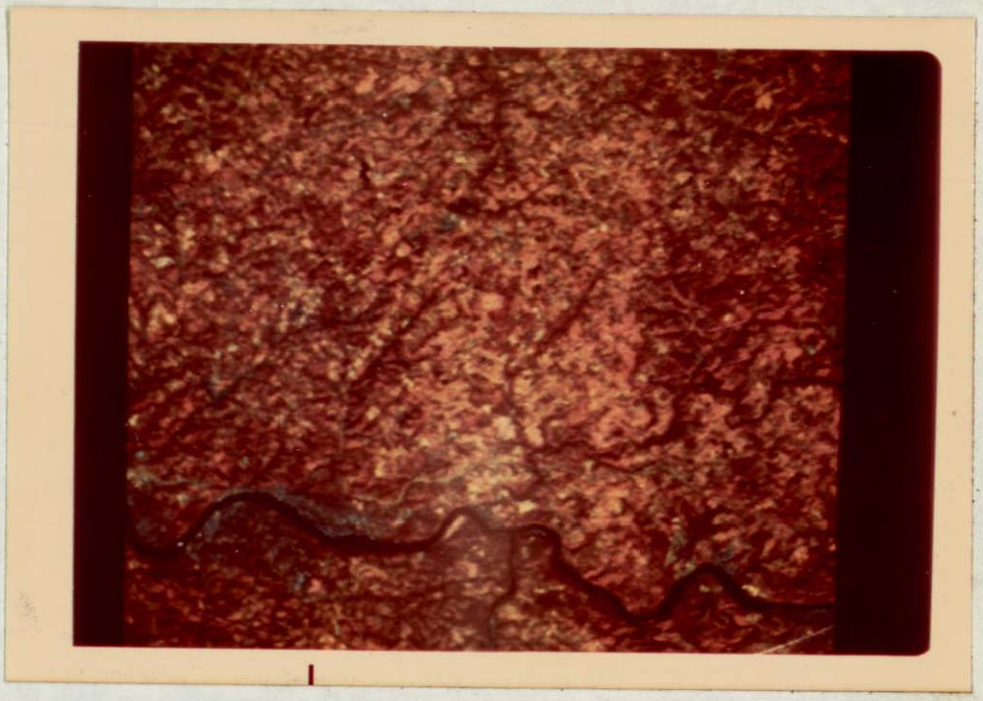

Figure 5-16: Dicomed film recorder display of three canonically transformed axes of S192 data.

Table 5-18: Colors and Location Key for Dicomed Image and Overlay[a]

Signature Number	Point Number	Target Type	Color
1	1	Non-forest vegetation	Orange-brown
2	2	Non-forest vegetation	Green-brown
3	3	Forest	Red-orange
4	4	Forest	Drab brown
5	5	Forest	Violet-pink
6	6	Non-forest vegetation	Yellow-brown
7	7	Forest	Violet
8	8	Forest	Purple-violet
9	9	Forest	Violet-red
10	10	Water	Dark blue-green
11	11	Water	Dark blue-green
12	12	Forest	Pink
13	13	Non-forest vegetation	Orange
14	14	Urban	Blue-green
15	-	(deleted)	
16	15	Urban	Green
17	16	Forest	Purple-violet
18	17	Forest	Olive green
19	18	Non-forest vegetation	Yellow-green
20	19	Non-forest vegetation	Pink-orange
21	20	Urban	Light blue
22	21	Non-forest vegetation	Drab green

[a]Refer to Figures 5-15 and 5-16.

These film recorder outputs are not classification maps. They are essentially color-coded displays of density slices of each of the three canonically transformed axes. Classification maps can easily be generated, however, by performing the classification based on the three axes as for printer maps followed by conversion of map symbols to color codes. For example, "other" may be coded to black by outputting 0, 0, 0 for the three channels. This translates to zero intensities for each of the red, green, and blue film colors for each such pixel. A maximum red can be obtained by the three channel values of 255, 0, 0; maximum green by 0, 255, 0; and maximum blue by 0, 0. 255.

The film recorder would have been used more, except for the week or more of turn-around time. The tape had to be generated, mailed to GSFC, processed, and the print mailed to ORSER. The advantages of this product, however, are outstanding; namely, a large area can be displayed and a permanent copy, ready for interpretation, is generated. In this last regard, a 35 mm slide, obtained by photographing a color CRT, must be converted to a 230 mm color print to be equivalent to the film recorder product.

Near the end of the classification and mapping phase of the project, an interactive color display system was implemented at ORSER. The system combines a color CRT and supporting hardware components marketed by the Ramtek Corporation, with a mini-computer, an interactive computer terminal, and a 1200 baud modem. This Ramtek system allows a dial-up connection with the main computer at The Pennsylvania State University Computation Center, through which ORSER program outputs may be transmitted for display on the CRT. The display may consist of 240 elements by 256 scan lines. Sixteen colors, from a possible 16^3 colors, may be displayed at one time and, by the interactive feature, color combinations may be manipulated. Through programs in the main computer and in the mini-computer, mapping symbols of map output from ORSER programs can be converted to any one of the 16 display colors.

At the time the machine became available for use, 30 signatures had been obtained. It was recognized that some confusion existed among signatures for strip mines and urban targets. Also, some confusion existed among various vegetation targets. At this stage of preparation for final map production, it was important to make proper assignments of signatures to map categories. In this respect, the Ramtek system was invaluable. Single and multiple signature classifications were displayed. On the basis of the spatial patterns, signatures could be assigned to the appropriate map categories.

Figures 5-17 and 5-18 were taken of the Ramtek display with a 35 mm S.L.R. camera mounted on a tripod. The Ramtek display presented in Figure 5-17 is that of a classification map. This is the same area used to produce the colored map shown in Figure 5-14. Here, the attempt was made to group all the signatures into 15 groups to achieve the best overall display. Table 5-19 is a listing of the signature groupings and the assigned color intensities. The ability to alter colors while observing the display and the large number of colors available make this a very useful device to compare spatial relationships among different

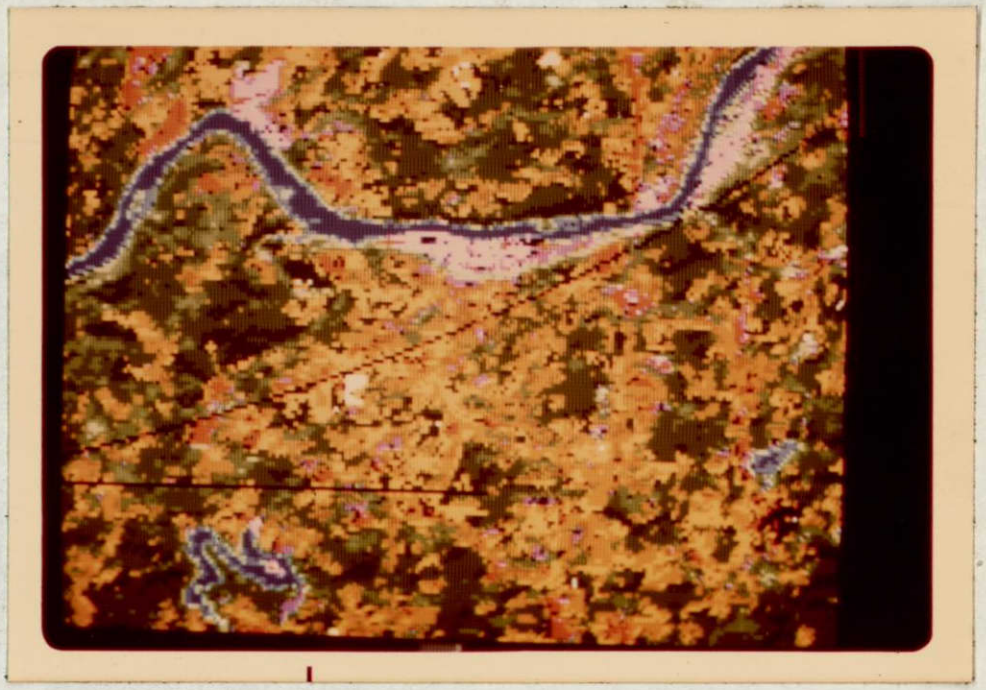

Figure 5-17: RAMTEK display of final classification map for same area as in Figure 5-14. See Table 5-19 for color key.

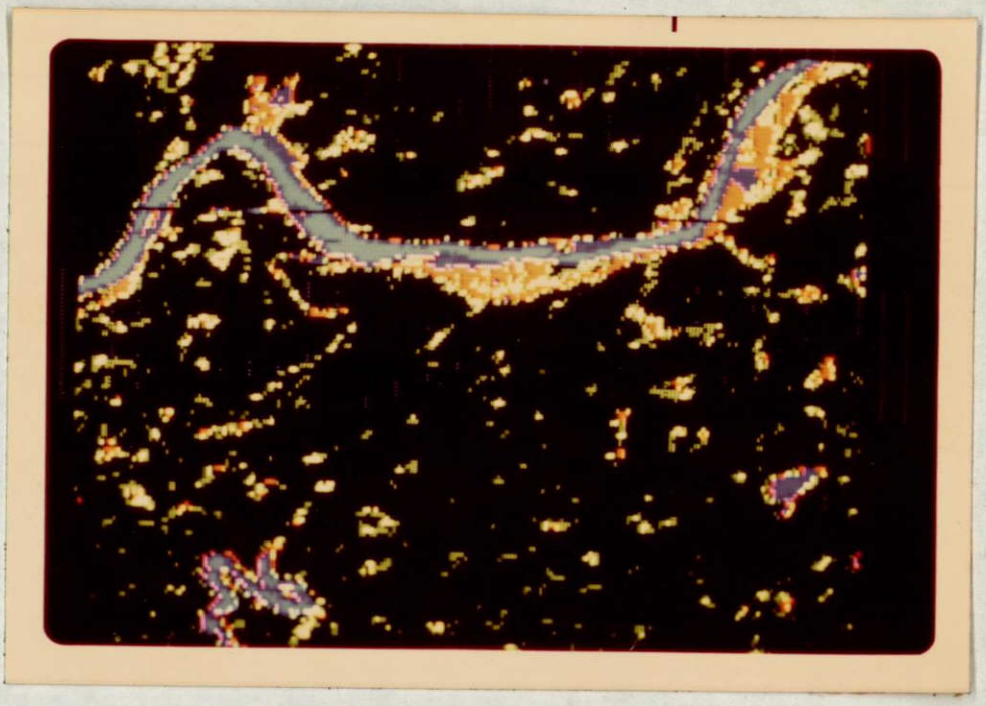

Figure 5-18: RAMTEK display of six density slices of the first canonically transformed axis for the same area as in Figures 5-14 and 5-17.

Table 5-19: Signature Grouping and Color Assignments for Display of the Final Classification Map on the Ramtek Device[a]

Ramtek Group	Classification	Gun Intensities Red	Green	Blue	Color	Signatures
1	Strip mine	15	0	0	Red	23, 24, 25, 31
2	Central urban	15	0	15	Pink	16, 28, 21
3	Residential urban	8	0	8	Purple	14
4	Water	0	0	15	Bright blue	10
5	Water	0	0	6	Dark blue	11
6	Non-forest vegetation	15	8	0	Bright orange	1,
7	Non-forest vegetation	12	5	0	Medium orange	2, 6
8	Forest	0	9	0	Medium 1 green	18, 25
9	Forest	0	15	0	Bright green	17, 26
10	Forest	0	7	0	Medium 2 green	4, 8
11	Forest	0	4	0	Medium 3 green	7, 5, 9
12	Forest	0	2	0	Dark green	3, 12
13	Open grassy	12	12	12	Gray	13
14	Non-forest vegetation	8	4	0	Dark orange	20
15	Clouds	0	0	0	Black	29, 30

[a]Refer to Figure 5-17.

signatures. This facility aids in the interpretation and final identification of the signatures. For instance, upon examination of the spatial relationship of signature number 24, it was decided that this was more representative of strip mines than of urban areas as had been previously decided. Therefore, the classification was changed to strip mine. Another signature (No. 12) was changed from non-forested to forested, a third (No. 21) was changed from urban to non-forested, and a fourth (No. 19) was dropped altogether, all by observing their spatial relationships.

Since colors can be changed during display on the Ramtek, it is possible to display only one of the 15 categories on the screen at a time, and then to add other categories later. This enables the user to view only selected categories at his discretion.

Figure 5-18 is a Ramtek display of a density slicing of axis one of canonically transformed data. That is, the information presented to the Ramtek comprised 15 density slices. The 16th color, black, was used for background. Therefore, each pixel was classified into one of the 15 slices according to the magnitude of its value in axis one. The display shows the first six of these slices. The other nine slices were assigned the background color to simplify the interpretation. The following are the classification limits for the six slices and the associated colors:

Slice	Response Magnitude Limits	Color
1	0.00-29.43	Bright blue
2	29.44-52.51	Medium blue
3	52.52-90.87	Dark blue
4	90.88-122.87	Red
5	122.88-133.11	Bright green
6	133.12-144.63	Medium green

It is evident in Figure 5-18 that all responses up through 90.87 are water. The higher responses of water could logically be shallow water or water and vegetation mixed as interpreted from the spatial patterns. The dark line that cuts across the scene is a bad line of data. Most of the urban area is fairly well separated and mapped in slices 4, 5, and 6, along with some vegetation. One interesting feature of this display is found between the Allegheny River and Crooked Creek Reservoir (in lower left). There is a stream running from the reservoir to the river. Attempts to find a signature to map the vegetation associated with the stream failed. Here, however, the location of the stream is visible as a composite of several of the density slices. The approximate

shape of the stream is represented in Figure 5-19:

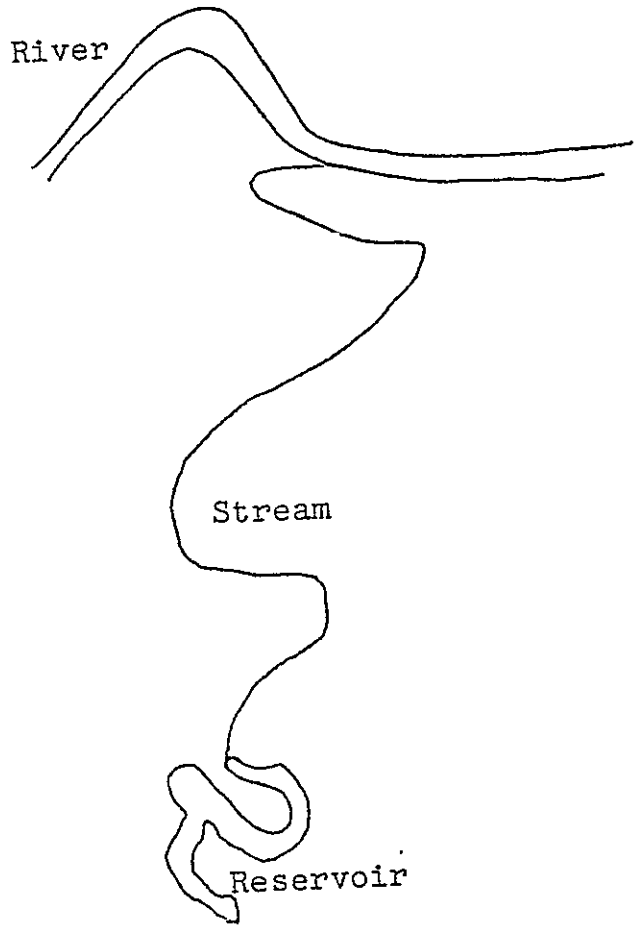

Figure 5-19: Sketch of stream between Crooked Creek Reservoir and the Allegheny River

This type of examination helps to reveal targets which do not have well-defined signatures and which, consequently, may be confused with other categories. Using canonically transformed data also gives assistance in determining the targets which can be discriminated by each axis.

Figure 5-20 represents a display which was originally generated on the Ramtek, but for the purpose of this report has been reproduced as a printer grey-scale map. The map shows only strip mines, urban areas, and water. The water category was mapped as a reference.

This display demonstrates the ability of the user to examine selected categories and ignore all others. This greatly reduces the visual confusion resulting when many categories are simultaneously mapped. In addition, small areas of classified data that may otherwise be overlooked now stand out.

Figure 5-20: Grey-scale printer output. The grey-scale assignment is:

Grey-scale	Category	Signatures
Dark	Strip mines	23, 24, 25, 31
Medium	Urban	14, 16, 21, 28
Light	Water	10, 11

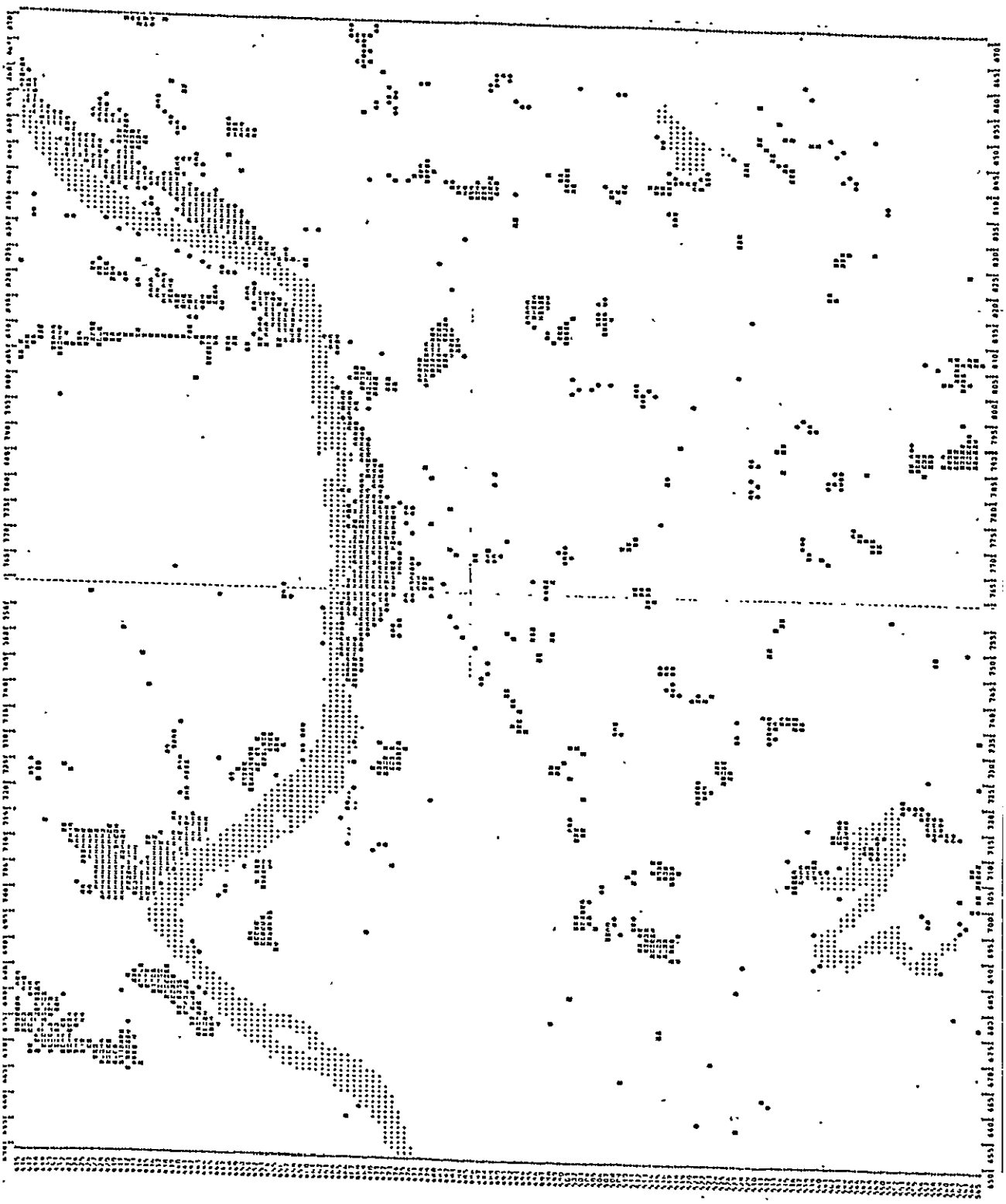

Although the Image 100 was not used for processing Skylab data, ORSER's experience on this system with Landsat data suggests certain comparative comments. The Image 100 is designed for analysis and, although the machine has versatile interactive capability, its high hourly cost mitigates against using it simply for display purposes. A serious shortcoming of the machine is that it has only eight colors for display and these cannot be modified. It was not easy with the fixed colors to obtain satisfactory photographic renditions.

5.3.12.4 Summary

In the early and intermediate stages of analysis of MSS data, standard printer maps are the preferred display means because of the minimum expense and rapid availability to the analyst. They are of limited utility for display of large areas with numerous map categories and as final products. In the later stages of analysis where large areas must be displayed and many signatures are involved, color display devices are preferred. For such use, the desirable features are ready access, a wide variety of colors to choose from, and interactive capability. The Ramtek system is ideally suited to these needs. A film recorder, if locally available, could meet the needs, except for its lack of interactive capability. For final display product generation, the film recorder is the preferred means. A large area can be displayed, a wide range of colors is available, and, of prime importance, a useful permanent copy (230 mm color print) is produced. The color CRT display devices, such as the Ramtek system and the Image 100, have the decided disadvantage that permanent copies can only be obtained by photographing the CRT and, for the usual 35 mm slide format, the final product is not directly useful. For final product generation, ready access is not so important as in the analysis stages.

5.4 S192 DIGITAL DATA EVALUATION (Borden)

The evaluation of S192 digital data will be presented in five parts:

1) tape management,
2) computer processing,
3) documentation,
4) inherent data quality, and
5) comparison with Landsat data.

Prior to specific evaluations, it must be stated that after initial problems with the tapes and the data within the tapes had been overcome, working with the data became desirably routine and productive. The data were of suitable quality, even without calibration, for use in thematic mapping at the resolution anticipated according to specifications of the S192 system.

5.4.1 Tape Management

The management of the tapes by JSC was found to be poor in that several deficiencies, noted in the following, caused serious interference with the planned conduct of the experiment. First, the preliminary test tape was of limited value since it contained no real or simulated data. Although it could be processed, it was a waste simply to work with a tape in an unconfirmed format containing no useful data. Second, a tape with real data was copied and sent from JPL for testing purposes. There was little value in that exercise because the data were in conical format and from a desert scene which contained no targets similar to the test site. It took considerable effort to uncover this information. It would have been much more productive if the test tape had been initially generated at JSC in a timely manner with data typical of the scenes in the test site. Third, the data for the test site arrived long after due and forced work plan revisions which were detrimental to a well-organized comprehensive effort. (A request for data evaluation was received prior to the arrival of the data, with a rapid response required in order to schedule reprocessing since beyond a given date no further S192 data processing was to take place.)

5.4.2 Computer Processing

The S192 data did not pose any major problems, although a number of minor problems were encountered. The header record did not contain any information regarding the number of records or scan lines in the file. To overcome this deficiency, some reprogramming and computer processing were required. It also required an additional, and otherwise unnecessary, pass of the data to determine the number of scan lines and produce a proper table of contents in the ORSER format. The table of contents is used in

ORSER programs as a check to avoid processing tape files which do not contain scan lines and elements requested by a user. Except in a few cases, such as with S192 original data, the feature avoids wasted computer time and expense. It would have been an improvement to have the number of scan lines or records in the header record or in the supporting documentation.

The organization of bands was perhaps logical with regard to sensor considerations but not for analysis. For analysis, the logical organization is by wavelength in a non-decreasing order. Although not a major problem, it led to a great deal of confusion when compounded with the following problem.

One band, namely 10, was misspecified in the header as 12.0 to 13.0 μ, instead of 1.20 to 1.30 μ. Subsequent confusion and misinterpretation resulted until the problem was recognized. This kind of error increases costs and wastes time.

5.4.3 Documentation

Documentary support was poor because a stream of drafts, revisions, etc., continuously arrived prior to and during data processing. It was impossible to keep users up-to-date and this kind of documentation and the management of it caused substantial doubt in the users' mind about the validity of any of the written material. Much effort could have been saved had the documentation been adequate and timely.

In summary, the inadequacies of documentation and tape management caused delays and inefficient processing on the part of the users. The S192 data used in the project were collected in August 1973, but were not furnished to ORSER until February 1975 and, even at that late date, documentation had not yet been developed to a reasonable final form.

5.4.4 Inherent Data Quality

Once the initial problems had been overcome in data processing, the data were found to be inherently quite satisfactory, even without calibration. These conclusions were reached as the result of successful classification and mapping of the S192 data. In this context, the relatively small number of erratically misclassified pixels, the low total variance in categories defined by a supervised method of analysis, and the absence of extreme outliers in the data indicated that the noise level relative to classification information was completely acceptable for thematic mapping purposes.

5.4.5 Comparison with Landsat Data

Only a general comparison of the quality of S192 and Landsat

data will be made. A comparison of the data utility based on thematic mapping of the same area with each data source is presented elsewhere in this report.

First, S192 data have greater resolution than Landsat data, but at the cost of a larger volume of data and the attendant increases in cost of processing. It cannot be conclusively stated here that the greater resolution is economically justified considering only analysis costs because:

1) the same area was not analyzed using both sources of data, and

2) start-up costs and first-time-through analysis costs for the S192 would yield bias in an unjustifiable way in favor of Landsat..

The greater number of channels in S192 data does not cause any greater analytical difficulty since the analysis methods were the same and not dependent upon the number of channels. Computer processing and data transfer from tapes are buffered so that costs are more in relation to data volume rather than to complexity of computation. The greater number of channels, along with the increased resolution of S192 data, cause processing cost increases resulting from the greater data volume per unit land area compared to Landsat.

From a statistical point of view, channels in the S192 data, not considering duplicate bands, are generally more strongly correlated than in Landsat data. This is to say, there is more redundancy in the S192 data. This is expected, since the band widths are narrower in the S192, while in Landsat they were designed for minimum redundancy for the general mix of land targets. One of the possible consequences is that, because of strong inter-channel correlation in the S192, classifiers and analyses which require the inverse of covariance matrices will, on mathematical grounds, be non-operational or of questionable utility if all channels are used simultaneously. Methods of this type were not used in this study.

In principal components or canonical analysis transformations, even with the greater number of channels, the S192 data can generally be cast onto two or three axes without serious loss of information. The same number of axes are usually required for Landsat data even with only four channels. This means that both kinds of data may be transformed for color display without losing a consequential amount of information.

A very strong point in favor of S192 data is that it is not seriously striped, as is frequently the case with Landsat data. Sixth-line and radiometric striping in Landsat data pose a serious challenge to its usefulness when using computer analysis and seem to promise large computing costs for its correction. Such is not true for the S192 data, in our experience.

In conclusion, it can be said with emphasis that the inherent quality of the S192 data is very satisfactory. But, also with emphasis, poor data management and planning caused substantial problems and delays in the initial stages of data processing.

5.5 DIGITAL MSS PROCESSING SUMMARY AND CONCLUSIONS

5.5.1 Summary

A limited amount of digital MSS data was provided to ORSER for processing and evaluation. This was a result of both the limited capacity of NASA to provide processing of the original MSS data due to sheer volume and also a result of the lack of MSS coverage on the Skylab passes of principal geographical interest to ORSER. As a result, ORSER did not have aircraft underflight photography in most of the areas covered by the S192 scanner. This was a handicap to digital processing, as ORSER has found such photography to be extremely helpful as a form of ground truth. Nevertheless, available digital data was processed and a summary of the results is included here.

Line-straightened but uncalibrated data were used in these evaluations. It was decided that data calibration would be attempted only if the uncalibrated data were found to be otherwise not useful. Although radiometric striping was detectable in images of some channels, it was not seen at any stage of the Skylab digital analysis. Calibration is seldom an easy task and would not necessarily be justified if the sensor systems were quite stable over a scene. Calibration to achieve linearization and particular units of measure are generally of little consequence in classification and mapping. In view of the above factors, calibration was deemed unnecessary considering the time and expense the development of calibration programs would have required.

The S192 data were found to be inherently quite satisfactory, even without calibration. The relatively small number of erratically misclassified pixels, the low total variance in categories defined by a supervised method of analysis, and the absence of extreme outliers in the data indicated that the noise level relative to classification information was completely acceptable for thematic mapping purposes.

Since ORSER has had considerable experience in processing Landsat MSS data digitally, it is natural to attempt to compare Skylab and Landsat MSS data from a processing standpoint. Although most of the Skylab MSS data processed was over areas and at times of the year for which ORSER did not have corresponding Landsat data, one area was covered by both sensing systems at about the same time of the year in south-central Pennsylvania. Signatures for four vegetative targets were obtained by using the unsupervised cluster analysis program, DCLUS, to classify data from Skylab and Landsat channels from approximately the same wavelength bands. Seven Skylab channels were used to span the spectral interval covered by the four Landsat channels. After correction for scaling in the two systems, the Skylab and Landsat spectral signatures for the four targets agreed extremely well, although the S192 near-infrared channel responses were slightly higher than the corresponding responses on Landsat.

A major objective of the investigation of the S192 digital data was the evaluation of the various spectral bands and channels for classification and thematic mapping. In order to meet the objective, it was necessary to produce satisfactory classifications and thematic maps according to the resolution of the S192.

Prior to the classification and mapping phase, an initial screening evaluation of the channel imagery was made in order to delete obviously poor channels. In addition to screening the imagery, intensity (grey level) maps were generated digitally for each of the 22 channels and statistical correlations were performed. As a result, channels 7, 11, 15, 16, 18, and 22 were dropped and the number of channels to be processed and evaluated was reduced to 16.

Initial classification and mapping by supervised classification based on the 16 selected channels resulted in the definition of eight categories. Fourteen more were added by unsupervised classification and nine more were identified after processing by canonical analysis. Two categories were eliminated due to insufficient numbers of pixels in those classes, and thus a total of 29 categories were mapped. As with Landsat data collected from Pennsylvania, a region with a large variety of land use targets and mixed spectral responses, the number of signatures required to map an area is fairly large. Thirty or more signatures has been the rule, rather than the exception, with Landsat data. The same situation occurred with the S192 data. Classification of the S192 was successful for the intended purpose; namely, for support in channel evaluation. The final classification maps were correct to the level of detail afforded by the limited ground truth.

Following mapping and classification, three methods were used to evaluate the spectral channels. The objectives were the evaluation of channels for redundancy, evaluation of each channel for its contribution to the total information content of a scene, and evaluation of each channel for its contribution to the discriminatory information content of a scene composed of a number of categories.

Evaluation of channels for redundancy was based on simple correlations of the digital data, but this method is limited to the identification of highly redundant channels. The criteria which were employed to identify strongly redundant pairs of channels were a high correlation between the two channels, and a very similar pattern of correlations of each with the other channels. The limitation of this method of channel evalution is that it is useful only in identifying pairs of channels which are redundant. The method does not help in determining the comparative value of channels for recognition of land features.

The method of channel evaluation based on the contribution of each channel to the total information content of a scene was a principal components analysis of data for a scene or a representative sample thereof. The main and secondary dimensions (axes) existing in the data were found by linearly transforming the original dimensions (channels) on the basis of principal components analysis. This was then followed by the determination of the correlation of each channel with each of the axes.

Channels which were strongly correlated with the important axes were, therefore, determined to be important in contributing to the total information content of the data. In this method, however, channel redundancy was not taken into account.

To evaluate channels regarding their contribution to discriminatory information content, canonical analysis was used. After recognizing the predominant categories in a scene, canonical analysis also performs a linear transform and identifies the discriminatory dimensions (axes) among categories. Correlations of channels with the important discriminatory axes then can be used to identify the importance of each channel for discrimination among the various categories. As with the prior method, channel redundancy is not considered. Furthermore, the success of the method is contingent upon satisfactorily identifying and defining the predominant categories in the scene.

The total among-category variance for a number of categories defines an upper bound on the amount of discriminatory information available in a data set and is called the discriminatory variance. Canonical analysis finds the fewest linear transformations which maximize the recovery of the discriminatory variance. Using the 22 categories which map all but an inconsequentially small area of the scene sensed by the S192, the correlation aspects of canonical analysis then give a reliable basis to evaluate channels with respect to their contribution to the discriminatory power of the data for the scene. This point is important, because if only a few categories were used and they comprised only a small part of the scene, it could be questioned whether the canonical analysis results would be applicable to the full set of categories or to the full scene.

Each of the methods has advantages and disadvantages, so that no one method could be singled out for exclusive use with complete success as the anticipated result. The various methods, therefore, were used in a complementary fashion and the combined interpretation of results was used as the basis for final channel evaluations.

The selection of these methods and the results of their use have a strong and intended orientation toward land use classification and mapping. The methods and resultant channel evaluations must be considered in this context. These methods do not lend themselves to direct use for identifying channels which measure subtle phenomena dispersed over large areas, such as certain geologic or phenologic expressions. In addition, the methods as used were not oriented toward discovering channels which would precisely identify any specific category against a background of other undifferentiated categories.

In the evaluation of the contribution of each channel to the total information content of the data, principal components analysis showed that of the total variance, 90% was recovered in the first three axes and 10% was distributed over the remaining 13 axes. A loss of 10% of the total variance would not be tolerable if further analyses for classification and mapping based on three axes were to be done. However, the first three axes were considered adequate for channel evaluation for the following reasons: 1) the percentage of total variance for each axis after the third

axis was quite small and decreased slowly with each additional axis; and 2) beyond the third axis, the correlations of channels with axes were usually small and, therefore, not particularly useful for interpretation.

For the first axis, which accounted for 71.5% of the total variance, all channels covering the spectrum from 0.68 through 1.75 μ were important. These channels cover a small portion of the long wavelengths of the visible spectrum and extend just beyond the photographic IR wavelengths. The correlations for these channels with the first axis were all greater than 0.80. Channels which were of little importance in the first axis were in the visible spectrum up to the red wavelength (0.52-0.67 μ), and the thermal IR band (10.20-12.50 μ). Their correlations with the first axis were all 0.30 or less. The non-photographic IR band, from 2.10-2.35 μ, was intermediate but not interpreted as important.

The second axis accounted for 14.4% of the total variance or about 20% of the amount recovered in the first axis. Those channels which were not important in the first axis were important in the second axis, with the exception of the thermal IR channel. The thermal IR was of questionable importance in axis two and of inconsequential importance in axis one. The important channels for axis two covered the visible spectrum, from 0.52-0.67 μ, and the IR wavelengths, from 2.10-2.35 μ. The correlations were all greater than 0.70 in absolute value. The correlation of -0.48 for the 1.55-1.75 μ band was considered marginal, relative to the other large correlations. In axis three, which recovered only 3.8% of the total variance, correlations were all much lower than for the first two axes. Only three channels were considered to be of relative importance; namely, those for the 0.78-0.88, 0.98-1.03 and 1.20-1.30 μ bands. These are a repetitious subset of the important channels in axis one, although the transformation vector, of course, is not the same.

The canonical analysis results showed that, for the first three axes only, nearly 99% of the discriminatory variance was recovered with almost 84% recovered in the first axis alone. The third axis is of little consequence, except for the existence of the strong correlation of the thermal IR channel with the axis.

In axis one, the bands from the long visible through short IR wavelengths (0.68-1.75 μ) are important. The bands from 0.52-0.67 μ, as well as the thermal IR, are definitely not important, since their correlations are all less than 0.08. The 2.10-2.35 μ band is of dubious importance, with a correlation for these two channels of 0.20.

In the second axis, the bands covering 1.55-2.35 μ are important, with correlations of 0.60 or greater. The bands covering the visible spectrum from 0.52-0.67 are important, but less so than for the 1.55-2.35 μ bands. It is difficult to make a firm statement about the bands covering 0.68-1.19 μ and 10.20-12.50 μ, but these were judged to be relatively unimportant. Judgments concerning these correlations are difficult because no sharp distinctions are evident.

In axis three only the thermal IR is of obvious importance, with a correlation of 0.85 with the axis, while the next most important, the

1.55-1.75 μ channel, is of dubious value with a -0.29 correlation value. All others are definitely unimportant in this axis.

In order to determine if any difference existed between pairs of channels in the same band, correlations between all pairs of channels were computed for selected bands using approximately 11,000 observations. For bands 6, 7, and 11, with correlations of 0.96 or 0.97, the pairs are almost perfect duplicates. For bands 3, 4, 5, and 12, correlations range from 0.85 to 0.91 and, since they are so strongly correlated, they may be considered to be effective duplicates. Correlations among the pairs of the thermal IR channels, band 13, are not strong enough to be considered as duplicates. It should be remembered that uncalibrated data were used and it is possible that calibration of these channels could improve the correlation.

In addition to the comparison of correlations, the within category variances were used for comparison. The within category variances are measures of the variability within channels, or channel noise relative to thematic mapping of the categories. For two channels in the same band which are essentially duplicates, the channel with the smallest within category variance is preferred because it is least noisy for thematic mapping purposes. The among category variance is a measure of the spectral differences of a channel among categories. The ability to distinguish among categories in general is dependent upon the relative differences between the among and within category variances for the aggregate of channels. The ratios of among to within category variances for all channels examined were very large, indicating that the ratio of discriminatory information to noise is very large. On the other hand, the pairwise comparison of channels in the same band shows that the within category variances are all essentially the same. That is to say, for any pair of channels in the same-band, there is no practical difference in noise level for bands 3, 4, 5, 7, or 12.

With the aim of selecting the minimum number of bands which could be used effectively to support thematic mapping at the same level as the S192, correlations between all pairs of bands were computed. The correlations were averaged for bands with duplicate channels. Two groups of associations emerged. In each of these associations, the correlations between all bands in a given group are generally quite strong. For bands 1 and 2, on the other hand, the correlations with all other bands are relatively small, indicating independence not only between the two bands but also between these and all other bands. Therefore, if either band contained discriminatory information for thematic mapping, it would have to be retained. Band 13 is marginally independent. The correlations are not particularly strong with the other bands but correlations with bands 3, 4, 5, 6, 11, and 12 indicate some redundancy with these bands. Because of this, and because of the prior finding of the possible importance of a band 13 channel in the third canonical axis, band 13 should not be eliminated.

Bands 3, 4, 5, 6, 11 and 12, which form association group A, are all mutually correlated in a fairly strong way. Except for bands 6 and 11, they are only weakly correlated with bands in association group B. Bands 6 and 11 appear to be intermediate, but with a stronger association with group B than group A. Because of their mutually strong

correlations, it would seem that only one of bands 3, 4, 5, and 12 would have to be retained. The choice would be band 12, inasmuch as it had the strongest correlation, 0.60, with the second canonical axis.

Bands 6, 7, 8, 9, 10, and 11, composing association group B, are mutually strongly correlated. For the same reasons as given for group A, it is likely only one band would be needed. Of this group, band 9 would be slightly preferred because it has the highest correlation, 0.75, with the first canonical axis.

As part of the channel evaluation, ORSER used several methods of displaying products. Color displays are extremely helpful in providing spatial relationships and interpretations and can save much time in analysis. Based on the displays utilized in this project, as well as previous experience with displays, a comparison of four color display systems was made. These are: 1) line printer output in color (using different colored ribbons); 2) the GE Image 100 interactive display and classification system; 3) a Dicomed color film recorder; and 4) the Ramtek color TV monitor display system at ORSER.

5.5.2 Conclusions

Based upon the results of processing the digital MSS (S192) data from Skylab, the following conclusions are drawn:

1. Channels which were duplicates in the bandwidth of their spectral response appear to contain approximately duplicate information and discriminatory power as applied to the types of ground targets being classified by ORSER. Therefore, the choice of the best sensor in each band should be determined by other factors, such as cost, design, and reliability.

2. The most important channels in defining both total information content and discriminatory variance cover the long visible through short IR wavelengths (0.68-1.75 μ) and the long reflected IR band from 2.10-2.35 μ; and, finally, the least important band is the thermal IR band (10.20-12.50 μ).

3. The relatively low information content in the thermal IR channels is somewhat surprising, but it is believed that such channels should not be considered useless in land use classification applications. After canonical transformation, three axes in the transformed data were found to be useful for classification. The third of these axes, although it contained the least discriminatory information (smallest variance), was still significant and the thermal IR content in this axis was relatively high. One possible explanation for the overall low rating of the thermal IR channels may be that their discriminatory power is relatively low in the daytime, since the energy measured is both reflected and radiated (as opposed to night sensing of radiated energy alone). Thermal IR measurements are more sensitive to time of day, atmospheric disturbances, etc., and calibration is very critical.

4. Skylab MSS data have greater resolution than Landsat data and this makes land use mapping somewhat easier in some cases. Simultaneously, however, the system features which result in greater resolution, along with the many spectral channels of Skylab, generates a much greater data volume to be handled and processed. This results in increased costs and time for processing. Overall, the quality of Skylab MSS data is quite good.

5. As a result of the application of principal components and canonical analysis to the MSS data, it was determined that a considerable reduction in data volume can be achieved by use of such transformations followed by feature selection (dimension reduction) based on information content of the transformed axes. The resulting savings in time and cost are substantial. In addition, the transformed data is ideally suited for use with color display devices.

It should be noted that the results of this study of the S192 digital data are for the general mix of land use patterns existing in the growing season for an area representative of western Pennsylvania. It would be conjectural to extrapolate the results to other substantially different climatic areas, such as semi-arid ones, or to another very different season of the year, such as winter. Although the methodology would be expected to be as satisfactory in channel evaluation under other conditions, the specific results might very well be quite different.

5.5.3 Recommendations

Based upon the results of ORSER's analysis of the S192 digital data, the following suggestions are recommended for serious consideration:

1. Future earth resources missions should use fewer spectral bands (and channels) and provide more areal coverage. Six bands (e.g., 0.5-0.7 μ, 0.7-0.9 μ, 0.9-1.1 μ, 1.1-1.3 μ, 2.10-2.35 μ, and 10.20-12.50 μ) would appear to be adequate.

2. The techniques used for channel evaluation in this investigation (correlation, principal components, and canonical analysis) should be applied to S192 data over other geographical areas and for other types of targets.

3. There is a need for a more extensive investigation of the value of daytime thermal IR data for land use mapping using digital MSS data. Consideration should be given to calibration, types of target, time of day, etc.

4. Canonical analysis should be applied to digital S192 data and the results displayed on color display devices for evaluation by photo-interpreters.

6.0 SUMMARY, CONCLUSIONS, AND RECOMMENDATIONS

This report describes an interdisciplinary effort to analyze Skylab EREP data by the Office for Remote Sensing of Earth Resources (ORSER) at The Pennsylvania State University. The research findings are presented for two major subject areas: 1) photographic analysis for geomorphic and geologic applications, and 2) evaluation of S192 multispectral scanner digital data. The first of these two areas is split, for purposes of this report, into two parts: 1) photographic analysis, and 2) geologic studies.

6.1 SUMMARY

ORSER received data from several passes of Skylab-3 and one of Skylab-4. The Skylab-4 scenes were of limited usefulness, being largely snow and cloud covered.

6.1.1 Summary of Photographic Analysis

Before commencing application of Skylab photography in detailed geologic studies, it was decided that Skylab photography should be evaluated for its general interpretive potential, especially in terrain mapping applications. A comparison of the various photographic products was made for three test sites selected as being representative of major physiographic regions in Pennsylvania. Standard techniques used for aerial photointerpretation were applied during the evaluation. The basis for the evaluation was an analysis and comparison of the various Skylab sensor/film/filter combinations available, utilizing study guides prepared from ground truth information for each test site. Photography from the S190A and S190B sensors were compared, with the result that the S190B color positive film was selected as the best in overall quality for terrain analysis.

The sensor/film/filter analysis revealed that the following features are visible on all of the photography: 1) major drainage, such as rivers and their tributary creeks and 2) the sandstone ridges of the Appalachian Ridge and Valley Region.

The following features are visible on all photography with the exception of that from S190A stations 1 and 2 (0.7 to 0.8 and 0.8 to 0.9 μ, respectively): 1) differences in vegetation (forest versus agricultural land), 2) color/tone variations in water bodies, 3) most cultural features, such as railroad rights-of-way, large industrial buildings, and roads (some with verification from underflight aircraft photography), and 4) hills formed by the Triassic igneous intrusions. Water bodies are most clearly visible on photography from stations 1 and 2 of the S190A photography, and on the S190B photography. Limestone quarries are visible on all photography but that of stations 5 and 6 (0.6-0.7 and 0.5-0.6 μ) from the snow-free passes of Skylab-3. Slope breaks and soil differences are not clearly seen on any of the Pennsylvania scenes. Differences in relief of 150-240 m can be seen on all but stations 1, 2, and 6 photographs,

using the Old Delft stereoscope. With the Bausch & Lomb Zoom 95R stereoscope, however, relief differences down to 30 m were seen on a black and white S190B scene from New York State.

S190B photographs were then used for terrain mapping of the three test areas in Pennsylvania, using standard aerial photointerpretation techniques and the Old Delft Scanning Stereoscope. Initially, the photos were analyzed without the assistance of ground truth information; later, a study guide for each area (prepared in advance) was used for re-evaluation of the scenes, in order to determine the maximum level of refinement possible.

Drainage to the level of third order streams (source streams are first order) can be consistently mapped, and second order streams are frequently discernible with the aid of vegetation and shadows. Vegetation at the level of forests versus agricultural land can be consistently mapped, and in some cases larger areas of conifers can be differentiated from deciduous trees, especially on color winter scenes. Regional geological features can be delineated from topography, and from patterns of drainage, vegetation, and cultural features. Regional strike and dip may be indicated, but should be verified by ground truth. Water and wind gaps, and drainage larger than second order are clearly visible. Changes in drainage density are an important indicator of lithologic types.

Color and tonal changes gave inconclusive evidence of soil and underlying bedrock. Tonal differences clearly differentiated forest vegetation from cultivated fields. Tonal differences in water bodies may indicate the presence of silt. Textural differences were used to identify urban, suburban and industrial, and agricultural land uses. The presence of utility and railroad rights-of-way, quarries, and large industrial buildings require aircraft underflight photography for verification. Field patterns can easily be seen, although crops were not identified. The level of generalization at which soils can be mapped compares well with the soil association maps prepared by the Soil Conservation Service.

Finally, it was felt that Skylab photography could be a useful form of ground truth which would be helpful in digital analysis of Landsat MSS data. A study was conducted to evaluate this potential application of Skylab photography.

6.1.2 Summary of Geologic Studies

One of the objectives of these studies was to map lineaments on the Skylab/EREP data and to determine how well these lineaments correlated with those mapped from the Landsat-1 imagery. As a basis for correlation of the two data sources, a lineament map of Pennsylvania produced from Landsat-1 imagery was used because of its complete coverage of Pennsylvania. Skylab photographs were then used to compare the distribution of visible lineaments and to help position them more accurately on larger scale maps. Lineaments (linear terrain features >1.5 km long) bear a strong resemblance to fracture traces (<1.5 km long) appearing to differ only in scale.

The proven relationship between fracture traces and zones of high permeability and increased weathering emphasizes the significance of lineaments in mineral and groundwater prospecting, foundation engineering studies, and pollution control.

The extent of correlation of lineaments with ore deposits was determined following the preparation of a Pennsylvania mineral deposit map. The lineaments were also related to groundwater well yields in the carbonate areas of Pennsylvania.

Structural studies were used to relate lineaments to problems of regional structure, joint orientation, and prospecting for mineral and groundwater resources. Lineaments, fracture traces and joints are shown to be coincident in direction in one area of the Allegheny Plateau. This relationship is more consistent with a tensional than a shear model of origin.

An important factor in lineament analysis is the determination of the actual lineament width in various topographic and lithologic settings. Study of a new road cut crossing several lineaments located accurately from Skylab photography has been an important first step in lineament width determination.

As a result of the comparison between Skylab and Landsat-1 lineaments, it became possible to determine the lineament sampling bias on both types of data.

A zone of lineation determined on Skylab photography was used in a study to investigate the origin and extent of a thermal anomaly in central Pennsylvania.

Finally, digital wavenumber analysis (spatial filtering) was attempted to determine if it can be used to enhance certain subtle features and, in particular, to locate and verify lineaments.

6.1.3 Summary of Digital Processing of S192 MSS Data

A limited amount of digital MSS data was provided to ORSER for processing and evaluation. This was a result of both the limited capacity to NASA to provide processing of the original MSS data due to sheer volume and also a result of the lack of MSS coverage on the Skylab passes of principal geographical interest to ORSER. As a result, ORSER did not have aircraft underflight photography in most of the areas covered by the S192 scanner. This was a handicap to digital processing, as ORSER has found such photography to be extremely helpful as a form of ground truth. Nevertheless, available digital data was processed and a summary of the results is included here.

Line-straightened, but uncalibrated, data were used in these evaluations. The S192 data were found to be inherently quite satisfactory, even without calibration, for thematic mapping purposes.

Since ORSER has had considerable experience in processing Landsat MSS data digitally, it was natural to compare Skylab and Landsat MSS data from a spectral signature standpoint. One area was covered by both sensing systems at about the same time of the year in south-central Pennsylvania. Signatures for four vegetative targets were obtained by using an unsupervised cluster analysis program to classify data from Skylab and Landsat channels from approximately the same wavelength bands. Seven Skylab channels were used to span the spectral interval covered by the four Landsat channels. After correction for scaling in the two systems, the Skylab and Landsat spectral signatures for the four targets agreed extremely well, although the S192 near-infrared channel responses were slightly higher than the corresponding responses on Landsat.

A major objective of the investigation of the S192 digital data was the evaluation of the various spectral bands and channels for classification and thematic mapping. In order to meet the objective, it was necessary to produce satisfactory classifications and thematic maps according to the resolution of the S192.

Prior to the classification and mapping phase, an initial screening evaluation of the channel imagery was made in order to delete obviously poor channels. In addition to screening the imagery, intensity (grey level) maps were generated digitally for each of the 22 channels and statistical correlations were performed. As a result, channels 7, 11, 15, 16, 18, and 22 were dropped and the number of channels to be processed and evaluated was reduced to 16.

A total of 29 categories were mapped for a region in southwestern Pennsylvania with a large variety of land use targets and mixed spectral responses. Classification of the S192 data was successful for the intended purpose; namely, for support in channel evaluation. The final classification maps were correct to the level of detail afforded by the limited ground truth.

Following mapping and classification, three methods were used to evaluate the spectral channels. The objectives were the evaluation of channels for redundancy, evaluation of each channel for its contribution to the total information content of a scene, and evaluation of each channel for its contribution to the discriminatory information content of a scene composed of a number of categories.

Evaluation of channels for redundancy was based on simple correlations of the digital data, but this method is limited to the identification of highly redundant channels. The criteria which were employed to identify strongly redundant pairs of channels were a high correlation between the two channels, and a very similar pattern of correlations of each with the other channels. The limitation of this method of channel evaluation is that it is useful only in identifying pairs of channels which are redundant. The method does not help in determining the comparative value of channels for recognition of land features.

The method of channel evaluation based on the contribution of each channel to the total information content of a scene was a principal

components analysis of data for a scene or a representative sample thereof. The main and secondary dimensions (axes) existing in the data were found by linearly transforming the original dimensions (channels) on the basis of principal components analysis. This was then followed by the determination of the correlation of each channel with each of the axes. Channels which were strongly correlated with the important axes were, therefore, determined to be important in contributing to the total information content of the data. In this method, however, channel redundancy was not taken into account.

To evaluate channels regarding their contribution to discriminatory information content, canonical analysis was used. After recognizing the predominant categories in a scene, canonical analysis also performs a linear transform and identifies the discriminatory dimensions (axes) among categories. Correlations of channels with the important discriminatory axes then can be used to identify the importance of each channel for discrimination among the various categories. As with the prior method, channel redundancy is not considered.

Each of the methods has advantages and disadvantages, so that no one method could be singled out for exclusive use with complete success as the anticipated result. The various methods, therefore, were used in a complementary fashion and the combined interpretation of results was used as the basis for final channel evaluations.

The selection of these methods and the results of their use have a strong and intended orientation toward land use classification and mapping. The methods and resultant channel evaluations must be considered in this context. These methods do not lend themselves to direct use for identifying channels which measure subtle phenomena dispersed over large areas, such as certain geologic or phenologic expressions. In addition, the methods as used were not oriented toward discovering channels which would precisely identify any specific category against a background of other undifferentiated categories.

As part of channel evaluation, ORSER used several methods of displaying products. Color displays are very helpful in providing spatial relationships and interpretations and can save much time in analysis. A comparison of four color display systems was made: 1) line printer output in color (using different colored ribbons); 2) the GE Image 100 interactive display and classification system; 3) a Dicomed color film recorder; and 4) the Ramtek color TV display system at ORSER.

6.2 CONCLUSIONS

6.2.1 Conclusions of Photographic Analysis

The significant findings and conclusions based upon the analysis of Skylab photography are:

1. The S190B color positive photography was clearly superior, for interpretive purposes, to any of the S190A photography. Within the S190A films, the panchromatic black and white is generally superior to the infrared black and white, although water feature definition and that of water and wind gaps are distinctly clearer on the infrared film. The visible color film of the S190A is superior to the color infrared film.

2. Photoanalysis techniques applied to Skylab S190B photography can yield a regional map of considerable value. Landforms with minimum relief differences of 150-240 m can be mapped relatively consistently, and lesser relief differences can be discerned in some instances, with the assistance of shadows and vegetation differences.

3. Drainage pattern mapping is a major key to successful identification of many features. The consistency with which three operators have identified features in three different geographic areas indicates that generalized regional mapping using S190B photography is feasible for areas for which little or no ground truth is available.

4. Skylab S190B photography was shown to be a very effective form of ground truth data when digitally processing Landsat MSS data. Its quality and resolution are excellent for this purpose. It is useful to a lesser degree as ground truth support for processing Skylab MSS data. Aircraft underflight photography with better resolution is more suitable as ground truth in this latter case.

6.2.2 Conclusions of Geologic Studies

The significant findings and conclusions based upon the geologic studies are:

1. Skylab photography is superior to both Landsat imagery and high altitude (U2 or RB57) aircraft photography for purposes of accurate location of lineaments initially detected on Landsat imagery.

2. A comparison of lineaments plotted on Skylab scenes with those plotted on Landsat images has revealed that the Landsat plots suffer from a significant bias by illumination and scan line directions.

3. Analysis of Skylab photography has shown that lineaments originally plotted on Landsat images are actually made up of several shorter segments. These segments may differ in orientation by several degrees from the mean orientation of the long lineament originally plotted from the Landsat data.

4. Groundwater studies have shown that intersections of lineaments and fracture traces should be used to obtain maximum well yields. The large number and wide distribution of lineaments and fracture traces in all terrains means that almost any community can exploit these features to increase their water supplies, avoiding the need for costly long distance pipe lines and reservoirs. Formations known to be very poor aquifers have been shown to yield large volumes of water from fractured zones.

5. Based upon relations observed between the mineral deposit map prepared for Pennsylvania and structural features identified from Skylab and Landsat scenes, there appears to be an indication that lineaments provide clues to possible controls of metallic mineralization in Pennsylvania. The Tyrone-Mount Union lineament complex and the Perkiomen Creek lineament are the most strongly associated with mineralization in Pennsylvania. Several other unnamed lineaments were geographically associated with 3 - 5 mineral occurrences each.

6. As a result of studying the wavenumber spectrum of the individual Skylab channels, it is concluded that each channel provides unique wavenumber information about a particular scene. The peaks and troughs produced in the wavenumber domain by a scene are shaped differently in different channels, and the separations of the intensities of peaks and troughs vary for different channels. The most detailed wavenumber spectrum is produced by the thermal IR which has higher intensities in higher wavenumbers than the other channels. The channels in the IR and near IR show a relatively distinct wavenumber signature for the dominant periodic feature in the scene. The channels in the visible range have a flatter wavenumber response, and the wavenumber signature associated with the dominant feature is not as sharp and as well defined as in the IR channels.

6.2.3 Conclusions of Digital Processing of S192 MSS Data

It should be noted that the results of this study of the S192 digital data are for the general mix of land use patterns existing in the growing season for an area representative of western Pennsylvania. It would be conjectural to extrapolate the results to other substantially different climatic areas, such as semi-arid ones, or to another very different season of the year, such as winter. Although the methodology would be expected to be as satisfactory in channel evaluation under other conditions, the specific results might very well be quite different.

Based upon the results of processing the digital MSS (S192) data from Skylab, the significant findings and conclusions are:

1. Channels which were duplicates in the bandwidth of their spectral response appear to contain approximately duplicate information and discriminatory power as applied to the types of ground targets being classified by ORSER. Therefore, the choice of the best sensor in each band should be determined by other factors, such as cost, design, and reliability.

2. The most important channels in defining both total information content and discriminatory variance cover the long visible through short IR wavelengths (0.68-1.75 μ) and the long reflected IR band from 2.10-2.35 μ; and, finally, the least important band is the thermal IR band (10.20-12.50 μ).

3. The relatively low information content in the thermal IR channels is somewhat surprising, but it is believed that such channels should not be considered useless in land use classification applications. After canonical transformation, three axes in the transformed data were found

to be useful for classification. The third of these axes, although it contained the least discriminatory information (smallest variance), was still significant and the thermal IR content in this axis was relatively high. One possible explanation for the overall low rating of the thermal IR channels may be that their discriminatory power is relatively low in the daytime, since the energy measured is both reflected and radiated (as opposed to night sensing of radiated energy alone). Thermal IR measurements are more sensitive to time of day, atmospheric disturbances, etc., and calibration is very critical.

4. Skylab MSS data have greater resolution than Landsat data and this makes land use mapping somewhat easier in some cases. Simultaneously, however, the system features which result in greater resolution, along with the many spectral channels of Skylab, generate a much greater data volume to be handled and processed. This results in increased costs and time for processing. Overall, the quality of Skylab MSS data is quite good.

5. As a result of the application of principal components and canonical analysis to the MSS data, it was determined that a considerable reduction in data volume can be achieved by use of such transformations followed by feature selection (dimension reduction) based on information content of the transformed axes. The resulting savings in time and cost are substantial. In addition, the transformed data is ideally suited for use with color display devices.

6.3 RECOMMENDATIONS

6.3.1 Recommendations for Photographic Analysis

As a result of the analysis of Skylab photography, the following recommendations are submitted:

1. The S190B color positive photography should be used for all terrain analysis studies involving Skylab photography, and studies of this nature should utilize an instrument such as the Bausch and Lomb Zoom 95R stereoscope mounted on an X-Y stage.

2. A "foreign" area - one for which there is little or no ground truth available and one with which the photointerpreter is unfamiliar - should be studied using Skylab S190B photography in an attempt to define the landforms, nature of the bedrock, structural features, nature of the soil cover, and relative depth to the groundwater table. After such a study, the ground truth should be established and the percentage of the area correctly mapped should be determined.

6.3.2 Recommendations for Geologic Studies

As a result of the Skylab geologic studies conducted in this investigation, the following recommendations are submitted:

1. Skylab photography, or imagery at that scale and resolution, should be obtained on a seasonal basis and over major geographical areas for continued lineaments work. Repetitive Skylab coverage is lacking for most areas, and some areas are not covered at all. Stereo coverage would also be recommended on future flights.

2. Investigation should be continued into the effects of operator, scan line, and illumination bias on Skylab and Landsat photography and imagery. Multiple operators should be used to increase the probability of detecting more subtle lineaments.

3. There should be an investigation to determine from ground-based observations the nature of the structural features which underlie lineaments and to determine the nature and tectonic significance of well known major lineaments to establish their relationship to less prominent surrounding lineaments.

4. An accurate lineament map of the Commonwealth of Pennsylvania should be prepared using Skylab-type data and evaluated for its use in groundwater and mineral prospecting, siting of proposed construction, and pollution controls.

5. It is recommended that thermal infrared channels be included on future geological remote sensing missions since the Skylab thermal channel consistently produced a wavenumber spectrum with contributions in all wavenumbers, with a greater intensity in the higher wavenumbers than in the other channels. Since periodic ground features, such as folds and multiple lineaments, are of interest geologically, channels containing a great amount of wavenumber character would be desirable for geological studies.

6. To realize the full potential of wavenumber analysis in remote sensing and geologic applications, computer programs must be developed which are capable of operating on large data blocks representing ground areas of the order of 1 to 4 x 10^4 km^2. Basically, the area considered must be large enough to contain the salient shape characteristics of the feature(s) of interest.

6.3.3 Recommendations for Digital Processing of S192 MSS Data

Based upon the results of ORSER's analysis of the S192 digital data, the following recommendations are submitted:

1. Future earth resources missions should use fewer spectral bands

(and channels) and provide more areal coverage. Six bands (e.g., 0.5-0.7 μ, 0.7-0.9 μ, 0.9-1.1 μ, 1.1-1.3 μ, 2.10-2.35 μ, and 10.20-12.50 μ) would appear to be adequate.

2. The techniques used for channel evaluation in this investigation (correlation, principal components, and canonical analysis) should be applied to S192 data over other geographical areas and for other types of targets.

3. There is a need for a more extensive investigation of the value of daytime thermal IR data for land use mapping using digital MSS data. Consideration should be given to calibration, types of target, time of day, etc.

4. Canonical analysis should be applied to digital S192 data and the results displayed on color display devices for evaluation by photo-interpreters.

REFERENCES

Anderson, E. M. (1951), The Dynamics of Faulting. Oliver and Boyd, Edinburgh.

Billingsley, F. C. (1970), Applications of Digital Image Processing. Appl. Opt. 9:289-299.

Borden, F. Y., D. N. Applegate, B. J. Turner, H. M. Lachowski, B. F. Merembeck, and J. R. Hoosty (1976), Satellite and Aircraft Multispectral Scanner Digital Data Users' Manual. ORSER-SSEL Technical Report 1-76. Office for Remote Sensing of Earth Resources, The Pennsylvania State University, University Park, Pa. 16802.

Butts, C., F. M. Swartz, and W. Bradford (1939), Tyrone Quadrangle, Atlas of Pennsylvania, No. A96. Fourth Pennsylvania Geological Survey.

Cline, G. D. (1968), Geologic Factors Influencing Well-Yields in a Folded Sandstone-Siltstone-Shale Terrane Within the East Manhantango Creek Watershed, Pennsylvania. M.S. thesis, Dept. Geology, The Pennsylvania State University, University Park, Pa. 16802.

Cline, G. D., and R. R. Parizek (1975), Factors Influencing Well-Yields in Folded Sandstone-Siltstone-Shale Terrane, Northumberland and Schuylkill Counties, Pennsylvania (unpublished manuscript).

Cooley, J. W., and J. W. Tukey (1965), An Algorithm for the Machine Calculation of Complex Fourier Series. Math Computation 19:297-301.

Corrêa, A. C., and R. J. Lyon (1974), An Application of Optical Fourier Analysis to the Study of Geological Linear Features in ERTS-1 Imagery of California. Stanford RSL Technical Report 74-9. Stanford University, Palo Alto, California.

DeMeyer, F. (1974), Filter Techniques in Gravity Interpretation. Advances in Geophysics 10:187-261.

Drahovzal, J. A., T. L. Neathery, and C. C. Wielchowski (1973), Significance of Selected Lineaments in Alabama. Third Earth Resources Technology Satellite - 1 Symposium, Technical Presentations 1:897-918

Embree, P., J. P. Burg, and M. M. Backus (1963), Wide Band Velocity Filtering -- The Pie Slice Process. Geophysics 28:948-976.

Fleming, R. S. (1975), Interpretation of Geophysical Anomalies Over the Arcuate Appalachians. GSA Northeastern Section Annual Meeting Vol. 7, 38 p.

Fuller, B. D. (1967), Two-Dimensional Frequency Analysis and Design of Grid Operators. Mining Geophysics, Vol. II, Theory. Society Exploration Geophysics. p. 658-708.

Gold, D. P. (1973), Crustal Control on the Emplacement of Kimberlites. Extended Abstracts of Papers: Conference on Kimberlites, University of Cape Town, South Africa. p. 131-134.

Gold, D. P., S. S. Alexander, and R. R. Parizek (1974), Applications of Remote Sensing of Natural Resource and Environmental Problems in Pennsylvania. Earth and Mineral Sciences (The Pennsylvania State University) 43:49-53.

Gold, D. P., R. R. Parizek, and S. S. Alexander (1973), Analysis and Application of ERTS-1 Data for Regional Geological Mapping. Symposium on Significant Results Obtained from the Earth Resources Technology Satellite - 1 1:231-245.

Gray, C., et al. (1960), Geologic Map of Pennsylvania. Scale of 1:250,000. Pennsylvania Geological Survey, 4th Series.

Gwinn, V. E. (1964), Thin-Skinned Tectonics in the Plateau and Northwestern Valley and Ridge Provinces of the Central Appalachians, Bull. Geol. Soc. of America 75:863-900.

HARM, (1966) Harmonic Analysis Subroutine for IBM 7090. SDA 3425. SHARE Distribution Agency, Program Information Department, IBM Corp. 40 Saw Mill Road, Hawthorne, NY 10532.

Horning, R. J., and J. A. Smith (1973), Application of Fourier Analysis to Multispectral/Spatial Recognition. Management and Utilization of Remote Sensing Data, Proceedings of Symposium on Remote Sensing, Sioux Falls, SD 57198.

Hsu, Fu-Tzu (1973), Geochemical Exploration in the Nittany Valley Area, Centre County, Pennsylvania. M.S. thesis, Dept. Geosciences, The Pennsylvania State University, University Park, Pa.

Hudleston, P.J. (1973), Fold Morphology and Some Geometrical Implications of Theories of Fold Development. Tectonophysics 16:1-46.

Jensen, M. L. (1973), Geology of Utah and Nevada by ERTS-1 Imagery. Symposium on Significant Results Obtained from the Earth Resources Technology Satellite - 1 1:247-257.

Keim, J. W. (1962), A Study of Photogeologic Fracture Traces Over the Bisbee Quadrangle, Cochise County, Arizona. M.S. thesis, Dept. Geology, The Pennsylvania State University, University Park, Pa. 16802.

Koppe, E. F. and D. R. Thompson (1972), Progress in the Recognition of Fractured Rock Zones in Prevention and Abatement of Mine Drainage. Papers presented before the 4th Symposium on Coal Mine Drainage Research, Mellon Institute, Pittsburgh, Pa. April 26-27, 1972. p. 41-47.

Kowalik, W. S. (1975), Use of Landsat-1 Imagery in the Analysis of Lineaments in Pennsylvania. M.S. Paper, Department of Geology, The Pennsylvania State University, University Park, Pa. 16802.

Kowalik, W. S., and Gold, D. P. (1975a), Lineament Map of Pennsylvania. ORSER-SSEL Technical Report 5-75. Office for Remote Sensing of Earth Resources, The Pennsylvania State University, University Park, Pa. 16802.

Kowalik, W. S., and D. P. Gold (1975b), Lineaments and Mineral Occurrences in Pennsylvania. ORSER-SSEL Technical Report 14-75. Office for Remote Sensing of Earth Resources, The Pennsylvania State University, University Park, Pa. 16802.

Krohn, M. D. (1975), The Relation of Lineaments to Gossans and Geochemical Anomalies Along Bald Eagle Mountain, Centre, Blair, and Huntingdon Counties, Pennsylvania. M.S. thesis, Dept. Geosciences, The Pennsylvania State University, University Park, Pa. 16802.

Krohn, M. D. and D. P. Gold (1975), Relation of Lineament to Sulfide Deposits: Bald Eagle Mountain, Centre County, Pennsylvania. ORSER-SSEL Technical Report 9-75. The Office for Remote Sensing of Earth Resources, The Pennsylvania State University, University Park, Pa. 16802.

Lattman, L. H. (1958), Techniques of Mapping Geologic Fracture Traces and Lineaments on Aerial Photographs. Photogram. Engineering 24:568-576.

Lattman, L. H. and R. P. Nickelson (1958), Photographic Fracture-Trace Mapping in Appalachian Plateau. Bull. Amer. Assoc. Petrol. Geology 42(9):2238-2245.

Lattman. L. H. and R. H. Matzke (1961), Geological Significance of Fracture Traces. Photogram. Engineering 27:635-638.

Lattman, L. H. and R. R. Parizek (1964), Relationship Between Fracture Traces and the Occurrence of Ground-water in Carbonate Rocks. Journ. Hydrology 2:73-91.

Lavin, P. M., and J. F. Devane (1970), Direct Design of Two-Dimensional Wavenumber Filters. Geophysics 35:1073-1078.

Levandowski, D. W., T. V. Jennings, and W. T. Lehman (1973), Applications of ERTS-1 Imagery to Mapping Lineaments Favorable to the Localization of Ore Deposits in North Central Nevada. LARS Information Note 101073. Laboratory for Applications of Remote Sensing, Purdue University, Lafayette, Indiana.

Lovell, H. L. and J. W. Gunnett (1974), Hydrogeological Influences in Preventive Control of Mine Drainage from Deep Coal Mining. Special Research Report SR-100. Coal Research Section, The Pennsylvania State University, University Park, Pa. 16802.

Maul, G. A., R. L. Charnell, and R. H. Qualset (1974) Computer Enhancement of ERTS-1 Images for Ocean Radiances. Remote Sensing of Environment 3:237-252.

McMurtry, G. J., F. Y. Borden, H. A. Weeden, and G. W. Petersen (1974), The Penn State ORSER System for Processing and Analyzing ERTS and Other MSS Data. Remote Sensing of Earth Resources 3:721-740.

Moody, J. D., and M. J. Hill (1956), Wrench Fault Tectonics. Bull. Geol. Soc. America 67:1207-1246.

Nickelsen, R. P. and V. N. D. Hough (1967), Jointing in the Appalachian Plateau of Pennsylvania. Bull. Geol. Soc. America 78:609-629.

Nicolias, S. M. (1973), Mineral Exploration with ERTS Imagery. Third Earth Resources Technology Satellite -1 Symposium, Technical Presentations 1:785-789.

Parizek, R. R. (1969), An Environmental Approach to Land Use in a Folded and Faulted Carbonate Terrane. Environmental Planning and Geology. U.S. Dept. Housing and Urban Development and U.S. Dept. Interior p. 122-143.

Parizek, R. R. (1971a), Hydrologic Framework of Folded and Faulted Carbonates -- Influence of Structure. In Mineral Conservation Series Circular 82: Hydrogeology and Geochemistry of Folded and Faulted Carbonate Rocks of the Central Appalachian Type and Land Use Problems, by R. R. Parizek, W. B. White, D. Langmuir, et al. College of Earth and Mineral Sciences, The Pennsylvania State University, University Park, Pa. 16802. p. 28-65.

Parizek, R. R. (1971b), Prevention of Coal Mine Drainage Formation by Well Dewatering. Special Research Report 82. Coal Research Section, The Pennsylvania State University, University Park, Pa. 16802.

Parizek, R. R. (1975), On the Nature and Significance of Fracture Traces and Lineaments in Prospecting for Groundwater. Proceedings: First Bilateral U.S. - Yugoslavia Seminar on Hydrology and Water Resources in Karst Regions, Dubrovnik, Yugoslavia, 2-5 June 1975. (in press).

Parizek, R. R. and B. Voight (1970), Question 37: On Remote Sensing Investigations for Dam and Reservoir Construction in Karst Terranes. Dixieme Congres des Grands Barrages (Tenth International Congress on Large Dams, Montreal, 1970) 6:538-546.

Pennsylvania Geological Survey (1972), Open File Report: Knisley Quarry, Blair County.

Pennsylvania Geological Survey (no date), Open File Report: U.S. 22 Roadcut, Mapleton, Huntingdon County.

Podwysocki, M. H. (1974), Fortran IV Programs for Summarization and Analysis of Fracture Trace and Lineament Patterns. NASA-Goddard Space Flight Center Document X-644-74-3. Goddard Space Flight Center, Greenbelt, Md. 20771

Price, N. J. (1966), Fault and Joint Development in Brittle and Sem-Brittle Rock. Pergamon Press, Oxford.

Rose, A. W. (1970) (Reprinted 1973), Atlas of Pennsylvania's Mineral Resources. Part 3: Metal Mines and Occurrences in Pennsylvania. Bulletin M50. Pennsylvania Geological Survey, 4th Series.

Sanders, J. E. (1963), Late Triassic Tectonic History of Northeastern United States. American Journal Science 261:501-524.

Selzer, R. H. (1968), The Use of Computers to Improve Biomedical Image Quality. Proceeding of Fall Joint Computer Conference 33:817-834.

Siddiqui, S. H. (1969), Hydrogeologic Factors Influencing Well Yields and Aquifer Hydraulic Properties of Folded and Faulted Carbonate Rocks of Central Pennsylvania. Ph.D. thesis. Dept. Geology and Geophysics, The Pennsylvania State University, University Park, Pa.

Siddiqui, S. H. and R. R. Parizek (1971a), Hydrogeologic Factors Influencing Well-Yields in Folded and Faulted Carbonate Rocks in Central Pennsylvania. Water Resources Research 7:1295-1312.

Siddiqui, S. H. and R. R. Parizek (1971b), Variations in Well-Yields and Controlling Hydrogeologic Factors. In Mineral Conservation Series Circular 82: Hydrogeology and Geochemistry of Folded and Faulted Carbonate Rocks of the Central Appalachian Type and Land Use Problems, by R. R. Parizek, W. B. White, D. Langmuir, et al. College of Earth and Mineral Sciences, The Pennsylvania State University, University Park, Pa. 16802. p. 87-95.

Smith, R. C., III, D. C. Herrick, A. W. Rose, and J. M. McNeal (1971), Zn-Pb Occurrences Near Mapleton, Huntingdon County, Pennsylvania. Earth and Mineral Sciences Experiment Station Circular 83. The Pennsylvania State University, University Park, Pa. 16802

Turner, B. J. (1974), Applications of Cluster Analysis in Natural Resources Research. Forest Science 20:343-349.

Wier, E. C., F. J. Wobber, O. R. Russell, R. V. Amata, and T. V. Leshendok (1973), Relationship of Roof Falls in Underground Coal Mines to Fractures Mapped on ERTS-1 Imagery. Third Earth Resources Technology Satellite - 1 Symposium, Technical Presentations 1:825-844.

Wise, D. U. (1968), Regional and Sub-Continental Size Fracture Systems Detectable by Topographic Shadow Techniques. Paper 68-72. Geol. Survey Canada, Ottawa. p. 175-199.